Argillite Disposal R&D and Argillite International Collaborations - LANL

Spent Fuel and Waste Disposition

Prepared for
U.S. Department of Energy
Spent Fuel and Waste Science and Technology

Kirsten B. Sauer, Florie A. Caporuscio, and Marlena J. Rock
Los Alamos National Laboratory

July 19, 2021
SF-21LA01030101 Rev2
SF-21LA01030102
LA-UR-21-26538

STANDARD CONTRACT DISCLAIMER

This is a technical report that does not take into account the contractual limitations under the Standard Contract for Disposal of Spent Nuclear Fuel and/or High-Level Radioactive Waste (Standard Contract) (10 CFR Part 961). For example, under the provisions of the Standard Contract, DOE does not consider spent nuclear fuel in multi-assembly canisters to be an acceptable waste form, absent a mutually agreed to contract amendment. To the extent discussions or recommendations in this report conflict with the provisions of the Standard Contract, the Standard Contract provisions prevail.

APPENDIX E

NFCSC DOCUMENT COVER SHEET [1]

Name/Title of Deliverable/Milestone/Revision No.	Argillite Disposal R&D - LANL M3SF-21LA010301011
Work Package Title and Number	Argillite Disposal R&D - LANL (FY-21)
Work Package WBS Number	SF-21LA01030101
Responsible Work Package Manager	Kirsten Sauer Kirsten Sauer Digitally signed by Kirsten Sauer Date: 2021.07.12 13:08:07 -06'00' (Name/Signature)
Date Submitted	

Quality Rigor Level for Deliverable/Milestone[2]	☐ QRL-1 ☐ Nuclear Data	☐ QRL-2	☒ QRL-3	☐ QRL-4 Lab QA Program[3]

This deliverable was prepared in accordance with _____
(Participant/National Laboratory Name)

QA program which meets the requirements of

☐ DOE Order 414.1 ☒ NQA-1 ☐ Other

This Deliverable was subjected to:

☐ Technical Review ☒ Peer Review

Technical Review (TR)
Review Documentation Provided

☐ Signed TR Report or,

☐ Signed TR Concurrence Sheet or,

☐ Signature of TR Reviewer(s) below

Name and Signature of Reviewers

Peer Review (PR)
Review Documentation Provided

☐ Signed PR Report or,

☐ Signed PR Concurrence Sheet or,

☒ Signature of PR Reviewer(s) below

Artas Migdissov
Artaches Migdissov Digitally signed by Artaches Migdissov Date: 2021.07.13 13:05:36 -06'00'

NOTE 1: *Appendix E should be filled out and submitted with the deliverable. Or, if the PICS:NE system permits, completely enter all applicable information in the PICS:NE Deliverable Form. The requirement is to ensure that all applicable information is entered either in the PICS:NE system or by using the NTRD Document Cover Sheet.*

- *In some cases there may be a milestone where an item is being fabricated, maintenance is being performed on a facility, or a document is being issued through a formal document control process where it specifically calls out a formal review of the document. In these cases, documentation (e.g., inspection report, maintenance request, work planning package documentation or the documented review of the issued document through the document control process) of the completion of the activity, along with the Document Cover Sheet, is sufficient to demonstrate achieving the milestone.*

NOTE 2: *If QRL 1, 2, or 3 is not assigned, then the QRL 4 box must be checked, and the work is understood to be performed using laboratory QA requirements. This includes any deliverable developed in conformance with the respective National Laboratory / Participant, DOE or NNSA-approved QA Program.*

NOTE 3: *If the lab has an NQA-1 program and the work to be conducted requires an NQA-1 program, then the QRL-1 box must be checked in the work Package and on the Appendix E cover sheet and the work must be performed in accordance with the Lab's NQA-1 program. The QRL-4 box should not be checked.*

SUMMARY

The United States' Department of Energy Spent Fuel and Waste Disposition program is investigating disposal concepts in a variety of host rock settings and thermal loads. Target geologic formations include crystalline (e.g., granite), argillite (e.g., sedimentary rocks with a high clay mineral content), and salt. Different configurations and loadings of spent nuclear fuel and waste within disposal canisters are also being investigated, some of which have the potential to generate repository temperatures higher than previously considered (i.e., temperatures > 100ºC) by foreign and domestic concepts. This report focuses on understanding geochemical and mineralogical changes in the engineered barrier system (EBS), consisting of waste canister, bentonite buffer, and cementitious materials, in a high temperature argillite-hosted repository.

Experiments were designed to develop EBS concepts in a high-temperature argillite environment in 1) bentonite-cement reactions, 2) interaction between waste canister materials and bentonite, and 3) influence of phosphate additives to the bentonite buffer. Experiment results are applied to understanding long-term repository performance.

Hydrothermal experiments completed in the rocking autoclaves at LANL in FY21 include: EBS-30 (Opalinus Clay + Wyoming bentonite + cured ordinary Portland cement + Opalinus Clay synthetic groundwater, 316SS, 200ºC/150 bar, 8 weeks), EBS-31 (Opalinus Clay + Wyoming bentonite + cured ordinary Portland cement + Opalinus Clay synthetic groundwater, 304SS, 300ºC/150 bar, 8 weeks). Characterization of the reaction products of experiments conducted in FY20 and FY21 was completed, including QXRD, aqueous geochemistry, XRF, and SEM analyses.

The addition of uncured Portland cement powder to the Wyoming bentonite + Opalinus Clay experimental system in EBS-23 through EBS-27 at 200ºC resulted in the formation of abundant aluminosilicate phases (phyllosilicates, feldspar, and zeolites), calcium silicate hydrate minerals, and amorphous material, coupled with the dissolution of clay phases. Structural degradation of the smectite mineral structure from within Wyoming bentonite, due to the formation of interlayered illite, silica cementation, and/or CSH mineral intergrowth, resulted in ~10% reduction in expandability. The composition of analcime determined by electron microprobe reveals a wide range of Ca and Na compositions and lower Si/Al values than observed in previous EBS experiments.

One experiment was conducted with Wyoming bentonite + Opalinus Clay + uncured Portland cement powder at 300ºC for 6 weeks (EBS-28). Aqueous chemistry and solid reaction products were notably different from the experiments conducted at 200ºC. Feldspar and zeolite formation was observed as well as significant degradation to the smectite structure and formation of interlayered illite-smectite and chlorite-smectite.

Two experiments (EBS-30 and EBS-31) were completed that contained a cured cement chip instead of uncured powder. Alteration to the bentonite was less extensive than in the experiments with the uncured powder. Zeolite, feldspar, and CSH formation was still observed but to a lesser extent. Smectite was observed to remain stable; detailed clay mineral structural analyses are in progress. Measured pH values reached near-neutral values by the second week of experiment time.

The new characterization efforts related to the interaction of stainless-steel coupons and bentonite clay focused on thickness and mineralogy of phases that formed at the steel surface. The mineral phases observed were dependent on the pH of the system (i.e., bulk chemistry). For

example, in the Wyoming bentonite + Opalinus Clay experiments, layered alteration products were observed on the surface of coupons that included alteration of the outermost steel edge to Fe,Cr-oxide phases, followed by Fe-rich phyllosilicates (Fe-saponite, chlorite) and interbedded Fe,Cr,Ni-sulfide phases (pentlandite). In contrast, under the alkaline solution conditions in the experiments with uncured cement powder, zeolite and CSH phases are observed attached to the steel surface; no Fe is transferred to the bentonite groundmass. In experiments with the cured cement chip, solutions evolved to neutral pH values and corrosion of steel coupons and the formation of Fe-rich clay phases was observed.

An experimental program was initiated in exploring apatite as an additive to the bentonite buffer. Objectives were to: 1) assess apatite interaction with bentonite clay under hydrothermal conditions and 2) apatite solubility at relevant geochemical and pressure-temperature conditions. One experiment was completed with Wyoming bentonite, apatite from Durango, Mexico, and Stripa brine at 250ºC/150 bar for 8 weeks. Characterization efforts revealed minimal apatite dissolution and the absence of newly formed phosphate phases. In the bentonite, XRD analyses reveal a reduction in smectite abundance and formation of muscovite. Future work will confirm these results and will be used to inform experiments on apatite retention of radionuclides in the EBS.

Work related to the new international collaboration with the Japan Atomic Energy Agency (JAEA) continued in FY21. Future experiments will be conducted at conditions relevant to full-scale EBS demonstrations at the Honorobe Underground Research Laboratory. Requests for material and experiment planning was conducted (presented in Chapter 2). Experiments relevant to the Japanese disposal concept on the effects of different treatments of stainless steel (e.g., polishing, welding) were conducted/planned (presented in Chapter 3).

The experimental results obtained in FY21 continue to document the wide-ranging effects of bulk composition and pressure-temperature conditions in the mineralogical and geochemical evolution of the repository environment. Concepts developed will be used to inform models of long-term material stability in a generic argillite-hosted repository.

This page is intentionally left blank.

CONTENTS

LIST OF FIGURES

LIST OF TABLES

Acronyms

DOE-	Department of Energy
DPC-	Dual-Purpose Canister
CSH-	Calcium Silicate Hydrate
EBS-	Engineered Barrier System
EDS-	Energy-dispersive X-ray spectroscopy
EPRI-	Electric Power Research Institute
FEBEX-	Full-scale High-Level Waste Engineered Barriers
FY-	Fiscal Year
JAEA-	Japanese Atomic Energy Agency
JNC-	Japan Nuclear Cycle Development Institute
LANL-	Los Alamos National Laboratory
LCS-	Low Carbon Steel
OC-	Opalinus Clay
OPC-	Ordinary Portland Cement
PR-	Prototype Repository
PWR-	Pressurized-Water Reactors
QXRD-	Quantitative X-Ray Diffraction
RH-	Relative Humidity
SEM-	Scanning Electron Microscope
SKB-	Svensk Kärnbränslehantering Ab (Swedish Nuclear Fuel and Waste Management Co.)
SS-	Stainless-Steel
SNL-	Sandia National Laboratories
URL-	Underground Research Laboratory
WB-	Wyoming Bentonite
WIPP-	Waste Isolation Pilot Plant
XRD-	X-Ray Diffraction
XRF-	X-Ray Fluorescence
YMP-	Yucca Mountain Project

Chapter 1

Argillite Disposal R&D

SPENT FUEL AND WASTE SCIENCE AND TECHNOLOGY

ARGILLITE DISPOSAL R&D AND ARGILLITE INTERNATIONAL COLLABORATIONS – LANL

CHAPTER 1: Argillite Disposal R&D

1. Introduction

The United States Department of Energy Spent Fuel and Waste Disposition program is investigating reference cases in multiple host rock types for the geologic disposal of spent nuclear fuel and waste. This report presents experimental results on engineered barrier system (EBS) interactions at elevated temperature and pressure in an argillite host rock formation. The generic disposal concept in argillite includes a horizontal waste package encapsulated in a bentonite clay barrier (pellets or compressed blocks) emplaced in a horizontal tunnel, likely lined with a form of concrete (e.g., shotcrete or pre-formed concrete blocks) (Figure 1). The bentonite barrier's function relies on the physical and chemical properties of swelling clay minerals (i.e. smectite), which are the main mineralogical components of bentonite (Pusch, 1979; Dohrmann et al., 2013; Sellin & Leupin, 2014). Smectite has unique swelling properties that 1) maintain in-drift pressure, 2) have the ability to seal cracks and fractures that may develop, and 3) retard the infiltration of fluid from the surrounding wall rock that may interact with the waste package. Further, clay minerals may act as a chemical barrier that attenuate actinide migration through sorption on clay mineral surfaces if a release occurs. However, there remain large uncertainties regarding the long-term stability of bentonite at potential repository conditions, particularly, under prolonged periods of high thermal loads in the presence of water and other repository materials such as cement and stainless steel.

U.S. DOE is interested in exploring repository concepts at higher temperatures than considered by foreign programs in order to vet disposal of large waste packages with a higher thermal load. For example, dual-purpose canisters (DPCs), designed for storage and transportation, may contain up to 37 spent-fuel assemblies (37 pressurized-water reactors (37-PWR)), whereas many of the European concepts are limited to four spent fuel assemblies (4-PWR) (Pusch, 2008; Hardin et al., 2015). The increased number of spent fuel assemblies within the U.S. DPCs have the potential to generate a greater amount of heat radiating into the EBS and host rock in a disposal scenario. For example, thermal modeling calculations show that the surface of a DPC containing 37-PWR (60 gigawatt-days per metric ton burnup) has the potential to reach 400ºC in a repository hosted in clay/shale rock (50-year decay storage and 100-year ventilation; 20 m package spacing; unsaturated bentonite thermal conductivity = 0.60 W/m-K, Hardin et al., 2015) (Figure 2). These calculations, based on a hypothetical repository layout, demonstrate the importance of thermal management and the potential for high temperatures in a clay/shale disposal environment. Thus, the thermal evolution of this potential repository design demonstrates the need for high temperature experimental work on the interaction of

wall rock, EBS backfill, cement liner, and canister materials that have not been explored previously by the foreign repository science programs.

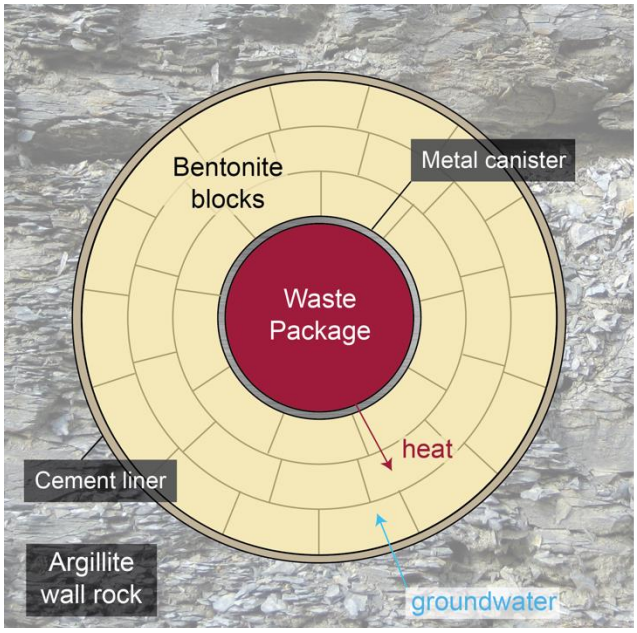

Figure 1: Schematic of a generic engineered barrier system concept in argillite host rock. Bentonite blocks surround a waste canister emplaced in a horizontal tunnel lined with cement.

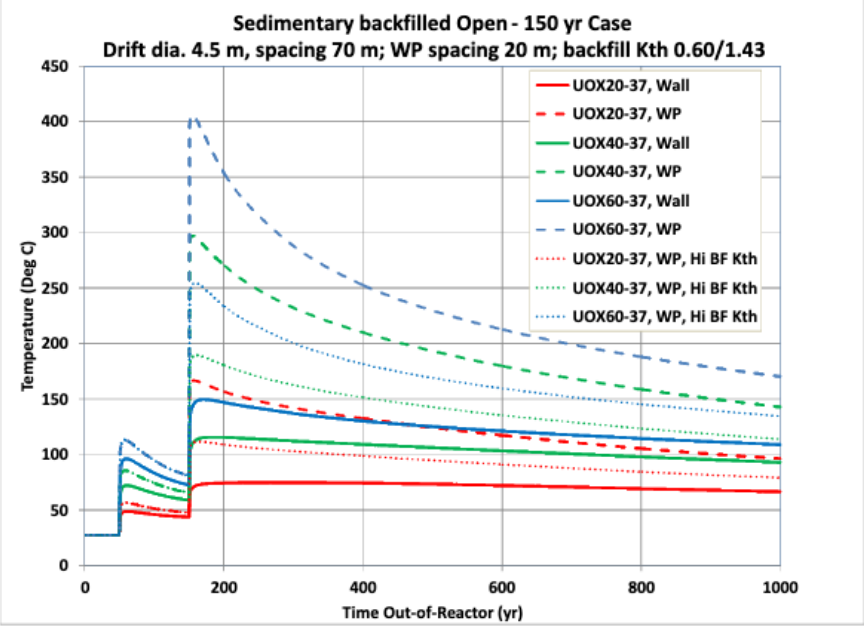

Figure 2: Calculated temperatures for various burnup levels (e.g., OUX20) of spent nuclear fuel 37-PWR at the repository drift wall (wall) and waste package surface (WP) in a backfilled sedimentary rock-hosted repository. The calculations include 50 years of decay storage and 100-year ventilation time. Waste package spacings and drift dimensions are listed on the figure. Thermal conductivity of the bentonite is either 0.60 W/m-K (unsaturated bentonite) or 1.43 W/m-K (fully hydrated bentonite). From Hardin et al. (2015).

Cementitious materials will likely make up a large component of the underground repository. Interaction between cement, bentonite, and steel will therefore likely occur at elevated temperature and pressure and in the presence of water. Experiments in FY21 included a comparison of the effects of uncured ordinary Portland cement (OPC) powder versus cured OPC chips on bentonite mineral and geochemical properties at temperatures of 200 to 300ºC.

The research scope of FY21 also included the investigation of "designer" EBS additives that may enhance the radionuclide retention capacity of the barrier system. Clay and zeolite minerals within bentonite have the potential to retain radionuclides in the case of a canister breach, through sorption on mineral surfaces or incorporation into the crystalline structure. For example, Redkin and Hemley (2020) studied the cesium (Cs) and strontium (Sr) sorption on analcime at 250 to 300ºC in rock buffered systems. They establish that there is a high sorption capacity for the albite-analcime assemblage at 250 to 300°C with respect to Cs and Sr. The interaction of Cs and Sr-bearing solution encouraged the mineralization of Cs-rich analcime, pollucite and Sr-analcime, especially in systems buffered at a higher pH. Phosphate minerals also have the potential for actinide element retention under ambient to hydrothermal conditions (e.g. Krejzker et al., 2003; Omel'yanenko et al., 2007; Rigali et al., 2016). It is unknown, however, how the presence of phosphate will affect bentonite mineral stability under repository temperature and pressures. One preliminary hydrothermal experiment was completed in FY20 with Wyoming bentonite and Durango apatite to assess bentonite-phosphate interaction and dissolution-reprecipitation of apatite, with the overall goal of understanding how phosphate additives may affect bentonite stability and/or enhance EBS function to retain radionuclides.

Overall, the hydrothermal experiments conducted at Los Alamos National Laboratory in FY21 aimed to develop concepts related to the function of EBS in the high-temperature isolation of spent fuel and waste in argillite host rock. Our work on bentonite interaction with Opalinus Clay in experimental hydrothermal systems was developed in the FY17, FY18, and FY19 reports and was published in Clays and Clay Minerals (Sauer et al., 2020). The FY21 report will focus on our current experimental focuses in argillite including: 1) the effects of cured and uncured Ordinary Portland cement on bentonite stability and Opalinus Clay mineralogy, 2) clay-steel interface mineralization and growth rates in systems with and without cement, and 3) the effects of phosphate additives to the EBS system.

1.1 Background

1.1.1 Wyoming Bentonite in EBS Applications

Bentonite performance in the EBS relies on the physical and chemical properties of the mineral components, especially the clay mineral montmorillonite. Under dry conditions, the bentonite mineral assemblage may be stable to over 350°C (Wersin et al., 2007); however, moisture is likely to be present in the natural geologic environment. Under water saturated conditions and temperatures > 100°C, alteration of clay minerals may occur (e.g. Mosser-Ruck et al., 2010; Ferrage et al., 2011; Cheshire et al., 2014). The stability of bentonite at repository conditions has been documented in both laboratory and in situ (full-scale) experiments and are used to assess the long-term function of a nuclear waste disposal site.

Mineralogical changes within the bentonite EBS materials that affect the ability of smectite to expand are a primary concern for the long-term function of a nuclear waste repository. The reduction of swelling capacity of smectite, due to the formation of non-swelling clays, cementation of smectite lamellae caused by silica precipitation, and/or recrystallization to other mineral phases (e.g. zeolites), is believed to be one of the greatest risks to the repository stability and isolation capability compared to other mineral reactions (Pusch et al., 1998; Pusch & Kasbohm, 2002). Previous laboratory-scale investigations have investigated clay mineral transformations relevant to EBS systems over a wide range of repository temperatures (i.e. ~25 - 300°C), alone and in contact with metals that approximate potential canister materials (Madsen, 1998; Meunier et al., 1998; Guillaume et al., 2003; Hofmann et al., 2004; Wersin et al., 2007; Mosser-Ruck et al., 2010; Ferrage et al., 2011; Cheshire et al., 2014). The reduction of swelling capacity of montmorillonite may be due dominantly to the formation of non-swelling clays (e.g. illite, $K(Al,Mg,Fe)_2(Si,Al)_4O_{10}[(OH)_2]$) (Wersin et al., 2007). For example, in experimental systems where K^+ was reacted with bentonite, the formation of non-swelling K^+ rich, collapsed layer smectite and/or illite was observed (e.g. Mosser-Ruck et al. 1999; Kaufhold & Dohrmann, 2010; Cheshire et al. 2014). In the alteration of montmorillonite to illite, silica is liberated through the generalized reaction:

$$\text{Na-montmorillonite} + K^+ + H^+ \rightarrow \text{illite} + SiO_{2\,(aq)} + Na^+ + Mg^+ + H_2O \qquad (1)$$

The low availability of K^+ and silica saturation in the system may limit illitization (Pusch & Madsen 1995; Cheshire et al. 2014; Savage et al. 2019). For example, in bentonite systems reacted with NaCl solutions, montmorillonite structural alteration is not observed (Kaufhold & Dohrmann, 2009; Cheshire et al., 2014) in comparison to experiments in a K^+ rich environment (Kaufhold & Dohrmann, 2010).

The influence of bulk chemistry on clay-mineral reactions is observed in full-scale experiments. In the full-scale Prospective Repository experiment at the Äspö Hard Rock Laboratory in Sweden, cation exchange was observed in the smectite, but no structural changes were observed in the bentonite blocks after a period of eight years at temperatures between 60 and 85°C (Dohrmann & Kaufhold, 2014). In the FEBEX experiment, smectite alteration was observed only close to the heater surface (100°C) and included recrystallization to saponite and chlorite and a decrease in cation exchange capacity and surface area (Fernandez et al., 2018).

Zeolite formation within bentonite EBS material has also been reported (e.g. Mosser-Ruck et al., 2010; Ferrage et al., 2011; Cheshire et al., 2013, 2014; Mosser-Ruck et al., 2016). Zeolites may form as a result of clinoptilolite dissolution under silica-saturated conditions (Cheshire et al., 2013; 2014) or clay-mineral reactions (Mosser-Ruck et al., 2010). Dissolution of clinoptilolite, which makes up roughly 13% of the Wyoming bentonite used in this study, and precipitation of analcime may result in a slight volume loss within the bentonite buffer (Cheshire et al., 2014).

1.1.2 Opalinus Clay

Opalinus Clay is considered to be a favorable medium for a repository based on its high clay content, low permeability, high sorption potential for radionuclides, and crack-sealing properties (Nagra, 2002; Bossart & Thury, 2008; Bossart & Milnes, 2017). Several experimental studies have examined the mineralogical and chemical evolution of Opalinus Clay at temperatures below 200°C. The interaction of high pH fluids and Opalinus Clay had been evaluated at ambient (e.g. Adler et al., 1999; Taubald et al., 2000) and elevated (e.g. 90–200°C; Honty et al., 2012; Chermak, 1992) temperatures. The presence of cement and/or high-pH solutions at ambient temperatures (25°C) results in the dissolution of the precursor chlorite in the Opalinus Clay (Taubald et al., 2000) and the formation of Ca-zeolites and calcium aluminum silicate hydrate minerals (Alder et al., 1999). At higher temperature (150–200°C) and similar pH, the formation of analcime, vermiculite, and narectorite was observed within powdered Opalinus Clay (Chermak, 1992). In situ EBS experiments at the Mont Terri underground research laboratory in Opalinus Clay are in progress (HE-E, up to 140°C; Wieczorek et al., 2017; FE, up to 150°C; Müller et al., 2018).

1.1.3 Hydrothermal Interaction of Wyoming Bentonite and Opalinus Clay

The results and analysis of Opalinus Clay ± Wyoming bentonite experiments (EBS-14 through EBS-22) were published in Sauer et al. (2020) and summarized in Caporuscio et al. (2020).

1.1.4 Previous Research in Bentonite-Portland Cement Interaction

There have been many studies on the interaction of bentonite and cementitious materials in EBS systems as both materials are integral to most repository designs (e.g., Karnland, 1997; Cuevas et al., 2006; Watson et al., 2009; Fernandez et al., 2009a; Savage et al., 2010; Watson et al., 2018). Cementitious materials, such as shotcrete, cast-in-place, and/or preformed cement blocks, are necessary elements of repository infrastructure and provide ground support to maintain drift integrity and prevent collapse. However, the reaction of cement with water may have a significant chemical effect on the repository system through the dissolution of portlandite ($Ca(OH)_2$), alkali-rich phases, calcium silicate hydrate (CSH) minerals, and other reactive components of the cement (e.g., sulfates). Thus, cement reactions have the potential to release significant amounts of OH^- and Ca^{2+} into the groundwater migrating into the EBS system, leading to increase in pore water pH in the bentonite buffer, montmorillonite dissolution, and the formation of diverse secondary mineral phases (e.g., Ca-zeolites, CSH phases, feldspars). Cement-bentonite interaction is observed to be a non-linear system that involves multiple coupled processes that occur simultaneously and affect each other (e.g., Savage et al., 2010). These processes include the reaction of concrete to release Ca^{2+} and OH^-, transport of hydroxide and cations into bentonite, montmorillonite ion exchange and dissolution, precipitation of secondary phases, dissolution of accessory minerals, and porosity and swelling changes (Takasa, 2004; Savage et al., 2010).

The potential for significant and wide-ranging geochemical and mineralogical effects of bentonite-cement interaction has led repository programs to implement a pH limit for cement porewater (e.g., B, pH < 11). The pH limit is achievable using low pH cements that replace traditional cement components (e.g., limestone aggregate) with siliceous materials (e.g. fly ash and silica fume) resulting the reduced abundance of portlandite in the cured

product and a lower Ca/Si ratio in the CSH minerals (Calvo et al., 2010; Lothenbach et al., 2011). Due to the potential for bentonite degradation in alkaline pore waters, low pH cement formulations are becoming increasingly standard for repository concepts. The experimental work reported here focuses on the effects of uncured Ordinary Portland cement (OPC) powder and cured chips containing 100% OPC. Future research will evolve to include low pH formulations. A summary of previous modeling and experimental (laboratory and full-scale) studies is provided here to contextualize our experimental results.

1.1.4.1 Experimental Studies

Many experimental studies have been performed on the interaction of bentonite and cementitious materials and bentonite stability in highly alkaline environments (e.g, Balmer et al., 2017; Chen et al., 2019; Cuevas et al., 2006; de la Villa et al., 2001; Dolder et al., 2014; Fernandez et al., 2006; 2009a; 2016; Karnland et al., 2007; Karnland, 1997; Kaufhold et al., 2020). Experimental work at the laboratory scale and in full-scale demonstrations, especially at low temperature, may not fully capture the evolution of the cement-bentonite system due to kinetically slow reactions, but can provide insight into the potential for geochemical and mineralogical changes. Experiments below ~100ºC show that the reaction of bentonite in contact with cement and alkaline porewaters over relatively short timescales (~months to 1–2 years) result in changes to the physical property clay minerals (e.g., swelling) and the formation of secondary phases. For example, 16-month experiments with MX-80 Wyoming bentonite and solutions mimicking cement porewater (pH = 12.8–13.7) at 40ºC resulted in minor illite and chlorite formation, cristobalite dissolution and quartz precipitation, and CSH mineral and CSH gel formation (Karnland, 1997). At 60ºC over a period of 6 to 12 months, in column tests with FEBEX bentonite and alkaline solutions, alteration was concentrated in a 2.0 to 2.5 mm reaction front, which included brucite, chlorite, Mg-smectite, and minor zeolite formation and montmorillonite dissolution (Fernandez et al., 2009a). In a comparative study of 40 different bentonites in contact with Portland cement powder at 80ºC for 3 months showed that the presence of reactive silica in bentonite helped to stabilize clay minerals (Kaufhold et al., 2020). Comparative experiments over a range of temperatures between 25 and 200ºC demonstrated expansion of the alteration zone with increasing temperature and changes in alteration mineralogy (Cuevas et al., 2006). Overall, these cement-bentonite experiments demonstrate the potential for montmorillonite dissolution, zeolite, feldspar, and CSH mineral formation near the bentonite-cement contact, and the influence of bulk-system chemistry. Further, experiments demonstrated that alteration is concentrated in a thin alteration zone at the bentonite-cement interface, which expands with higher temperatures.

Observations from long-term, full-scale, in situ demonstrations at underground research facilities provide insight into cement-bentonite interactions in the natural environment, including potential effects on groundwater geochemistry, host-rock properties, and hydrologic processes. Several full-scale experimental studies at underground research laboratories have been conducted, including the PR (Prototype Repository) at the Äspö Hard Rock Laboratory in Sweden (Johannesson et al., 2007) and FEBEX at the Grimsel Test Site (Martin et al., 2006). Observations of cement-bentonite interaction after 13 years in the FEBEX demonstration are reported in Alonso et al. (2017) and Fernandez et

al. (2017). The FEBEX experiment consisted of a heater that was held at 100ºC resulting in an observed maximum temperature of 28ºC in the concrete liner (Martinez et al., 2016). Therefore, the observed alteration was likely due only to water-rock interaction, and not temperature effects. Important observations, reported in Alonso et al. (2017) and Fernandez et al. (2017), include that both the shotcrete plug and bentonite experienced alteration due to groundwater interaction. In the concrete, portlandite dissolution occurred at the host rock-concrete interface and CSH phases in the concrete were altered due to the incorporation of aluminum, sulfur, and magnesium. At the bentonite-concrete interface, the main alteration mineral observed was ettringite ($Ca_6Al_2(SO_4)_3(OH)\cdot 26\ H_2O$), indicating that the breakdown of sulfur-rich phases in the bentonite, concrete, and/or sulfur sourced from the groundwater resulted in mineral precipitation (Alonso et al., 2017). In the bentonite, alteration was mostly limited to the immediate interface zone, mostly in the form of precipitation Mg-rich phases and the change in exchangeable cations in the bentonite (Fernandez et al., 2017). These results highlight the potential for alteration at the cement-bentonite interface at ambient temperatures in a realistic repository scenario.

1.1.4.2 Modeling

Modelling efforts on cement-bentonite interaction are informed by experimental, thermodynamic, and natural analogue data. Models aim to predict the effect of cement degradation on bentonite physical properties (e.g., swelling capacity, cation exchange, and/or surface area) and clay-mineral stability over time in a repository environment. However, as mentioned above, the complex, non-linear processes involved in cement-interaction may complicate modelling efforts. In general, modeling studies show rapid development of porosity and pH changes in a zone ~1 m from the cement-bentonite interface within 100 years of repository operation (e.g., Steefel & Lichtner, 1994, 1998; Soler, 1998; Savage et al., 2002). For example, simulations at 25 and 70ºC over a 3.2 ka period predict that extensive bentonite dissolution occurs in a ~60 cm zone in the buffer adjacent to the cement boundary (Savage et al., 2002). The model results also show that bentonite dissolution results in CSH-mineral precipitation closest to the cement interface; sheet silicates and zeolites form farther away from the boundary. The precipitation of secondary minerals is the mechanism for the increase in porosity. The results from Savage et al. (2002) also show that the extent of bentonite alteration is highly dependent on the water-rock ratio and transport of high-pH pore fluid through the bentonite. In comparison, models that examine the effects of low-pH cement pore water (i.e., pH < 11) show that bentonite interaction with low pH cement water (at 25ºC) does not result in observable bentonite dissolution (Watson et al., 2007). This study highlights that increased amounts of aqueous silica and aluminum (sourced from the siliceous materials included in the low pH cement) may stabilize clay minerals. Models based on results from bentonite-cement column experiments predict the formation of secondary minerals such as zeolites, hydroxides, phyllosilicates, and CSH minerals in the bentonite in a ~cm-scale zone (Fernandez et al., 2009b). Overall, the modelling studies support experimental observations that cement alteration effects only affect the portion of the bentonite buffer in contact with cement materials. Further, modelling results highlight the importance of pore water pH and secondary mineral precipitation in understanding the long-term geochemical and mineralogical evolution of the cement-bentonite interface.

1.1.5 Steel Canister-Clay Interface Zone Alteration in an Argillite-Hosted Repository

The findings of our previous investigations on mineral precipitation at the steel-bentonite interface in EBS hydrothermal experiments have been described in Caporuscio et al. (2015; 2017; 2018; 2019) and Cheshire et al. (2018). These studies describe the layered alteration sequence observed on the surface of steel coupons included in Wyoming bentonite-only experiments. In general, an oxide layer forms directly at the surface of steel coupons mixed in with bentonite and wall rock components. The oxide layer is followed by newly crystallized Fe-saponite at the steel-clay interface with Fe being supplied by steel corrosion. Concurrent with Fe-saponite formation, sulfides precipitated from sulfide-bearing fluids, likely from pyrite dissolution, near the steel interface. The thickness of the Fe-rich phyllosilicate minerals perpendicular to the SS surface ranges from 9 to 44 µm. There was no significant change in the precipitation thicknesses between the three different temperature profiles for 300°C (ramped, cooling and constant).

In general, the metal waste canister overpack (likely carbon steel) in a shale (argillite) hosted repository will be expected to corrode over time (e.g., Bryan et al., 2011). The steel will corrode at the bentonite buffer interface in the presence of oxygen according to one of the following reactions (aerobic corrosion) (Kursten at al., 2004):

$$4\ Fe^{o} + 3\ O_2 \rightarrow 2\ Fe_2O_3 \qquad (2)$$

$$2\ Fe + 2\ H_2O + O_2 \rightarrow 2\ Fe(OH)_2 \qquad (3)$$

The corrosive reaction (3) can be fairly fast for carbon steel, whereas corrosion can be slowed for stainless steels by an oxide film (i.e., Fe-oxide). In the presence of oxygen, the ferrous hydroxide in the second reaction can corrode further (Kursten et al., 2004):

$$4\ Fe(OH)_2 + 2\ H_2O + O_2 \rightarrow 4\ Fe(OH)_3 \qquad (4)$$

$$4\ Fe^{o} + 6\ H_2O + 3\ O_2 \rightarrow 4\ Fe(OH)_3 \qquad (5)$$

If magnetite is formed by the corrosion potential exceeding equilibrium (2), a resistant oxide film will precipitate on the metal surface. The oxide film will act as a protective coating against further corrosion in the effect called passivation. In an alkali solution where a porous $Fe(OH)_2$ develops, a passive layer may not form, but $Fe(OH)_2$ may still decrease the corrosion rate (5) (Kursten et al., 2004). Therefore, stainless steel and carbon steel are protected against corrosion by the presence of a thin “passive” layer in environments with cement that are highly alkaline conditions. The stainless steel is covered by a corrosion-resistant film of chromium oxy-hydroxide, whereas carbon steel forms a less resilient film composed of a mixture of Fe(II) and Fe(III) oxy-hydroxides (4 & 5) (Kursten et al., 2004).

Nevertheless, these oxide passive films can break down at lower pHs and/or by reactions with aggressive species, e.g., chlorides (Kursten et al., 2004). The passive film overlaying carbon steel can more easily be broken down by chloride corrosion than on stainless steel. Carbon steel, therefore, tends to suffer for general/uniform corrosion, whereas stainless steel tends to be highly localized (i.e. pitting corrosion, stress corrosion) (Smart, 2011).

Previous study by Smailos et al. (1997) and subsequently Kursten et al. (1996; 1997) examined the effect of the solid clay phase on the formation of the corrosion layers (16°C (baseline) increasing to 170°C, five years). The corrosion layer on the unheated carbon steel average about 10 to 20 µm thick. Both experiments had a precipitation thickness on

average 30 to 50 μm thick in total. The experiment at 16°C had the multi-layered precipitation, but this layering was less obvious at 170°C. The precipitation could be subdivided into 3 sub-layers with the middle layer having a higher Fe/O ratio than the other two layers. A possible explanation for the middle layer having a higher Fe/O ratio was that the initial passive layer had cracked and further corrosion had occurred.

Other research by Schlegal et al. (2008) studied the interaction of ferrite iron and argillite (approximate mineralogy: 30 wt.% quartz, 30 wt.% calcite, 35 wt.% interstratified illite–smectite, traces of pyrite and feldspars) interface reacted in saturated condition at 90°C and 50 bars for 8 months. Their results show the presence of a corrosion layer (magnetite, Fe-phyllosilicate), an external sublayer enriched in sodium followed by a clay transformation layer (mainly Ca-rich siderite). The clay layer was depleted in Al and K, signifying the dissolution of rock-forming minerals. There was a transitional layer of irregular thickness (~100 μm) present between the new precipitation layer and unaltered argillite made up of small crystals containing argillite markers, such as quartz and clay minerals.

1.1.6 Steel Corrosion in a Cement Environment

The cement buffer in an EBS can provide a favorable geochemical environment (high pH), in which corrosion of the carbon steel overpack will be limited. In the high alkaline condition created by the cement, both stainless and carbon steel should also be protected against corrosion in the presence of a thin "passive" layer similar to as discussed above (Kursten et al., 2004; Smart, 2011). For low carbon steel with cement in anoxic solutions the corrosion rate increased with decreasing pH. The corrosion rates were about 5 to 15 times higher, at pH 7 and 4 respectively, than at a solution pH of 13 (Kursten et al., 2004). A common layer at the steel-cement interface is "laitance," a weak, easily-crumbled layer consisting of cement and fine aggregates. This laitance can act as a controlling factor for the rate of corrosion of steel in cement and has exhibited the ability to limit diffusion of chloride species (Smart et al., 1999). In cases where calcium hydroxides precipitation, they can reduce pitting corrosion by hindering the ability of chloride ions. The calcium hydroxides can provide hydroxides to counter local acidification caused by corrosion product hydrolysis (Smart et al., 1999).

1.1.7 Designer EBS Additives

The main function of the EBS is to enhance the radionuclide retention and geotechnical aspects of the repository system. As described above, bentonite has favorable properties for the overall function of the repository in terms of hydrologic processes and radionuclide sorption. Other materials have been proposed to enhance the overall radionuclide sorption capacity, including adding phosphates as a radionuclide "getter". Phosphate minerals are known to incorporate radionuclides into their crystal structure and can efficiently immobilize uranium and its mobile fission products through uptake from an aqueous solution by formation of U-rich phosphate minerals.

1.1.7.1 Apatite Stability

Apatite ($Ca_5(PO_4)_3(F,Cl,OH)$) is the tenth most abundant mineral on earth and is uncommonly versatile (Rigali et al., 2016). The ubiquitous nature of the apatite mineral group dictates an extremely large stability field, from accessory phases in garnet lherzolites (Konzett et al., 2012) at its upper P,T limit, to being an integral component of

human teeth (Larsen & Jenson, 1989). In human dental enamel, apatite is stable from neutral to high pH. At low pH (<4) apatite converts to brushite (Larsen & Jenson, 1989). The durable nature of apatite is demonstrated by the observation of detrital apatite grains in Precambrian sandstones and gneisses.

In planned nuclear repositories, apatite could be used in permeable reactive barriers to isolate radionuclides in groundwater. The phosphorus produced from dissolving apatite could remove radionuclides, particularly cationic radionuclides including Sr, U, Pu, and Np, from solution by forming insoluble radionuclide-containing solids through incorporation into the apatite via substitution (Moore et al., 2002; Rigali et al., 2016). The surface of apatite may also exchange anionic radionuclides for surface phosphates/hydroxyl groups (Moore et al., 2002). A radionuclide "getter" safety case study on the Yucca Mountain Project (YMP) in 2006 by Lukens et al. (2006) focused on the radioisotopes I-127, Tc-99 and Np-237, and U-238 primarily due to their high mobility in a Yucca Mountain scenario (oxidizing, unsaturated, depth to groundwater). Apatite was identified in this study as a material that could preferentially sorb I, Tc and Np. Further, Lukens et al. (2006) identified apatite's potential for high attraction of actinides, and recognized apatite as an inexpensive and readily available mineral. Apatite, however, was identified as slightly soluble, and likely not sufficiently durable if placed in the invert placed below the canister, but could be utilized elsewhere in the design.

Radiation effects on apatite are also important to consider in EBS applications. Meldrum et al. (1997) irradiated single crystals of natural F-rich apatite and ion-beam amorphized apatite to determine phase transition/structural change. Irradiation of amorphized apatite using a high current density (16 A/cm^2) caused the precipitation of cubic CaO from the crystalline apatite matrix. The lower beam current (1.6 A/cm^2) resulted in nanometer-sized voids and CaO did not crystallize even after prolonged irradiation. The natural apatite underwent extensive void formation followed by the precipitation of cubic CaO under a 200 keV electron irradiation (Cameron et al. 1992).

Apatite has a strong tendency to crystallize under electron irradiation (Meldrum et al., 1997). The crystallization products depend on the dose rate and on the ambient temperature. These results suggest that beta-decay in natural or nuclear-waste loaded apatite has the potential to inhibit amorphization, contrary to the traditional understanding that beta decay may weakly enhance the damage-accumulation process.

Few previous experiments have been performed to evaluate the stability of apatites in hydrothermal conditions. Betkowski et al. (2016) performed experiments on fluoroapatites in Na- and Si-rich fluids to evaluate the mineral reactions. In the experiments performed at 300 and 400°C (100 MPa), the observed little reactivity or dissolution of the fluoroapatite. However, at 600°C, the fluorapatite was more reactive and partially altered into its pseudomorph, britholite.

The experimental results from the current study will be used to quantify apatite stability in the EBS, including possible phase transformations at high temperature repository conditions. The results would then help inform radionuclide-speciation in phosphate solution experiments in our partner radionuclide hydrothermal lab at LANL. For example, experiments would be conducted with apatite and relevant aqueous radionuclide species at 300ºC and 150 bar (i.e., maximum temperatures expected in the disposal of dual purpose canisters) in order to understand the potential for apatite to form

radionuclide-bearing phases and/or how much sorption potential phosphate minerals may provide under relevant repository chemical, temperature, and pressure conditions. Experiments with apatite and U would address the formation of autunite (U-bearing phosphate) as an example of a phosphate mineral by-product that may enhance the radionuclide-retention potential of the EBS. Further, phosphate-based minerals may also incorporate other elements that are of particular concern for repository performance such as radiocesium, radiostrontium, and trivalent americium and curium (Krejzler et al., 2003).

2. Methods

Experiments EBS-23 through EBS-31, with the exception of EBS-29, were designed to explore the effect of ordinary Portland cement (OPC) on bentonite stability in the argillite system. The starting components and experiment parameters are reported in Table 1. The starting solid materials were mixed at 60 wt.% Wyoming bentonite (powder and granules), 20 wt.% Opalinus Clay (powder and fragments), and 20 wt.% uncured OPC powder or cured OPC chip. Experiment variations included: water:rock ratio (11 to 13 and 6.8 for the 6-month experiment), temperature (200 or 300ºC), duration (eight weeks or 6 months), and inclusion of different types of stainless steel (316SS, 304SS and LCS).

An experimental program on the effect of phosphate additives to the bentonite EBS was initiated in FY20. Experiment EBS-29 (250ºC, eight weeks) was completed in FY20 and characterized in FY21. EBS-29 included 80 wt.% Wyoming bentonite, 20 wt.% apatite from Durango, Mexico (referred to as Durango apatite), and Stripa V2.3 brine at a water-rock ratio of 7:1. Three sealed gold capsules that included only apatite crystals and brine at a water rock ratio of 11:1 were included at the bottom of the titanium vessel (Table 2).

In all experiments, fluid chemistry was monitored in aqueous samples extracted during and after the experiment. Solid phase reaction products were evaluated with X-ray diffraction (bulk and clay mineralogy), scanning electron and petrologic microscopy (mineralogy and textural observations), and electron microprobe and electron dispersive spectroscopy (mineral phase chemistry). Solid and aqueous phase characterization methods are reported in Appendix A.

Table 1: Initial components and reaction conditions for EBS experiments in the presence of Opalinus Clay. Experiments completed in FY21 are highlighted in green. Abbreviations: WB, Wyoming bentonite; OPC, ordinary Portland cement; OC, Opalinus Clay; SS, stainless steel; LCS, low carbon steel.

Exp.	Components	Temp (°C)	Run time	Synthetic GW (g)	Opalinus Clay (g)	WY bentonite (g)	Portland cement (g)	Durango apatite (g)	steel type	EBS metal (g)	Fe° (g)	Fe_3O_4 (g)	Deviations	Water:Rock
EBS-23	OC + WB + OPC Powder	200	8 weeks	150	2.0	5.9	2.1	-	-	-	0.57	0.48	-	13.6
EBS-24	OC + WB + OPC Powder + 316 SS	200	8 weeks	150	2.0	6.0	2.0	-	316 SS	4.52	0.52	0.51	-	13.6
EBS-25	OC + WB + OPC Powder + 304 SS	200	8 weeks	126	2.0	6.0	2.0	-	304 SS	3.27	0.55	0.51	-	11.4
EBS-26	OC + WB + OPC Powder + LCS	200	8 weeks	130	2.0	6.0	2.0	-	LCS	5.02	0.5	0.5	-	11.8
EBS-27	OC + WB + OPC Powder +316 SS	200	6 months	270	7.6	22.8	7.6	-	316 SS	5.06	0.95	0.95	-	6.8
EBS-28	OC + WB + OPC Powder + 316 SS	300	8 weeks	138	2.2	6.6	2.2	-	316 SS	5.06	0.50	0.50	-	11.7
EBS-29	WB + Durango apatite	250	8 weeks	156	-	17.8	-	4.5	-	-	0.63	0.63	Apatite + Stripa V2.3	7.0
EBS-30	OC + WB + Cured OPC chip + 316 SS	200	8 weeks	104	2.1	6.4	2.1	-	316 SS	5.1	0.5	0.5	-	11.7
EBS-31	OC + WB + Cured OPC chip + 316 SS	200	8 weeks	131	2.0	6.1	2.1	-	304 SS	4.7	0.5	0.5	-	11.6

Table 2: Initial components and reaction conditions for the capsules included in the EBS-29 with Durango apatite.

Capsule ID	Temp (°C)	Run Time	Stripa V2.3 Synthetic GW (g)	Durango apatite (g)	Fe° (g)	Fe_3O_4 (g)	Water:Rock
C1	250	8 weeks	1.10	0.104	0.003	0.003	11:1
C2	250	8 weeks	1.11	0.103	0.003	0.003	11:1
C3	250	8 weeks	1.11	0.100	0.003	0.003	11:1

3. Results

3.1 Starting Material Characteristics

Opalinus Clay. Opalinus Clay used in this study was sourced from the Mont Terri Underground Rock Laboratory in Canton Jura, northern Switzerland. The rock used was from the shaley facies of Opalinus Clay at Mont Terri (drill core BFE-A10) and was exposed to air (i.e. oxidizing conditions) before the experiment. Opalinus Clay is thinly laminated, dark grey shale with a dry density of 2.2 to 2.4 g/cm^3 and water content of 6.5 to 8.0% (Pearson et al., 2003). Opalinus Clay is dominantly composed of clay minerals, with lesser carbonates and silicates. The Opalinus Clay used in our experiments is composed of mixed illite, smectite, and illite-smectite (24%), kaolinite (17%), calcite (16%), chlorite (9%), mica (7%), K-feldspar (6%), and plagioclase (3%), with minor dolomite and pyrite, as determined by QXRD analyses (Table C-1). In the QXRD datasets, illite and smectite are typically reported together due to the difficulty of quantifying these mineral phases when they are mixed. Na^+ is the dominant exchangeable cation in the Opalinus Clay followed by Ca^{2+}, Mg^{2+}, K^+, and Sr^{2+}; however, the bulk composition is dominated with CaO (7.96 wt.%), K_2O (3.05 wt.%), MgO (2.38 wt.%), and Na_2O (0.48 wt.%) (Pearson et al., 2003). These exchangeable cations should be in equilibrium with the pore water described below (synthetic Opalinus Clay groundwater, Table 2). Other minerals present include calcite, ankerite, dolomite, quartz, and biotite. Well-preserved pyrite occurs primarily as < 2 μm octahedral crystals, filling fractures and/or along bedding planes. Calcite primarily occurs as pocket filling agglomerates showing layered structures with alternating calcite and clay layers (Figure 3).

Wyoming bentonite. The bentonite used in the present study is unprocessed and was provided by Bentonite Performance Minerals LLC from Colony, Wyoming, U.S.A. It is composed dominantly of Na-montmorillonite (general composition: $Na_{0.33}(Al,Mg)_2(Si_4O_{10})(OH)_2 \cdot nH_2O$), lesser clinoptilolite and feldspar, and minor biotite, pyrite, quartz, opal, and sulfide minerals. The QXRD results from unheated bentonite are presented in Table C-1.

Opalinus Clay synthetic groundwater. Synthetic groundwater was created to mimic the pore water found in the Mont Terri Opalinus Clay (Pearson et al., 2003). This solution has a pH of around 7.5 and is a Na-Cl type solution. The initial chemistry is reported in Table 3.

Stripa V2.3 synthetic groundwater. The synthetic solution composition was chosen to represent that of a deep groundwater in granitic rock (Stripa sample V2) (Frape et al., 2003). This is a Na-Ca-Cl type solution of high pH (8–10). The initial chemistry is reported in Table 3.

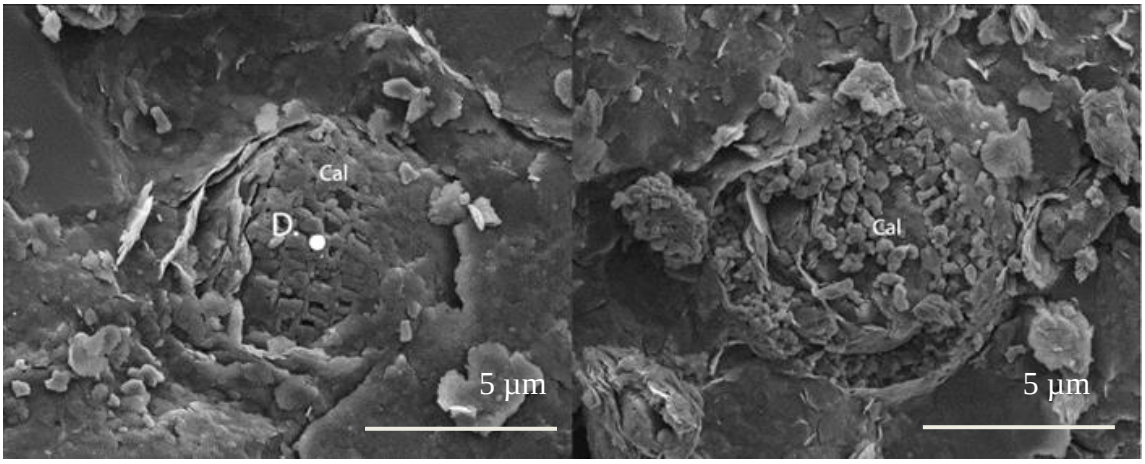

Figure 3: SEM images of unheated Opalinus Clay. [Left] Biogenic calcite (Cal) filling a pocket with in the Opalinus Clay matrix. [Right] Disturbed pocket-filling calcite showing layered structure with alternating calcite and clay layers.

Table 3: Brine compositions for synthetic Opalinus Clay solution modelled after data reported from the Mont Terri site (Pearson et al., 2002) used in the Opalinus Clay experiments and the composition of the Stripa synthetic solution used in the apatite experiment (after Frape et al., 2003). The Los Alamos Municipal tap water was used in the curing of the ordinary Portland cement. All values were measured at 25°C (n.m. = not measured)

	Opalinus Clay	**Stripa V2.3**	**Los Alamos Tap Water**
Species	mg/L	mg/L	mg/L
Ca^{2+}	426	670	9.62
Cl^-	6470	n.m.	24.7
CO_3^{2-}	n.m.	291	n.m.
K^+	225	163	2.04
Na^+	3846	1	12.8
Si	1	64	35.4
SO_4^{2-}	998	0.09	6.93
Sr^{2+}	0.16	7.1	0.0445
TDS	12153	46	n.m.
pH	7.50	6.70	6.61
Experiment Used	EBS-14 to -28, -30 to -31	EBS-29	Cured Cement in EBS-30 to -31

316SS. (NIST SRM 160b) is an iron alloy primarily with 18.37 wt.% Cr, 12.35 wt.% Ni, 2.26 wt.% Mo, 1.619 wt.% Mn, 0.5093 wt.% Si, and 0.175 wt.% Cu.

304SS. An ion alloy which differs from 316SS in Cr/Ni ratio. Along with Fe, it contains 18 wt.% Cr, 8 wt.% Ni, < 2 wt.% Mn, < 1 wt.% Si, < 0.045 wt.% P, and < 0.03 wt.% S, and < 0.08 wt.% C.

Low carbon steel (LCS). Composed of Fe along with ~0.2 wt.% C, 0.9 wt.% Mn, < 0.04 wt.% P, and < 0.05 wt.% S.

Ordinary Portland cement. Ordinary Portland cement consists of ~77% of calcium silicates, (3 $CaO{\cdot}SiO_2$, and 2 $CaO{\cdot}SiO_2$), the remainder consisting of aluminum- and iron-containing silicate phases and other compounds. The ratio of CaO to SiO_2 is ~3.2. The magnesium oxide content (MgO) is ~2.6 wt.%. The mineralogy consisted of larnite, hatrurite, and brownmillerite. Uncured, powdered OPC was used in the experiments EBS-23 through EBS-28.

Cured OPC cement chips were included in EBS-30 and -31 experiments. Cement curing began in November of 2018 using Los Alamos Municipal tap water (Table 3). Mineralogy of the cured OPC differed from the uncured powder with the formation of portlandite. The CaO to SiO_2 ratio increased to ~3.6 and the magnesium wt.% was unchanged.

Durango apatite. The apatite used in this study is from the Cerro de Mercado mine in Durango, Mexico, which is an open-pit iron mine known for the occurrence of abundant coarse-grained fluoroapatite ($Ca_5(PO_4)_3F$). The apatite crystals are readily available and have a consistent chemical composition; Durango apatite is commonly used as a standard material for isotope and trace element analyses (e.g., Chew et al., 2016).

3.2 Aqueous Geochemistry (EBS-23 to -28)

pH. All experiments began with a near neutral pH at 25ºC of ~7.4. Of the 200ºC cement experiments, the pH of reaction fluids measured at 25ºC of EBS-23 and EBS-25 initially dropped to ~5 to 6, whereas EBS-24 and EBS-26 initially increased to ~11. The first measured pH value from EBS-27 was around 9, before stabilizing around 8.5 for the duration of the 6-month experiment. Although the 200ºC cement experiments diverged in pH initially, all experiments stabilized to pH values from ~8 to 9 around 3 weeks into the experiment duration, and remained around the same values for the rest of the experiment (Figure 4). In comparison, pH values from EBS-28 (300ºC) initially rose from 7.5 to 9.5 in the first week of the experiment before stabilizing to values of around 6 for the duration of the 6-week experiment. In EBS-30 and EBS-31, which included a cured cement chip, pH values dropped to ~6 within the first two weeks of experiment time before gradually increasing to values between 6 and 7 by the end of the experiment.

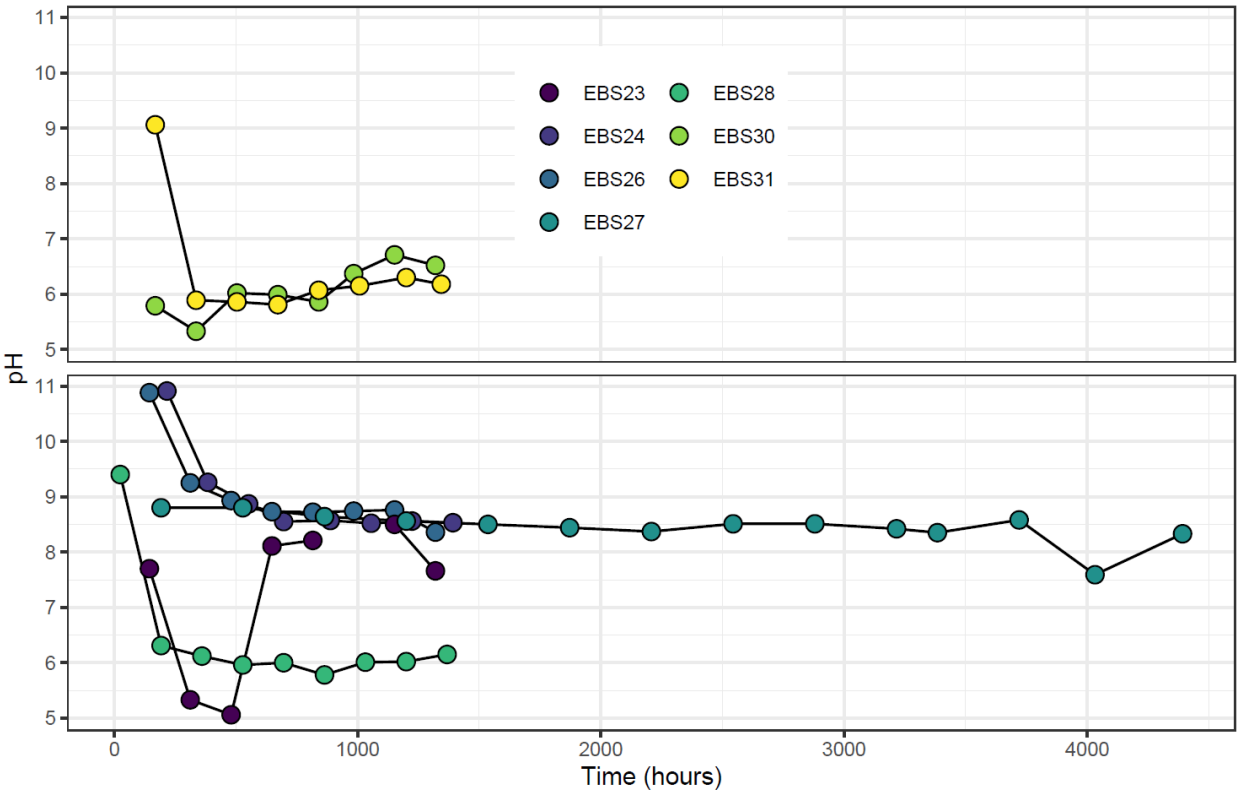

Figure 4: pH (measured at 25ºC) throughout each cement EBS experiments.

Silica. In all experiments, aqueous silica generally increases during each experiment (Figure 5). Aqueous silica increases rapidly until 1000 hours in EBS-25, and plateaus ~180 mg/L by 1200 hours into the experiment. The other three 200ºC/8 week experiments reach ~100 to 130 mg/L by 1200 hours. In comparison, EBS-27 (six months) shows significant variability in silica concentrations throughout the experiment duration; values vary between ~100 and 200 mg/L. In the 300ºC experiment, silica increases to 500 mg/L in the first 6 weeks, before slightly plateauing. In EBS-30 and EBS-31, silica reaches concentrations of ~300 mg/L by the end of the experiments.

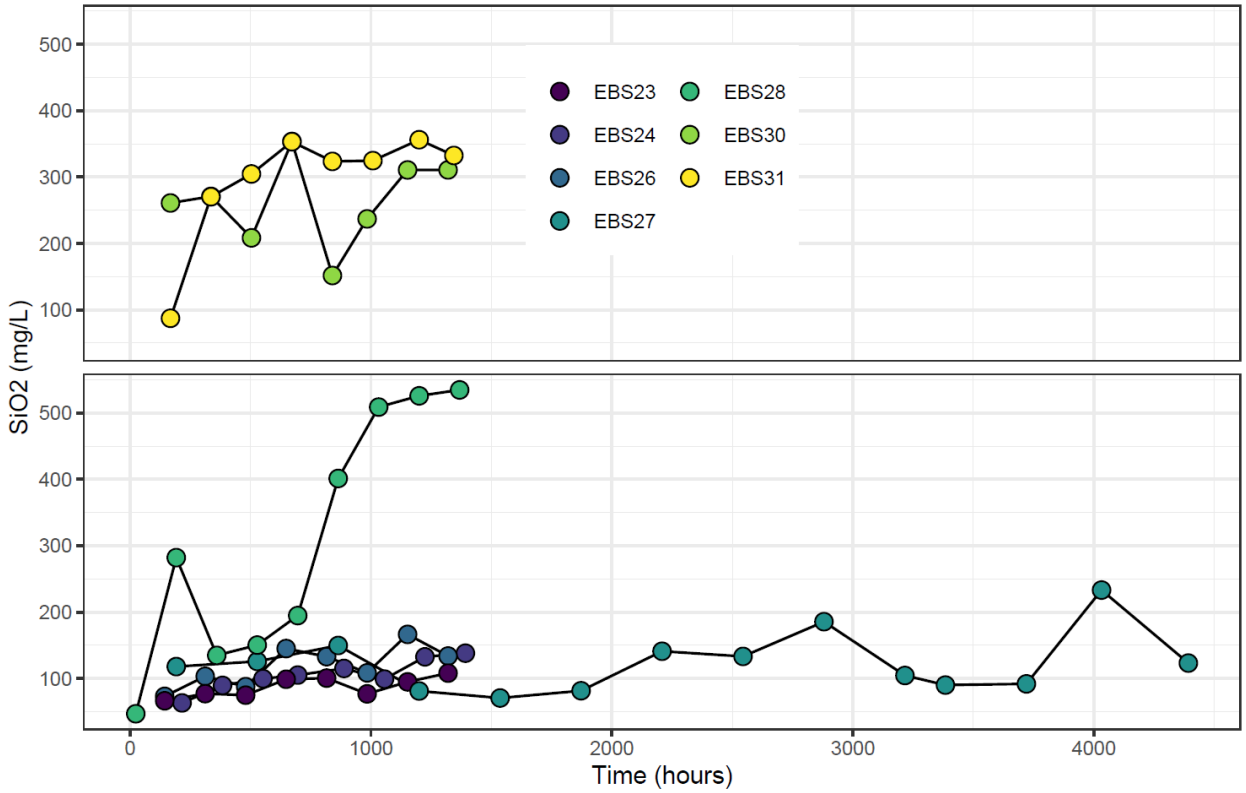

Figure 5: $SiO2_{(aq)}$ concentration (mg/L) throughout each cement EBS experiments.

Aluminum and Magnesium. Aqueous aluminum remains constant, near detection-limit values, or steadily decreases throughout each experiment. All values end below detection limits (< 0.032 mg/L). In experiments with cement powder, $Mg^{2+}{}_{(aq)}$ remains generally constant and below 0.15 mg/L throughout each experiment. In the experiments with the cured cement chip, Mg^{2+} values are initially elevated around 30 mg/L before reaching < 1 mg/L by the end of the experiments.

K^+, Na^+, Ca^{2+}. Sodium and potassium follow a decreasing trend throughout each 200ºC cement powder experiment (Figure 6). Calcium either remains constant (EBS-23 and EBS-24) or gradually increases (EBS-25 and EBS-26). $[Ca^{2+}]$ continues to increase throughout the whole 6-month duration of EBS-27. The concentrations of these cations in aqueous solutions of EBS-23 and EBS-24 versus EBS-25 and EBS-26 differ by about 50% during the experiment. The starting solution for these four experiments had very similar concentrations of these cations; however, the water:rock ratio differed between these experiments. EBS-23 and EBS-24 had a higher water:rock ratio (~13.6) versus the ratio in EBS-25 and EBS-26 (~11.5). The 300ºC experiment (EBS-28) has a much higher $[K^+]$ that initially rose during the first three weeks before beginning to decrease for the remainder of the experiment. Calcium concentrations are similar in magnitude to observations from the 200ºC experiments but follow a different trend: values increase initially and then drop in a similar manner to the potassium values. Sodium values in EBS-28 are initially elevated but sharply decrease during the experiment.

In the cement chip experiments, EBS-30 and EBS-31, sodium and potassium concentrations follow a decreasing trend. Calcium concentrations are constant around 150 mg/L throughout both experiments.

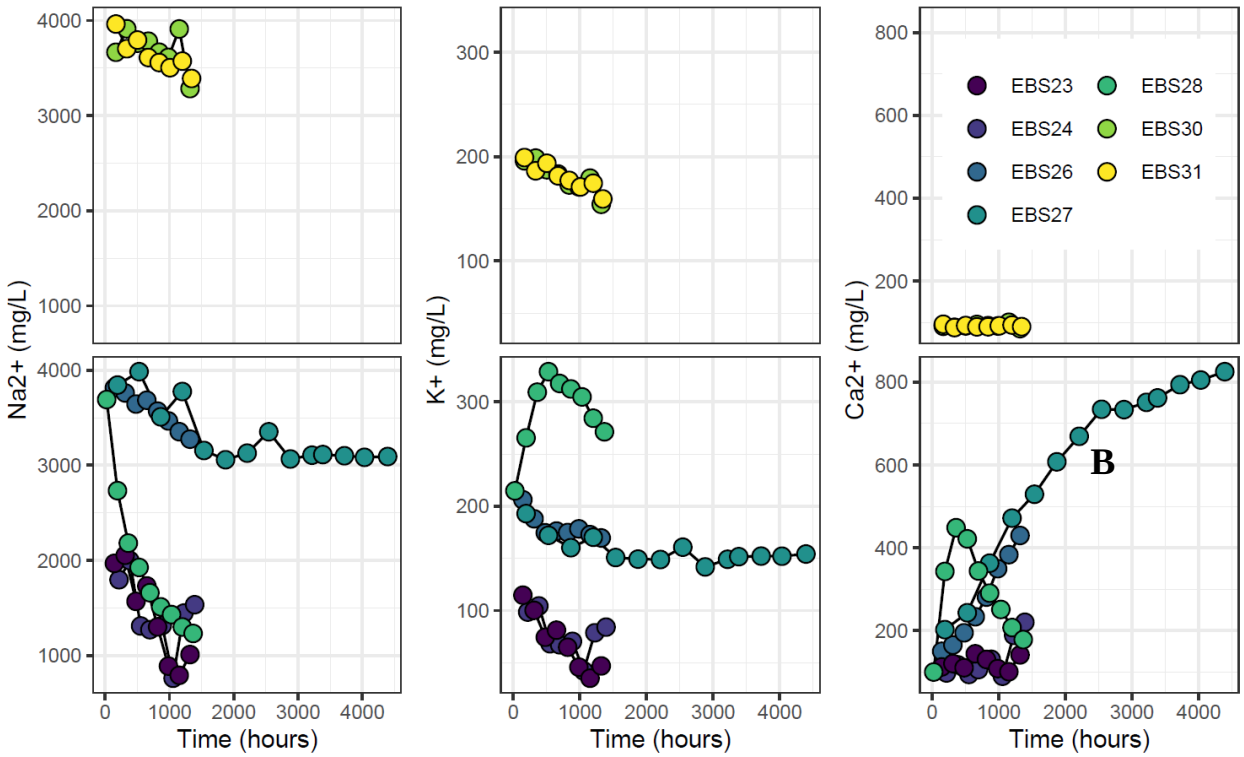

Figure 6: Sodium, potassium, and calcium concentrations in the cement EBS experiments.

Chloride. Chloride concentrations cover a wide range of values (2500 to 10000 mg/L) in the EBS cement powder experiments (Figure 7). [Cl^-] generally decreases gradually in 200ºC experiments and decreases more rapidly at 300ºC (EBS-28). In the experiments with the cement chip (EBS-30 and EBS-31), chloride values generally decrease and reach 5000 mg/L by the end of the experiment.

Sulfate. Sulfate generally decreases in all experiments, for at least the first 3000 hours of elapsed time (Figure 7). An increase from ~50 mg/L to ~125 mg/L is observed around 3000 hours in the 6-month experiments, followed by a return to decreasing concentrations. Sulfate concentrations are lower magnitude in the 300ºC experiment ([SO_4^{2-}] = ~10 mg/L at 1000 hours) compared to the 200ºC runs ([SO_4^{2-}] = ~50–80 mg/L at 1000 hours). In the cement chip experiments, sulfate generally remains around 250 mg/L.

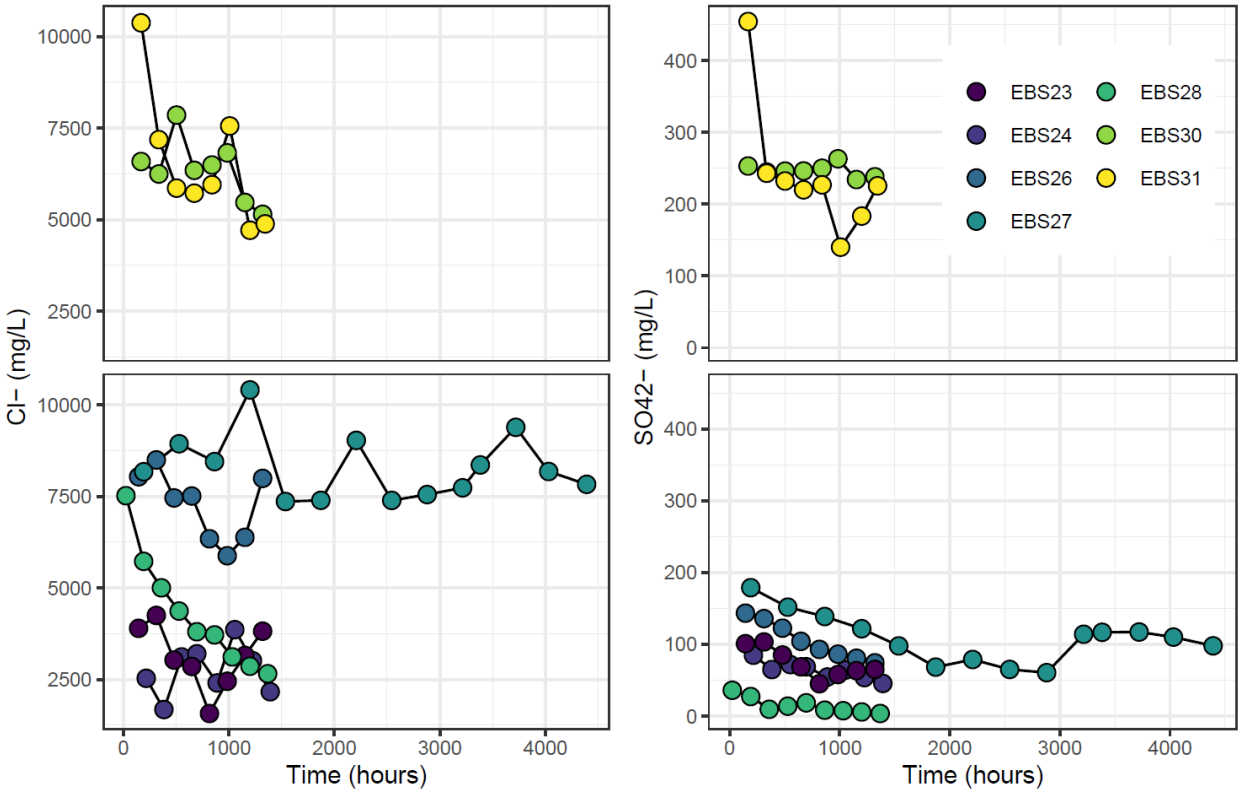

Figure 7: Concentrations of chloride and sulfate ions in solution in the cement EBS experiments.

3.3 XRF Results

XRF analyses for bulk rock oxide chemistry were performed on the unreacted starting material and the bulk reaction products (Table D-1).

In the 200ºC experiments with uncured OPC powder, the bulk chemistry of the reaction products generally matched the composition of the starting mix. In the 6-month Wyoming bentonite + Opalinus Clay + powered OPC experiment (EBS-27), the solid reaction products were stratified at the end of the experiment. Samples were divided based on their depth in the reaction cell. EBS-27-1 was taken from the top layer inside the reaction cell contained a higher concentration of CaO and Fe_2O_3 (16.4 wt.% versus 11.6 wt.% and 8.4 wt.% versus 7.5 wt.%, respectively) in comparison to EBS-27-4, which was taken from near the bottom of the reaction cell. EBS-27-4 had increased wt% of SiO_2 and Al_2O_3 compared to EBS-27-1 (49.5 wt.% versus 41.5 wt.% and 15.4 wt.% versus 13.7 wt.%, respectively).

In the 300ºC experiment with uncured OPC powder (EBS-28), Fe_2O_3 was elevated in the reaction products in comparison to the starting mix.

The Wyoming bentonite + Opalinus Clay + cured OPC chip experiments (EBS-30 and -31) only differed in the stainless steel type used and measured weight percent oxide values were consistent between the two experiments. There were only slight variations in Fe_2O_3 and loss

on ignition (LOI). In comparison to the starting mixture chemistry, weight percent CaO decreased.

3.4 QXRD Results

QXRD results from the bulk reaction product mineralogy from the Wyoming bentonite + Opalinus Clay + OPC experiments and the bulk mineralogy of the starting materials, are shown in Table C-1 and -2 and Figure 8. Results are presented from the 8-week 200ºC experiments (EBS-24, EBS-25, and EBS-26), the 6-month 200ºC experiment (EBS-27), the 300ºC experiment (EBS-28), and the 200ºC experiments with the cured cement chip (EBS-30 and EBS-31). In general, the addition of OPC powder to the starting experiment mixture resulted in significant changes to the bulk mineralogy of the reaction products at 200ºC. For example, in all reaction products from the cement experiments, precursor portlandite is not detected, indicating that it was consumed in mineral-forming reactions. Newly formed mineral phases include analcime, garronite, tobermorite, plagioclase feldspar, zeolites, calcite, illite-smectite mixed layers, illite, and amorphous material. The bulk abundance of smectite, illite-smectite, and illite is reduced. Increasing temperature to 300ºC resulted in different mineralogical changes, including a decrease in zeolites and formation of feldspars, chlorite-smectite mixed layers, and abundant Fe-saponite.

Swapping powder OPC for a cement chip resulted in less alteration to the bentonite at 200ºC (Figure 8). For example, combined smectite + illite + smectite-illite comprised 67 to 78 wt.% of the cement chip experiment versus 16 to 30 wt.% in the experiments containing cement powder. Further, the patterns preliminarily indicate that mixed layer phases are not abundant (i.e., the prominent peak at 6º 2 theta); detailed clay mineral XRD analyses are in progress. In addition, there was a reduction in zeolite and CSH mineral formation and amorphous material with the addition of the cement chip in comparison to cement powder.

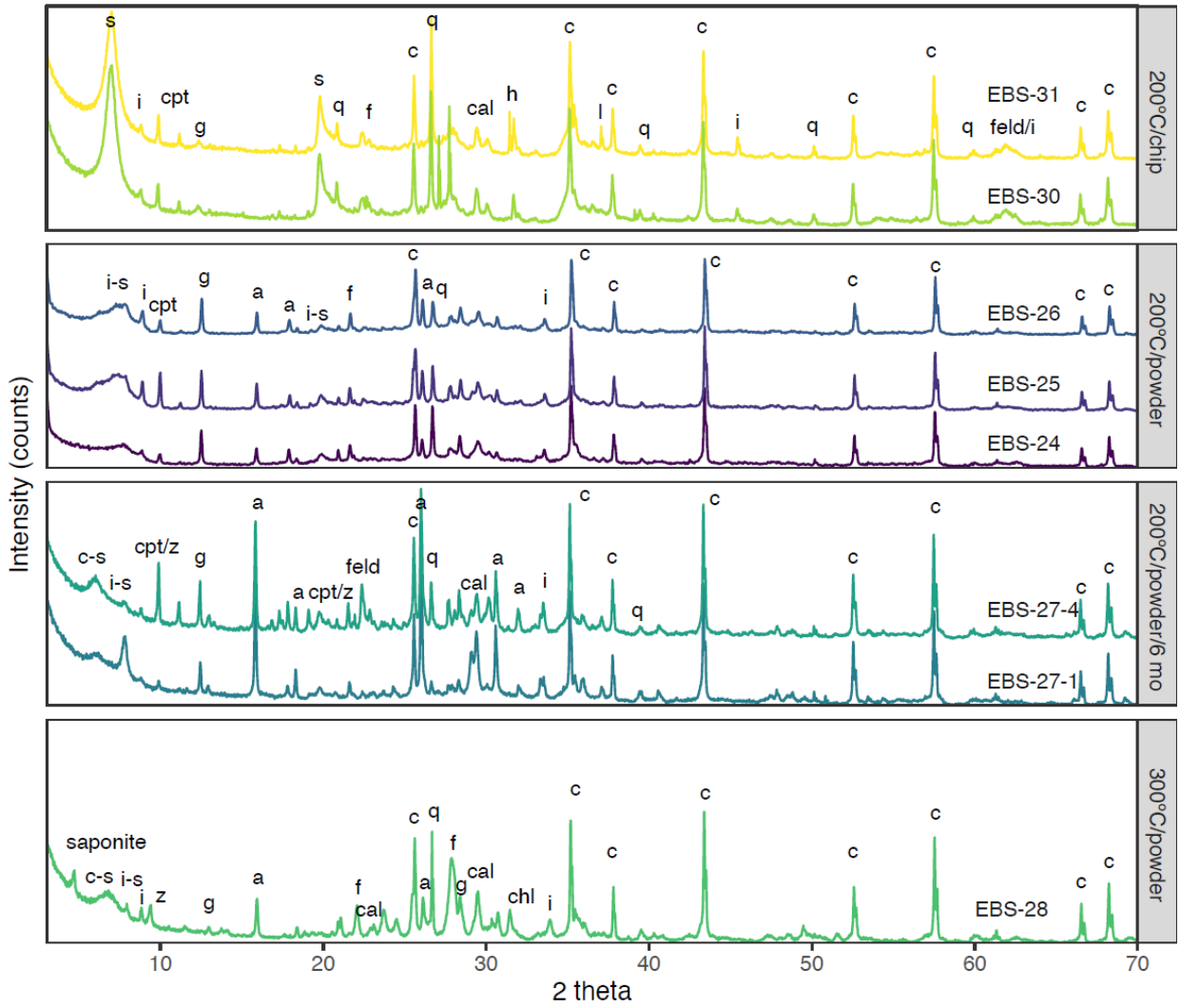

Figure 8: QXRD pattern of the bulk post-reaction products from the cement experiments. Peaks corresponding to corundum (c), smectite (s), illite (i), illite-smectite (I-S), clinoptolite (cpt), calcite (cal), quartz (q), zeolite (z), garronite (g), feldspar (f/feld), analcime (a), chlorite (chl) and chlorite-smectite (c-s).

3.5 Clay Mineral XRD

The addition of OPC to the experimental system affected the clay mineralogy in the reaction products, as observed in the reduction in illite, smectite, and illite-smectite mixed layers mineral abundance in the bulk system in the QXRD results from EBS-24, EBS-25, and EBS-26. XRD analyses of oriented clay fractions from both the Opalinus Clay fragments and the clay groundmass show significant shifts in mineral structure. Shifts of the glycolated smectite (GS) 002 and 003 peaks from the 2 µm fraction from the clay groundmass (mostly reacted bentonite with trace amounts of Opalinus Clay) correspond to ~10% reduction in expandability and ~10 to 20% increase in interlayered illite in the 8 week, 200ºC experiments (EBS-24, EBS-25, and EBS-26) (Table 4). The <2 µm clay fraction separated from EBS-28 (8 weeks, 300ºC) revealed a similar reduction in expandability to the 200ºC experiments, but

also included multiple other phases (e.g., chabazite, other unidentified peaks, Figure 9). The expandability of the remaining montmorillonite in experiment EBS-27 (6 months, 200ºC) was not able to be quantified. Amorphous material was present in the sample, resulting in a broad peak between 18 and 25º2θ, which obscured the position of the d003 glycolated smectite peak. Tobermorite is identified in all the clay fraction results, indicating potential CSH mineral interlayering in smectite.

In Opalinus Clay fragments extracted from the experiments EBS-24, EBS-25, and EBS-26, clay phases include I-S, illite, and chlorite (Figure 10). Tobermorite is detected in EBS-26. There was not enough sample of EBS-23 to analyze the Opalinus Clay fragments. The exact percentage of illite in illite-smectite mixed layers is difficult to quantify, but is likely < 40% illite based on the position of the 001 illite/002 GS-smectite peak (~8.9 Å).

Analyses of the clay mineral structure for EBS-30 and EBS-31 are in progress.

Table 4: Glycolated smectite (GS) peak positions for the <2 µm clay fraction separated from the Opalinus Clay–Wyoming bentonite experiments (EBS-23 to -28). Expandability was calculated based on the position of the 002 and 003 GS peaks.

EG-smectite	**001**		**002**		**003**		**002/003**	**1**	**2**	**3**
Sample	**d (Å)**	**2θ**	**d (Å)**	**2θ**	**d (Å)**	**2θ**	**Δ 2θ**	**%Exp**	**%Exp**	**%Exp**
WY Bentonite	17.0	5.2	8.5	10.4	5.7	15.7	5.3	100	102	103
EBS-23	16.4	5.4	8.3	10.7	5.5	16.0	5.4	95	95	97
EBS-24	16.5	5.3	8.3	10.7	5.5	16.1	5.5	90	89	92
EBS-25	16.5	5.4	8.3	10.7	5.5	16.1	5.4	93	92	95
EBS-26	16.5	5.3	8.3	10.7	5.5	16.2	5.4	91	90	93
EBS-27	16.9	5.2	8.4	10.5	–	–	–	–	–	–
EBS-28	16.9	5.2	8.5	10.5	5.6	15.9	5.4	91	90	93

1: %Exp = 973.76 – 323.45Δ + 38.43Δ2 – 1.62Δ3 (Eberl et al., 1993)

2: %Exp = 1517.8 – 548.49Δ + 68.35Δ2 – 2.90Δ3 (Eberl et al., 1993)

3: %Exp = 766.01 – 194.10Δ + 12.924Δ2 (Moore and Reynolds, 1997)

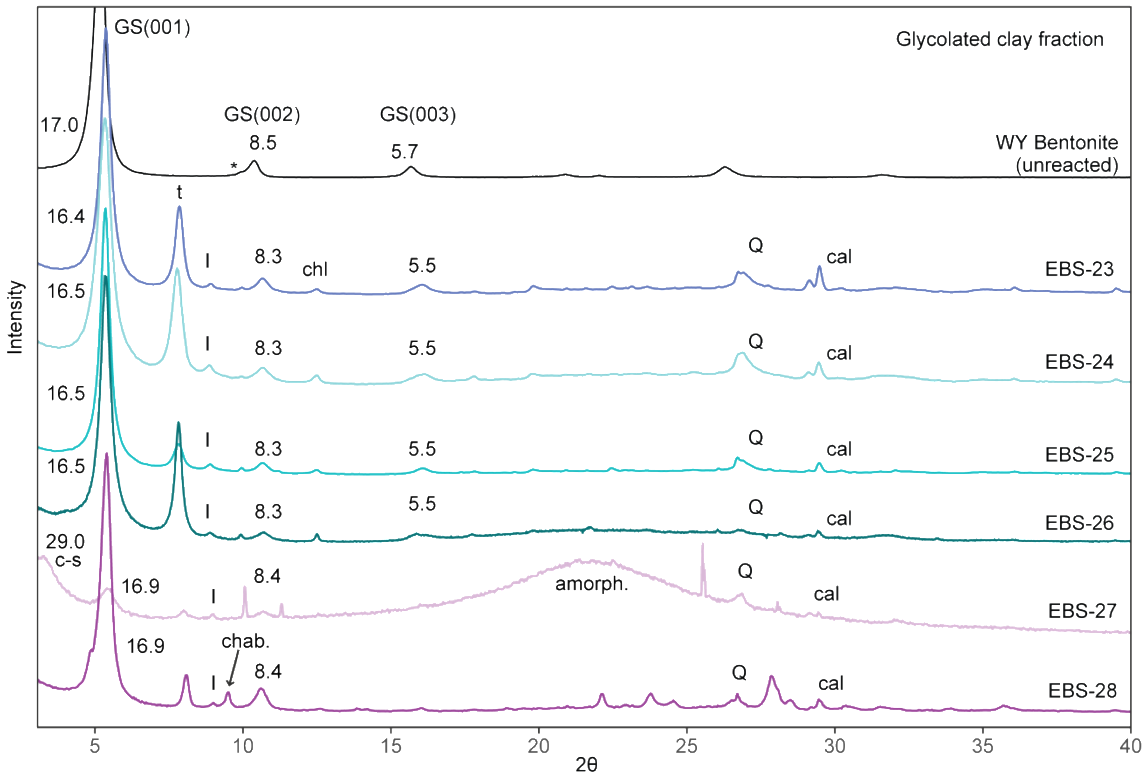

Figure 9: XRD patterns of the oriented and ethylene glycol saturated < 2 µm clay fraction from the clay groundmass of the cement experiments, compared to unheated Wyoming bentonite from the OPC experiments. Peaks correspond to amorphous material (amorph.), illite-smectite (I-S), chabazite (chab.), chlorite (chl), chlorite-smectite (c-s), illite (I), kaolinite (kao), quartz (Q), tobermorite.

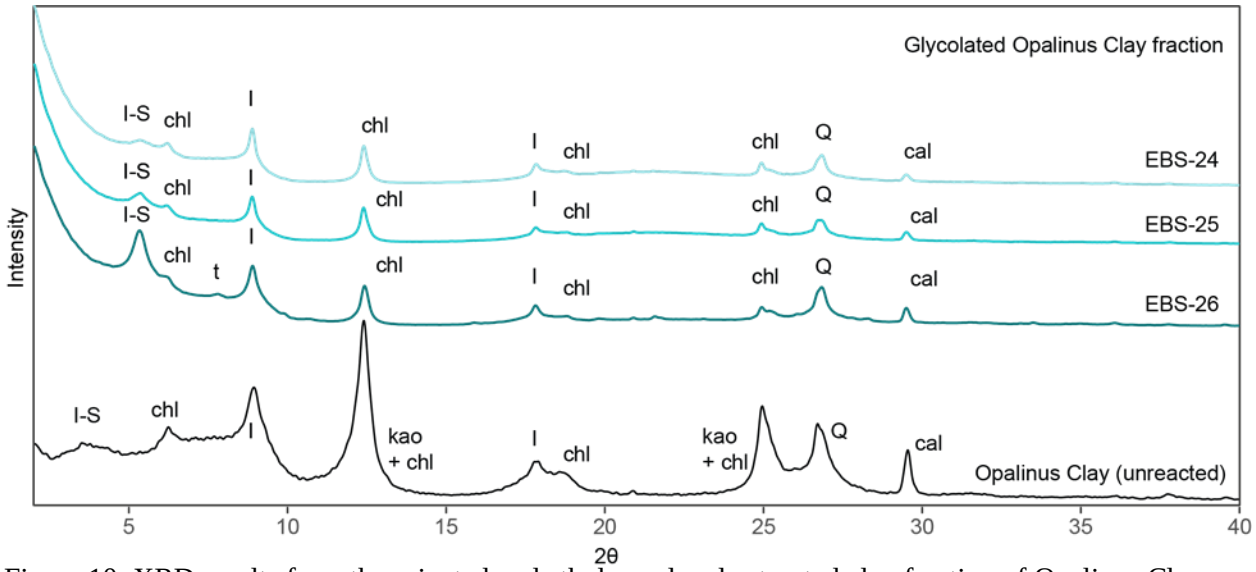

Figure 10: XRD results from the oriented and ethylene glycol saturated clay fraction of Opalinus Clay fragments extracted from each cement experiment and unreacted Opalinus Clay. Peaks correspond to illite-smectite (I-S), chlorite (chl), illite (I), kaolinite (kao), quartz (Q), tobermorite (t) and and calcite (cal) are labelled.

3.6 Cement Chip XRD

The surface of the unreacted cured cement chip and reacted cement chips from EBS-30 and EBS-31 was analyzed with XRD (Figure 11). The resulting patterns show that mineral reactions occurred at the chip surface. The unreacted chip is characterized by portlandite with calcite and larnite. The reacted chip pattern is dominated by calcite with smectite and CSH minerals.

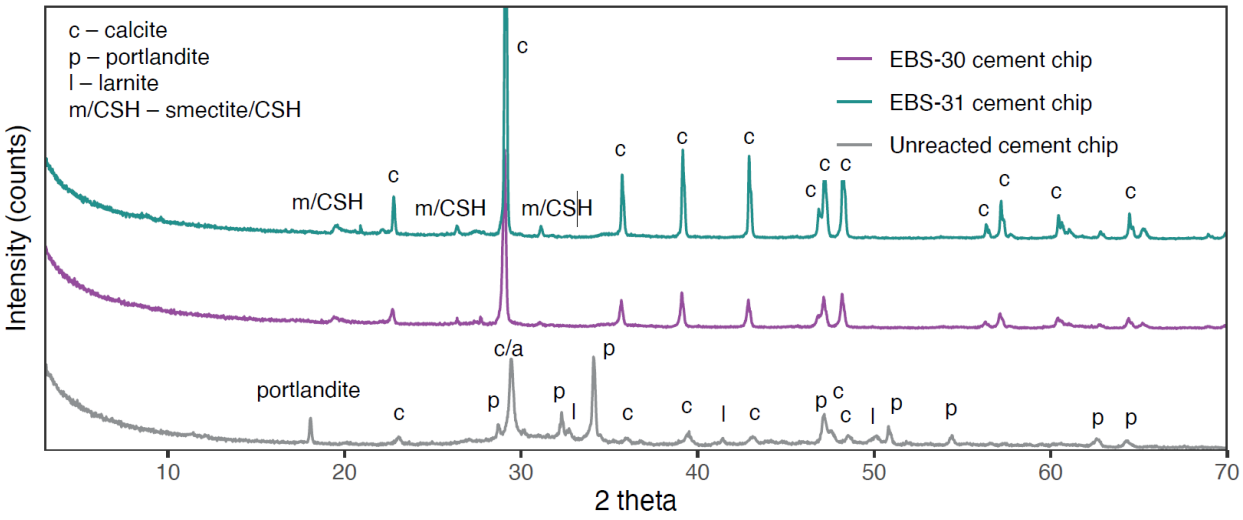

Figure 11: XRD pattern on the unreacted and reacted cement chip from EBS-30 and -31.

3.7 Electron Microprobe Analyses (Appendix E)

In experiments that included OPC powder/chips (EBS-23 through EBS-28, EBS-30, EBS-31), abundant analcime and Ca-rich zeolite and aluminosilicate phases (feldspars, garronite, and chabazite) were formed (Figure 12). Major element compositions of these aluminosilicate phases were analyzed via electron microprobe for samples EBS-24, EBS-25, and EBS-26. Analyses for EBS-27, EBS-28, EBS-30, and EBS-31 were collected in July 2021; data reduction is in progress and will be reported next year. In general, garronite was typically found near the Opalinus Clay fragments (Figure 12). Analcime was observed in several contexts: (1) in the fine-grained clay (bentonite) groundmass, (2) rimming grains of Opalinus Clay, and (3) in the porous "cement" matrix (Figure 13), and (4) at the steel-clay/cement interface. The porous cement fraction of the samples is a different color (lighter), texture, and composition compared to the clay matrix. It contains silica, calcium, and likely water, with a similar composition to tobermorite. In experiments that contained steel coupons, analcime and garronite formed directly at the steel interface. The analyses of EBS-23 through EBS-26 reveal a wide range of Si/Al values and/or cation (Na^+, Ca^{2+}) compositions (Figure 14).

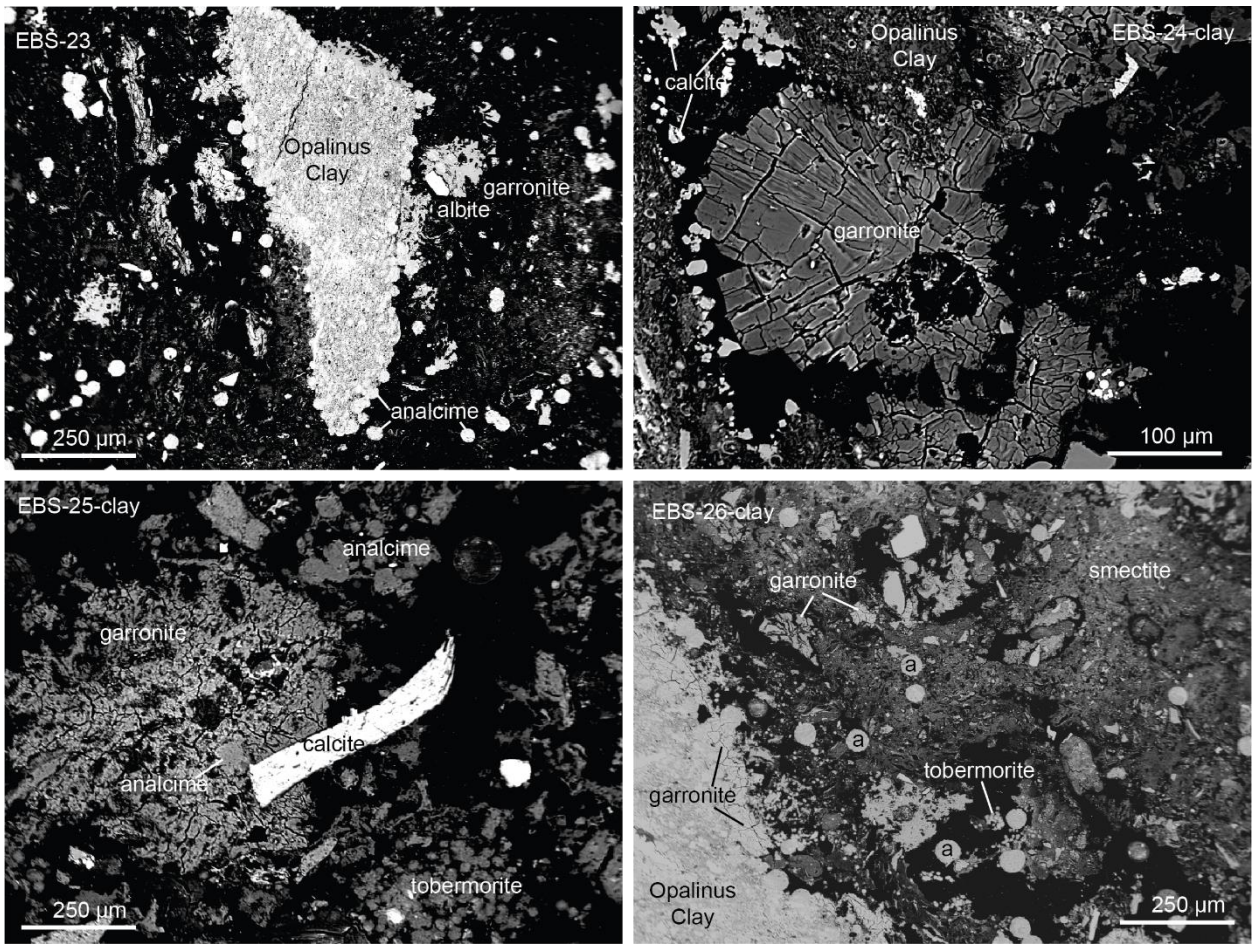

Figure 12: BSE images of thin sections from EBS-23, EBS-24, EBS-25, and EBS-26 showing the petrographic context of authigenic zeolite and CSH minerals (tobermorite). Analcime (a) and garronite crystals form at the interface of the Opalinus Clay fragments and the Wyoming bentonite.

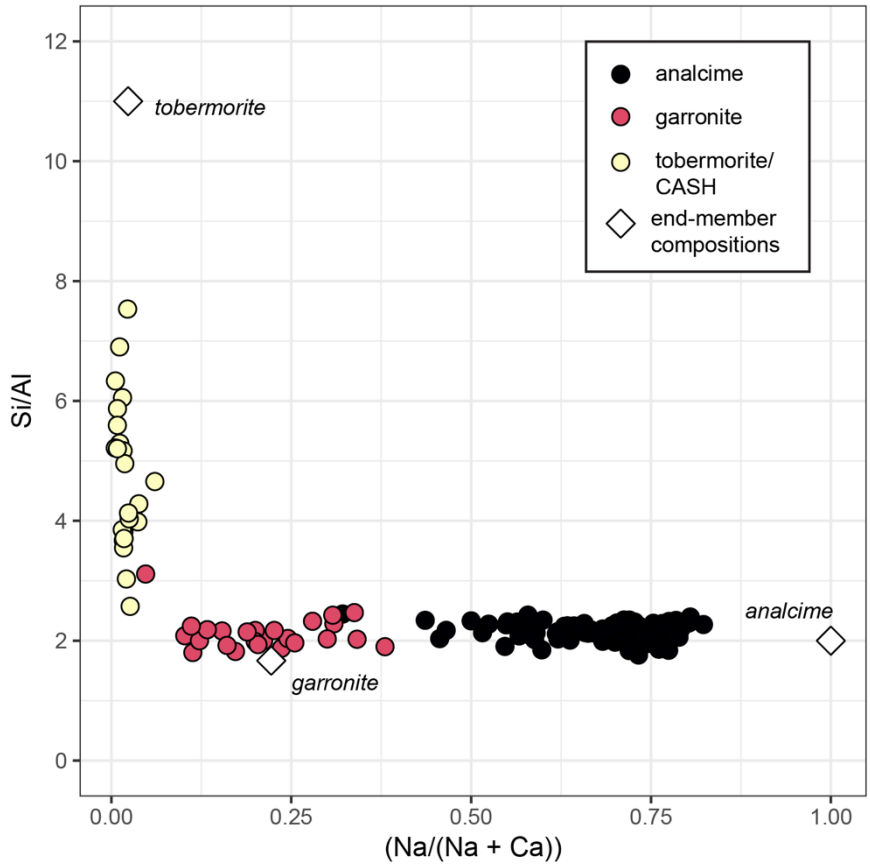

Figure 13: Electron microprobe analyses of zeolite and CSH minerals from EBS-23 through EBS-26. Each point represents a single analysis from the sample set.

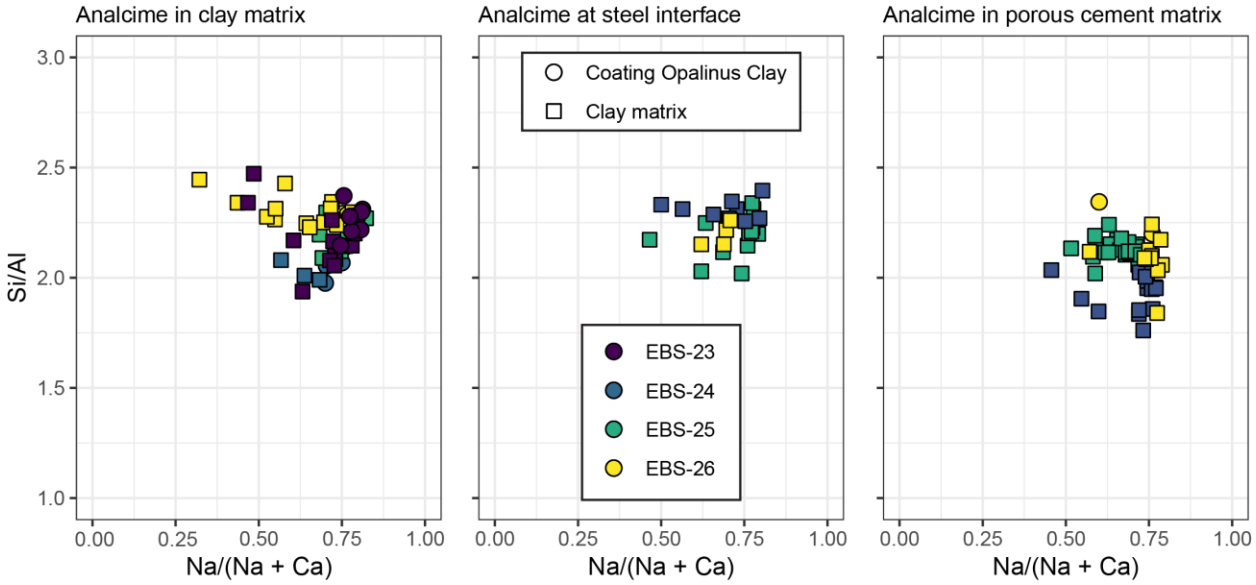

Figure 14: Analcime compositions divided by petrographic context within EBS-23 through EBS-26. Each point represents a single analysis as a wide range of compositions were observed in each sample.

3.8 SEM/EDS Clay Results (Appendix F)

EBS-23. Significant silicate mineral formation occurred in EBS-23. Images in Appendix F focus on analcime crystals in different petrographic contexts, for example, rimming Opalinus Clay fragments (Figure F-1 A, B, C, D). Figure F-1 E shows a feldspar crystal adjacent to garronite. Bright Fe-oxide crystal next to the garronite cluster with a cluster of analcime with mottled cores below (Figure F-1 F). Figure F-2 shows a calcite fragment surrounded by analcime crystals.

EBS-24. Two rough analcime spheres are depicted in Figure F-3 A). Fibrous minerals, identified as xonotlite, were found locally in clusters (Figure F-3 B). Phases associated with Opalinus Clay fragments formed around cracks and edges of fragments, for example garronite and calcite observed in Figure F-3 C. Figure F-3 D shows an example of intergrown analcime, garronite, and feldspar in the clay fraction of the EBS-24 reaction products. The reaction products also contained porous "cement" fragments, composed of a matrix of hydrous CSH-type minerals with dispersed analcime crystals (Figure F-3 E).

EBS-25. SEM images from EBS-25 demonstrate the association of analcime with CSH, feldspar, and garronite phases. For example, Figure F-5 A shows a cluster of large analcime spheres with blocky Ca-rich feldspar (anorthite) and smaller tobermorite spheres. Some phases common in cement materials are formed as well; Figure F-5 B shows fibrous xonotlite with clay.

EBS-26. SEM images from EBS-26 (Figure F-7 A–D) show analcime (large spheres) and tobermorite (smaller spheres) in a clay matrix (fine grained material). Gypsum was also observed locally (Figure F-7 C).

EBS-27. The 6-month EBS-27 was stratified in the reaction cell. SEM samples were taken from the top and bottom third of the matrix. The SEM images from the top showed analcime–wairakite, gypsum, and minor xonotlite in the smectite groundmass (Figure F-9 A-B and F-10 A-B). SEM images from the sample of the bottom third contained an abundance of analcime–wairakite with minor garronite and CSH phases in smectite groundmass (Figure F-11 A-B).

EBS-28. The SEM images collected from EBS-28 show the formation of abundant CSH and aluminosilicate minerals. The clay groundmass is coated with fine grained platelet CSH phases. Tobermorite rosettes and a bladed CSH mineral were observed embedded in the clay matrix (Figure F-14 A-B). Also observed was an example of a hexagonal portlandite crystal (Figure F-15 A). Ca-rich zeolites, including wairakite and garronite, were commonly observed to form together (Figure F-15 B).

EBS-29. The bentonite SEM images from EBS-29 showed montmorillonite with "cornflake" texture with minor apatite, plagioclase, and pyroxene impurities throughout (Figure 18 A-B). The apatite from the main reaction cell showed a planar texture with minor irregular and stepped texturing (Figure F-19 A-B). Apatite from the apatite-only capsules showed the same planar and stepped textures with some pitting. Impurities from the Durango apatite were more apparent (Figure F-20 A-B).

EBS-30 SEM images of the clay-bentonite matrix show predominantly smectite with minor calcite and plagioclase phenocrysts (Figure F-22 A-B). The cured cement chip was coated with a CSH gel and calcite with minor smectite (Figure F-21 A-B).

EBS-31. The SEM of the post-reaction bentonite showed smectite and Fe-saponite with interbedded garronite (Figure F-25 A). A spherical mineral of either lime or CSH phase was observed sporadically throughout the sample (Figure F-25 B). Minor amounts of plagioclase phenocrysts are embedded within the smectite. The cement chip included in the experiment has a layer of calcite on the surface (Figure F-24 A-B).

3.9 Wyoming Bentonite + Durango Apatite: EBS-29

Characterization of EBS-29 and the effects on phosphate additives on bentonite stability were completed in FY21. Analyses include: electron microprobe, SEM, aqueous geochemistry of major anions and cations, QXRD, and XRD of clay mineral structures and apatite crystals.

The pH of the EBS-29 started around 7.4, the pH of the synthetic Opalinus Clay groundwater. The pH, measured at 25ºC (i.e., solution quench), dropped within the first week of the experiment to ~6.5 and remained relatively stable between 6.5 and 7 for the duration of the experiment (Figure 15).

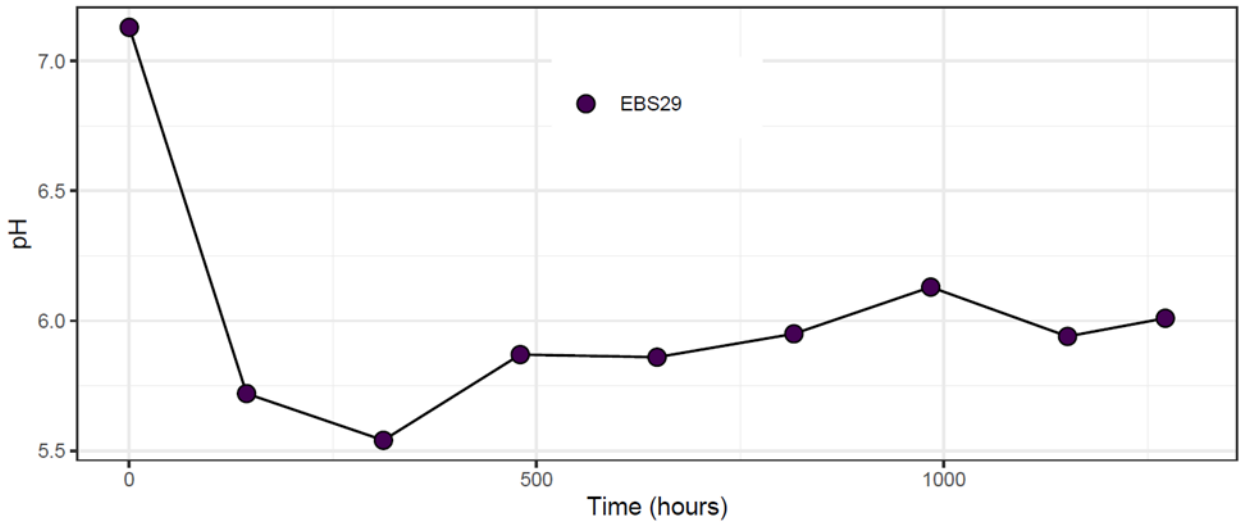

Figure 15: pH at 25ºC throughout the duration of experiment EBS-29.

Major cation concentrations (Na^+, K^+, Ca^{2+}) all showed decreasing trends throughout EBS-29 (Figure 16). At the first sampling, [Na^+] concentrations increased from the starting solution brine (162 mg/L) to 450 mg/L. Concentrations decreased to ~325 mg/L by the end of the experiment. For [K^+], concentrations sharply decreased from initial brine concentrations (290 mg/L) to 50 mg/L by the first sampling, reaching ~20 mg/L by the end of the experiment. Calcium concentrations were observed to decrease from 9 mg/L to 2 mg/L during the experiment from a starting brine concentration of 46 mg/L.

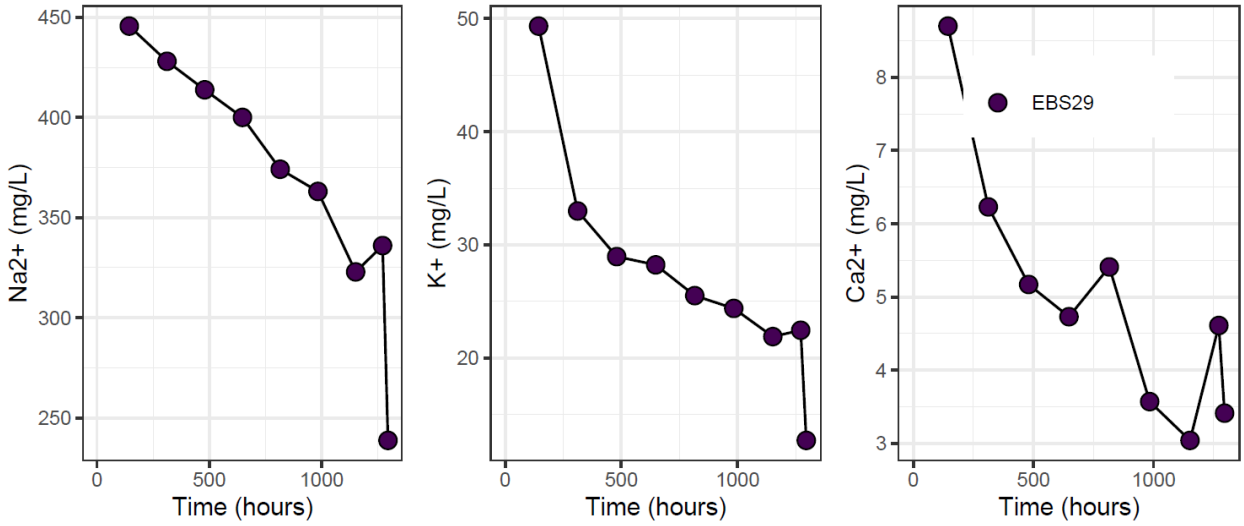

Figure 16: Cation concentrations throughout the duration of experiment EBS-29.

Phosphate concentrations remained ~0.2 mg/L throughout the experiment. Upon experiment quench, concentrations reached ~0.75 mg/L (Figure 17). The initial chloride in the starting brine was around 670 mg/L but dropped to near the detection limit by the first sampling (Figure 18). Sulfate concentrations initially increased from 150 mg/L to 175 mg/L in the first week of the experiment and then steadily decreased to 125 mg/L by the end of the experiment (Figure 18).

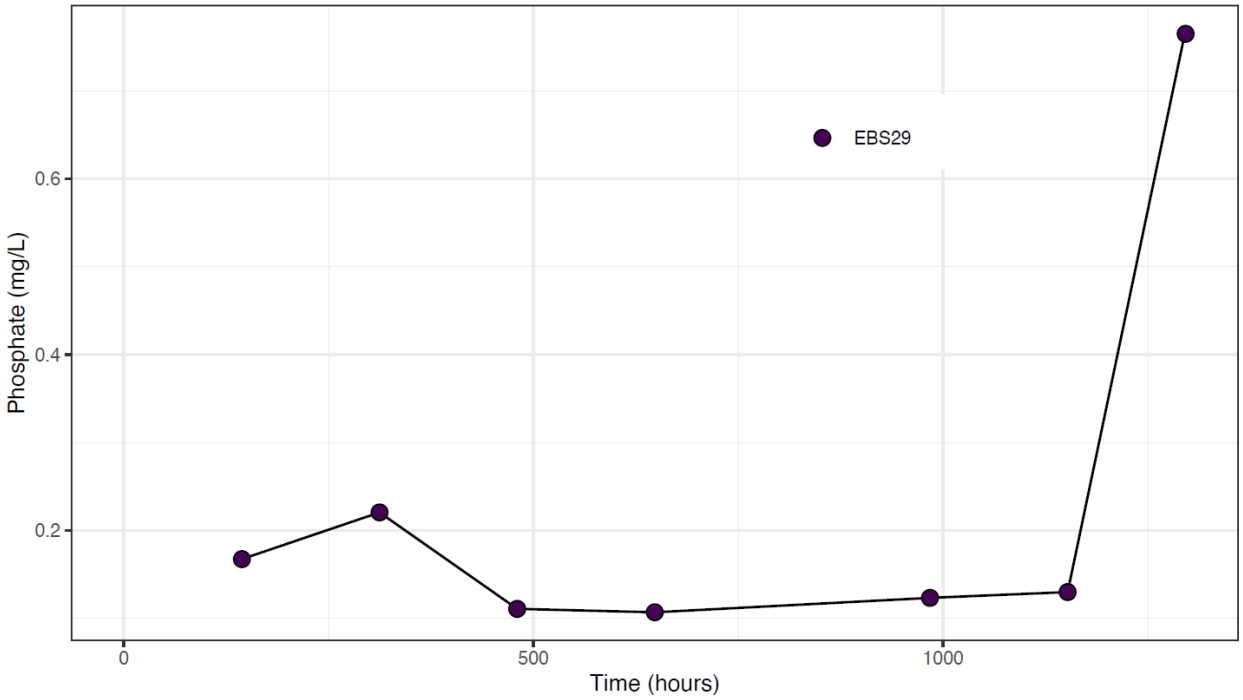

Figure 17: Phosphate concentrations throughout the duration of experiment EBS-29.

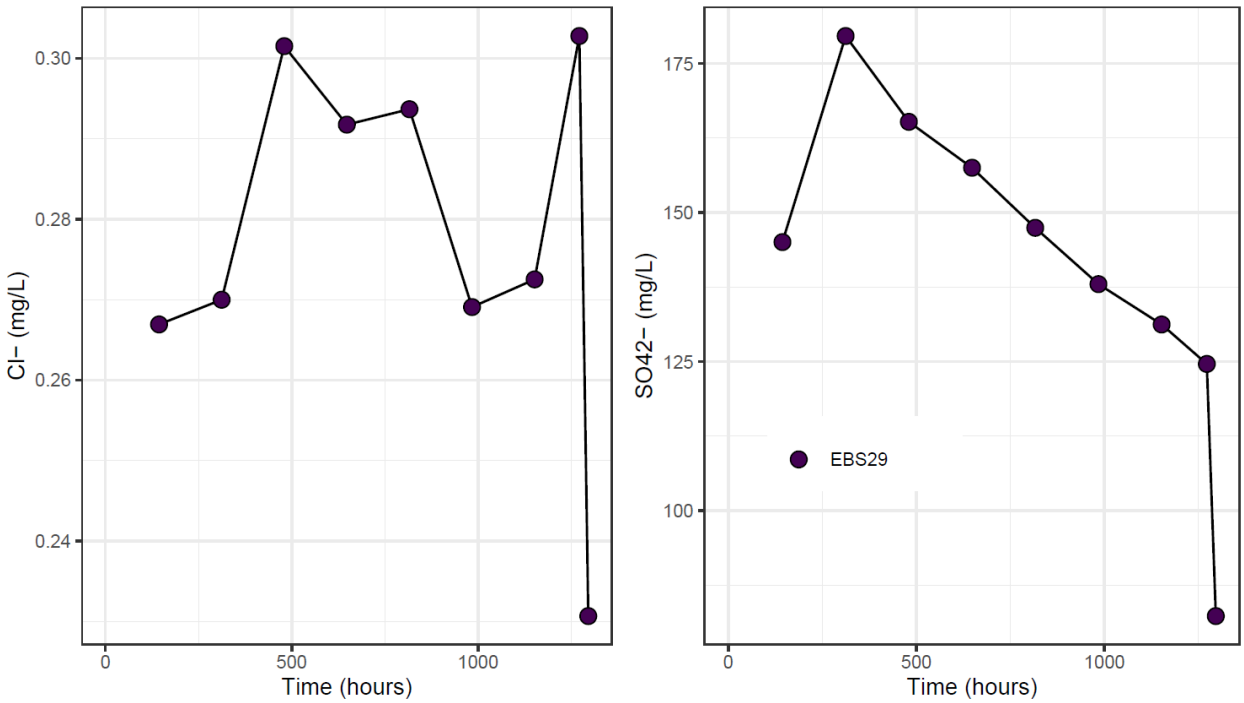

Figure 19: Anion concentrations throughout the duration of experiment EBS-29.

Silica concentrations remained constant around 700 mg/L throughout the experiment. Concentrations dropped to 500 mg/L on experiment quench (Figure 19).

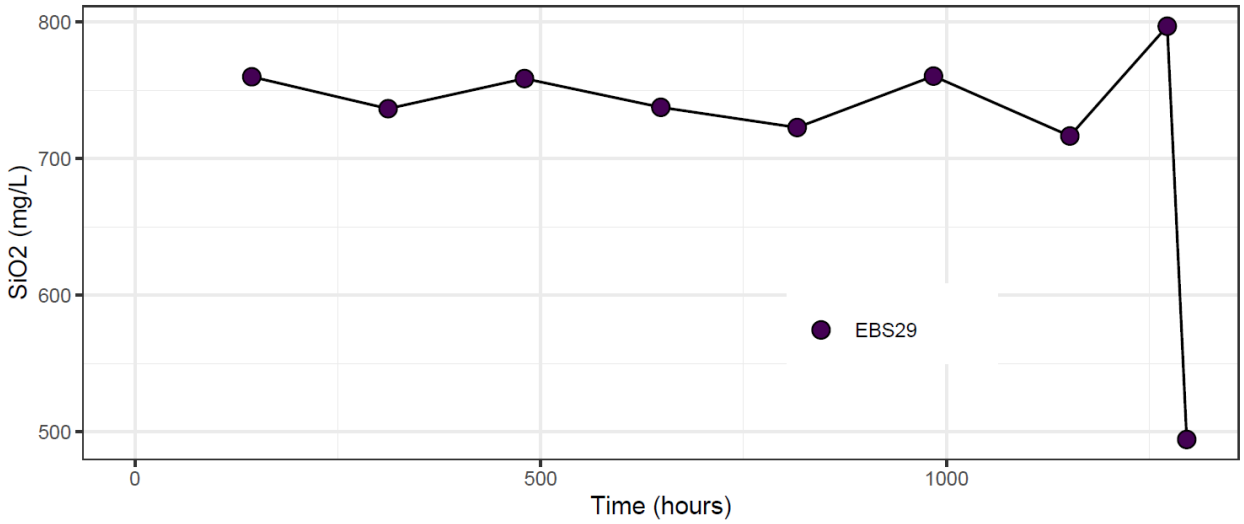

Figure 18: Silica concentrations throughout the duration of experiment EBS-29.

The XRD pattern of the < 2 μm clay fraction from the EBS-29 reaction products shows that the structure of montmorillonite was unchanged with respect to the characteristics of the starting bentonite (Figure 20). Peak positions show no significant shifts or loss of swelling (Table 6). QXRD analyses of the bulk reaction product and SEM images indicate that there was newly formed zeolite (analcime) and an amorphous phase, along with a reduction of combined smectite + illite + smectite-illite.

Table 5: Ethylene glycol saturated smectite (GS) peak positions for the clay fraction extracted from the Wyoming bentonite-Apatite experiment. Expandability was calculated based on the position of the 002 and 003 GS peaks.

EG-smectite	**001**		**002**		**003**		**002/003**	**1**	**2**	**3**
Sample	**d (Å)**	**2θ**	**d (Å)**	**2θ**	**d (Å)**	**2θ**	**Δ 2θ**	**%Exp**	**%Exp**	**%Exp**
WY Bentonite	17.0	5.2	8.5	10.4	5.7	15.7	5.3	100	102	103
EBS-29	17.1	5.2	8.6	10.3	5.7	15.6	5.3	100	102	103

1: %Exp = 973.76 – 323.45Δ + 38.43Δ2 – 1.62Δ3 (Eberl et al., 1993)
2: %Exp = 1517.8 – 548.49Δ + 68.35Δ2 – 2.90Δ3 (Eberl et al., 1993)
3: %Exp = 766.01 – 194.10Δ + 12.924Δ2 (Moore and Reynolds, 1997)

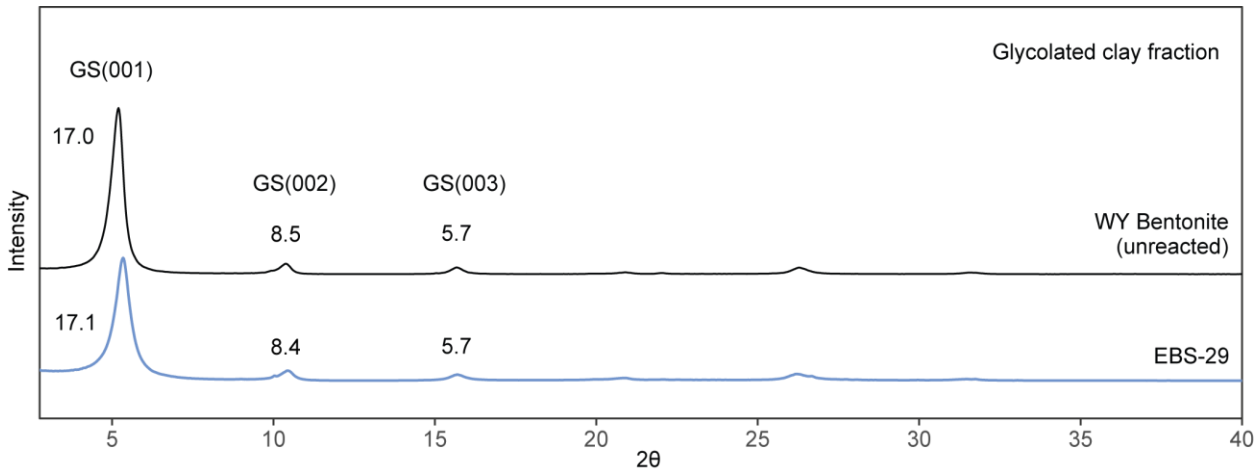

Figure 20: XRD results from the oriented clay fraction of heated bentonite from EBS-29 and unreacted Wyoming bentonite. Peaks corresponding to ethylene glycol saturated smectite are labelled.

Apatite crystals that reacted with synthetic Opalinus Clay groundwater in a sealed gold capsule at the bottom of the titanium experiment vessel were crushed and analyzed in a randomly oriented powder mount. The pattern of the reaction product did not show any significant shifts from the starting material pattern (Figure 21). The lack of peaks corresponding to secondary phases suggests that precipitation of other phosphate phases did not occur.

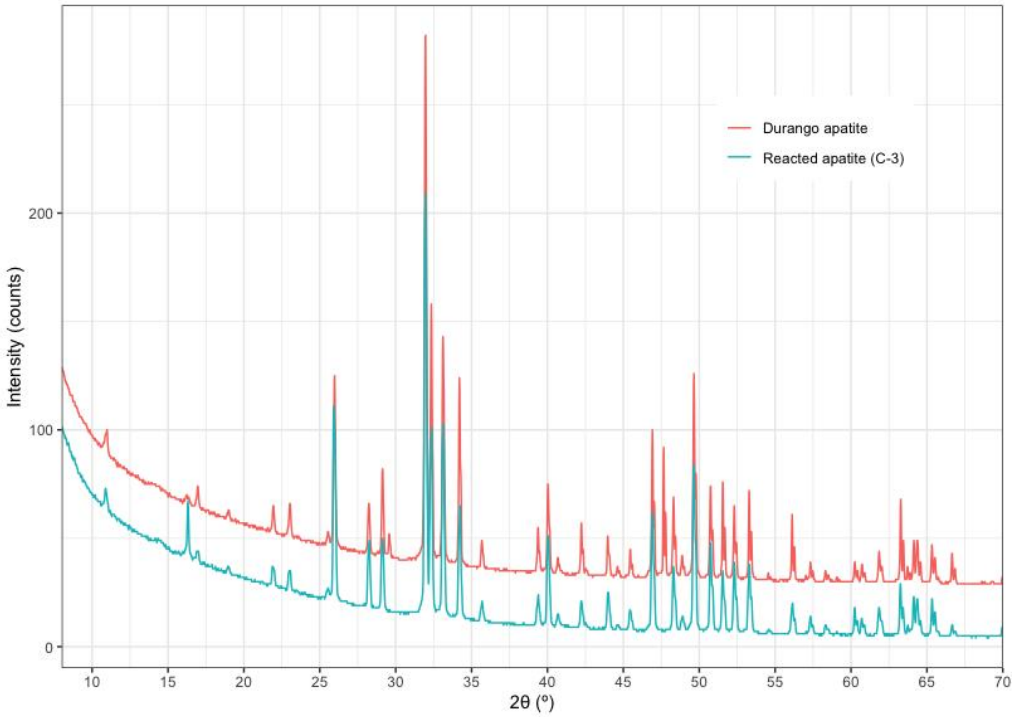

Figure 21: XRD of the apatite crystals that reacted with synthetic Opalinus Clay groundwater in a sealed gold capsule in EBS-29.

3.10 Steel-Bentonite Interface Mineralization

Steel coupons (316SS, 304SS, and LCS) were included in most Wyoming bentonite + Opalinus Clay ± OPC experiments (Table 1). Proportions of Wyoming bentonite:Opalinus Clay:OPC were either (in wt.% values) 80:20:0, 50:50:0, or 60:20:20. Experiments with Wyoming bentonite and Opalinus Clay were performed at either 200 or 300ºC and experiments containing Portland cement were run at 200ºC. Steel coupons were separated from the other solid reaction products. Interface mineralization was observed via secondary electron SEM imaging of the coupon surface and in cross-section view of a coupon mounted in epoxy and polished to show mineralization perpendicular to the coupon edge. The chemical composition of mineral phases on the surface of the steel coupons was analyzed via SEM-EDS and electron microprobe.

3.10.1 Experiment with Wyoming Bentonite and Opalinus Clay

In the set of experiments with Wyoming bentonite and Opalinus Clay, the following mineral phases were identified growing at the interface of the various steels: Fe-saponite, pentlandite, smectite, feldspars, and zeolites.

304SS: EBS-19. Post-reaction 304SS exhibited a layer of Fe-saponite with minor smectite and pentlandite crystals (Figure 22 C) covering the surface of the steel plate. Analcime-wairakite was embedded in the Fe-saponite. The Fe-saponite exhibited a honeycomb texture (Figure 22 A, B).

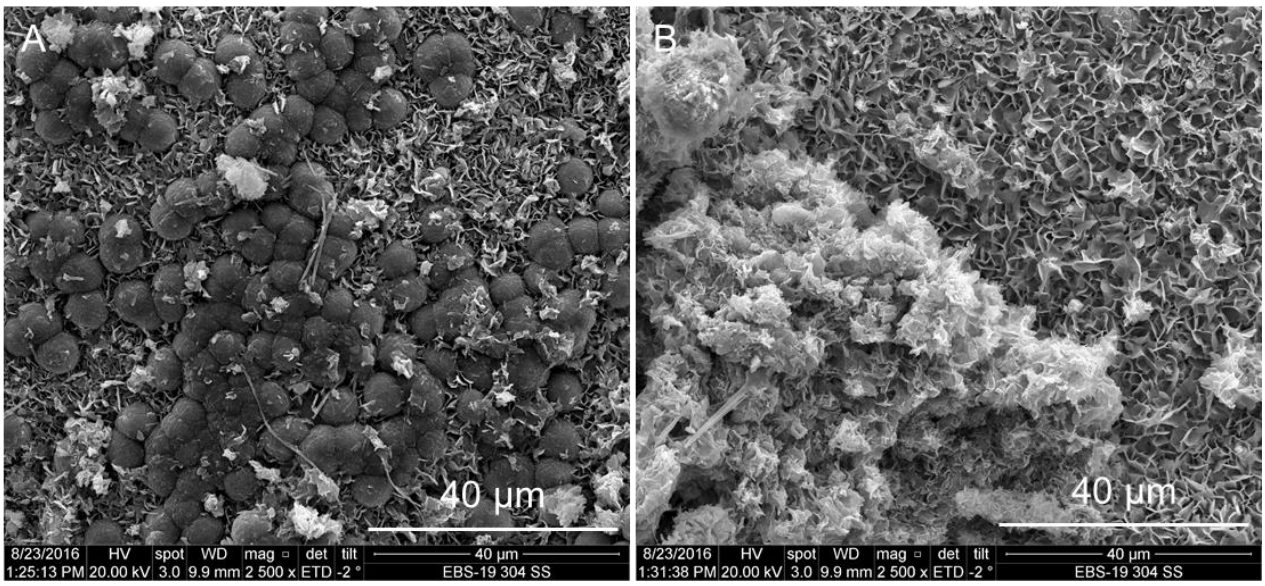

Figure 22: Secondary electron SEM images of the 304SS surface from EBS-19. [C] Fe-saponite with embedded zeolites (rounded) and [D] smectite overlying honeycomb-texture Fe-saponite from EBS-19.

LCS: EBS-18. Fe-saponite crystals grew perpendicular to the low carbon steel followed by secondary smectite rosettes. Minor analcime and millerite are embedded in the saponite mat (Figure 23). This experiment failed (i.e., developed a leak) before reaching the full experiment duration.

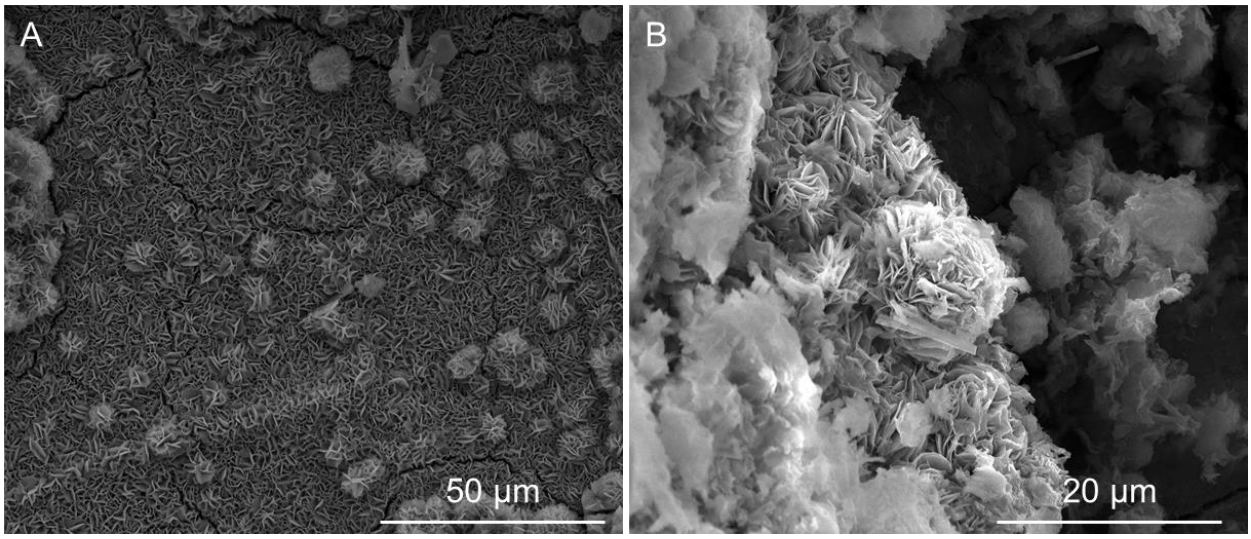

Figure 23: Secondary electron SEM images of the LCS surface from EBS-18. [A, B] Fe-saponite rosettes.

316SS: EBS-15 & -20. In the 6-week experiment, saponite formed in a honeycomb texture on the 316SS steel surface with lesser smectite (Figure 24 A-B). Minor minerals include millerite and analcime-wairakite on the saponite with feldspars embedded on the surface.

The 6-month experiment, EBS-20, was similar to the 6-week experiment with the presence of Fe-saponite with embedded analcime-wairakite, except the late-stage pentlandite were present in the Fe-saponite (Figure 24 C-D).

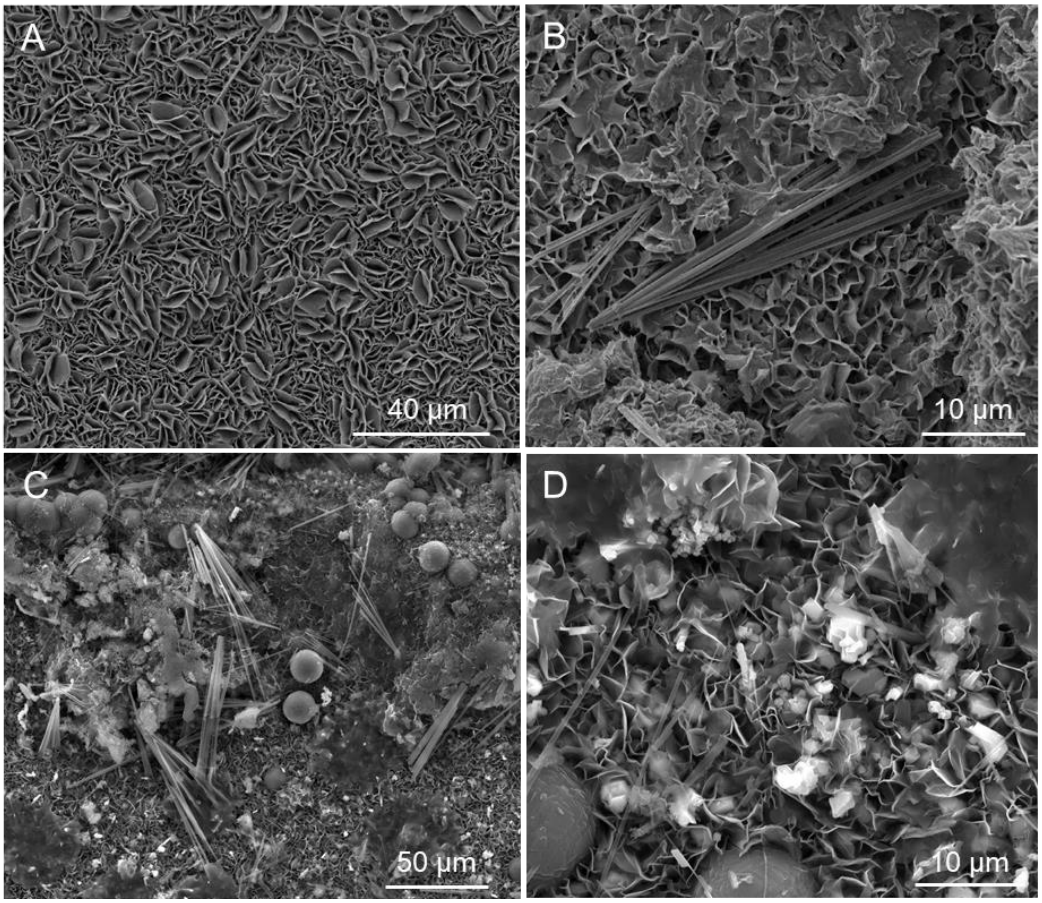

Figure 24: Secondary electron SEM images of the 316SS surface from EBS-15 and EBS-20. [A] Fe-saponite overlaying the 316SS in EBS-15 [B] Smectite, zeolites, and millerite from EBS-15 [C] Fe-saponite and smectite (around the edges) with millerite (bladed mineral) and zeolites and [C]. Pentlandite (blocky mineral) overtop smectite from EBS-20.

3.10.2 Experiments with Portland Cement

Fe-saponite growth on the surface of the steel coupons was not observed in the experiments containing OPC powder, unlike the coupons extracted from EBS experiments without OPC (described above) and experiments containing the cured cement chip. In experiments with OPC powder, mineral phases such as calcite, analcime, tobermorite (CSH minerals), Fe-oxides and Fe-Ni-Cr sulfides/oxides are observed at the steel coupon interface. In experiments containing the cured cement chip, observed newly formed mineral phases include Fe-saponite and gypsum. The SEM images of the steel coupons from the cement experiments can be found in Appendix F.

316SS: EBS-24, -27, -28. The surface of the 316SS coupon was not characterized by a layer of Fe-rich clay (as observed in previous EBS experiments). The 316 stainless-steel surface is altered to granular Fe-oxide with platy/bladed Fe-Ni-Cr oxide interbedded. Analcime and calcite are also observed on the layer of minerals attached to the steel surface (Figure F-4, A-D).

Similarly to the other 200ºC experiments, the 6-month experiment did not have Fe-rich silicate reaction products on the steel surface. The steel surface is coated in Fe-oxides (Figure F-13 A-B). CSH and smectite are attached to the steel surface as well as large (~100 µm diameter) analcime–wairakite crystals (Figure F-12 A-B). Garronite is locally observed.

At 300 ºC, the post-reaction 316SS shows that the steel surface was covered in tobermorite and wairakite in a CSH-clay matrix (Figure F-16 A,B). Gypsum and xonotlite were also present on the reacted coupon (Figure 17 A,B).

EBS-30. The reacted 31SS from the cured cement experiment was coated with smectite with large gypsum crystals (~100-300 µm in length) and corroded plagioclase embedded in the clay (Figure F-23 A). Fe-saponite is also observed on the steel coupon (Figure F-23 B).

304SS: EBS-25. Newly formed minerals attached to the stainless-steel surface outboard of the CSH layer include calcite splays, tobermorite rosettes, and analcime (Figure F-6 A–D). Point EDS analyses on the EBS-25 bentonite-304SS interface show little to no alteration or oxidation (Figure F-6, A-D). A thin fibrous mineral layer is observed attached to the 304SS and locally exhibits a honeycomb texture. EDS analyses indicate this thin layer was likely a CSH phase. Locally, Fe-Cr-Ni-sulfides are observed to separate the CSH layer from the steel surface. Similar to EBS-24, Fe-saponite is not observed on the surface of the coupon.

EBS-31: In the experiment with the cured cement chip, Fe-saponite formed a honeycomb texture on the 304SS steel surface with lesser smectite (Figure-26 B). Calcite and garronite were present sporadically throughout the smectite and Fe-saponite (Figure F-26 A-B).

LCS: EBS-26. Analcime crystals formed mats along the surface (Figure F-7 E). Gypsum and Fe-oxides were also observed (Figure F- 7 F). BSE images of the post-reaction coupon also show the formation of a zeolite layer adjacent to the surface (Figure F-8 A, B). BSE images also show the formation of other newly formed secondary phases of garronite, analcime, and tobermorite, similar to the other EBS experiments with cement (Figure F-8 A-D). No iron-rich clay was observed at the clay-steel interface.

3.10.3 Chemical Gradient across the Steel Surface

Chemical analyses were collected via SEM-EDS along a line perpendicular to the surface of the mounted steel coupon for EBS-15 (Wyoming bentonite + Opalinus Clay, 316SS, 300ºC, 6 weeks) and EBS-25 (Wyoming bentonite + Opalinus Clay + Portland cement, 304SS, 200ºC, 8 weeks). Analyses of the remaining stainless steel coupon chemical gradients are in progress. The results from the steel coupons from two different experiment sets demonstrate the differences in steel surface mineralization with changes in bulk chemistry in the experimental system. The outermost surface of the 316SS coupon of EBS-15 is altered to Fe,Cr-oxide in which Cr is slightly enriched with respect to the steel (Figure 25). The portion of the surface of the 316SS appears to have delaminated from the surface

and Fe-saponite formed between the layers of steel (Figure 25). In comparison, zeolite minerals (analcime) formed at the surface of the coupon from the cement-bearing experiment (EBS-25). It does not appear that Fe or Cr were transferred to reaction products away from the coupon surface. Further, a distinct oxide rind is not observed at the coupon margin (Figure 18). There is a sharp chemical boundary of the steel and the attached reaction products in the EBS-25 sample, whereas a more diffuse, gradual boundary is observed in EBS-15 with respect to elements such as Fe and Cr.

Preliminary observations from experiments EBS-30 and EBS-31 indicate that the presence of the cement chip instead of OPC powder results in different reactions at the steel interface. Fe-saponite is observed, indicating that Fe is transferred from the coupon to the clay matrix. In progress analyses of the steel coupon surface will be compared with previous results.

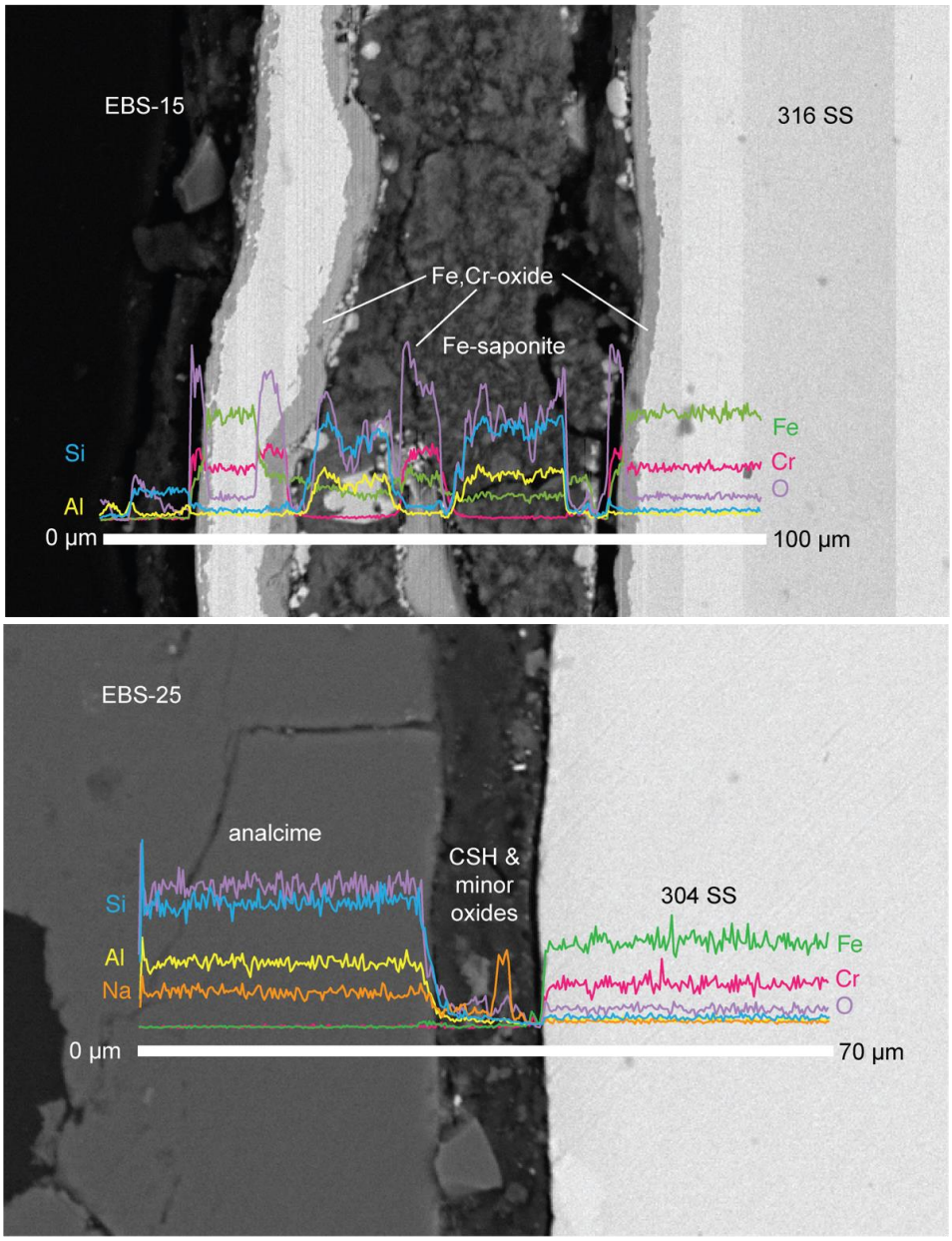

Figure 25: Energy dispersive X-ray spectroscopy (EDS) chemical results collected along a line (white) perpendicular to the steel surface in EBS-15 (top) and EBS-25 (bottom).

3.10.4 Steel Precipitation Thickness

Estimates of the thickness of the zone of alteration products at the steel-bentonite interface were measured for experiments EBS-15 through EBS-26 that contained stainless-steel coupons. Precipitation thicknesses (Table 6) were determined from backscattered electron (BSE) images of a cross section of two steel coupons per experiment. Fifty measurements were taken from each long side at equal intervals with an additional eight measurements on each short side. Measurements were made in Adobe Photoshop using the measurement

tool. Precipitation rates (Table 7) were determined by dividing the average precipitation thickness by the number of experimental run days. The stainless-steel sample for EBS-18 could not be located; subsequently, the thicknesses recorded are from an older measurement technique and were included for completeness. It is also important to note that EBS-18 did not run the full duration of the experimental time due to the gold bag failure.

The Fe-rich phyllosilicate mineral growth rates at the bentonite-steel interface were the highest in the 300ºC experiments that included Wyoming bentonite (80%) and Opalinus Clay (20%). In these 300ºC runs, LCS had the fastest average growth rate (3.56 µm/day, 6 weeks), followed by 316SS (0.67 µm/day, 6 weeks), 304SS (0.45 µm/day, 6 weeks) and 316SS (0.13 µm/day, 6 months). The 200ºC experiments, EBS-21 and -22, had lower precipitation rates than the higher temperature experiments (316SS, 0.14 µm/day and 0.38 µm/day over 8 weeks, respectively), likely due to experiment parameters such as lower temperature, longer run time, starting mixtures, and groundwater composition.

The thickness of zeolite and CSH phases that formed perpendicular to the stainless-steel surface in the 8-week experiments with OPC varied with steel type. Mineral formation on the LCS surface occurred at the fastest average growth rate (0.56 µm/day), followed by 304SS (0.40 µm/day) and 316SS (0.14 µm/day).

Table 6: Phyllosilicate (Fe-saponite/chlorite)/zeolite (analcime) thickness and growth rates. Rates are represented in µm per day. Three steel types were examined: 304SS, 316SS and LCS from EBS-15 through -26.

Sample	Steel	Matrix	Water: Rock	Temp	Time	Ave Precip (µm)	Prec./Day (µm/day)
EBS-19	304	Bent + Clay	6.0	300°C	6 weeks	12.58 (±11.67)	0.45
EBS-25		Bent + Clay + Cement	11.3	200°C	8 weeks	16.99 (±12.15)	0.40
					AVERAGE:	14.79	0.43
EBS-15	316	Bent + Clay	8.1	300°C	6 weeks	28.30 (±16.06)	0.67
EBS-20		Bent + Clay	7.1	300°C	6 months	24.10 (±19.59)	0.13
EBS-21		Bent + Clay (1 M NaCl)	9.1	200°C	8 weeks	7.37 (±8.89)	0.14
EBS-22		Bent + Clay (=)	8.4	200°C	8 weeks	21.10 (±24.75)	0.38
EBS-24		Bent + Clay + Cement	13.5	200°C	8 weeks	7.91 (±8.39)	0.14
					AVERAGE:	17.76	0.29
EBS-18*	LCS	*Bent + Clay*	*8.3*	*300°C*	*3 weeks*	*71.13*	*3.56*
EBS-26		Bent + Clay + Cement	11.7	200°C	8 weeks	31.63 (±16.11)	0.56

* Sample EBS-18 was analyzed with an older technique and did not run to completion. It was included for completeness.

4. Discussion

4.1 Portland Cement Effects

4.1.1 Aqueous Geochemistry

The solution chemistry changes observed in the extracted reaction fluids likely reflect mineral-brine reactions. The hydrothermal reaction of the solid reactants with the synthetic Opalinus Clay brine likely resulted in precursor phase dissolution/recrystallization and the precipitation of new mineral phases. As described above, the addition of OPC powder or cured chips to the reaction mixture resulted in changes in the observed newly formed mineral phases in comparison with the set of experiments without cement. In addition, temperature (200 or 300ºC) also affected the observed aqueous geochemistry changes. The main observations from the experiments with Opalinus Clay and Wyoming bentonite at 200ºC were silica undersaturation and difference in pH values. Increases in temperature resulted in different pH, silica, and cation concentrations in comparison to the 200ºC experiments. Swapping out OPC powder for a cured chip also resulted in different effects, described below.

4.1.2 Silica Saturation

Previous studies identified silica saturation as a major factor in the alteration of EBS materials (Smyth, 1982; Bish & Aronson, 1993; Neuhoff & Ruhl, 2006; Cheshire et al., 2014). The presence of Opalinus Clay wall rock and synthetic groundwater had significant effects on the aqueous chemistry of the system, in particular, on the silica saturation state throughout each experiment. Cheshire et al. (2014) observed saturation with respect to cristobalite throughout the experiment duration of 300°C Wyoming bentonite only experiments. In comparison, measurements from the 300°C Opalinus Clay ± Wyoming bentonite experiments of this study showed similar silica concentrations throughout each experiment, regardless of the proportions of starting material (Sauer et al., 2020). Silica saturation calculations of the reaction fluids from the experiments with Portland cement are in progress.

4.1.3 pH

The pH (measured at 25ºC) of the reaction fluids extracted from the 300ºC experiment that contained cement (EBS-28) dropped to ~6 within two weeks of the experiment, indicating that OH^- derived from portlandite ($CaOH_2$) dissolution is quickly consumed at 300ºC (Figure 4). Mineral phases such as zeolites (e.g., analcime, garrnonite) and aluminosilicates (e.g., feldspar) likely buffered the pH, as has been observed in other experimental systems (e.g., Johnston & Miller, 1984; Heimann, 1993; Gailhanou et al., 2017; Sauer et al., 2020). Portlandite dissolution initially occurred as indicated by the pH of ~9.5 at the first sampling and the XRD pattern of the reacted mixture (Figure 4).

The pH values (measured at 25ºC) in the 200ºC experiments increased from the starting groundwater solution pH to values between 8 and 9. The elevated pH values are likely related to the OH^- contributed to the system from the OPC powder related to portlandite dissolution. In comparison to 300ºC, the OH^- was not immediately consumed in mineral-forming reactions. The increase of pH is likely related to the dissolution of portlandite and the presence of alkaline components (Na^+, K^+ and Ca^{2+}) in the cement powder entering into

the solution (see the increase of Ca^{2+} in Figure 6). The pH of the pore water should gradually decrease during the evolution of cement degradation; however, this was not observed over the period of the 8-week 200ºC experiments. A slight decreasing trend in pH values was observed in the values recorded from the six-month experiment (EBS-27; Figure 3).

In experiments EBS-30 and EBS-31 that contained a cured cement chip at 200ºC, pH values were lower than were observed in the 200ºC powder experiments. A slight increasing trend is observed over time from pH = 6 to pH = 6.5 to 7. Portlandite dissolution is indicated by the XRD patterns of the chip surface. A thin section was made of a cross section of the cement chip; future work will include the assessment of the extent of the reaction into the center of the chip. Future work will also assess if calcite formation/recrystallization occurred.

The evolution of the pH pore water in a cementitious environment is modeled over time at 25ºC by Jacques et al. (2010). The reaction between an aqueous fluid and cement is a gradual change in composition, from a "young" concrete pore water (pH > 13) to more mature pore water with a lower pH (~10). Changes in solution pH are observed in stages, which can be related to mineral-brine reactions. The first stage of the pH evolution, when the pH is ~12.5, Na^+ and K^+ concentrations are elevated due to leaching of Na_2O and K_2O from the dissolution of portlandite from OPC. The pH will begin to decrease as all the portlandite is consumed from the cement and the pore water is then buffered by other cement phases, such as CSH minerals. When the pH drops below 10, the formation of calcite and aggregate minerals will likely be the phases responsible for buffering the pH (Jacques et al., 2010).

Significant solution chemistry differences are observed in the concentrations of aqueous species (e.g., SiO_2, K^+) and the pH between the reaction fluids from the 200 and 300ºC cement experiments. Reactions were likely kinetically faster at 300ºC, e.g., as demonstrated by the rapid changes observed within the first week of the 300ºC experiment duration (e.g., drop in pH values, silica, cations) (Figure 4-6). The differences in the observed solution trends also reflect the formation of different mineral phases, potentially through different reaction pathways. In the experiments with cement powder, at 300ºC the formation of feldspar and analcime was favored versus at 200ºC where abundant zeolite phases (garronite, clinoptilolite/heulandite, analcime) were formed. Further, differences in the experiments with cured cement chips indicate that cured cement is less reactive and has less of an effect on the pH of the system than OPC powder.

4.2 Clay Alteration

The addition of uncured OPC powder affected the smectite mineral structure in the bentonite fraction, resulting in ~10% reduction in expandability from 8 weeks of hydrothermal treatment at 200ºC and 300ºC. In the 6-month experiment, the formation of mixed layer chlorite-smectite was also observed. A prominent tobermorite peak is present in the clay mineral fraction of all the cement-bentonite experiments (Figure 9). Previous investigations on the interaction of bentonite and cement materials have documented the formation of Al-tobermorite from the reaction of portlandite ($Ca(OH)_2$) with montmorillonite (Fernandez et al., 2014; 2016). Fernandez et al. (2016) similarly observed reduced expandability in smectite

post hydrothermal reaction at 60 to 120ºC. Thus, montmorillonite in the Wyoming Bentonite used in our experiments likely reacted with Portland cement to create interlayered tobermorite in the clay mineral structure. Further, QXRD results indicate that combined illite, illite-smectite, and smectite in the bulk system was reduced by ~12 to 19 wt.%, whereas tobermorite comprises 2 to 4 wt.% of the reaction products and amorphous material comprises 9–26 wt.% in the reaction products from the 8 week, 200ºC experiments. Amorphous material that has an aluminosilicate composition (analyzed via SEM-EDS) indicates potential breakdown of clay minerals, as has previously been recognized in alkali-rich experimental systems (i.e., Khalifa et al., 2020).

In experiments with the cured OPC chip (EBS-30 and EBS-31), the clay mineral structure was less affected than in experiments with uncured OPC powder. Clay mineral separations are in progress for these experiments but XRD patterns from the bulk powder suggest that smectite remained stable during the experiment period and that mixed layer illite-smectite or chlorite-smectite phases were not formed.

4.3 Zeolite and CSH-Mineral Formation

The addition of uncured ordinary Portland cement powder to the Opalinus Clay + Wyoming bentonite system at 200ºC (EBS-23 through EBS-27) resulted in abundant zeolite and CSH mineral formation. Phases observed in previous EBS experiments (Wyoming bentonite only and Wyoming bentonite + Opalinus Clay) such as analcime likely formed through different reaction pathways involving different mineral phases. QXRD data from EBS-24, EBS-25, and EBS-26 correspond to 5 to 6 wt.% analcime, 6 to 9 wt.% garronite (a rare Ca-rich zeolite), 2 to 4 wt.% Al-tobermorite (CSH), and 9 to 26 wt.% amorphous material (CSH gel). In the 6-month experiment (EBS-27), more analcime–wairakite and other zeolites and less garronite, tobermorite, and amorphous material were observed. The minerals analcime, garronite, and tobermorite are commonly observed together (e.g., Figure 11). Garronite and tobermorite crystals from EBS-23 through EBS-26 are very sensitive to the microprobe electron beam and thus did not yield reliable compositional data (e.g., low silica and total oxide numbers). The compositions of analcime, garronite, and tobermorite/CSH phases obtained are plotted in Figure 12a. Feldspar, analcime, and garronite analyses have a wide range of Na/Na+Ca values between the end-member phase values. The observed compositional spread and textural association of these phases in the 200ºC experiments and the reduction in garronite and CSH abundance after 6 months of reaction time indicates that garronite and CSH phases may be metastable precursors to more stable silicate phases, such as analcime–wairakite. Potential reactions related to this mineral sequence have been outlined by Bayliss and Levinson (1970) based on results from hydrothermal experiments involving quartz, kaolinite, and calcite/dolomite. Garronite and analcime are commonly found at the interface of the Opalinus Clay fragments, which contain calcite and kaolinite. Thus, the formation of garronite may be described by the reaction, generalized from Bayliss and Levinson (1970):

$$Na^{+} + \text{calcite} + \text{quartz} + \text{kaolinite} + H_2O \rightarrow \text{garronite} + CO_{2\,(gas)} \qquad (6)$$

Analcime produced in the OPC powder-containing experiments has a distinct composition with respect to the analcime formed in previous EBS experiments (Figure 26). The Si/Al ratios of

analcime from EBS-23 to EBS-26 have similar Si/Al ratio to analcime from EBS-14 (Opalinus Clay only). The Na/(Na+Ca) ratios are similar to analcime formed in experiments without Portland Cement (i.e., lower bulk Ca compositions). Future experiments with different parameters (length, temperature) could explore this difference. Petrographic evidence of intergrowth of analcime and garronite and mottled textures in analcime cores, along with the range of compositions, may suggest that the reaction from garronite to analcime was not complete. Therefore, intergrowth of garronite, or other Ca-rich phases (e.g., tobermorite), may be the reason for the wide range in Na and Ca contents observed in analcime in the electron microprobe results. Electron microprobe results from EBS-27 through EBS-31 will be included in the FY22 report.

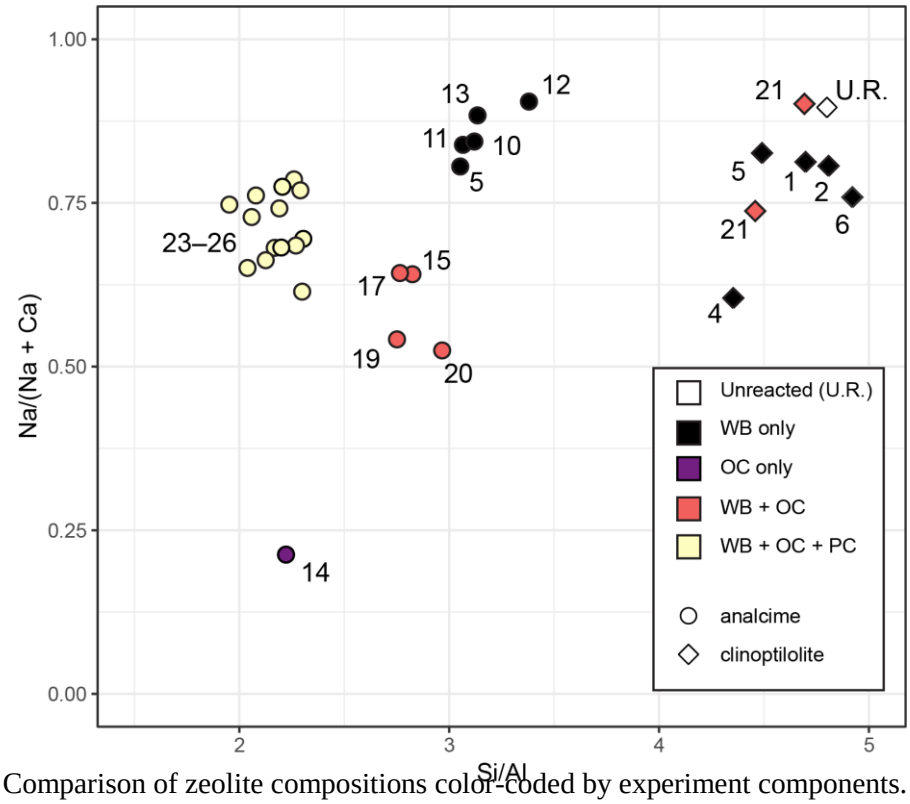

Figure 26: Comparison of zeolite compositions color-coded by experiment components. The numbers represent the EBS experiment identifier. The run conditions are as follows: 1–4, 6: 4–5 week bentonite only experiments with a ramped thermal profile (25/100/200/300/25 °C); 5, 10–13: 6 week bentonite only at 300 °C; 14: Opalinus Clay only for 6 weeks at 300 °C; 15–20: Opalinus Clay + bentonite 6–8 week experiments at 300 °C; 21: Opalinus Clay + bentonite 200 °C; and 23–26: Opalinus Clay + Wyoming bentonite + Portland cement for 8 weeks at 200 °C. Bentonite-only experiments generally have higher Na/Na+Ca and Si/Al values. Experiments with Opalinus Clay and/or Portland cement shift to lower Si/Al. Abbreviations: OC, Opalinus Clay; PC, Portland cement; WB, Wyoming bentonite.

4.4 Phosphate Effects

Phosphate minerals are a potential EBS additive that would function to enhance radionuclide-retention properties. Results from EBS-29, which included 80 wt.% Wyoming bentonite and 20 wt.% Durango apatite, showed that hydrothermal treatment at 250ºC and 150 bar for 8 weeks did not result in significant changes to the apatite but montmorillonite was decreased

in abundance. Aqueous geochemical analyses of reaction fluids show a slight increase in phosphate, indicating minor apatite dissolution occurred. XRD/SEM analyses did not identify the formation of secondary phosphate mineral phases that may have formed. The amount of phosphate dissolved will inform hydrothermal experiments with relevant radionuclides at observed phosphate concentrations to understand the formation of radionuclide-bearing phosphate byproducts. Further, the sorption of radionuclides to phosphate mineral surfaces will also be explored at the relevant repository temperatures, pressures, and chemical conditions.

4.5 Steel Corrosion and Interface Mineral Precipitation

Results from these experiments show a dynamic environment in the experimental systems at the bentonite-metal interface. The bulk chemistry likely controls the alteration mineralogy, as demonstrated by the differences in mineral precipitation in the experiments with and without uncured/cured Portland cement (Figure 20). The new growth of surface-bound minerals is likely due to direct crystallization in the localized environments surrounding the metal with the steel material acting as a substrate for mineral growth in response to corrosion. The following describes our finding from the (1) general argillite environment and (2) from the cement environment.

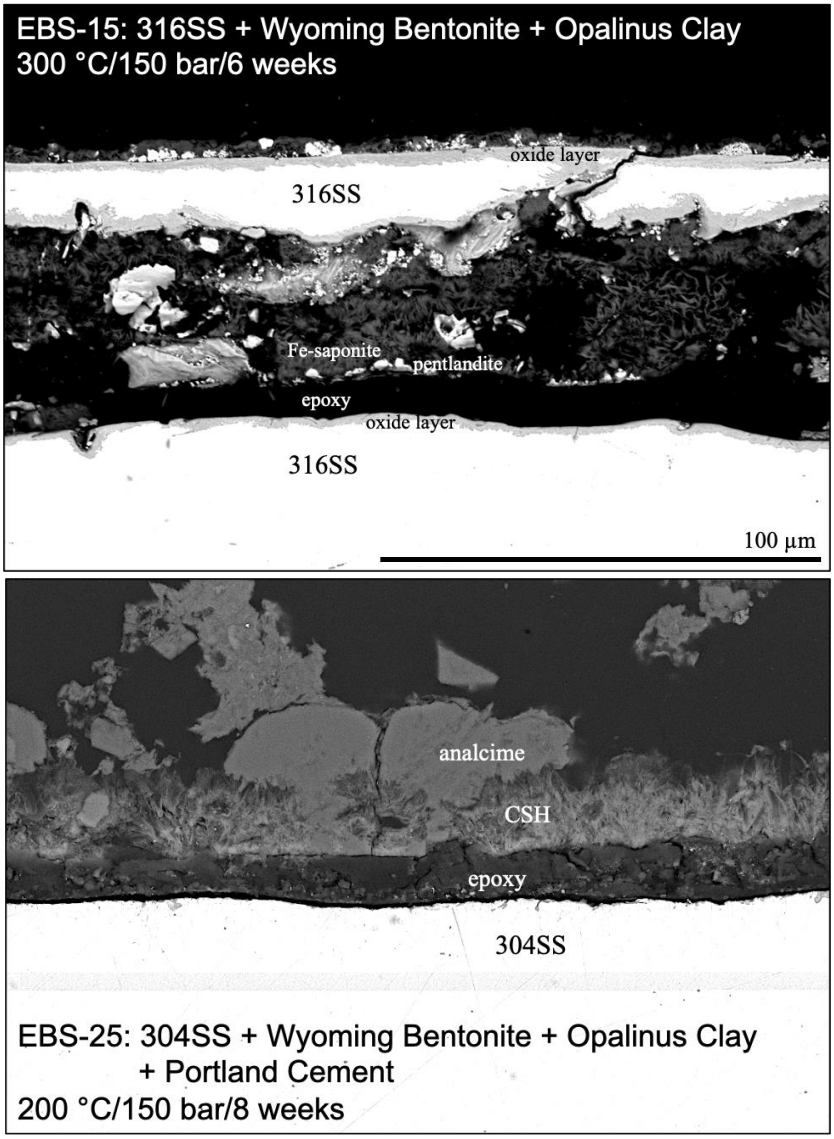

Figure 27: Backscattered electron SEM images showing layered mineral growth that the stainless-steel surface. [Top] The edge of a 316SS coupon from EBS-15. The edge of the steel is an Fe,Cr-oxide layer (medium gray), iron rich phases such as Fe-saponite and pentlandite are observed attached to the steel surface. [Bottom] The edge of the 304SS coupon from EBS-25. On the edge of the steel, a CSH layer formed followed by analcime.

4.5.1 Steel Corrosion in the Argillite Environment

In EBS-15 to 22 (Wyoming bentonite + Opalinus Clay experiments), iron corrosion products that formed on the steel coupon surface reacted with bentonite, resulting in the Fe/Cr/Ni-rich phases (Fe-saponite, chlorite, pentlandite, chromite). These reaction products are only observed in a thin (< ~50 µm) rind on the reacted coupons. Outboard of the Fe-rich phases, unaltered montmorillonite is observed.

In the Wyoming bentonite only experiment series described in Cheshire et al. (2018), a magnetite-like oxide layer developed at the outermost surface of the steel coupon. Further, an oxide layer on the steel coupon surface is observed in the Wyoming bentonite + Opalinus Clay experiments (reported above) that remained around circum-neutral pH values. Outboard of the oxide products, Fe-rich phyllosilicates (i.e., trioctahedral, Fe-rich saponite and chlorite) crystallized, forming a reactive zone with a high surface area in comparison to the original steel surfaces. The surface-bound Fe-rich minerals likely directly crystallized from solution in the local environments surrounding the metal plates as these phases are not observed elsewhere in the clay reaction products. Both steel surfaces for experiments with Wyoming bentonite only and experiments with Wyoming bentonite and Opalinus Clay (argillite environment) have Fe-rich minerals at the steel interface. The localized presence of the newly formed Fe-rich phases together with the lack of significant increase in aqueous Fe in the reaction fluids indicate that steel coupon reactions did not influence solution chemistry of the bulk system.

The general reaction between the steel and bentonite is depicted in Figure 28. The stainless-steel interaction with bentonite via congruent dissolution/oxidation can be detailed by the following reactions:

Stainless steel dissolution

$$Fe_{1.22}Cr_{0.37}Ni_{0.22} = 1.22\ Fe^{2+} + 0.37\ Cr^{+} + 0.22\ Ni^{2+} + 3.99e^{-} \quad (7)$$

Smectite evolution

$$Fe^{2+} + Ni^{2+} + Cr^{3+} + H_2S_{(aq)} + (Na,K,Ca)_{0.33}(Al_{1.67},Fe_3{+}0.20,Mg_{0.13})Si_4O_{10}(OH)_2 = \text{smectite}$$

$$(Fe,Ni,Cr)_9S_8 + (Na, K, Ca)_{0.33}Fe_3(Si_{3.67},Al_{0.33})O_{10}(OH)_2 \quad (8)$$

pentlandite Fe-saponite

Synthetic Fe-saponites have been crystallized in dilute solutions and gels of silica, Fe-, Al-chlorides at temperatures up to 850°C and pH of 8.5 to 9.5 (Kloprogge et al. 1999). In our experiments, the partial dissolution of the steel plates likely contributed ferrous iron into the fluid phase and, together with silica and aluminum from montmorillonite and other precursor aluminosilicate phases in the bentonite, resulted in Fe-saponite crystallization on the steel surface growth substrate. Further, Fe-saponite alteration into chlorite has been suggested (Mosser-Ruck et al., 2010) in the presence of ferrous iron at temperatures approaching 300°C and near-neutral pH. This was confirmed by Mosser-Ruck et al. (2016) through long duration experiments (up to 9 years). The authors were able to demonstrate that smectite is consumed by dissolution to produce chlorite (chamosite) by precipitation. Mosser-Ruck et al. (2016) depicts this reaction by:

$$3\ \text{smectite} + 3\ Fe + 4\ H_2O \rightarrow 1\ \text{chlorite} + 3\ \text{quartz} + 2\ \text{albite} + 3\ H_2 + \text{zeolite} \quad (9)$$

Electron microprobe analyses and SEM observations of our experimental reaction products show some instances of chlorite formation in contact with the steel, likely due to the relatively Si-deficient environment) Fe-saponite forms outboard of the chlorite layer, where Si is more abundant (Figure 28).

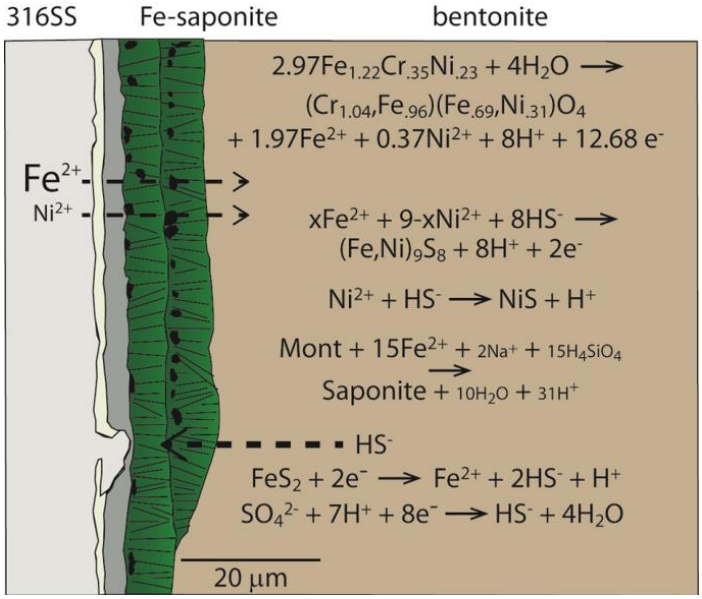

Figure 28: A stylized representation of phyllosilicate mineral growth at the steel interface. Of particular interest is the reaction: montmorillonite → Fe-saponite.

4.5.2 Corrosion in the Cement Environment

In experiments that included uncured OPC powder or cured OPC chips, at 200 and 300ºC, different mineral reactions occurred at the steel-bentonite interface. As described above, in the experiments without cement, an oxide layer formed on the outermost edge of the steel coupons. At 200ºC with uncured OPC powder (EBS-24 through EBS-27), an oxide layer was only locally observed and did not appear to be continuous along the steel surface (Figure 29). At 300ºC, Fe-saponite formation at the steel surface is observed. With the inclusion of a cured cement chip at 200ºC, an oxide layer and Fe-saponite is observed.

In general, pH can considerably influence the corrosion behavior of metals by forming or dissolving the protective oxide layers on the metal surface (Kursten et al., 2004). The corrosion rate of steel in an anoxic solution increases with decreasing pH. For example, observed steel corrosion rates were ~5 and 15 times higher at solution values pH of 7 and 4, respectively, than the corrosion rates in pH 13 solutions (Kursten et al., 2004). We interpret that the increased pH of the experiments with uncured ordinary Portland cement powder at 200ºC likely slowed oxide layer formation at the steel interface, leading to the lack of Fe-rich phyllosilicate minerals. Similarly, the surface of the steel coupon at 300ºC lacks iron rich clay phases. In comparison, pH values in the experiments with the cured cement chips (EBS-30 and EBS-31), observed values are much lower, between 6 and 7. When the pH of the experimental fluid is high, the corrosion of steel occurs at a much slower rate and is unable to provide iron into the system (e.g., Kursten et al., 2004). For the experiments without cement, pH values between 5 and 6 before the conclusion of the

experiment are conducive for oxide precipitation for the corrosion of the steel coupons. The experiments with Portland cement (EBS-24 to 27), the pH is higher, hovering between 8 and 9 before termination. Overall, the elevated pH observed in our experiments with uncured Portland cement powder slowed the corrosion of the steel coupons, and, therefore, the formation of an oxide layer and Fe-rich minerals.

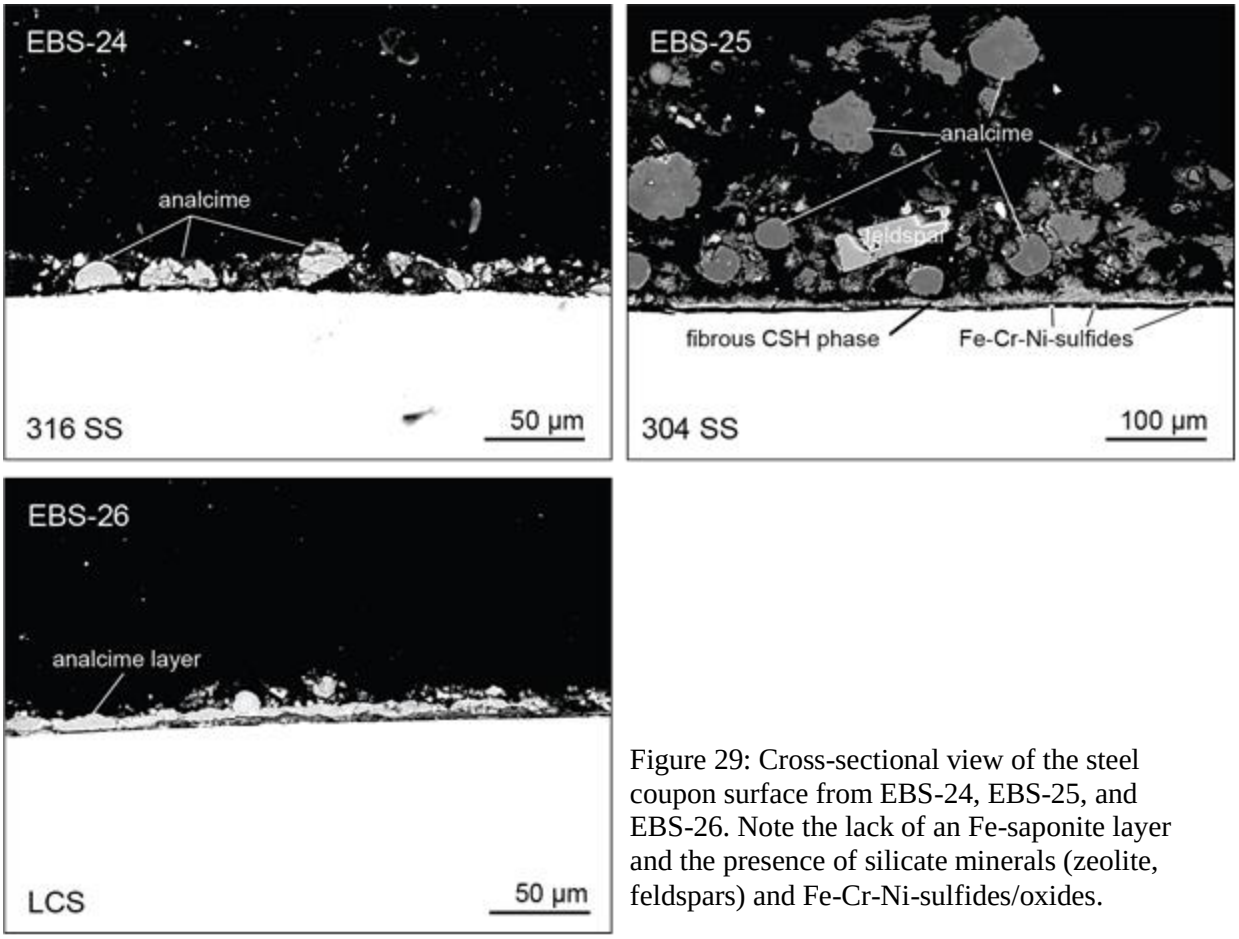

Figure 29: Cross-sectional view of the steel coupon surface from EBS-24, EBS-25, and EBS-26. Note the lack of an Fe-saponite layer and the presence of silicate minerals (zeolite, feldspars) and Fe-Cr-Ni-sulfides/oxides.

In experiments that included ordinary Portland cement powder, different mineral phases were observed at the steel coupon surface. In comparison, in the cement experiments, the steel surface provides a substrate for the formation of zeolite (analcime) and CSH phases. Instead, calcium-silicate-hydrate minerals (e.g., tobermorite), analcime, garronite (Ca-rich zeolite) and amorphous CSH minerals. The alkaline pH of the bulk system and difference in bulk chemistry in the system are reflected in the localized environment around the steel coupons, which ultimately inhibited steel corrosion and instead provided a substrate for the newly precipitated layers of CSH minerals and analcime at the steel interface.

In the cement experiments where circum-neutral pH values were observed (EBS-30 and EBS-31) the mineral phases attached to the steel coupon surface more closely matched the assemblage observed in the Wyoming bentonite + Opalinus Clay experiments (i.e., an oxide layer followed by a layer of Fe-saponite).

4.5.3 Steel Corrosion Summary

The results from the experiments discussed here indicate that the waste container will act as a substrate for mineral growth. At pH values between 4 and 7, we observe surface-bound minerals in response to steel corrosion that likely formed via direct crystallization from the solution in their specific localized environment surrounding the metal plates. The iron in the newly precipitated mineral layers at the steel interface is sourced as the steel corrodes; however, the steel coupons from this study have yet to be evaluated for general and localized corrosion. Future work is needed to address the extent these mineral precipitants influence the engineered barrier performance or the repository system as a whole, and to whether these minerals (e.g., Fe-saponite) will act as a passive protecting layer against further corrosion of the waste containers. In experiments where pH is elevated due to the influence of OPC powder, steel corrosion is inhibited and the surface of the coupons act as substrates for zeolite and CSH mineral crystallization.

5. Conclusions

The work in FY21 aimed to further develop concepts for a high-temperature, argillite-hosted repository with respect to: 1) bentonite-cement interaction, 2) bentonite-steel interaction, and 3) novel EBS additives. Characterization of a 6-month experiment and two 8-week experiments were completed during the FY (EBS-27, EBS-28, and EBS-29) and two 6-week experiments were completed (EBS-30 and EBS-31). This report presents new results and interpretations from our series of experiments with Opalinus Clay, Wyoming bentonite, and ordinary Portland cement (EBS-23 through EBS-28, EBS-30, EBS-31), new measurements of mineral (e.g., Fe-saponite, zeolite) growth rates on the surface of reacted steel coupons, and results from our first experiment investigating the use of apatite as a radionuclide isolating additive material.

Concepts developed include:

1. Bentonite stability in argillite:
   - Montmorillonite is stable over the experimental time period (6 weeks to 6 months) at circum-neutral pH values and low bulk system [K^+]
   - Zeolite formation is observed at 300ºC but not 200ºC
   - Zeolite/aluminosilicate mineral reactions buffer the solution chemistry and pH
   - Recrystallization of montmorillonite to illite is not observed, zeolite forming reactions are kinetically favored

2. Portland cement effects:

Uncured OPC powder
   - The addition of uncured ordinary Portland cement powder results in precursor montmorillonite dissolution and the formation of abundant feldspar, zeolite, CSH, and amorphous phases
   - Significant montmorillonite alteration occurs in the experiments with OPC powder, including recrystallization to illite and loss of swelling capacity

- The pH increase observed with the inclusion of OPC powder is temperature dependent: the pH of the cement-bearing experimental system at 200ºC stabilizes at pH (at 25ºC) values around 8 to 9, whereas at 300ºC, pH rapidly drops to ~6.

Cured OPC chip

- Inclusion of cured cement results in different geochemical and mineralogical effects in comparison to OPC powder
- Lower pH values are observed in the experiments with cured Portland cement
- Portlandite dissolution results in early elevated pH values, but pH values stabilize to 6–7 by the second week of experiment time.
- Montmorillonite is likely stable in the experiments with the cured chip.
- Zeolite formation is observed throughout the clay groundmass of the reaction products.

3. Steel-bentonite interface alteration:
   - Mineralization at the steel-bentonite interface varies with system bulk chemistry
   - Fe is transferred to the bentonite buffer in the form of Fe-rich phyllosilicate phases at circum-neutral pH
   - In a cementitious, high-pH environment, Fe-rich aluminosilicate phases are not observed; zeolite and CSH minerals are observed attached to the steel surface

4. Apatite-bentonite interaction:
   - Preliminary results suggest that apatite was unreactive in the bentonite
   - Minor apatite dissolution may have occurred based on observed phosphate concentrations in reaction fluids

Future research will emphasize the following areas:

- Detailed geochemical modelling of the effects of cement on aqueous geochemistry of the experimental system.
- Incorporation of low-pH cement materials into the argillite experimental system.
- Clay mineral analyses of experiment products with cured cement.
- Conduct investigation into the physical properties of Fe-saponite and other mineral products observed at the steel-bentonite interface.
- Apatite stability in different geochemical EBS environments (i.e., cementitious).
- Incorporate results into generic modeling codes.

6. Acknowledgements

We would like to thank Oana Marina for water chemistry analyses and Rose Harris for the XRF analyses. Scanning electron microscopy facilities were provided by the Materials Science and Technology group at Los Alamos National Laboratory. Dr. Lindsey Hunt at the University of Oklahoma was instrumental in the obtaining of EMP analyses. Funding was through the Department of Energy's Spent Fuel and Waste Science and Technology.

7. References

Adler, M., Mäder, U. K. ,and Waber, H. N. (1999). High-pH alteration of argillaceous rocks: an experimental study. Schweizerische Mineralogische und Petrographische Mitteilungen, 79, 445–454.

Alonso, M. C., Calvo, J. L. G., Cuevas, J., Turrero, M. J., Fernández, R., Torres, E., and Ruiz, A. I. (2017). Interaction processes at the concrete-bentonite interface after 13 years of FEBEX-Plug operation. Part I: Concrete alteration. Physics and Chemistry of the Earth, Parts A/B/C, 99, 38-48.

Balmer, S., Kaufhold, S. and Dohrmann, R. (2017). Cement-bentonite-iron interactions on small scale tests for testing performance of bentonites as a barrier in high-level radioactive waste repository concepts. Applied Clay Science, 135, 427-436.

Bayliss, P. and Levinson, A. A. (1970). Clay-mineralogy and boron determinations of the shales from the Reindeer well, Mackenzie River delta, NWT, Canada. Bulletin of Canadian Petroleum Geology, 18(1), 80-83.

Betkowski, W. B., Harlov, D. E., and Rakovan, J. F. (2016). Hydrothermal mineral replacement reactions for an apatite-monazite assemblage in alkali-rich fluids at 300–600°C and 100 MPa. American Mineralogist, 101, 2620-2637.

Bish, D. L. and Aronson, J. L. (1993). Paleogeothermal and paleohydrologic conditions in silicic tuff from Yucca Mountain, Nevada. Clays and Clay Minerals, 41(2), 148-161.

Bossart, P.J. and Thury, M. (2008). Mont Terri Rock Laboratory: Project, Programme 1996 to 2007 and Results, no. 3. Reports of the Swiss Geological Survey, Wabern.

Bossart, P. and Milnes, A. G. (2017). Mont Terri Rock Laboratory, 20 Years: Two Decades of Research and Experimentation on Claystones for Geological Disposal of Radioactive Waste (Vol. 5): Birkhäuser.

Bryan, C. R., Enos, D. G., Brown, N., Brush, L., Miller, A. and Norman, K. (2011). Engineered Materials Performance: Gap Analysis and Status of Existing Work. FCRD-USED-2011-000407. US Department of Energy.

Calvo, J. G., Hidalgo, A., Alonso, C. and Luco, L. F. (2010). Development of low-pH cementitious materials for HLRW repositories: Resistance against ground waters aggression. Cement and Concrete Research, 40(8), 1290-1297.

Cameron, M., Wang, L. M., Crowler, K. D. and Ewing, R. C. (1992). HRTEM observations on electron-irradiation damage in F-apatite. In G.W. Bailey, J. Bentley, and A. Small, Eds., Proceedings of the 50th Annual Meeting of the Electron Microscopy Society of America, p. 378. San Francisco Press, California.

Caporuscio, F. A., Cheshire, M. C., Rearick, M. S., and Jove Colón, C. (2014). LANL argillite EBS experimental program 2014. (FCRD-USED-2014-000491). Los Alamos National Lab. (LANL), Los Alamos, NM (United States).

Caporuscio, F. A., Cheshire, M. C., Palaich, S., Norskog, K. and Jove Colón, C. (2015). Argillite Disposal R&D-LANL 2015. Summary of baseline experiments for generic repository engineered barriers. (FY 2015). (FCRD-UFD-2015-000356, LA-UR-15-26110). Los Alamos National Lab. (LANL), Los Alamos, NM (United States).

Caporuscio, F.A., and Norskog, K. (2017). Disposal Overpack and Waste Package Options – LANL Petrographic descriptions of FEBEX Section 49 - Dismantlement Phase operation. (SFWD-SFWST-2017-000116, LA-UR -17-28576) Los Alamos National Lab. (LANL), Los Alamos, NM (United States).

Caporuscio, F. A., Sauer, K. B., Houser, L., Rock, M. (2018). Argillite R&D and International Collaborations – LANL. (SF-18LA01030102 Rev.2/SF-18LA01030106, LA-UR-18-27277) Los Alamos National Lab. (LANL), Los Alamos, NM (United States).

Caporuscio, F. A., Sauer, K. B., Rock, M. (2019). Argillite Disposal R&D – LANL (FY19). (SF-19LA01030801/SF-19LA01030805, LA-UR-19-24397). Los Alamos National Lab. (LANL), Los Alamos, NM (United States).

Caporuscio, F. A., Sauer, K. B., Rock, M. (2019). Argillite Disposal R&D – LANL (FY20). (SF-21LA01030101 Rev2/ SF-21LA01030102, LA-UR-20-24308). Los Alamos National Lab. (LANL), Los Alamos, NM (United States).

Chen, Y. G., Sun, Z., Cui, Y. J., Ye, W. M. and Liu, Q. H. (2019). Effect of cement solutions on the swelling pressure of compacted GMZ bentonite at different temperatures. Construction and Building Materials, 229, 116872.

Chermak, J.A. (1992). Low temperature experimental investigation of the effect of high pH NaOH solutions on the opalinus shale, Switzerland. Clays and Clay Minerals, 40, 650-658.

Cheshire, M. C., Caporuscio, F. A., Jove Colón, C. and McCarney, M. K. (2013). Alteration of clinoptilolite into high-silica analcime within a bentonite barrier system under used nuclear fuel repository conditions. Proceeding from the 14th International High-Level Radioactive Waste Management Conference, 410-415.

Cheshire, M. C., Caporuscio, F. A., Jove Colón, C. and McCarney, M. K. (2014). Bentonite Clay evolution at elevated pressures and temperatures: An experimental study for generic nuclear repositories. American Mineralogist, 99, 1662-1675.

Cheshire, M. C., Caporuscio, F. A., Jove Colón, C. and Norskog K. E. (2018). Fe-saponite growth on low-carbon and stainless steel in hydrothermal-bentonite experiments. Journal of Nuclear Materials, 2018. 511: p. 353-366.

Chew, D. M., Babechuk, M. G., Cogné, N., Mark, C., O'Sullivan, G. J., Henrichs, I. A., ... and McKenna, C. A. (2016). (LA, Q)-ICPMS trace-element analyses of Durango and McClure Mountain apatite and implications for making natural LA-ICPMS mineral standards. Chemical Geology, 435, 35-48.

Chipera, S. J. and Bish, D. L. (2002). FULLPAT: a full-pattern quantitative analysis program for X-ray powder diffraction using measured and calculated patterns. Journal of Applied Crystallography, 35, 744–749.

Chung, F. H. (1974). Quantitative interpretations of X-ray diffraction patterns of mixtures. I. Matrix flushing method for quantitative multicomponent analysis. Journal of Applied Crystallography, 7, 519-525.

Cuevas, J., De La Villa, R. V., Ramírez, S., Sánchez, L., Fernández, R. and Leguey, S. (2006). The alkaline reaction of FEBEX bentonite: a contribution to the study of the performance

of bentonite/concrete engineered barrier systems. Journal of Iberian Geology, 32(2), 151-174.

De La Villa, R. V., Cuevas, J., Ramírez, S. and Leguey, S. (2001). Zeolite formation during the alkaline reaction of bentonite. European Journal of Mineralogy, 13(3), 635-644.

Dohrmann, R. and Kaufhold, S. (2014). Cation exchange and mineral reactions observed in MX 80 buffer samples of the Prototype repository in situ experiment in Äspö, Sweden. Clays and Clay Minerals. 62, 357–373. https://doi.org/10.1346CCMN.2014.0620501.

Dohrmann, R., Kaufhold, S. and Lundqvist, B. (2013). The role of clays for safe storage of nuclear waste. Pp. 677–710 in: Developments in Clay Science (Vol. 5). Elsevier. doi: https://doi.org/10.1016/B978-0-1201 08-098259-5.00024-X.

Dolder, F., Mäder, U. and Jenni, A. (2014). Stability of bentonite under high-pH conditions. https://www.researchgate.net/profile/Florian_Dolder/publication/274390805_Stability_of_bentonite_under_high-pH_conditions/links/551ed2860cf2f9c1304da570.pdf

Eberl, D. D. (1993). Three zones for illite formation during burial diagenesis and metamorphism. Clays and Clay Minerals, 41(1), 26-37.

Fernández, R., Cuevas, J., Sánchez, L., de la Villa, R. V. and Leguey, S. (2006). Reactivity of the cement–bentonite interface with alkaline solutions using transport cells. Applied Geochemistry, 21(6), 977-992.

Fernández, R., Cuevas, J., & Mäder, U. K. (2009a). Modelling concrete interaction with a bentonite barrier. European Journal of Mineralogy, 21(1), 177-191.

Fernández, R., Mäder, U. K., Rodríguez, M., De La Villa, R. V., & Cuevas, J. (2009b). Alteration of compacted bentonite by diffusion of highly alkaline solutions. European Journal of Mineralogy, 21(4), 725-735.

Fernández, R., González, L., Ruiz, A. I., and Cuevas, J. (2014). Nature of C-(A)-S-H Phases Formed in the Reaction Bentonite/Portlandite. Journal of Geochemistry, vol. 2014, Article ID 145425, 8 pages, 2014. https://doi.org/10.1155/2014/145425.

Fernandez, Raúl, Ruiz, A. I. and Cuevas, J. (2016). Formation of C-A-S-H phases from the interaction between concrete or cement and bentonite. Clay Minerals, 51(02), 223-235. doi:10.1180/claymin.2016.051.2.09

Fernández, R., Torres, E., Ruiz, A. I., Cuevas, J., Alonso, M. C., Calvo, J. L. G., ... and Turrero, M. J. (2017). Interaction processes at the concrete-bentonite interface after 13 years of FEBEX-Plug operation. Part II: Bentonite contact. Physics and Chemistry of the Earth, Parts A/B/C, 99, 49-63.

Fernandez, A. M., Kaufhold, S., Sánchez-Ledesma, D. M., Rey, J. J., Melón, A., Robredo, L. M., ... and Clavero, M. A. (2018). Evolution of the THC conditions in the FEBEX in situ test after 18 years of experiment: Smectite crystallochemical modifications after interactions of the bentonite with a C-steel heater at 100° C. Applied Geochemistry, 98, 152-171.

Ferrage, E., Vidal, O., Mosser-Ruck, R., Cathelineau, M. and Cuadros, J. (2011). A reinvestigation of smectite illitization in experimental hydrothermal conditions: Results from X-ray diffraction and transmission electron microscopy. American Mineralogist, 96, 207-223.

Frape, S. K., Blyth, A., Blomqvist, R., McNutt, R. H., Gascoyne, M. (2003). 5.17 - deep fluids in the continents: II. Crystalline rocks A2 - holland, heinrich D, in: K.vK. Turekian (Ed.), Treatise on Geochemistry, Pergamon, Oxford, 541-580.

Gailhanou, H., Lerouge, C., Debure,M., Gaboreau, S., Gaucher, E. C., Grangeon, S., Grenèche, J.M., Kars,M.,Madé, B.,Marty, N. C.M. and Warmont, F. (2017). Effects of a thermal perturbation on mineralogy and pore water composition in a clay-rock: an experimental and modeling study. Geochimica et Cosmochimica Acta, 197, 193–214. https://doi.org/10.1016/j.gca.2016.10.004.

Guillaume, D., Neaman, A., Cathelineau, M., Mosser-Ruck, R., Peiffert, C., Abdelmoula, M., Dubessy, J., Villieras, F., Baronnet, A. and Michau, N. (2003). Experimental synthesis of chlorite from smectite at 300°C in the presence of metallic Fe. Clay Minerals, 38, 281-302.

Hardin, Ernest, Hadgu, Teklu, and Clayton, Daniel James. (2015). Cavern/Vault Disposal Concepts and Thermal Calculations for Direct Disposal of 37-PWR Size DPCs. United States: N. Web. doi:10.2172/1172177.

Heimann, R. B. (1993). Brønsted acidification observed during hydrothermal treatment of a calcium montmorillonite. Clays and Clay Minerals, 41, 718–725. https://doi.org/10.1346/CCMN.1993.0410610.

Hofmann, H., Bauer, A. and Warr, L. N. (2004). Behavior of smectite in strong salt brines under conditions relevant to the disposal of low-to medium-grade nuclear waste. Clays and Clay Minerals, 52, 14–24. https://doi.org/10.1346/CCMN.2004.0520102.

Honty, M., Wang, L., Osacký, M., Uhlík, P., Czímerová, A., & Madejová, J. (2012). Experimental interactions of the Opalinus Clay and Boom Clay with various repository relevant solutions at 90 C under closed conditions. Applied Clay Science, 59, 50–63. https://doi.org/10.1016/j.clay.2012.02.011.

Jacques, D., Wang, L., Martens, E. and Mallants, D. (2010). Modelling chemical degradation of concrete during leaching with rain and soil water types. Cement and Concrete Research, 40(8), 1306-1313.

Johannesson, L. E., Börgesson, L., Goudarzi, R., Sandén, T., Gunnarsson, D. and Svemar, C. (2007). Prototype repository: A full scale experiment at Äspö HRL. Physics and Chemistry of the Earth, Parts A/B/C, 32, 58–76. https://doi.org/10.1016/j.pce.2006.04.027. 1252

Johnston, R.M. and Miller, H.G. (1984). The effect of pH on the stability of smectite (No. AECL–8366). Atomic Energy of Canada Ltd.

Karnland, O. (1997). Cement/bentonite interaction. Results from 16 month laboratory tests (No. SKB-TR--97-32). Swedish Nuclear Fuel and Waste Management Co.

Karnland, O., Olsson, S., Nilsson, U. and Sellin, P. (2007). Experimentally determined swelling pressures and geochemical interactions of compacted Wyoming bentonite with highly alkaline solutions. Physics and Chemistry of the Earth, Parts A/B/C, 32(1-7), 275-286.

Kaufhold, S. and Dohrmann, R. (2009). Stability of bentonites in salt solutions | sodium chloride. Applied Clay Science, 45, 171–177. https://doi.org/10.1016/j.clay.2009.04.011.

Kaufhold, S. and Dohrmann, R. (2010). Stability of bentonites in salt solutions: II. Potassium chloride solution—Initial step of illitization? Applied Clay Science, 49, 98–107. https://doi. org/10.1016/j.clay.2010.04.009.

Kaufhold, S., Dohrmann, R. and Ufer, K. (2020). Determining the extent of bentonite alteration at the bentonite/cement interface. Applied Clay Science, 186, 105446.

Khalifa, A. Z., Cizer, Ö., Pontikes, Y., Heath, A., Patureau, P., Bernal, S. A., & Marsh, A. T. (2020). Advances in alkali-activation of clay minerals. Cement and Concrete Research, 132, 106050.

Kloprogge, J. T., Komarneni, S. and Amonette, J. E. (1999). Synthesis of Smectite Clay Minerals: A Critical Review. Clay and Clay Minerals, 47, 529–554.

Konzett, J., Rhede, D., and Frost, D. J. (2012) The high PT stability of apatite and Cl partitioning between apatite and hydrous potassic phases in peridotite: an experimental study to 19 GPa with implications for the transport of P, Cl and K in the upper mantle. Contributions to Mineralogy and Petrology volume 163, pages 277–296.

Krejzler, J., and Narbutt, J. (2003) Adsorption of strontium, europium, and americium(III) ions on a novel adsorbent Apatite II. Nukleonika, 48, 171–175.

Kursten, B., Cornelis, B., Labat, S. and Van Iseghem, P. (1996). Geological Disposal of Conditioned High-Level and Long Lived Radioactive Waste. In situ experiments, Report R-3121, SCK•CEN (Mol, Belgium).

Kursten, B., Cornelis, B., Labat, S. and Van Iseghem, P. (1997). Completion of the Corrosion Programme in Boom Clay – in situ experiments, Report EUR-17105, SCK•CEN (Mol, Belgium).

Kursten, B., Smailos, E., Azkarate, I., Werme, L., Smart, N.R. and Santarini, G. (2004). COBECOMA. State of the art document on the Corrosion Behaviour of Container Materials.

Larsen M.J., Jensen, S.J. (1989) Stability and mutual conversion of enamel apatite and brushite at 20 °C as a function of pH of the aqueous phase. Archive Oral Biology, 34, 963-968.

Lothenbach, B., Scrivener, K. and Hooton, R. D. (2011). Supplementary cementitious materials. Cement and concrete research, 41(12), 1244-1256.

Lukens, W. W., Moore, R. C., and Holt, K.C. (2006) Workshop on Development of Radionuclide Getters for the Yucca Mountain Waste Repository: Proceedings. Sandia Report, SAND2006-0947. Sandia National Laboratory, Albuquerque, N.M. 68pp.

Madsen, F.T. (1998). Clay mineralogical investigations related to nuclear waste disposal. Clay Minerals, 33, 109-129.

Martin, P. L., Barcala, J. M. and Huertas, F. (2006). Large-scale and long-term coupled thermo-hydro-mechanic experiments with bentonite: the FEBEX mock-up test. Journal of Iberian Geology, 32, 259–282.

Martinez, V., Abós, H. and García-Siñeriz, J. L. (2016). FEBEXe: Final Sensor Data Report (FEBEX "in situ" Experiment) - Arbeitsbericht NAB 16-19, National Cooperative for the Disposal of Radioactive Waste (NAGRA), Wettingen, Switzerland.

Meldrum, A., Wang, L.M., and Ewing, R.C. (1997) Electron-irradiation-induced phase segregation in crystalline and amorphous apatite: A TEM study. American Mineralogist, (82), 858–869.

Meunier, A., Velde, B., and Griffault, L. (1998). The reactivity of bentonites: A Review. An application to clay barrier stability for nuclear waste storage. Clay Minerals, 33, 187-196.

Moore, D. M. and Reynolds, R.C. (1989). X-ray Diffraction and the identification and analysis of clay minerals. Oxford University Press, New York, New York, 377.

Moore, R. C., Zhao, H., Sanchez, C. A., Holt, K. C., Salas, F., Hasan, A. A. M. and Lucero, D. A. (2002). In situ formation of apatite in soil and groundwater for containment of radionuclides and heavy metals (No. SAND2002-3642). Sandia National Labs., Albuquerque, NM (US); Sandia National Labs., Livermore, CA (US).

Mosser-Ruck, R., Cathelineau, M., Baronnet, A. and Trouiller, A. (1999). Hydrothermal reactivity of K-smectite at 300°C and 100 bar: dissolution-crystallization process and non-expandable dehydrated smectite formation. Clay Minerals, 34, 275–290.

Mosser-Ruck, R., Cathelineau, M., Guillaume, D., Charpentier, D., Rousset, D., Barres, O., and Michau, N. (2010). Effects of Temperature, pH, and Iron/Clay and Liquid/Clay Ratios on Experimental Conversion of Dioctahedral Smectite to Berthierine, Chlorite, Vermiculite, or Saponite. Clays and Clay Minerals, 58, 280-291.

Mosser Ruck, R., Pignatelli, I., Bourdelle, F., Abdelmoula, M., Odile Barres, O., Guillaume, D., Charpentier, D., Rousset, D., · Cathelineau, M., and Michau, N. (2016). Contribution of long term hydrothermal experiments for understanding the smectite to chlorite conversion in geological environments. Contributions to Mineralogy and Petrology, 171, 97-118.

Müller, H.R. et al. (2018) Implementation of the full-scale emplacement (FE) experiment at the Mont Terri rock laboratory. In: Mont Terri Rock Laboratory, 20 Years (P. Bossart and A.Milnes, editors). Swiss Journal of Geosciences Supplement, vol 5. Birkhäuser, Cham. https://doi.org/10.1007/978-3-319-70458-6_15

NAGRA (2002). Technischer Bericht 02-03, Projekt Opalinuston: Synthese der geowissenschaftlichen Untersuchungsergebnisse, December 2002.

Neuhoff, P. S., & Ruhl, L. S. (2006). Mechanisms and geochemical significance of Si–Al substitution in zeolite solid solutions. Chemical Geology, 225, 373–387.

Omel'yanenko, B. I., Livshits, T. S., Yudintsev, S. V. and Nikonov, B. S. (2007). Natural and artificial minerals as matrices for immobilization of actinides. Geology of Ore Deposits, 49(3), 173-193.

Pearson, F.J., Arcos, D., Bath, A., Boisson, J.-Y., Fernandez, A.M., Gabler, H.-E., Gaucher, E., Gautschi, A., Griffault, L., Hernan, P., and Waber, H.N. (2003). Mont Terri Project-geochemistry of water in the opalinus clay formation at the Mont Terri Rock Laboratory. Reports of the Federal Office for Water and Geology (FOWG), Geology Series No. 5.

Pouchou, J. L. and Pichoir, F. (1985). "PAP" φ(ρz) correction procedure for improved quantitative microanalysis. Microbeam Analysis, Ed. Armstrong, J.T., San Francisco Press, 104-106.

Pusch, R. (1979). Highly compacted sodium bentonite for isolating rock-deposited radioactive waste products. Nuclear Technology, 45, 153-157.

Pusch, R. (2008). Geological Storage of Radioactive Waste. Springer-Verlag, Berlin, Germany, 379.

Pusch, R. and Madsen, F. T. (1995). Aspects on the illitization of the Kinnekulle bentonites. Clays and Clay Minerals, 43(3), 261-270.

Pusch, R. and Kasbohm, J. (2002). Alteration of MX-80 by hydrothermal treatment under high salt content conditions. Svensk Kärnbränslehantering Technical Report, TR-02-06, 44.

Pusch, R. Takase, H., and Benbow, S. (1998) Chemical Processes causing cementation in heat-affected smectite- the Kinnekulle bentonite. Svensk Kärnbränslehantering Technical Report, TR-98-25, 62.

Redkin, A. F. and Hemley, J. J. (2000). Experimental Cs and Sr sorption on analcime in rock-buffered systems at 250–300 C and Psat and the thermodynamic evaluation of mineral solubilities and phase relations. European Journal of Mineralogy, 12(5), 999-1014.

Rigali, M.J., Brady, P.V., and Moore, R.C. (2016). Radionuclide removal by apatite. Am Min, 101, 2611–2619.

Sauer K., Caporuscio, F., Rock, M., Cheshire, M. and Jove Colon, C. (2020). Hydrothermal interactions of Wyoming bentonite and Opalinus clay. Clay and Clay Minerals, in press.

Savage, D., Noy, D., & Mihara, M. (2002). Modelling the interaction of bentonite with hyperalkaline fluids. Applied Geochemistry, 17(3), 207-223.

Savage, D., Watson, C., Benbow, S. and Wilson, J. (2010). Modelling iron-bentonite interactions. Applied Clay Science, 47(1-2), 91-98.

Savage, D., Wilson, J., Benbow, S., Sasamoto, H., Oda, C. and Walker, C. (2019). Natural systems evidence for the effects of temperature and the activity of aqueous silica upon montmorillonite stability in clay barriers for the disposal of radioactive wastes. Applied Clay Science, 179, 105146. https://doi.org/10.1016/j.clay.2019.105146.

Schlegel, M. L., Bataillon, C., Benhamida, K., Blanc, C., Menut, D. and Lacour, J. L. (2008). Metal corrosion and argillite transformation at the water-saturated, high-temperature iron–clay interface: a microscopic-scale study. Applied Geochemistry, 23(9), 2619-2633.

Sellin, P., & Leupin, O. (2014). The use of clay as an engineered barrier in radioactive waste management – a review. Clays and Clay Minerals, 61, 477–498. https://doi.org/10.13461361/CCMN.2013.0610601.

Seyfried, J.R., Janecky, D.R., and Berndt, M.E. (1987). Rocking autoclaves for hydrothermal experiments II. The flexible reaction-cell system. Hydrothermal Experimental Techniques, Eds. Ulmer, G.C. and Barnes, H.L. John Wiley & Sons, 216-239.

Smailos, E., Cuñado, M. A., Azkarate, I., Kursten, B. and Marx, G. (2002). Long-Term Performance of Candidate Materials for HLW/Spent Fuel Disposal Containers, Report FZKA 6706, FZK.INE (Karlsruhe, Germany).

Smart, N. R., Fennell, P. A. H., Rance, A. P., Winsley, R. J., Reddy, B. and Kursten, B. (2011). Experimental studies of the effect of irradiation on the anaerobic corrosion of carbon steel in relation to the Belgian supercontainer concept. In EPJ Web of Conferences (Vol. 12, p. 02003). EDP Sciences.

Smart N. R., Naish C. C. And Pritchard A. M. (1999). Corrosion Principles for the Assessment of Stainless Steel Radioactive Waste Containers, Report AEAT-1337, issue C, AEAT Technologye (Harwell, UK).

Smyth, J.R. (1982). Zeolite stability constraints on radioactive waste isolation in zeolite-bearing volcanic rocks. Journal of Geology, 90, 195-201.

Środoń, J. (1980). Precise identification of illite/smectite interstratifications by X-ray powder diffraction. Clays and Clay Minerals, 28, 401-411.

Soler, J.M. (1998). Reactive transport modelling of the interaction between a high pH plume and a fractured marl. V.M. Goldschmidt Abstracts, Toulouse. Min. Mag. 62A, 1427–1428.

Steefel, C. I. and Lichtner, P. C. (1994). Diffusion and reaction in rock matrix bordering a hyperalkaline fluid-filled fracture. Geochimica et Cosmochimica Acta, 58(17), 3595-3612.

Steefel, C. I. and Lichtner, P. C. (1998). Multicomponent reactive transport in discrete fractures: II: Infiltration of hyperalkaline groundwater at Maqarin, Jordan, a natural analogue site. Journal of Hydrology, 209(1-4), 200-224.

Takase, H. (2004). Discussion on PA model development for bentonite barriers affected by chemical interaction with concrete: do we have enough evidence to support bentonite stability? International Workshop on Bentonite–Cement Interaction in Repository Environments, Nuclear Waste Management Organisation of Japan (NUMO), NUMO Report TR-04-05 (2004), pp. 172-177

Taubald, H., Bauer, A., Schäfer, T., Geckeis, H., Satir, M. and Kim, J. I. (2000). Experimental investigation of the effect of high-pH solutions on the Opalinus Shale and the Hammerschmiede Smectite. Clay Minerals, 35(3), 515-524.

Watson, C., Benbow, S., & Savage, D. (2007). Modelling the interaction of low pH cements and bentonite. Issues affecting the geochemical evolution of repositories for radioactive waste (No. SKI-R--07-30). Swedish Nuclear Power Inspectorate.

Watson, C., Hane, K., Savage, D., Benbow, S., Cuevas, J. and Fernandez, R. (2009). Reaction and diffusion of cementitious water in bentonite: results of 'blind' modelling. Applied Clay Science, 45(1-2), 54-69.

Watson, C., Wilson, J., Savage, D. Norris, S. (2018). Coupled reactive transport modelling of the international Long-Term Cement Studies project experiment and implications for radioactive waste disposal. Applied Geochemistry, 97, 134-146.

Wersin, P., Johnson, L.H., and McKinley, I.G. (2007). Performance of the bentonite barrier at temperatures beyond 100°C: A critical review. Physics and Chemistry of the Earth, 32, 780-788.

Wieczorek, K., Gaus, I., Mayor, J. C., Schuster, K., García-Siñeriz, J.-L., & Sakaki, T. (2017). In-situ experiments on bentonite-based buffer and sealing materials at the Mont Terri rock laboratory (Switzerland). Swiss Journal of Geoscience., 110, 253–268. https://doi.org/10.1007/s00015-016-0247-y.

This page is intentionally left blank.

Chapter 2

Argillite International Collaboration

SPENT FUEL AND WASTE SCIENCE AND TECHNOLOGY

ARGILLITE DISPOSAL R&D AND ARGILLITE INTERNATIONAL COLLABORATIONS – LANL

CHAPTER 2: Argillite International Collaborations

1. Horonobe URL Research

1.1 Background

The geologic disposal of high-level radioactive waste at the Horonobe Underground Research Center is the focus of this research. Japan initiated a 20-year investigation on deep geologic disposal of high-level radioactive waste in 2000. The Japan Nuclear Cycle Development Institute (JNC) and later the Japanese Atomic Energy Agency (JAEA) have investigated disposal in both crystalline and argillite rock types. The first underground research laboratory (URL) was emplaced in a crystalline rock type, with fresh groundwater, and is located in Mizunami, Gifu. The second URL is located in an argillite rock type, with saline groundwater, and is centered at Horonobe (Hokkaido). Operational activities at the Horonobe URL, including detailed in-situ experiments, were detailed in Hama et al. (2007). The most recent full scale experimental design was described at the DECOLOVEX 2023 meeting (JAEA, 2021) and is illustrated in Figure 1.

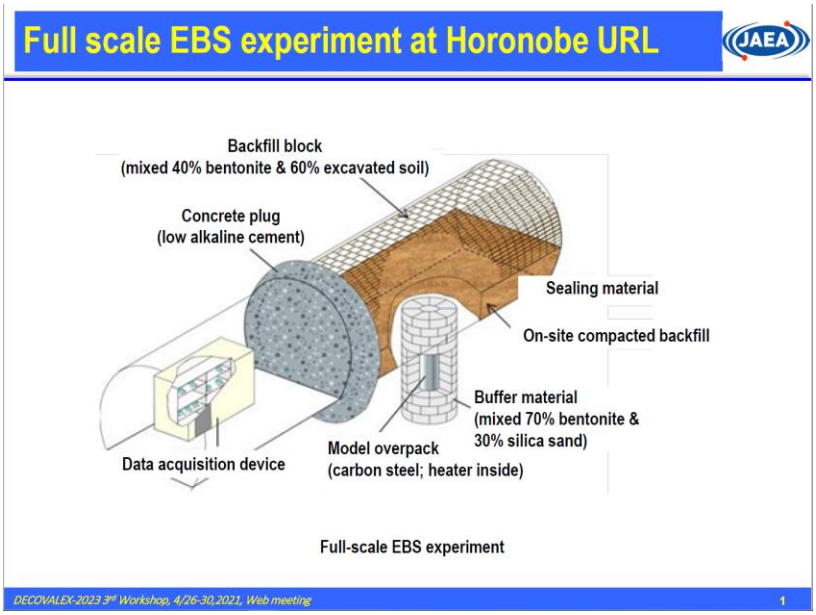

Figure 30: Simplified depiction on the full-scale EBS experiment at the Horonobe URL (JAEA, 2021).

1.2 Summary of FY20 Horonobe Report

We requested Kunigel bentonite and target Horonobe URL host rock (Wakkanai Formation) from the JAEA. This request was recommended to our Sandia project managers in November 2019. At present, we have not received an update from our JAEA counterparts as to when the material will be shipped.

In FY20, we performed a literature review and summarized the following: 1). Regional geology of the western coastal plain of Hokkaido, northern Japan. Major documents included geologic maps and stratigraphic columns of the region encompassing the URL (Wei & Seno, 1998; Ishii, 2012; Ishii et al., 2010). 2). Lithology of the Wakkanai and Koetoi Formations (the target URL repository horizon), which were well documented by Iijima and Tada, 1981; Tada and Iijima, 1982, Kemp et al., 2002; Barnes & Milodowski, 2004; Milodowski et al., 2004, Ishii et al., 2010. 3). Regional structural geology, such as faults and large-scale structures were addressed by Kunimari et al. (2010) and Milodowski et al. (2004), and 4). Finally, the water chemistry of the URL area was discussed by Hama et al. (2007).

All of these summarized four sections are described in more detail in Caporuscio et al. (2020).

1.3 FY21 LANL Experiments

Our initial experimental plan for FY21 was to mimic the full-scale EBS test that is currently underway at the Honorobe URL. The full-scale test includes multiple phases of heating and groundwater injection (Figure 1). The experiments we proposed to run would contain combinations of the following components: Kunigel bentonite (EBS buffer material) + quartz, Wakkanai Formation wall rock, synthetic Wakkanai groundwater (formulated after Hama et al., 2007), and low carbon steel (waste canister material). The experiments will be conducted between 125 to 200°C and at hydrostatic pressure (~150 bar). The synthetic groundwater composition was developed from water chemistry described by Hama et al. (2007) for the Horonobe area. The full data set was presented in Caporuscio et al. (2020). From the 14 analyses, we restricted the field to Wakkanai Formation waters greater than 300 meters in depth. The resulting seven analyses were then averaged to produce a “synthetic” Wakkanai groundwater (Table 1). This methodology is similar to the one used to develop the synthetic brines (example ERDA-9) used for Waste Isolation Pilot Plant (WIPP) experiments by DOE. Our experiments would provide insight into mineralogical and geochemical changes that may occur in the EBS region.

Table 7: Average synthetic groundwater composition developed to mimic Wakkanai Formation groundwater at depths greater than 300 meters. The composition is an average of seven different groundwater samples with an average depth of 431 m.

	pH	Na^+	K^+	Ca^{2+}	Mg^{2+}	Si	Fe_T	Cl^-	Br-	I^-	SO_4	HCO_3
Synthetic Wakkanai Groundwater	7.1	3577	81.0	100	66.0	26.0	1.0	4740	17.0	12.0	17.0	1745

Chemical concentrations in mg/L.

There were logistical problems obtaining the Kunigel bentonite and Wakkanai Formation wall rock from JAEA. After our Sandia National Laboratory contact informed us that samples may be held up for longer than this past year, we made contact with the mining company, Kunimine Kogyo Co., Ltd, in Japan that produces Kunigel V. Upon my request, within one week, one kilogram of Kunigel V1 arrived at Los Alamos National Laboratory on April 30, 2021 from Kunimine Kogyo Co., Ltd.

We plan to run a series of experiments using Kunigel bentonite in FY22 for the Argillite International Collaboration work package. The experiment will be at 200ºC and 150 bar with Kunigel bentonite/quartz sand (70:30 ratio) with or without low carbon steel coupons. The water rock ratio will be set at 11:1. Once the experiments are complete, the mineralogy and geochemistry of the reaction products will be evaluated by a variety of characterization methods (e.g. scanning electron microscopy, X-ray diffraction, electron microprobe, aqueous geochemistry analyses, and modelling).

1.4 References

Barnes, R. P. and Milodowski, A. E. (2004): Characterisation of Fractures in Horonobe. Boreholes HDB-6, HDB-7 and HDB-8: Results of core examination, February 2004. BGS Report CR/04/043, BGS, Keyworth, UK.

Caporuscio, F.A., Sauer, K.B., and Rock, M.J. (2020) Argillite Disposal R&D and Argillite International Collaborations – LANL. (SF-20LA01030102 / SF-20LA01030106, LA-UR-20-24308). Los Alamos National Lab. (LANL), Los Alamos, NM (United States).

Hama, K., Kunimaru, T., Metcalfe, R., and Martin, A. J. (2007) The hydrochemistry of argillaceous rock formations at the Horonobe URL site, Japan. *Phys. Chem. Earth*, 32, 170-180.

Iijima, A. and Tada, R. (1981). Silica diagenesis of Neogene diatomaceous and volcaniclastic sediments in northern Japan. *Sedimentology*, 28, 185-200.

Ishii, E. (2012). Microstructure and origin of faults in siliceous mudstone at the Horonobe Underground Research Laboratory site, Japan. *Jour. Struc. Geol*., 34, 20-29.

Ishii, E., Funaki, H., Tokiwa, T., and Ota, K. (2010). Relationship between fault growth mechanism and permeability variations with depth of siliceous mudstones in northern Hokkaido, Japan. *Jour. Struc. Geol*., 32, 1792-1805.

JAEA (2021) Presentation at DECOVALEX-2023 3rd Workshop, April 23-30, 2021, Web meeting.

Kemp, S. J., Cave, M. R., Hodgkinson, E., Milodowski, A. E. and Kunimaru, T. (2002). Mineralogical Observations and Interpretation of Porewater Chemistry from the Horonobe Deep Boreholes HDB-1 and HDB-2, Hokkaido, Japan. *BGS Report CR/02/303*, BGS, Keyworth, UK.

Kunimaru, T., Ota, K., Alexander, W. R., and Yamamoto, H. (2010). Groundwater/Porewater Hydrochemistry at Horonobe URL: Data Freeze I - Preliminary Data Quality Evaluation for Boreholes HDB-9, 10 and 11 - Geological Isolation Research and Development Directorate, Japan Atomic Energy Agency, JAEA-Research 2010-035.

Milodowski, A. E., Barnes, R. P., Kemp, S. J., Bouch, J. and Wagner, D. (2004). Characterisation of fractured rock and fracture mineralisation. *Horonobe Boreholes HDB-6, HDB-7 and HDB-8: Final report. BGS Report CR/04/251*, BGS, Keyworth, UK. 8.

Minoura, K, Susaki, T and Horiuchi, K. (1996). Lithification of biogenic siliceous sediments: Evidence from Neogene diatomaceous sequences of northeast Japan. *Sedimentary Geology*, 107, 45-59.

Tada, R. and Iijima, A. (1982). Petrology and diagenetic changes of Neogene siliceous rocks in northern Japan. *Journal of Sedimentary Petrology*, 53, 911–930.

Wei, D. and Seno, T. (1998). Determination of the Amurian plate motion. In: Flower, M.,Chung, S.L., Lo, C.H., Lee, T.Y. (Eds.), Mantle Dynamics and Plate Interactions in East Asia. Geodynamics Series, *American Geophysical Union*, 27, 337-346.

2. Steel corrosion experiments – FY21

2.1 Background

Steel corrosion with respect to waste canister integrity has been of significant concern to both the SFWST (Spent Fuel and Waste Science and Technology) program and international research programs for decades. The LANL experimental program in FY21 explored the effect of stainless steel welds and surface treatments (i.e., polishing) on corrosion in a high temperature and pressure EBS environment. The following summarizes previous studies that provide context for the experimental work.

Hanson et al. (2012) performed a gap analysis to evaluate the type(s) of research needed to identify data and modeling needs to develop the technical bases to enable the extended storage of UNF (Used Nuclear Fuel). Additional research is needed for most structures, systems, and components important to safety in more modern fuels and dry storage cask systems. There is also limited data on the effects of high burnup and extended storage times. Research of canister corrosion under a variety of conditions (atmospheric, aqueous, of both welded and bolted casks) was ranked as high importance. Over the years, Sandia National Laboratories (SNL) have studied stainless steel (SS) corrosion at low temperatures and various redox conditions.

Enos et al. (2013) assessed localized corrosion on 304SS due to salt delinquency. Researchers used synthetic sea water as the salt source; however, although they did not control gas phases in the experiments, they recognized that in field conditions other salt components, ammonium, and nitrate are significant in atmospheric aerosols. As a reference point, they collected dust from Calvert Cliffs interim storage site, located near the Chesapeake Bay, where the majority of the dust particles were not salt, but rather terrestrial in nature. Furthermore, they investigated the cause of localized corrosion due to deliquescence of brines and the potential for stifling at elevated temperatures and times up to 100 days. Although localized (crevice) corrosion occurred, the effect of stifling was inconclusive.

Bryan and Enos (2014) produced an interim SNL report on the results of stainless steel corrosion. In summary, the report was a continuation of the Enos et al. (2013) research and centered on four pieces of research. First, they continued a collaboration with the Electric Power Research Institute (EPRI) to collect airborne particles at two other storage sites. The sites, Hope Creek NJ, and Diablo Canyon CA, were located near marine coastal waters. The dust particles collected at Hope Creek, NJ were primarily terrestrial in nature, while the Diablo Canyon particles were more marine salts in composition. Second, they designed and fabricated a full-diameter canister mockup. Third, experimental work was carried out to evaluate crevice corrosion of 304SS in the presence of limited reactants, hoping to prove limited salt loads would limit corrosion penetration over time. However, in experiments of up to 100 days, no stifling occurred. And finally, the fourth project was to design and implement a device to deposit sea salts onto metal surfaces in a controlled manner.

Bryan and Schundelholz (2017) calculated the chemical composition of the brines that form by deliquescence of sea-salt aerosols using thermodynamic methods. With this data, they estimated brine volumes and salt/brine volume ratios as a function of temperature and atmospheric relative humidity. The authors performed experiments of simple brine compositions where they mixed representative brines and measured the physical and

electrochemical properties of those brines over a range of temperatures (up to 80ºC). The focus of these experiments was on carbonation of magnesium chloride brines, which are quite corrosive at higher temperatures.

A cooperative study between Ohio State University and SNL (Weirich et al., 2019) investigated the effect of relative humidity (RH) on the corrosion of 304SS exposed to sea salt. In their study, the total corrosion damage accumulation was higher at 40% RH than at 76% RH. These preliminary atmospheric exposure results showed that even though calculation that pit growth at 40% RH should have been slower, a lower anodic current caused by the oxidation allowed the pits to grow similar to the size of the metal exposed to the 76% RH. The researchers concluded that this phenomenon coupled with a higher pit initiation leads to higher accumulation of steel damage at 40% RH than a RH of 78%.

Chatzidakis et al. (2021) employed neutron diffraction to investigate residual stress behavior in welds. The authors determined that significant tensile residual stresses would occur in welded samples. Following weld repairs, they observed a stress redistribution and introduction of beneficial compressive stresses. By using welding repair techniques, Chatzidakis et al. (2021) believes that through-thickness growth of cracks in the welds may be avoidable.

2.2 Steel Corrosion Experiments at LANL

The main research thrust for the Argillite International Collaboration for FY21 was to focus on Japanese EBS mineralogy alteration at high temperature. However, samples were never received from the Horonobe URL site and only recently Kunigel V1 bentonite was obtained from the source mine.

To make use of the hydrothermal laboratory facilities at LANL, three experiments focusing on corrosion of welded or polished stainless steel at high temperature were requested instead. Welded stainless steel and polished stainless steel samples were obtained from SNL.

2.2.1 Methods

Experiments were designed to explore the effect stainless steel welds and polished surfaces on steel corrosion in the argillite system. The starting components and experiment parameters are reported in Table 2. One experiment was completed in FY21 and two experiments are planned to be completed in FY22. The starting solid materials include Wyoming bentonite (powder and granules) and a steel coupon. All experiments have a set water:rock ratio of 11:1 and will be run at 300ºC, 150 bars for 6 weeks. The only variation in experiment parameters will be the types/treatment of stainless steel included.

In all experiments, fluid chemistry is monitored in aqueous samples extracted during and after the experiment. For the completed experiment, solid phase reaction product characterization is ongoing and will include X-ray diffraction, scanning electron and petrologic microscopy (mineralogy and textural observations), and electron microprobe and electron dispersive spectroscopy (mineral phase chemistry). Solid and aqueous phase characterization methods are reported in Appendix A.

Table 8: Initial components and reaction conditions for STL experiments. Initial components and reaction conditions for STL experiments. Abbreviations: SS, stainless steel; WB, Wyoming Bentonite; GW, groundwater.

Exp.	Components	Temp (°C)	Pressure	Brine	Water:Rock	Run Time
STL-(W)-1	Welded 304SS + WB	300	150 bar	Opalinus GW	11:1	6 weeks
STL-(P)-2*	Polished 316SS + WB	300	150 bar	Opalinus GW	11:1	6 weeks
STL-(P)-3*	Polished 304SS + WB	300	150 bar	Opalinus GW	11:1	6 weeks

* indicates future experiments

2.2.2 Starting Material

Welded 304SS: The welded sample was originally from the SNL canister mockup (Figure 2). The larger welded 304SS was cut into smaller coupons (Figure 3). Along with Fe, 304SS contains 18 wt.% Cr, 8 wt.% Ni, < 2 wt.% Mn, < 1 wt.% Si, < 0.045 wt. % P, and < 0.03 wt.% S, and < 0.08 wt.% C.

Polished Steel: The 316SS and 304SS polished samples were used in long-term (2-year) corrosion exposure tests in an RH chamber at SNL (Figure 3). The one side was reground with 600 grit sandpaper and pitted extensively (Figure 3). Both samples were cleaned with acetone prior to use. The 304SS was similar to the welded steel sample, but the 316SS differs in the Cr/Ni ratio. The 316SS is 18.37 wt.% Cr, 12.35 wt.% Ni, 2.26 wt.% Mo, 1.619 wt.% Mn, 0.5093 wt.% Si, and 0.175 wt.% Cu.

Wyoming bentonite. The bentonite used in the present study is unprocessed and was provided by Bentonite Performance Minerals LLC from Colony, Wyoming, U.S.A. It is composed dominantly of Na-montmorillonite (general composition: $Na_{0.33}(Al,Mg)_2(Si_4O_{10})(OH)_2 \cdot nH_2O$), lesser clinoptilolite and feldspar, and minor biotite, pyrite, quartz, opal, and sulfide minerals. The QXRD results from unheated bentonite are presented in Chapter 1, Table C-1.

Opalinus Clay synthetic groundwater. Synthetic groundwater was created to mimic the pore water found in the Mont Terri Opalinus Clay (Pearson et al., 2003). This solution has a pH of around 7.5 and is a Na-Cl type solution. The initial chemistry is reported in Chapter 1, Table 3.

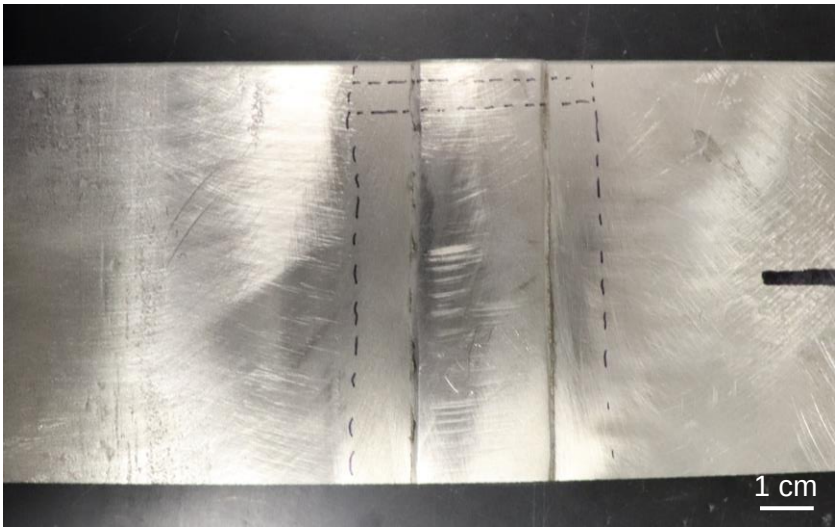

Figure 31: Original welded steel sample with cut lines. The left and right dashed lines indicate the cut to include the weld and unaltered 304SS. The smaller center dotted lines are cuts to isolate coupons across the weld that will be suitable for the experiment.

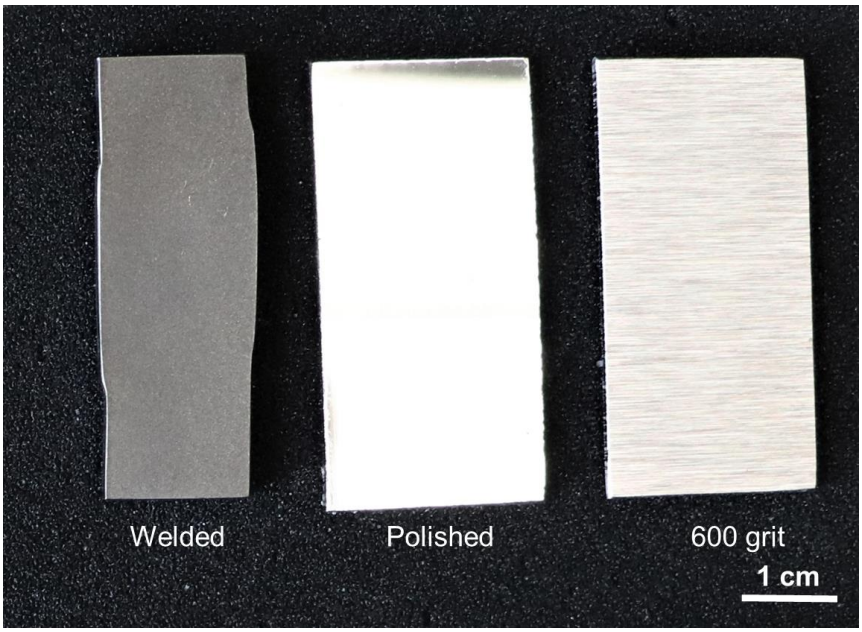

Figure 12: Examples of the welded, polished, and reground (600 grit) coupons used in the STL experiments.

2.2.3 Current Status

The steel corrosion experiments are currently ongoing. STL-(W)-1 is the only completed experiment and is undergoing characterization. More data will be provided in FY22.

2.3 References

Bryan, C., and Enos, D. (2014) Results of Stainless Steel Corrosion Studies and Environmental Sample Investigations. Sandia National Laboratory, DOE - Used Fuel Disposition Campaign, FCRD-UFD-2014-000055, SAND2014-20347 O

Bryan, C., and Schindelholz, E. (2017) Properties of Brines formed by Deliquescence of Sea-Salt Aerosols. Sandia National Laboratory, SAND2017-11231C.

Chatzidakis, S., Tang, W., Miller, R., Payzant, A., Bunn, J., Bryan, C., Scaglione, J., and Wang, J-A. (2021) Neutron diffraction illustrates residual stress behavior of welded alloys used as radioactive confinement boundary. Intl Jour of Press Vessels and Piping, 191, 104348

Enos, D., Bryan, C., and Norman, K. (2013) Data Report on Corrosion Testing of Stainless Steel SNF Storage canisters. Sandia National Laboratory, DOE - Used Fuel Disposition Campaign, FCRD-UFD-2013-000324

Hanson, B., Alsaed, H., Stockman, C., Enos, D., Meyer., R, Sorenson, K. (2012) Gap Analysis to support extended storage of Used Nuclear Fuel Rev.0. Pacific Northwest National Laboratory, DOE - Used Fuel Disposition Campaign, PNNL -20509

Weirich, T.D., Srinivasan, J., Taylor, J.A., Melia, M., A., Noell, P., J., Bryan, C.,R., Frankel, G.,S., Locke, J.,S., and Schindelholz, E.J. (2019) Humidity Effects on Pitting of Ground Stainless Steel Exposed to Sea Salt Particles. Jour. Electrochem. Soc., 166, C3477-C3487.

This page is intentionally left blank.

Appendix

A. Methods and Characterization

Experimental Setup

The bentonite used in this experimental work was mined from a reducing horizon in Colony, Wyoming. The bentonite was pulverized and sieved to < 3 mm and used with a free moisture content of ~15.5 wt.%. The groundwater solution was prepared using reagent grade materials dissolved in double deionized water. NaOH and HCl were added to adjust the initial solution pH. This solution was then filtered through a 0.45 μm filter and sparged with He before each experiment. The synthetic brine solution was added at 9:1 water:bentonite ratio. Initial components for wall rock experiments have been summarized in Table 2 of text.

Experiments were performed to examine the bentonite system with host rock, waste canister, and cement inclusion. Host-rock experiments focused on Opalinus Clay from the Swiss Underground Research Laboratory located at Mont Terri. The core was collected from BFE-A10 drill core (interval from 11 to 12 m and interval from 33 to 34 m from the borehole head). A portion of the Opalinus Clay was crushed and sieved with 10 mesh (~2 mm). Opalinus Clay to be used in experiments was reconstituted at 80 wt.% -10 mesh and 20 wt.% +10 mesh. Synthetic groundwater was chosen to replicate the groundwater composition that represents Opalinus Clay pore water (Table 2 of text, Pearson et al., 2003). The salt solution was added at 9:1 water: rock ratio.

The redox conditions for each system were buffered using a 1:1 mixture (by mass) of Fe_3O_4 and Fe° added at 0.07 wt.% of the bentonite mass. Approximately 7 wt.% (of total solids mass) 304 stainless steel (NIST SRM 101g), 316 stainless steel (NIST SRM 160b), and low-carbon steel (provided by Sandia National Laboratory) were added to the experiments to mimic the presence of a waste canister.

Reactants were loaded into a flexible gold bag and fixed into a 500 mL Gasket Confined Closure reactor (Seyfried et al., 1987). Experiments were pressurized to 150 to 160 bar and were heated isothermally to temperatures of either 200 or 300°C for 6–8 weeks or 6 months. Reaction liquids were extracted during the experiments and analyzed to investigate the aqueous geochemical evolution in relationship to mineralogical alterations. The sampled reaction liquids were split three-ways producing aliquots for unfiltered anion, unfiltered cation, and filtered (0.45 μm syringe filter) cation determination. All aliquots were stored in a refrigerator at 1°C until analysis.

Mineral Characterization

QXRD

Quantitative X-ray diffraction (XRD) analyses of experimental materials determined relative mineral abundances in the starting materials and reaction products. Each sample was ground with 20 wt. % corundum (Al_2O_3) for quantitative XRD analysis of the bulk rock (Chung, 1974). XRD measurements were conducted with a Siemens D500 diffractometer using Cu-Kα radiation. Data were collected from 2 to 70 º2θ with a 0.02 º2θ step-size and count times of 8 to 12 seconds

per step. Quantitative phase analysis (QXRD) was performed using FULLPAT (Chipera and Bish, 2002) and Jade© 9.5 X-ray data evaluation software with the ICDD PDF-4 database.

Los Alamos National Laboratory Clay Mineral XRD

X-ray diffraction analyses at Los Alamos National Laboratory were conducted on a Bruker D8 Discover using Cu-Kα radiation. To better analyze the non-clay and clay fractions, the < 2 μm particles were separated via sedimentation in DI H2O. An aliquot of the < 2 μm suspension was dropped on a zero-background quartz plate and dried. This oriented mount was X-rayed from 2 to 40º2θ at 8 to 12 s per step. The oriented mount was then saturated with ethylene glycol in a 60ºC oven for 24 hours and XRD analysis was repeated. A portion of the > 2 μm particles was ground with a mortar/pestle, deposited on a zero-background quartz plate, and X-rayed under the same parameters as the bulk powder material. The remaining > 2 μm portion was used for electron microscopy. Mineral identification and unit-cell parameters analysis was performed using Jade© 9.5 X-ray data evaluation program with ICDD PDF-4 database. Illite-smectite composition of higher-ordered (R1-3) illite-smectites were modeled via ClayStrat+ (developed by Hongji Yuan and David Bish). Expandable component abundances for the disordered illite-smectites were calculated via the D°2Q method (Środoń, 1980; Eberl et al., 1993; Moore and Reynolds, 1997). A regression from calculated data were used to calculate the % expandable (%Exp) component in each untreated and reacted bentonite. The equation is:

$$\%Exp = 973.76 - 323.45\Delta + 38.43\Delta 2 – 1.62\Delta 3$$

(Eberl et al., 1993, Eq. 3, R^2=0.99)

with Δ corresponding to D°2Q between the 002 and 003 peak positions for the oriented, ethylene glycol saturated samples.

Bulk X-ray Fluorescence (XRF) Spectroscopy analyses

Major elements were analyzed using the Rigaku Primus II wavelength-dispersive X-ray fluorescence (XRF) spectrometer. Samples were first crushed and homogenized in 5 to 10 g portions in a tungsten-carbide ballmill. Sample splits were heated at 110°C for 4 hrs, and then allowed to equilibrate at ambient laboratory conditions for 12 hrs to minimize weighing errors from atmospheric water gain. Fusion discs were prepared for analyses of the samples, by mixing 1.25 gram splits with 8.75 grams of lithium metaborate-tetraborate flux and heated in a muffle furnace for 45 minutes at 1050°C. Additional one-gram splits were heated at 1000°C to obtain the loss-on-ignition measurements used in the data reduction program.

SEM analyses

Analytical electron microscopy was performed using a FEI™ Inspect F scanning electron microscope (SEM) at Los Alamos National Laboratory. All samples were Au/Pd-coated prior to SEM analysis. Imaging with the SEM was performed using a 5.0 kV accelerating voltage and 1.5 spot size. Energy dispersive X-ray spectroscopy (EDS) was performed at 30 kV and a 3.0 spot size.

Aqueous Geochemical Analyses

Major cations and trace metals were analyzed via inductively coupled plasma-optical emission spectrometry (Perkin Elmer Optima 2100 DV) and inductively coupled plasma-mass spectrometry (Elan 6100) utilizing EPA methods 200.7 and 200.8. Ultra-high purity nitric acid was used in sample and calibration preparation prior to sample analysis. Internal standards (Sc, Ge, Bi, and In) were added to samples and standards to correct for matrix effects. Standard Reference Material (SRM) 1643e Trace Elements in Water was used to check the accuracy of the multi-element calibrations. Inorganic anion samples were analyzed by ion chromatography (IC) following EPA method 300 on a Dionex DX-600 system. Aqueous geochemical results are presented in Appendix B.

B. Water Chemistry: EBS-23 to 28

EBS-23 UNFILTERED

Lab ID	Sample Date	Al	B	Ba	Br	Ca	Cl	Cr	F	Fe	K	Li	Mg	Mn	Na	NO_3	Si	SiO_2	SO_4	Sr	Ti	Zn
		ppm	ppm	ppm	ppm	ppm	ppm	ppm	ppm	ppm	ppm	ppm	ppm	ppm	ppm	ppm	ppm	ppm	ppm	ppm	ppm	ppm
EBS-23-1 UF	3/22/2018	0.19	<2.03	0.41	0.33	105.02	3897.19	<0.03	0.29	<0.18	104.28	0.24	<0.1	<0.03	1951.46	0.79	30.79	65.89	100.87	0.53	<0.02	<0.52
EBS-23-1 UF	3/22/2018	0.41	<2.03	<0.11	0.33	112.64	3897.19	<0.03	0.29	<0.18	114.72	0.31	0.80	<0.03	1968.58	0.79	31.04	66.42	100.87	0.55	<0.02	<0.52
EBS-23-2 UF	3/29/2018	0.54	<2.03	0.37	0.64	120.72	4249.60	<0.03	0.27	<0.18	100.20	0.34	<0.1	<0.03	2053.47	1.23	36.04	77.12	103.28	0.65	<0.02	<0.52
EBS-23-3 UF	4/5/2018	0.17	<2.03	0.15	0.56	110.66	3029.12	<0.03	0.28	<0.18	74.37	0.43	0.13	<0.03	1568.50	0.79	35.00	74.89	85.12	0.56	<0.02	<0.52
EBS-23-4 UF	4/12/2018	<0.16	<2.03	0.34	0.49	144.40	2854.58	<0.03	0.41	0.21	81.18	0.50	<0.1	<0.03	1730.95	0.67	46.19	98.85	68.63	0.67	<0.02	<0.52
EBS-23-5 UF	4/19/2018	0.32	<2.03	0.39	0.29	130.65	1568.73	<0.03	0.51	0.19	64.82	0.50	<0.1	<0.03	1300.11	0.72	47.00	100.57	45.06	0.53	<0.02	<0.52
EBS-23-6 UF	4/26/2018	<0.16	<2.03	0.39	0.44	108.63	2449.86	<0.03	0.64	0.26	45.74	0.45	0.77	1.06	888.26	0.59	35.91	76.85	57.92	0.40	<0.02	8.09
EBS-23-7 UF	5/3/2018	0.18	<2.03	0.19	0.56	101.00	3154.84	<0.03	0.41	0.19	35.10	0.42	<0.1	<0.03	791.08	0.37	44.36	94.92	63.29	0.33	<0.02	<0.52
EBS-23-8 UF	5/10/2018	<0.16	<2.03	0.17	0.32	141.60	3818.39	<0.03	0.50	0.23	46.91	0.49	<0.1	<0.03	1009.65	0.26	50.52	108.12	65.02	0.42	<0.02	<0.52
EBS-23-9 UF	5/11/2018	<0.16	2.18	0.20	0.42	673.73	5172.97	<0.03	0.43	0.31	113.40	0.96	<0.1	<0.03	2557.81	0.10	62.12	132.94	734.01	1.72	<0.02	<0.52

EBS-23 FILTERED

Lab ID	Sample Date	Al	B	Ba	Ca	Cr	Fe	K	Li	Mg	Mn	Na	Si	SiO_2	Sr	Ti	Zn
		ppm	ppm	ppm	ppm	ppm	ppm	ppm	ppm	ppm	ppm	ppm	ppm	ppm	ppm	ppm	ppm
EBS-23-1 F	3/22/2018	2.58	2.27	<0.11	<0.45	<0.03	0.64	<5.61	<0.06	<0.1	<0.03	131.19	264.20	565.39	0.01	<0.02	<0.52
EBS-23-1 F	3/22/2018	2.98	<2.03	<0.11	1.52	<0.03	0.50	<5.61	0.08	<0.1	<0.03	149.12	273.74	585.80	0.01	<0.02	<0.52
EBS-23-2 F	3/29/2018	0.72	<2.03	0.30	123.26	<0.03	<0.18	104.26	0.38	<0.1	<0.03	2114.05	38.97	83.40	0.67	<0.02	<0.52
EBS-23-3 F	4/5/2018	0.44	<2.03	0.23	110.74	<0.03	<0.18	73.98	0.42	<0.1	<0.03	1593.41	42.04	89.97	0.57	<0.02	<0.52
EBS-23-4 F	4/12/2018	0.33	<2.03	0.21	141.70	<0.03	<0.18	80.53	0.50	<0.1	<0.03	1710.55	48.11	102.95	0.66	<0.02	<0.52
EBS-23-5 F	4/19/2018	0.27	<2.03	0.14	131.50	<0.03	<0.18	61.87	0.47	<0.1	<0.03	1318.94	48.63	104.08	0.53	<0.02	<0.52
EBS-23-6 F	4/26/2018	<0.16	<2.03	0.20	101.32	<0.03	<0.18	39.71	0.39	<0.1	<0.03	865.24	42.37	90.67	0.36	<0.02	<0.52
EBS-23-7 F	5/3/2018	<0.16	<2.03	<0.11	97.75	<0.03	<0.18	37.55	0.42	<0.1	<0.03	769.90	41.82	89.50	0.33	<0.02	<0.52
EBS-23-8 F	5/10/2018	0.17	<2.03	0.13	138.94	<0.03	<0.18	47.12	0.50	<0.1	<0.03	1001.69	50.21	107.46	0.42	<0.02	<0.52
EBS-23-9 F	5/11/2018	<0.16	2.07	0.12	658.93	<0.03	<0.18	113.02	0.94	<0.1	<0.03	2525.67	61.51	131.63	1.70	<0.02	<0.52

EBS-24 UNFILTERED

Lab ID	Sample Date	Br	B	Cl	F	NO_3	P	SO_4	Al	Ca	Cr	Fe	K	Li	Mg	Mn	Na	Si	SiO_2	Sr	Ti	Zn
		ppm	ppm	ppm	ppm	ppm	ppm	ppm	ppm	ppm	ppm	ppm	ppm	ppm	ppm	ppm	ppm	ppm	ppm	ppm	ppm	ppm
EBS-24-1 UF	6/13/2018	0.22	0.24	2530.63	0.60	3.60	0.10	84.76	0.85	98.09	0.02	0.27	98.51	0.38	0.02	0.01	1,796.42	29.53	63.20	0.52	0.00	0.10
EBS-24-2 UF	6/20/2018	0.21	0.09	1677.53	0.55	2.73	0.10	64.85	0.84	117.74	0.01	0.14	104.41	0.48	0.02	0.01	1998.39	41.90	89.66	0.65	0.00	0.10
EBS-24-3 UF	6/27/2018	0.33	0.09	3114.66	0.67	2.30	0.10	71.70	0.53	94.48	0.01	0.14	68.15	0.49	0.02	0.01	1310.29	46.61	99.74	0.48	0.00	0.10
EBS-24-4 UF	7/3/2018	0.32	0.06	3201.25	0.65	2.17	0.52	68.74	0.42	106.20	0.01	0.14	67.14	0.53	0.02	0.01	1270.70	49.13	105.14	0.50	0.00	0.10
EBS-24-5 UF	7/11/2018	0.21	0.05	2404.09	0.88	2.05	0.10	54.46	0.37	130.98	0.01	0.16	70.45	0.59	0.03	0.01	1315.55	53.80	115.13	0.55	0.00	0.10
EBS-24-6 UF	7/18/2018	0.35	0.10	3859.82	0.97	1.68	0.10	64.27	0.21	90.09	0.01	0.14	42.14	0.49	0.02	0.01	760.66	46.30	99.08	0.34	0.00	0.10
EBS-24-7 UF	7/25/2018	0.25	0.10	3011.73	0.94	1.59	0.10	53.60	0.25	188.85	0.02	0.15	78.69	0.71	0.02	0.01	1445.49	61.98	132.63	0.65	0.00	0.11
EBS-24-8 UF	8/1/2018	0.20	0.10	2163.15	0.82	1.90	0.10	45.51	0.19	220.40	0.02	0.11	84.11	0.76	0.02	0.02	1533.79	64.54	138.11	0.69	0.00	0.12
EBS-24-9 UF	8/2/2018	0.40	0.10	5228.65	1.52	1.08	0.10	667.54	0.03	732.47	0.02	0.18	136.24	1.19	0.08	0.02	2815.76	55.60	118.98	2.00	0.00	0.15

EBS-24 FILTERED

Lab ID	Sample Date	Al	B	Ba	Ca	Cr	Fe	K	Li	Mg	Mn	Na	Si	SiO_2	Sr	Ti	Zn
		ppm	ppm	ppm	ppm	ppm	ppm	ppm	ppm	ppm	ppm	ppm	ppm	ppm	ppm	ppm	ppm
EBS-24-1 F	6/13/2018	0.79	1.38	0.16	99.37	0.01	0.12	99.85	0.38	0.05	0.01	1843.61	29.95	64.10	0.53	0.00	0.10
EBS-24-2 F	6/20/2018	0.79	2.06	0.15	110.56	0.01	0.12	98.45	0.46	0.03	0.01	1870.35	40.12	85.85	0.61	0.00	0.10
EBS-24-3 F	6/27/2018	0.50	1.21	0.13	92.60	0.01	0.13	67.31	0.48	0.02	0.01	1271.70	45.21	96.75	0.47	0.00	0.10
EBS-24-4 F	7/3/2018	0.42	1.24	0.13	105.58	0.01	0.14	67.29	0.53	0.02	0.01	1281.50	49.77	106.52	0.50	0.00	0.10
EBS-24-5 F	7/11/2018	0.32	1.35	0.12	130.69	0.02	0.14	69.62	0.59	0.02	0.01	1290.56	53.70	114.91	0.55	0.00	0.10
EBS-24-6 F	7/18/2018	0.23	0.78	0.15	94.41	0.01	0.14	44.38	0.51	0.02	0.01	799.85	48.39	103.55	0.35	0.00	0.10
EBS-24-7 F	7/25/2018	0.32	1.73	0.18	189.10	0.01	0.18	77.70	0.70	0.02	0.01	1433.33	62.00	132.69	0.65	0.00	0.10
EBS-24-8 F	8/1/2018	0.18	1.90	0.21	219.05	0.01	0.13	83.91	0.77	0.02	0.01	1535.20	65.74	140.68	0.70	0.00	0.12
EBS-24-9 F	8/2/2018	0.03	3.77	0.20	760.64	0.03	0.13	139.46	1.24	0.04	0.01	2878.14	59.69	127.73	2.06	0.00	0.17

EBS-25 UNFILTERED																			
Lab ID	Sample Date	Al	B	Ba	Ca	Cl	Cr	F	Fe	K	Li	Mg	Mn	Na	NO_3	Si	SiO_2	SO_4	Sr	Zn
		ppm	ppm	ppm	ppm	ppm	ppm	ppm	ppm	ppm	ppm	ppm	ppm	ppm	ppm	ppm	ppm	ppm	ppm	ppm
EBS-25-1 UF	8/15/2018	0.56	0.35	6437.67	0.65	0.10	0.71	0.10	137.30	3.85	3.24	0.17	158.43	0.01	0.13	212.71	0.33	0.46	0.01	4094.82
EBS-25-2 UF	8/22/2018	0.44	0.28	6220.20	0.59	0.10	0.71	0.10	126.63	2.49	4.52	0.10	181.28	0.01	0.04	195.68	0.54	0.02	0.01	4036.88
EBS-25-3 UF	8/29/2018	0.46	0.18	6189.46	0.63	0.10	0.58	0.10	114.98	1.53	5.43	0.08	211.02	0.01	0.04	179.04	0.68	0.03	0.01	3819.05
EBS-25-4 UF	9/5/2018	0.45	0.13	5927.57	0.70	0.10	0.54	0.10	101.76	1.09	5.56	0.06	247.57	0.01	0.04	171.89	0.83	0.02	0.01	3626.44
EBS-25-5 UF	9/12/2018	0.45	0.07	5937.69	0.83	0.10	0.49	0.10	85.49	0.73	5.66	0.07	296.54	0.01	0.06	169.04	0.97	0.05	0.01	3493.40
EBS-25-6 UF	9/19/2018	0.47	0.05	5849.89	1.03	0.10	0.52	0.10	78.25	0.45	5.96	0.08	349.66	0.01	0.07	162.77	1.08	0.08	0.01	3291.00
EBS-25-7 UF	9/26/2018	0.43	0.08	5539.00	1.27	0.10	0.45	0.10	70.50	0.28	5.71	0.08	405.94	0.01	0.26	162.86	1.18	0.12	0.01	3121.34
EBS-25-8 UF	10/3/2018	0.42	0.03	5448.03	1.61	11.48	0.40	0.10	66.62	0.17	5.44	0.11	431.00	0.01	0.11	151.69	1.22	0.05	0.01	2885.50

EBS-25 FILTERED																	
Lab ID	Sample Date	Al	B	Ba	Ca	Cr	Fe	K	Li	Mg	Mn	Na	Si	SiO_2	Sr	Ti	Zn
		ppm	ppm	ppm	ppm	ppm	ppm	ppm	ppm	ppm	ppm	ppm	ppm	ppm	ppm	ppm	ppm
EBS-25-1 F	8/15/2018	4.09	3.78	0.18	178.84	0.01	0.04	245.43	0.38	0.02	0.01	4639.56	19.57	41.88	0.98	0.00	0.10
EBS-25-2 F	8/22/2018	2.49	4.98	0.09	183.60	0.01	0.09	191.50	0.53	0.04	0.01	4027.53	42.62	91.20	1.02	0.00	0.10
EBS-25-3 F	8/29/2018	1.58	5.60	0.08	216.66	0.01	0.04	184.81	0.71	0.02	0.01	3904.28	60.82	130.16	1.16	0.00	0.10
EBS-25-4 F	9/5/2018	1.13	5.57	0.07	245.99	0.01	0.04	171.04	0.82	0.03	0.01	3613.37	69.67	149.09	1.20	0.00	0.10
EBS-25-5 F	9/12/2018	0.77	5.57	0.07	288.25	0.01	0.04	166.51	0.94	0.03	0.01	3400.79	75.10	160.72	1.26	0.00	0.10
EBS-25-6 F	9/19/2018	0.45	5.85	0.09	350.26	0.01	0.06	166.90	1.10	0.05	0.01	3316.41	82.50	176.55	1.33	0.00	0.10
EBS-25-7 F	9/26/2018	0.25	5.85	0.09	419.08	0.01	0.11	165.46	1.21	0.05	0.01	3226.31	87.36	186.96	1.36	0.00	0.10
EBS-25-8 F	10/3/2018	0.17	5.65	0.10	454.70	0.01	0.10	158.68	1.27	0.05	0.01	3020.06	89.59	191.71	1.32	0.00	0.10

EBS-26 UNFILTERED

Lab ID	Sample Date	Al	B	Ba	Ca	Cl	Cr	F	Fe	K	Li	Mg	Mn	Na	NO_3	Si	SiO_2	SO_4	Sr	Zn
		ppm	ppm	ppm	ppm	ppm	ppm	ppm	ppm	ppm	ppm	ppm	ppm	ppm	ppm	ppm	ppm	ppm	ppm	ppm
EBS-26-1 UF	10/24/2018	<0.032	2.10	0.19	150.32	8039.51	<0.006	0.14	<0.036	206.21	0.26	0.05	<0.006	3814.15	0.20	34.18	73.14	143.34	0.82	<0.104
EBS-26-2 UF	10/31/2018	0.24	3.51	0.16	165.47	8498.41	0.01	0.16	<0.036	187.97	0.49	<0.02	<0.006	3759.93	0.23	48.28	103.32	135.75	0.95	<0.104
EBS-26-3 UF	11/7/2018	<0.032	3.64	1.09	194.97	7460.12	0.02	0.33	0.43	174.52	0.69	0.09	<0.006	3643.74	0.41	40.99	87.71	122.48	1.07	<0.104
EBS-26-4 UF	11/14/2018	<0.032	4.59	0.27	233.72	7513.14	0.01	0.26	<0.036	176.20	0.90	0.09	<0.006	3683.99	0.12	67.79	145.08	104.12	1.25	<0.104
EBS-26-5 UF	11/21/2018	<0.032	4.42	0.17	281.15	6344.72	<0.006	0.38	<0.036	174.74	1.03	0.07	<0.006	3569.29	0.20	62.11	132.92	92.88	1.37	<0.104
EBS-26-6 UF	11/28/2018	<0.032	4.75	1.03	349.71	5880.37	<0.006	0.52	3.34	178.30	1.18	0.48	<0.006	3465.81	0.23	50.69	108.47	86.26	1.54	<0.104
EBS-26-7 UF	12/5/2018	<0.032	4.98	0.25	383.56	6384.05	<0.006	0.70	0.13	172.75	1.27	0.10	<0.006	3353.11	0.19	77.79	166.47	80.58	1.57	<0.104
EBS-26-8 UF	12/12/2018	<0.032	5.04	0.48	429.81	7994.74	<0.006	1.34	0.55	169.58	1.35	0.43	<0.006	3274.27	0.27	62.55	133.85	74.22	1.63	<0.104
EBS-26-9 UF	12/13/2018	<0.032	4.60	0.12	897.68	6002.34	0.02	1.77	0.74	132.88	1.50	0.44	<0.006	3151.35	0.4282	46.80	100.16	772.58	2.64	<0.104

EBS-26 FILTERED

Lab ID	Sample Date	Al	B	Ba	Ca	Cr	Fe	K	Li	Mg	Mn	Na	Si	SiO_2	Sr	Ti	Zn
		ppm	ppm	ppm	ppm	ppm	ppm	ppm	ppm	ppm	ppm	ppm	ppm	ppm	ppm	ppm	ppm
EBS-26-1 F	10/24/2018	<0.08	1.42	0.28	148.89	<0.015	0.09	200.51	0.22	<0.05	<0.015	3723.62	15.76	33.72	0.82	<0.01	<0.26
EBS-26-2 F	10/31/2018	0.072	3.70	0.17	167.35	0.01	0.11	186.59	0.50	<0.02	0.012909	3768.62	45.28	96.91	0.95	<0.004	<0.104
EBS-26-3 F	11/7/2018	0.038	4.00	0.20	197.51	0.02	<0.036	178.34	0.69	<0.02	<0.006	3690.35	54.70	117.06	1.09	<0.004	<0.104
EBS-26-4 F	11/14/2018	0.053	4.13	0.21	246.10	0.03	1.48	181.37	0.95	0.15	0.407302	3629.71	71.54	153.09	1.23	<0.004	1.05
EBS-26-5 F	11/21/2018	<0.032	4.55	0.19	280.71	<0.006	<0.036	174.83	1.04	0.08	<0.006	3547.87	45.32	96.98	1.36	<0.004	<0.104
EBS-26-6 F	11/28/2018	<0.032	4.94	0.46	350.83	<0.006	0.28	176.93	1.19	0.28	<0.006	3521.27	59.77	127.90	1.54	<0.004	<0.104
EBS-26-7 F	12/5/2018	<0.032	4.64	0.23	383.80	<0.006	0.07	172.77	1.27	0.07	<0.006	3336.39	76.48	163.68	1.56	<0.004	<0.104
EBS-26-8 F	12/12/2018	<0.032	5.20	0.21	429.31	<0.006	0.06	166.68	1.32	0.17	<0.006	3195.24	41.14	88.04	1.56	<0.004	<0.104
EBS-26-9 F	12/13/2018	<0.032	4.62	0.20	866.80	<0.006	0.05	132.18	1.47	<0.02	<0.006	3140.30	51.90	111.06	2.63	<0.004	<0.104

EBS-27 UNFILTERED																				
Lab ID	Sample Date	Al	B	Ba	Ca	Cl	Cr	F	Fe	K	Li	Mg	Mn	Na	NO_3	Si	SiO_2	SO_4	Sr	Zn
		ppm	ppm	ppm	ppm	ppm	ppm	ppm	ppm	ppm	ppm	ppm	ppm	ppm	ppm	ppm	ppm	ppm	ppm	ppm
EBS-27-1 UF	7/17/19	0.75	4.33	0.12	202.61	8177.06	<0.006	0.50	<0.036	192.93	0.32	5.63	<0.006	3843.33	0.59	55.11	117.93	178.86	0.85	<0.104
EBS-27-2 UF	7/31/19	0.48	7.21	0.10	243.43	8941.11	<0.006	0.58	0.08	172.10	0.76	0.67	<0.006	3983.94	0.57	58.77	125.76	151.73	1.15	<0.104
EBS-27-3 UF	8/14/19	0.06	7.82	0.10	363.07	8453.37	<0.006	0.68	<0.036	160.23	1.21	0.08	<0.006	3509.07	0.59	69.97	149.74	138.68	1.54	<0.104
EBS-27-4 UF	8/28/19	<0.032	8.52	0.49	471.69	10412.62	0.01	0.80	0.23	170.27	1.47	0.47	<0.006	3775.12	0.52	37.92	81.14	121.71	1.72	<0.104
EBS-27-5 UF	9/11/19	<0.032	8.20	0.17	529.28	7361.86	0.01	0.80	0.05	150.82	1.56	0.14	<0.006	3155.43	0.36	33.00	70.61	97.78	1.79	<0.104
EBS-27-6 UF	9/25/19	<0.032	7.90	0.23	607.60	7395.23	<0.006	0.10	0.12	149.28	1.67	0.38	<0.006	3058.12	n.a.	38.11	81.55	68.23	1.79	<0.104
EBS-27-7 UF	10/9/19	<0.032	8.78	0.39	669.19	9033.62	<0.006	0.12	0.14	148.90	1.86	0.34	<0.006	3127.49	n.a.	65.90	141.03	78.83	1.81	<0.104
EBS-27-8 UF	10/23/19	<0.032	9.04	0.32	734.33	7392.65	<0.006	0.14	0.17	160.76	2.25	0.39	0.02	3351.95	n.a.	62.27	133.25	65.02	1.90	<0.104
EBS-27-9 UF	11/6/19	<0.16	6.66	<0.11	733.58	7552.51	<0.03	0.14	<0.18	141.83	2.23	<0.1	<0.03	3065.81	n.a.	86.71	185.55	60.51	1.80	<0.52
EBS-27-10 UF	11/20/19	<0.032	9.38	0.14	751.15	7737.09	<0.006	1.28	0.07	149.15	2.57	0.11	<0.006	3105.98	<0.1	48.85	104.53	113.99	1.90	<0.104
EBS-27-11 UF	11/27/19	<0.032	9.17	0.15	761.82	8360.80	<0.006	1.33	0.05	151.65	2.65	0.15	<0.006	3112.39	<0.1	42.10	90.09	116.69	1.87	<0.104
EBS-27-12 UF	12/11/19	<0.032	9.50	0.12	793.75	9390.77	<0.006	1.43	0.05	152.18	2.83	0.06	<0.006	3099.71	<0.1	42.94	91.90	117.08	1.88	<0.104
EBS-27-13 UF	12/24/19	<0.032	9.53	0.12	804.98	8182.25	<0.006	1.52	0.06	152.08	2.93	0.04	<0.006	3083.58	<0.1	108.95	233.15	110.01	1.89	<0.104
EBS-27-14 UF	1/8/20	<0.032	9.88	0.12	825.15	7832.05	<0.006	1.31	<0.036	154.18	3.12	0.03	<0.006	3091.58	<0.1	57.58	123.23	97.86	1.94	<0.104
EBS-27-15 UF	1/9/20	<0.032	9.16	0.05	1274.68	8786.66	<0.006	1.38	0.08	113.95	3.18	0.56	<0.006	2942.30	<0.1	79.05	169.16	1161.13	2.90	<0.104

EBS-27 FILTERED																
Lab ID	Sample Date	Al	B	Ba	Ca	Cr	Fe	K	Li	Mg	Mn	Na	Si	SiO_2	Sr	Zn
		ppm	ppm	ppm	ppm	ppm	ppm	ppm	ppm	ppm	ppm	ppm	ppm	ppm	ppm	ppm
EBS-27-1 F	7/17/19	0.80	4.25	0.11	208.95	<0.006	<0.036	204.13	0.35	5.85	<0.006	3903.21	56.10	120.04	0.83	<0.004
EBS-27-2 F	7/31/19	0.75	7.19	0.11	242.08	<0.006	<0.036	170.82	0.75	0.46	<0.006	3949.78	60.91	130.35	1.15	<0.004
EBS-27-3 F	8/14/19	<0.032	7.79	0.10	367.54	<0.006	<0.036	161.20	1.21	0.10	<0.006	3508.50	64.92	138.92	1.54	<0.004
EBS-27-4 F	8/28/19	<0.032	8.62	0.14	465.68	<0.006	0.04	163.38	1.43	0.20	<0.006	3576.11	63.69	136.31	1.69	<0.004
EBS-27-5 F	9/11/19	<0.032	8.43	0.17	556.30	<0.006	0.07	156.50	1.63	0.18	<0.006	3260.34	35.01	74.92	1.86	<0.004
EBS-27-6 F	9/25/19	<0.032	8.27	0.24	602.12	<0.006	0.11	150.04	1.73	0.38	<0.006	3109.43	38.37	82.11	1.82	<0.004
EBS-27-7 F	10/9/19	<0.032	8.42	0.19	649.53	<0.006	0.09	147.55	1.81	0.17	<0.006	3021.01	41.99	89.86	1.77	<0.004
EBS-27-8 F	10/23/19	<0.032	7.76	0.09	704.64	<0.015	<0.09	146.18	2.10	<0.05	<0.015	3122.37	44.99	96.27	1.84	<0.01
EBS-27-9 F	11/6/19															
EBS-27-10 F	11/20/19	<0.032	9.20	0.14	758.69	<0.006	0.05	150.40	2.61	0.07	<0.006	3119.00	55.17	118.05	1.89	<0.004
EBS-27-11 F	11/27/19	<0.032	9.28	0.12	767.08	<0.006	0.04	151.10	2.69	0.08	<0.006	3104.81	61.88	132.42	1.90	<0.004
EBS-27-12 F	12/11/19	<0.032	9.59	0.13	803.93	<0.006	0.07	154.46	2.86	0.05	<0.006	3079.41	105.44	225.64	1.91	<0.004
EBS-27-13 F	12/24/19	<0.032	9.96	0.12	799.79	<0.006	0.06	152.80	2.95	0.06	<0.006	3070.71	52.30	111.92	1.91	<0.004
EBS-27-14 F	1/8/20	<0.032	9.88	0.11	817.61	<0.006	<0.036	157.14	3.09	<0.02	<0.006	3091.34	59.39	127.09	1.93	<0.004
EBS-27-15 F	1/9/20	<0.032	9.21	0.05	1253.46	<0.006	<0.036	114.48	3.19	<0.02	<0.006	2929.86	85.39	182.74	2.94	<0.004

* The two runs of EBS-27-9-UF CAT were attempted on the ICP-OES, but due to bad spike recovery the results were not reliable. There was no sample left to rerun the analysis.

EBS-28 UNFILTERED

Lab ID	Sample Date	Al	B	Ba	Ca	Cl	Cr	F	Fe	K	Li	Mg	Mn	Na	NO_3	Si	SiO_2	SO4	Sr	Zn
		ppm	ppm	ppm	ppm	ppm	ppm	ppm	ppm	ppm	ppm	ppm	ppm	ppm	ppm	ppm	ppm	ppm	ppm	ppm
EBS-28-1 UF	9/11/19	0.31	2.57	0.33	100.32	7521.64	<0.01	0.29	<0.04	214.74	0.25	<0.02	<0.01	3691.03	0.17	21.91	46.89	35.96	0.42	<0.10
EBS-28-2 UF	9/18/19	<0.03	5.96	0.67	343.09	5726.85	<0.01	1.06	<0.04	265.53	2.63	<0.02	<0.01	2732.89	<0.1	131.80	282.05	27.24	0.63	<0.10
EBS-28-3 UF	9/25/19	<0.03	5.80	0.92	448.60	5003.46	0.01	0.12	<0.04	309.35	2.76	<0.02	<0.01	2181.36	n.a.	63.01	134.84	9.50	0.67	<0.10
EBS-28-4 UF	10/2/19	<0.03	5.37	1.19	421.75	4367.68	<0.01	0.11	<0.04	329.00	2.63	<0.02	<0.01	1925.69	n.a.	70.24	150.31	13.84	0.68	0.1
EBS-28-5 UF	10/9/19	<0.03	4.70	1.15	344.09	3803.29	<0.01	0.07	<0.04	317.69	2.34	<0.02	<0.01	1659.87	n.a.	91.01	194.76	18.45	0.63	<0.10
EBS-28-6 UF	10/16/19	<0.03	4.30	1.23	290.82	3717.25	0.01	n.a.	<0.04	312.45	2.20	<0.02	<0.01	1511.29	n.a.	187.51	401.26	8.28	0.60	<0.10
EBS-28-7 UF	10/23/19	<0.03	4.15	1.37	251.32	3115.60	0.01	n.a.	<0.04	304.80	2.11	<0.02	<0.01	1429.93	n.a.	237.75	508.79	7.51	0.59	<0.10
EBS-28-8 UF	10/30/19	<0.03	3.68	1.43	207.69	2859.75	<0.01	0.13	<0.04	284.36	1.96	<0.02	<0.01	1299.28	n.a.	245.65	525.70	5.77	0.54	<0.10
EBS-28-9 UF	11/6/19	<0.03	3.34	1.35	178.58	2656.73	0.01	0.11	<0.04	271.35	1.86	<0.02	<0.01	1231.40	n.a.	249.82	534.62	3.63	0.53	<0.10
EBS-28-10 UF	11/7/19	<0.03	2.11	0.55	470.50	1821.21	<0.01	0.12	0.63	154.22	1.27	1.91	0.02	864.48	n.a.	174.18	372.74	533.87	0.92	<0.10

EBS-28 FILTERED

Lab ID	Sample Date	Al	B	Ba	Ca	Cr	Fe	K	Li	Mg	Mn	Na	Si	SiO_2	Sr	Ti	Zn
		ppm	ppm	ppm	ppm	ppm	ppm	ppm	ppm	ppm	ppm	ppm	ppm	ppm	ppm	ppm	ppm
EBS-28-1 F	9/11/19	0.36	2.61	0.34	99.86	0.01	<0.036	209.79	0.25	<0.02	<0.006	3686.94	22.69	48.56	0.42	<0.004	<0.104
EBS-28-2 F	9/18/19	<0.032	6.06	0.68	349.20	<0.006	<0.036	269.60	2.74	<0.02	<0.006	2806.50	127.47	272.78	0.64	<0.004	<0.104
EBS-28-3 F	9/25/19	<0.032	5.55	1.03	440.28	<0.006	<0.036	304.57	2.72	0.05	<0.006	2186.03	83.61	178.93	0.69	<0.004	<0.104
EBS-28-4 F	10/2/19	<0.032	5.23	1.10	410.76	0.01	<0.036	318.69	2.59	<0.02	<0.006	1900.08	96.68	206.91	0.67	<0.004	<0.104
EBS-28-5 F	10/9/19	<0.032	4.70	1.17	344.77	0.01	<0.036	319.69	2.36	<0.02	<0.006	1663.26	89.03	190.52	0.63	<0.004	<0.104
EBS-28-6 F	10/16/19	<0.032	4.29	1.23	292.55	0.01	<0.036	307.25	2.19	<0.02	<0.006	1504.80	241.80	517.46	0.60	<0.004	<0.104
EBS-28-7 F	10/23/19	<0.032	4.17	1.36	246.77	0.01	0.16	298.25	2.10	<0.02	<0.006	1405.04	231.39	495.17	0.59	<0.004	<0.104
EBS-28-8 F	10/30/19	<0.032	3.71	1.48	206.50	0.01	0.10	286.21	1.97	<0.02	<0.006	1310.56	250.41	535.87	0.55	<0.004	<0.104
EBS-28-9 F	11/6/19	<0.032	3.36	1.39	179.97	<0.006	<0.036	272.24	1.88	<0.02	<0.006	1238.12	254.51	544.64	0.52	<0.004	<0.104
EBS-26-10 F	11/7/19	<0.032	1.95	0.70	466.10	0.01	<0.036	155.34	1.29	0.52	0.01	874.30	171.92	367.91	0.92	<0.004	<0.104

EBS-29 UNFILTERED

Lab ID	Time (Hours)	Al	B	Ba	Ca	Cl	Cr	F	Fe	K	Li	Mg	Mn	Na	NO_3	P	Si	SiO_2	SO4	Sr	Zn
		ppm	ppm	ppm	ppm	ppm	ppm	ppm	ppm	ppm	ppm	ppm	ppm	ppm	ppm	ppm	ppm	ppm	ppm	ppm	ppm
EBS-29-1 UF	144	1.70	8.23	0.030	8.70	0.27	0.01	597.36	0.13	49.33	0.19	0.16	<0.01	445.68	0.12	0.17	355.07	759.86	145.06	0.10	<0.10
EBS-29-2 UF	312	1.01	7.63	0.028	6.23	0.27	<0.01	550.73	0.09	32.99	0.15	0.02	1.56	428.10	0.25	0.22	344.16	736.50	179.62	0.09	<0.10
EBS-29-3 UF	480	0.96	7.59	0.035	5.17	0.30	0.01	535.60	0.06	28.96	0.14	<0.02	0.68	413.86	0.10	0.11	354.46	758.55	165.22	0.08	<0.10
EBS-29-4 UF	648	1.00	7.48	0.037	4.73	0.29	<0.01	506.84	0.04	28.23	0.15	0.02	0.12	400.06	0.30	0.11	344.63	737.51	157.52	0.08	<0.10
EBS-29-5 UF	816	1.08	6.82	0.056	5.41	0.29	0.01	469.09	0.08	25.51	0.14	0.12	0.07	374.17	0.24	<0.1	337.71	722.71	147.45	0.07	<0.10
EBS-29-6 UF	984	1.12	6.47	0.036	3.57	0.27	0.01	435.33	<0.04	24.38	0.14	<0.02	0.05	363.10	0.22	0.12	355.31	760.36	138.00	0.06	<0.10
EBS-29-7 UF	1152	1.08	5.81	0.035	3.04	0.27	0.01	414.36	<0.04	21.89	0.13	<0.02	0.02	322.88	0.13	0.13	334.81	716.50	131.24	0.05	<0.10
EBS-29-8 UF	1272	1.43	6.09	0.055	4.61	0.30	<0.01	404.00	<0.04	22.45	0.12	0.13	0.03	336.03	0.11	<0.1	372.36	796.86	124.62	0.06	<0.10
EBS-29-9 UF	1296	2.084	3.755	0.038	3.412	0.23	<0.01	250.31	0.873	12.716	0.208	0.320	0.010	238.706	0.06	0.77	231.000	494.340	82.33	0.041	<0.10

EBS-29 FILTERED

Lab ID	Time (Hours)	Al	B	Ba	Ca	Cr	Fe	K	Li	Mg	Mn	Na	Si	SiO_2	Sr	Ti	Zn
		ppm	ppm	ppm	ppm	ppm	ppm	ppm	ppm	ppm	ppm	ppm	ppm	ppm	ppm	ppm	ppm
EBS-29-1 F	144	1.13	8.04	0.03	8.82	<0.01	<0.04	48.56	0.17	<0.02	<0.01	447.92	326.26	698.20	0.09	<0.01	<0.10
EBS-29-2 F	312	0.93	8.01	0.04	6.86	0.02	0.09	33.78	0.16	0.04	1.53	440.27	343.74	735.61	0.09	<0.01	<0.10
EBS-29-3 F	480	0.98	7.62	0.04	5.33	0.01	0.06	28.72	0.15	0.07	0.67	413.88	346.47	741.44	0.08	<0.01	<0.10
EBS-29-4 F	648	1.01	7.22	0.04	4.70	0.01	0.06	27.15	0.14	<0.02	0.12	396.09	345.18	738.68	0.07	<0.01	<0.10
EBS-29-5 F	816	1.02	6.77	0.04	4.12	0.01	<0.04	25.22	0.14	<0.02	0.09	366.67	349.32	747.54	0.07	<0.01	<0.10
EBS-29-6 F	984	1.11	6.58	0.03	3.42	0.01	<0.04	24.72	0.14	<0.02	0.05	360.83	363.27	777.40	0.06	<0.01	<0.10
EBS-29-7 F	1152	1.17	6.17	0.03	3.12	<0.01	<0.04	23.13	0.13	<0.02	0.02	341.66	355.12	759.96	0.06	<0.01	<0.10
EBS-29-8 F	1272	1.30	6.10	0.04	3.52	<0.01	0.04	22.80	0.12	<0.02	0.02	343.84	361.63	773.90	0.05	<0.01	<0.10
EBS-29-9 F	1296	0.21	3.79	0.05	3.24	<0.01	0.08	12.65	0.21	0.02	<0.01	237.95	226.95	485.66	0.04	<0.01	<0.10

EBS-29 CAPSULES UNFILTERED																					
Lab ID	Time (Hours)	Al	B	Ba	Ca	Cl	Cr	F	Fe	K	Li	Mg	Mn	Na	NO_3	P	Si	SiO_2	SO4	Sr	Zn
		ppm	ppm	ppm	ppm	ppm	ppm	ppm	ppm	ppm	ppm	ppm	ppm	ppm	ppm	ppm	ppm	ppm	ppm	ppm	ppm
EBS-29-A1 UF	1296	0.12	<0.406	0.38	50.35	0.13	0.02	8.07	275.85	<0.012	0.65	0.63	171.05	0.02	0.35	<0.10	13.29	28.43	39.38	0.13	<0.10
EBS-29-A2 UF	1296	3.30	<0.406	0.08	51.33	0.14	0.02	26.87	270.82	<0.012	1.07	0.63	167.74	0.02	0.11	<0.10	17.29	37.00	40.15	0.11	<0.10
EBS-29-A3 UF	1296	0.48	<0.406	0.17	51.37	0.14	0.01	8.87	285.88	0.01	1.51	0.97	172.17	0.01	0.35	<0.10	16.48	35.27	39.07	0.12	0.27

EBS-30 UNFILTERED																				
Lab ID	Time (Hours)	Al	B	Ba	Ca	Cl	Cr	F	Fe	K	Li	Mg	Mn	Na	NO_3	Si	SiO_2	SO4	Sr	Zn
		ppm	ppm	ppm	ppm	ppm	ppm	ppm	ppm	ppm	ppm	ppm	ppm	ppm	ppm	ppm	ppm	ppm	ppm	ppm
EBS-30-1 UF	168	<0.03	4.15	0.50	90.92	6587.06	0.02	0.34	1.46	195.92	0.59	33.00	0.21	3665.92	0.12	121.92	260.91	253.06	0.89	1.78
EBS-30-2 UF	336	<0.03	4.66	0.53	88.39	6246.12	0.02	0.39	1.51	198.54	0.75	8.71	0.16	3913.66	<0.1	126.54	270.81	244.64	1.11	0.15
EBS-30-3 UF	504	<0.03	4.7	0.50	91.84	7856.02	0.01	0.67	0.59	187.40	0.78	2.94	0.11	3761.58	0.13	97.38	208.4	245.98	1.32	<0.10
EBS-30-4 UF	672	<0.03	4.69	0.50	95.3	6346.07	0.02	1.04	0.19	183.28	0.79	1.38	0.08	3782.28	0.11	165.17	353.46	246.18	1.46	<0.10
EBS-30-5 UF	840	<0.03	4.4	0.45	92.45	6491.68	<0.01	0.82	0.11	172.78	0.71	0.77	0.08	3666.70	0.22	70.88	151.69	249.94	1.41	<0.10
EBS-30-6 UF	984	<0.03	4.34	0.43	91.67	6824.29	<0.01	0.9	0.12	171.03	0.7	0.59	0.07	3612.07	0.18	110.73	236.96	263.13	1.4	<0.10
EBS-30-7 UF	1152	0.08	5.18	0.46	100.62	5468.65	0.02	0.69	0.10	179.34	0.76	0.54	0.07	3911.01	<0.1	145.17	310.67	234.21	1.53	<0.10
EBS-30-8 UF	1320	<0.03	4.45	0.40	85.34	5144.25	0.02	0.66	0.07	154.23	0.63	0.22	0.04	3284.24	<0.1	145.2	310.72	238.07	1.32	<0.10
EBS-30-9 UF	1344	1.96	3.15	0.41	498.87	5261.46	0.01	0.57	2.91	114.68	0.53	11.9	0.40	2712.02	0.12	107.88	230.86	1070.41	2.38	<0.10

EBS-30 FILTERED																	
Lab ID	Time (Hours)	Al	B	Ba	Ca	Cr	Fe	K	Li	Mg	Mn	Na	Si	SiO_2	Sr	Ti	Zn
		ppm	ppm	ppm	ppm	ppm	ppm	ppm	ppm	ppm	ppm	ppm	ppm	ppm	ppm	ppm	ppm
EBS-30-1 F	168	<0.03	3.96	0.51	95.95	0.01	1.04	193.8	0.58	33.48	0.21	3880.38	93.39	199.85	0.91	<0.01	1.12
EBS-30-2 F	336	<0.03	5.09	0.54	89.32	0.01	1.17	194.98	0.74	8.57	0.16	3757.92	119.02	254.7	1.1	<0.01	0.19
EBS-30-3 F	504	<0.03	4.98	0.52	92.33	0.02	0.22	184.58	0.78	2.93	0.11	3635.39	96.76	207.07	1.3	<0.01	0.12
EBS-30-4 F	672	<0.03	4.96	0.51	93.70	0.05	0.30	179.78	0.78	1.34	0.09	3646.71	100.45	214.97	1.41	<0.01	0.13
EBS-30-5 F	840	<0.03	4.76	0.48	92.00	0.02	0.14	175.45	0.74	0.84	0.09	3574.45	154.98	331.66	1.45	<0.01	<0.10
EBS-30-6 F	984	<0.03	4.58	0.45	89.90	0.02	0.13	169.25	0.72	0.60	0.07	3470.23	165.19	353.52	1.43	<0.01	0.12
EBS-30-7 F	1152	<0.03	4.37	0.43	87.96	0.02	0.12	159.98	0.68	0.42	0.06	3373.60	157.72	337.51	1.4	<0.01	0.11
EBS-30-8 F	1320	<0.03	4.45	0.41	83.39	0.02	0.27	154.18	0.64	0.25	0.05	3287.00	145.54	311.46	1.33	<0.01	<0.10
EBS-30-9 F	1344	<0.03	3.14	0.39	445.34	0.02	1.06	108.44	0.51	2.59	0.33	2534.34	112.51	240.77	2.32	<0.01	<0.10

EBS-31 UNFILTERED																				
Lab ID	Time (Hours)	Al	B	Ba	Ca	Cl	Cr	F	Fe	K	Li	Mg	Mn	Na	NO_3	Si	SiO_2	SO4	Sr	Zn
		ppm	ppm	ppm	ppm	ppm	ppm	ppm	ppm	ppm	ppm	ppm	ppm	ppm	ppm	ppm	ppm	ppm	ppm	ppm
EBS-31-0 UF	0	<0.03	<0.41	0.06	405.66	7834.05	<0.01	<0.1	<0.04	225.04	0.02	188.92	<0.01	3820.62	0.12	31.94	68.35	1024.92	0.18	<0.10
EBS-31-1 UF	168	<0.03	2.74	0.49	95.81	10377.62	0.01	0.44	<0.04	199.07	0.54	36.33	0.08	3962.97	1.65	40.78	87.27	454.23	0.95	<0.10
EBS-31-2 UF	336	<0.03	3.12	0.49	87.83	7184.93	0.01	0.66	0.42	186.37	0.63	13.07	0.06	3703.22	0.38	126.31	270.31	243.01	1.14	<0.10
EBS-31-3 UF	504	<0.03	3.23	0.51	92.69	5859.01	0.01	0.49	0.35	193.61	0.68	5.27	0.04	3794.43	0.20	142.35	304.63	232.17	1.33	<0.10
EBS-31-4 UF	672	<0.03	3.08	0.50	89.54	5721.63	0.01	0.54	0.11	181.52	0.64	2.33	0.03	3610.70	0.16	165.08	353.27	219.93	1.38	<0.10
EBS-31-5 UF	840	<0.03	3.08	0.54	89.81	5953.12	0.02	0.53	0.27	177.15	0.63	1.50	0.04	3558.08	0.40	151.20	323.57	226.85	1.44	<0.10
EBS-31-6 UF	1008	<0.03	3.04	0.53	92.05	7558.41	0.01	0.36	0.05	170.89	0.62	0.98	0.02	3503.37	<0.1	151.73	324.71	140.06	1.47	<0.10
EBS-31-7 UF	1200	<0.032	3.03	0.54	93.91	4708.86	0.01	0.44	0.05	174.48	0.67	0.72	0.01	3573.14	0.47	166.44	356.19	183.34	1.54	<0.10
EBS-31-8 UF	1344	<0.03	3.25	0.56	90.03	4882.16	<0.01	0.61	<0.04	159.41	0.57	0.56	0.02	3390.49	0.15	155.36	332.46	225.45	1.48	<0.10
EBS-31-9 UF	1368	<0.03	3.14	0.58	437.43	4977.27	0.01	0.59	0.16	148.68	0.59	5.63	0.14	3531.55	0.19	146.03	312.51	983.32	3.07	<0.10

EBS-31 FILTERED																	
Lab ID	Time (Hours)	Al	B	Ba	Ca	Cr	Fe	K	Li	Mg	Mn	Na	Si	SiO_2	Sr	Ti	Zn
		ppm	ppm	ppm	ppm	ppm	ppm	ppm	ppm	ppm	ppm	ppm	ppm	ppm	ppm	ppm	ppm
EBS-31-0 F	0	<0.03	<0.41	<0.02	390.61	0.01	<0.04	215.22	0.02	180.34	<0.01	3632.47	1.22	2.61	0.16	<0.01	<0.10
EBS-31-1 F	168	<0.03	2.70	0.48	93.06	0.01	<0.04	197.37	0.54	35.93	0.08	3904.06	41.24	88.25	0.94	<0.01	<0.10
EBS-31-2 F	336	<0.03	3.10	0.49	87.02	0.01	0.42	185.07	0.62	12.98	0.06	3710.31	123.57	264.43	1.12	<0.01	<0.10
EBS-31-3 F	504	<0.03	2.96	0.49	86.95	<0.01	0.20	173.85	0.61	4.87	0.04	3551.17	151.11	323.38	1.26	<0.01	<0.10
EBS-31-4 F	672	<0.03	3.09	0.51	87.96	0.01	0.18	173.18	0.63	2.23	0.03	3624.92	157.38	336.80	1.34	<0.01	<0.10
EBS-31-5 F	840	<0.03	2.99	0.51	90.56	0.01	0.08	169.48	0.61	1.36	0.03	3507.71	162.46	347.67	1.41	<0.01	<0.10
EBS-31-6 F	1008	<0.03	2.39	0.49	84.54	<0.01	0.08	152.29	0.55	0.84	0.01	3232.77	144.28	308.76	1.35	<0.01	<0.10
EBS-31-7 F	1200	<0.032	2.93	0.53	89.55	0.01	0.06	167.64	0.63	0.71	0.01	3489.70	158.75	339.72	1.49	<0.01	<0.10
EBS-31-8 F	1344	<0.03	2.36	0.50	84.13	0.01	0.07	148.67	0.52	0.49	0.01	3149.30	146.33	313.16	1.36	<0.01	<0.10
EBS-31-9 F	1368	0.30	2.74	0.50	427.93	0.01	1.07	138.67	0.53	7.64	0.14	3255.90	137.79	294.87	2.87	<0.01	<0.10

C. X-Ray Powder Diffraction Data: EBS-24 to EBS-31

Table C-1. Quantitative X-Ray Diffraction (QXRD) analyses of the starting materials and the experimental mixes. Abbreviations: OPC, ordinary Portland cement; OC, Opalinus Clay; WB, Wyoming bentonite.

SAMPLE ID	WB	OC	60 WB: 20 OC: 20 OPC Powder	60 WB: 20 OC: 20 Cured OPC	OPC Powder	Cured OPC	Durango Apatite	80 WB: 20 Apatite
Starting Material								
NON-CLAY FRACTION								
Quartz	1.5	13.8	3.7	3.7	-	-	-	1.2
K-Feldspar	0.7	5.9	1.6	1.6	-	-	-	0.6
Plagioclase	6.2	3.0	4.3	4.3	-	-	-	5.0
Apatite	-	-	-	-	-	-	100.0	20.0
Calcite	-	16.4	3.3	3.3	-	-	-	-
Dolomite	-	0.7	0.1	0.1	-	-	-	-
Gypsum	0.1	-	0.1	0.1	-	-	-	0.1
Sphalerite/Pyrite	0.2	1.1	0.3	0.3	-	-	-	0.1
Clinoptilolite	13.0	-	7.8	7.8	-	-	-	10.4
Cristobalite	1.5	-	0.9	0.9	-	-	-	1.2
Portlandite	-	-	-	7.8	-	38.9	-	-
Larnite	-	-	2.9	1.8	14.6	8.8	-	-
Hatrurite	-	-	13.4	5.9	67.1	29.7	-	-
Brownmillerite	-	-	3.2	3.8	16.0	18.9	-	-
Amorphous	-	-	0.5	0.7	2.3	3.7	-	-
TOTAL	**23.2**	**40.9**	**42.1**	**42.1**	**100.0**	**100.0**	**100.0**	**38.6**
CLAY FRACTION								
Smectite + Illite + I/S	71.0	24.1	47.4	47.4	-	-	-	56.8
Mica	3.8	7.4	3.8	3.8	-	-	-	3.0
Chlorite	2.0	9.1	3.0	3.0	-	-	-	1.6
Kaolinite	0.0	16.9	3.4	3.4	-	-	-	0.0
TOTAL	**76.8**	**57.5**	**57.6**	**57.6**	**0.0**	**0.0**	**0.0**	**61.4**

Table C-2. Quantitative X-Ray Diffraction (QXRD) analyses of the post-reaction product results from experiments EBS-24 to EBS-31. Values are in weight percent. Abbreviations: OPC, ordinary Portland cement; OC, Opalinus Clay; WB, Wyoming bentonite

SAMPLE ID	EBS-24	EBS-25	EBS-26	EBS-27-1	EBS-27-4	EBS-28	EBS-29	EBS-30	EBS-31
	OC + WB + OPC Powder						Apatite + WB	OC + WB + Cured OPC	
NON-CLAY FRACTION									
Quartz	3.1	1.8	1.2	0.6	2.1	5.2	5.5	3.5	1.0
K-Feldspar	0.4	0.1	0.1	0.7	-	-	1.4	1.4	3.6
Plagioclase	7.3	4.8	6.8	1.4	3.9	22.5	3.9	-	-
Apatite	0.6	0.6	0.6	0.6	-	-	26.0	-	-
Calcite	5.6	4.0	3.5	10.9	2.4	5.8	-	2.2	1.7
Dolomite	1.2	1.0	1.0	-	0.6	-	-	-	-
Gypsum	0.2	0.1	0.1	-	-	-	-	-	-
Halite	0.2	0.1	0.3	0.4	0.3	-	-	-	-
Anatase	0.3	0.3	0.3	-	-	-	-	-	-
Sphalerite/Pyrite	0.4	0.3	-	-	-	-	-	0.1	0.5
Clinoptilolite	6.9	7.8	3.9	5.5	12.3	-	11.7	4.3	5.8
Analcime	6.4	4.9	4.9	22.9	13.9	1.3	0.3	-	-
Garronite	7.2	6.2	9.5	-	5.1	-	-	-	-
Cristobalite	-	-	-	-	-	-	-	-	-
Magnetite	3.4	1.1	0.9	0.8	0.3	2.6	2.9	0.9	1.7
Wairakite	-	-	-	18.6	2.0	7.3	-	-	-
Tobermorite	2.1	4.0	3.1	6.5	0.4	-	-	0.5	4.9
Heulandite	-	-	-	-	3.4	-	-	-	-
Amorphous-Missing (gel?)	8.8	18.1	25.6	5.6	3.9	1.6	7.6	2.9	5.6
TOTAL	**54.2**	**55.2**	**61.8**	**74.5**	**50.5**	**61.9**	**59.3**	**16.0**	**24.6**
CLAY FRACTION									
Smectite + Illite + I/S	34.2	35.1	28.1	15.4	39.3	35.7	25.6	78.0	67.7
Fe-saponite	-	-	-	-	-	15.6	-	-	-
Mica	3.8	3.7	4.9	3.7	1.9	2.4	14.5	2.6	4.3
Chlorite	4.7	4.0	3.4	6.4	8.0	-	0.6	1.8	0.7
Kaolinite	3.0	2.0	1.8	-	0.3	-	-	1.8	2.7
TOTAL	**45.8**	**44.8**	**38.2**	**25.5**	**49.5**	**38.1**	**40.7**	**84.0**	**75.4**

D. X-Ray Fluorescence Data: EBS-27 to -31

Table D-1. X-Ray Fluorescence (XRF) analyses of the starting materials and the post-reaction product results from experiments EBS-24 to EBS-31. Values are in weight percent. Abbreviations: OPC, ordinary Portland cement; OC, Opalinus Clay; WB, Wyoming bentonite

	Opal. Clay + WY Bent. + Uncured OPC+ Steel			WY Bent. + Apatite	Opal. Clay + WY Bent. + Cured OPC + Steel		Unreacted						
Oxide	**EBS-27-1**	**EBS-27-4**	**EBS-28**	**EBS-29**	**EBS-30**	**EBS-31**	**Cured OPC**	**Uncured OPC**	**WY bent**	**Opal. Clay**	**Apatite**	**Uncured mix**	**Cured mix**
CaO	16.4	11.6	14.0	11.0	3.3	3.2	55.0	66.9	0.9	8.3	60.0	15.6	13.2
K_2O	1.1	1.1	0.7	0.7	1.4	1.4	0.4	0.6	0.6	3.1	0.0	1.1	1.0
SiO_2	41.5	49.4	43.5	47.4	50.8	48.4	17.4	18.7	61.9	44.2	0.5	49.7	49.5
Al_2O_3	13.7	15.4	13.7	14.4	16.3	16.3	3.2	4.4	19.5	19.6	0.0	16.5	16.3
Na_2O	3.0	2.5	2.4	2.3	2.4	2.6	0.1	0.1	2.9	0.4	0.3	1.8	1.8
MgO	2.3	1.7	1.9	1.2	1.8	2.0	2.6	2.5	1.6	2.5	0.0	2.0	2.0
P_2O_5	0.1	0.1	0.1	7.2	0.2	0.1	0.1	0.1	0.0	0.2	38.4	0.1	0.1
Fe_2O_3	9.4	7.5	17.5	10.3	14.6	19.4	2.9	3.2	4.1	5.8	0.5	4.3	4.2
TiO_2	0.4	0.4	0.6	0.3	0.6	0.6	0.2	0.3	0.1	0.3	0.0	0.2	0.2
MnO	0.1	0.4	0.1	0.0	0.1	0.1	0.1	0.1	0.0	0.1	0.0	0.0	0.0
LOI	11.6	10.1	5.3	5.0	8.1	5.7	17.8	3.1	8.2	14.8	0.2	8.5	11.4

E. Electron Microprobe Data

Electron Microprobe analyses

Electron microprobe (EMP) analyses were performed at the University of Oklahoma using a Cameca SX50 electron microprobe equipped with five wavelength-dispersive spectrometers and PGT PRISM 2000 energy-dispersive X-ray detector. Petrographic characterization was performed by backscattered electron imaging coupled with energy-dispersive X-ray analysis, using beam conditions of 20 kV acceleration and 20 nA sample current. Quantitative analysis was performed by wavelength-dispersive spectrometry using 20 kV accelerating voltage, 20 nA beam current, and 2 µm spot size. Matrix corrections employed the PAP algorithm (Pouchou and Pichoir, 1985), with oxygen content calculated by stoichiometry. Counting times were 30 seconds on peak for all elements, yielding minimum levels of detection (calculated at 3-σ above mean background) in the range of 0.01 to 0.03 wt. % of the oxides for all components except F (0.16 wt.%). All standards for elements in the silicates were analyzed using 30 second count times on peak, using K-alpha emissions. The standards and oxide detection limits, along with analytical data, are presented here in Appendix E.

Electron Microprobe Standards and Detection Limits

EMP standards and oxide detection limits for silicate analyses

Element	Standard Material	Minimum Detection Limit[a]
Mg	Synthetic Phlogopite	0.02
F	Synthetic Phlogopite	0.11
Na	Albite (Amelia, NC, U.S.A, Rutherford Mine)	0.02
Al	Labradorite (Chihuahua, Mexico)	0.02
Si	Labradorite (Chihuahua, Mexico)	0.02
Ca	Labradorite (Chihuahua, Mexico)	0.01
Cl	Tugtupite (Greenland)	0.01
K	Adularia (St. Gotthard, Switzerland)	0.01
Ti	Titanite glass (Penn State)	0.02
Cr	Synthetic Magnesio-chromite	0.04
Mn	Rhodonite (unknown locality)	0.02
Fe	Augite (unknown locality)	0.02
Ni	Synthetic Liebenbergite	0.06
Zn	Gahnite	0.05

[a] Minimum Detection Limit (MDL) values for oxides of respective elements

EBS-23															
Analcime in matrix	**Pt #**	**SiO_2**	**TiO_2**	**Al_2O_3**	**Cr_2O_3**	**FeO**	**NiO**	**MnO**	**MgO**	**CaO**	**Na_2O**	**K_2O**	**Cl**	**F**	**TOTAL**
EBS-23-A1 Anl-m	1	58.72	0.01	23.59	0.00	0.07	0.00	0.02	0.00	3.44	5.11	0.01	0.00	0.00	90.98
EBS-23-A1 Anl-m	2	58.52	0.01	23.14	0.00	0.04	0.02	0.00	0.00	3.39	6.64	0.02	0.01	0.00	91.79
EBS-23-A1 Anl-m	3	60.31	0.01	23.25	0.00	0.05	0.00	0.00	0.01	3.20	6.61	0.02	0.01	0.00	93.47
EBS-23-A1 Anl-m	4	56.92	0.01	22.26	0.00	0.10	0.01	0.02	0.06	5.87	4.96	0.02	0.02	0.00	90.25
EBS-23-A3Anl-rim-m	12	56.31	0.02	22.98	0.00	0.07	0.00	0.01	0.01	4.22	5.82	0.02	0.02	0.00	89.49
EBS-23-A3Anl-core-m	13	59.62	0.02	23.37	0.00	0.07	0.00	0.00	0.00	3.60	5.21	0.03	0.02	0.03	91.93
EBS-23-A3 Anl-m	14	60.43	0.00	22.46	0.00	0.05	0.02	0.01	0.00	3.11	6.49	0.04	0.01	0.07	92.62
EBS-23-A5 Anl-m	22	58.15	0.15	19.96	0.00	0.57	0.00	0.03	0.03	6.71	3.49	0.03	0.04	0.12	89.15
EBS-23-A6Anl-rim-m	24	61.82	0.00	23.19	0.00	0.05	0.00	0.00	0.00	3.22	4.56	0.01	0.01	0.03	92.87
EBS-23-A6Anl-core-m	25	59.40	0.02	21.54	0.00	0.18	0.00	0.00	0.03	7.16	3.47	0.05	0.07	0.04	91.92
EBS-23-A7 Anl-m	28	54.56	0.01	23.89	0.00	0.09	0.00	0.02	0.03	5.27	4.99	0.02	0.01	0.00	88.89
EBS-23-A7 Anl-m	29	58.02	0.00	23.95	0.00	0.05	0.00	0.00	0.01	3.96	5.84	0.02	0.01	0.02	91.86
AVERAGE		**58.56**	**0.02**	**22.80**	**0.00**	**0.12**	**0.00**	**0.01**	**0.02**	**4.43**	**5.27**	**0.03**	**0.02**	**0.03**	**91.27**
Std. Dev.		**1.98**	**0.04**	**1.13**	**0.00**	**0.15**	**0.01**	**0.01**	**0.02**	**1.45**	**1.08**	**0.01**	**0.02**	**0.04**	**1.51**
		6 oxygen atoms per formula unit (sum excludes F & Cl)													
	Pt #	**Si**	**Ti**	**Al**	**Cr**	**Fe**	**Ni**	**Mn**	**Mg**	**Ca**	**Na**	**K**	**Cl**	**F**	**Sum**
EBS-23-A1 Anl-m	1	2.10	0.00	0.99	0.00	0.00	0.00	0.00	0.00	0.13	0.35	0.00	0.00	0.00	3.58
EBS-23-A1 Anl-m	2	2.09	0.00	0.97	0.00	0.00	0.00	0.00	0.00	0.13	0.46	0.00	0.00	0.00	3.65
EBS-23-A1 Anl-m	3	2.11	0.00	0.96	0.00	0.00	0.00	0.00	0.00	0.12	0.45	0.00	0.00	0.00	3.64
EBS-23-A1 Anl-m	4	2.08	0.00	0.96	0.00	0.00	0.00	0.00	0.00	0.23	0.35	0.00	0.00	0.00	3.62
EBS-23-A3Anl-rim-m	12	2.07	0.00	0.99	0.00	0.00	0.00	0.00	0.00	0.17	0.41	0.00	0.00	0.00	3.64
EBS-23-A3Anl-core-m	13	2.11	0.00	0.97	0.00	0.00	0.00	0.00	0.00	0.14	0.36	0.00	0.00	0.00	3.58
EBS-23-A3 Anl-m	14	2.13	0.00	0.93	0.00	0.00	0.00	0.00	0.00	0.12	0.44	0.00	0.00	0.01	3.63
EBS-23-A5 Anl-m	22	2.14	0.00	0.87	0.00	0.02	0.00	0.00	0.00	0.26	0.25	0.00	0.00	0.01	3.55
EBS-23-A6Anl-rim-m	24	2.15	0.00	0.95	0.00	0.00	0.00	0.00	0.00	0.12	0.31	0.00	0.00	0.00	3.53
EBS-23-A6Anl-core-m	25	2.12	0.00	0.91	0.00	0.01	0.00	0.00	0.00	0.27	0.24	0.00	0.00	0.00	3.55
EBS-23-A7 Anl-m	28	2.69	0.00	1.39	0.00	0.00	0.00	0.00	0.00	0.28	0.48	0.00	0.00	0.00	4.85
EBS-23-A7 Anl-m	29	2.76	0.00	1.34	0.00	0.00	0.00	0.00	0.00	0.20	0.54	0.00	0.00	0.00	4.84
AVERAGE		**2.21**	**0.00**	**1.02**	**0.00**	**0.00**	**0.00**	**0.00**	**0.00**	**0.18**	**0.39**	**0.00**	**0.00**	**0.00**	**3.81**

Std. Dev.		**0.24**	**0.00**	**0.17**	**0.00**	**0.00**	**0.00**	**0.00**	**0.00**	**0.07**	**0.09**	**0.00**	**0.00**	**0.00**	**0.49**
Analcime coating Opalinus Clay	**Pt #**	**SiO_2**	**TiO_2**	**Al_2O_3**	**Cr_2O_3**	**FeO**	**NiO**	**MnO**	**MgO**	**CaO**	**Na_2O**	**K_2O**	**Cl**	**F**	**TOTAL**
EBS-23-A2 Anl-c	7	60.42	0.01	23.11	0.00	0.11	0.00	0.01	0.00	2.91	6.73	0.04	0.01	0.00	93.36
EBS-23-A2 Anl-c	8	60.34	0.01	22.16	0.02	0.11	0.00	0.01	0.01	2.95	7.03	0.04	0.01	0.04	92.68
EBS-23-A2 Anl-c	9	59.04	0.00	21.79	0.01	0.08	0.00	0.02	0.00	2.94	6.89	0.04	0.04	0.00	90.85
EBS-23-A3 Anl-c/m	10	58.10	0.01	22.29	0.00	0.05	0.00	0.02	0.00	3.13	6.09	0.03	0.01	0.01	89.73
EBS-23-A4 Anl-c	19	60.51	0.01	23.92	0.00	0.09	0.01	0.01	0.00	3.16	5.11	0.03	0.01	0.05	92.84
EBS-23-A5 Anl-c	20	61.99	0.02	23.09	0.00	0.10	0.00	0.01	0.00	2.63	4.97	0.04	0.01	0.03	92.85
EBS-23-A5 Anl-c	21	61.81	0.02	22.11	0.00	0.13	0.00	0.02	0.00	2.89	4.93	0.04	0.01	0.02	91.96
AVERAGE		**60.31**	**0.01**	**22.64**	**0.00**	**0.10**	**0.00**	**0.01**	**0.00**	**2.94**	**5.96**	**0.04**	**0.01**	**0.02**	**92.04**
Std. Dev.		**1.39**	**0.01**	**0.75**	**0.01**	**0.03**	**0.00**	**0.01**	**0.00**	**0.17**	**0.95**	**0.01**	**0.01**	**0.02**	**1.30**
		6 oxygen atoms per formula unit (sum excludes F & Cl)													
	Pt #	**Si**	**Ti**	**Al**	**Cr**	**Fe**	**Ni**	**Mn**	**Mg**	**Ca**	**Na**	**K**	**Cl**	**F**	**Sum**
EBS-23-A2 Anl-c	7	2.11	0.00	0.95	0.00	0.00	0.00	0.00	0.00	0.11	0.46	0.00	0.00	0.00	3.64
EBS-23-A2 Anl-c	8	2.13	0.00	0.92	0.00	0.00	0.00	0.00	0.00	0.11	0.48	0.00	0.00	0.00	3.65
EBS-23-A2 Anl-c	9	2.13	0.00	0.93	0.00	0.00	0.00	0.00	0.00	0.11	0.48	0.00	0.00	0.00	3.65
EBS-23-A3 Anl-c	10	2.11	0.00	0.96	0.00	0.00	0.00	0.00	0.00	0.12	0.43	0.00	0.00	0.00	3.62
EBS-23-A4 Anl-c	19	2.11	0.00	0.98	0.00	0.00	0.00	0.00	0.00	0.12	0.35	0.00	0.00	0.01	3.57
EBS-23-A5 Anl-c	20	2.16	0.00	0.95	0.00	0.00	0.00	0.00	0.00	0.10	0.33	0.00	0.00	0.00	3.54
EBS-23-A5 Anl-c	21	2.17	0.00	0.92	0.00	0.00	0.00	0.00	0.00	0.11	0.34	0.00	0.00	0.00	3.54
AVERAGE		**2.13**	**0.00**	**0.94**	**0.00**	**0.00**	**0.00**	**0.00**	**0.00**	**0.11**	**0.41**	**0.00**	**0.00**	**0.00**	**3.60**
Std. Dev.		**0.02**	**0.00**	**0.02**	**0.00**	**0.00**	**0.00**	**0.00**	**0.00**	**0.01**	**0.07**	**0.00**	**0.00**	**0.00**	**0.05**
Unknown hydrous phase (garronite)	**Pt #**	**SiO_2**	**TiO_2**	**Al_2O_3**	**Cr_2O_3**	**FeO**	**NiO**	**MnO**	**MgO**	**CaO**	**Na_2O**	**K_2O**	**Cl**	**F**	**TOTAL**
EBS-23-A3-chaz	11	45.89	0.00	21.24	0.00	0.05	0.00	0.00	0.00	6.43	8.01	0.18	0.02	0.01	81.82
EBS-23-A3-chaz	15	45.47	0.00	20.70	0.00	0.03	0.00	0.00	0.00	7.63	6.42	0.13	0.02	0.02	80.41
AVERAGE		**45.68**	**0.00**	**20.97**	**0.00**	**0.04**	**0.00**	**0.00**	**0.00**	**7.03**	**7.22**	**0.16**	**0.02**	**0.01**	**81.12**
Std. Dev.		**0.30**	**0.00**	**0.38**	**0.00**	**0.01**	**0.00**	**0.00**	**0.00**	**0.85**	**1.12**	**0.04**	**0.00**	**0.01**	**1.00**

		12 oxygen atoms per formula unit (sum excludes F & Cl)													
	Pt #	**Si**	**Ti**	**Al**	**Cr**	**Fe**	**Ni**	**Mn**	**Mg**	**Ca**	**Na**	**K**	**Cl**	**F**	**Sum**
EBS-23-A3-chaz	11	3.82	0.00	2.08	0.00	0.00	0.00	0.00	0.00	0.57	1.29	0.02	0.00	0.00	7.79
EBS-23-A3-chaz	15	3.84	0.00	2.06	0.00	0.00	0.00	0.00	0.00	0.69	1.05	0.01	0.00	0.01	7.66
AVERAGE		**3.83**	**0.00**	**2.07**	**0.00**	**0.00**	**0.00**	**0.00**	**0.00**	**0.63**	**1.17**	**0.02**	**0.00**	**0.00**	**7.72**
Std. Dev.		**0.01**	**0.00**	**0.02**	**0.00**	**0.00**	**0.00**	**0.00**	**0.00**	**0.08**	**0.17**	**0.00**	**0.00**	**0.00**	**0.10**
K-Feldspar	**Pt #**	**SiO_2**	**TiO_2**	**Al_2O_3**	**Cr_2O_3**	**FeO**	**NiO**	**MnO**	**MgO**	**CaO**	**Na_2O**	**K_2O**	**Cl**	**F**	**TOTAL**
EBS-23-A3-kfs	17	65.07	0.00	18.53	0.01	0.08	0.00	0.01	0.00	0.14	3.23	11.87	0.01	0.03	98.93
EBS-23-A7-kfs	27	63.31	0.01	17.88	0.00	0.09	0.00	0.01	0.01	0.23	3.18	11.38	0.00	0.04	96.09
AVERAGE		**64.19**	**0.01**	**18.20**	**0.00**	**0.09**	**0.00**	**0.01**	**0.01**	**0.18**	**3.20**	**11.62**	**0.01**	**0.04**	**97.51**
Std. Dev.		**1.24**	**0.00**	**0.46**	**0.00**	**0.00**	**0.00**	**0.00**	**0.00**	**0.07**	**0.03**	**0.35**	**0.00**	**0.01**	**2.01**
		8 oxygen atoms per formula unit (sum excludes F & Cl)													
	Pt #	**Si**	**Ti**	**Al**	**Cr**	**Fe**	**Ni**	**Mn**	**Mg**	**Ca**	**Na**	**K**	**Cl**	**F**	**Sum**
EBS-23-A3-kfs	17	2.99	0.00	1.00	0.00	0.00	0.00	0.00	0.00	0.01	0.29	0.70	0.00	0.00	5.00
EBS-23-A7-kfs	27	3.00	0.00	1.00	0.00	0.00	0.00	0.00	0.00	0.01	0.29	0.69	0.00	0.01	4.99
AVERAGE		**3.00**	**0.00**	**1.00**	**0.00**	**0.00**	**0.00**	**0.00**	**0.00**	**0.01**	**0.29**	**0.69**	**0.00**	**0.01**	**4.99**
Std. Dev.		**0.00**	**0.00**	**0.00**	**0.00**	**0.00**	**0.00**	**0.00**	**0.00**	**0.00**	**0.00**	**0.01**	**0.00**	**0.00**	**0.00**
Shard	**Pt #**	**SiO_2**	**TiO_2**	**Al_2O_3**	**Cr_2O_3**	**FeO**	**NiO**	**MnO**	**MgO**	**CaO**	**Na_2O**	**K_2O**	**Cl**	**F**	**TOTAL**
EBS-23-A4-shard	18	57.27	0.00	11.90	0.01	0.20	0.01	0.00	0.02	4.99	0.84	0.43	0.05	0.00	75.73
		18 oxygen atoms per formula unit (sum excludes F & Cl)													
	Pt #	**Si**	**Ti**	**Al**	**Cr**	**Fe**	**Ni**	**Mn**	**Mg**	**Ca**	**Na**	**K**	**Cl**	**F**	**Sum**
EBS-23-A4-shard	18	7.24	0.00	1.77	0.00	0.02	0.00	0.00	0.00	0.68	0.21	0.07	0.01	0.00	10.00
Plagioclase	**Pt #**	**SiO_2**	**TiO_2**	**Al_2O_3**	**Cr_2O_3**	**FeO**	**NiO**	**MnO**	**MgO**	**CaO**	**Na_2O**	**K_2O**	**Cl**	**F**	**TOTAL**
EBS-23-A5-plag	23	65.46	0.01	22.62	0.01	0.22	0.00	0.00	0.00	3.87	8.03	1.02	0.01	0.06	101.24
EBS-23-A6-plag	26	60.08	0.00	25.65	0.00	0.16	0.00	0.01	0.01	7.24	6.85	0.63	0.01	0.00	100.64
AVERAGE		**62.77**	**0.00**	**24.13**	**0.00**	**0.19**	**0.00**	**0.01**	**0.00**	**5.55**	**7.44**	**0.82**	**0.01**	**0.03**	**100.94**
Std. Dev.		**3.80**	**0.00**	**2.14**	**0.01**	**0.04**	**0.00**	**0.01**	**0.01**	**2.39**	**0.83**	**0.28**	**0.00**	**0.04**	**0.43**
		8 oxygen atoms per formula unit (sum excludes F & Cl)													

	Pt #	Si	Ti	Al	Cr	Fe	Ni	Mn	Mg	Ca	Na	K	Cl	F	Sum
EBS-23-A5-plag	23	2.85	0.00	1.16	0.00	0.01	0.00	0.00	0.00	0.18	0.68	0.06	0.00	0.01	4.94
EBS-23-A6-plag	26	2.66	0.00	1.34	0.00	0.01	0.00	0.00	0.00	0.34	0.59	0.04	0.00	0.00	4.98
AVERAGE		**2.76**	**0.00**	**1.25**	**0.00**	**0.01**	**0.00**	**0.00**	**0.00**	**0.26**	**0.63**	**0.05**	**0.00**	**0.00**	**4.96**
Std. Dev.		**0.13**	**0.00**	**0.13**	**0.00**	**0.00**	**0.00**	**0.00**	**0.00**	**0.12**	**0.06**	**0.02**	**0.00**	**0.01**	**0.03**

EBS-24		**WEIGHT PERCENT**													
SAMPLE	**Pt#**	**SiO_2**	**TiO_2**	**Al_2O_3**	**Cr_2O_3**	**FeO**	**NiO**	**MnO**	**MgO**	**CaO**	**Na_2O**	**K_2O**	**Cl**	**F**	**TOTAL**
ANALCIME coating O.C.															
EBS 24 clay A1 zeolites	1	59.77	0.04	25.65	0.00	0.72	0.00	0.02	0.32	3.29	4.22	0.15	0.05	0.00	94.24
EBS 24 clay A1 zeolites	5	59.44	0.02	24.32	0.01	0.18	0.00	0.01	0.01	2.54	4.17	0.04	0.00	0.03	90.73
EBS 24 clay A1 zeolites	7	60.43	0.04	24.94	0.01	0.20	0.01	0.01	0.05	3.22	4.25	0.10	0.02	0.02	93.28
EBS 24 clay A1 zeolites	8	60.67	0.00	24.01	0.01	0.10	0.01	0.00	0.01	2.87	4.91	0.03	0.00	0.00	92.63
AVERAGE		**60.08**	**0.03**	**24.73**	**0.00**	**0.30**	**0.01**	**0.01**	**0.10**	**2.98**	**4.39**	**0.08**	**0.02**	**0.01**	**92.72**
Std. Dev.		**0.50**	**0.02**	**0.63**	**0.00**	**0.24**	**0.01**	**0.01**	**0.13**	**0.30**	**0.31**	**0.05**	**0.02**	**0.01**	**1.28**
12 oxygen atoms per formula unit (sum excludes F & Cl)															
		Si	**Ti**	**Al**	**Cr**	**Fe**	**Ni**	**Mn**	**Mg**	**Ca**	**Na**	**K**	**Cl**	**F**	**SUM**
EBS 24 clay A1 zeolites	1	4.13	0.00	2.09	0.00	0.04	0.00	0.00	0.03	0.24	0.56	0.01	0.01	0.00	7.12
EBS 24 clay A1 zeolites	5	4.22	0.00	2.04	0.00	0.01	0.00	0.00	0.00	0.19	0.57	0.00	0.00	0.01	7.05
EBS 24 clay A1 zeolites	7	4.19	0.00	2.04	0.00	0.01	0.00	0.00	0.01	0.24	0.57	0.01	0.00	0.01	7.07
EBS 24 clay A1 zeolites	8	4.24	0.00	1.98	0.00	0.01	0.00	0.00	0.00	0.21	0.67	0.00	0.00	0.00	7.11
AVERAGE		**4.20**	**0.00**	**2.04**	**0.00**	**0.02**	**0.00**	**0.00**	**0.01**	**0.22**	**0.59**	**0.01**	**0.00**	**0.00**	**7.09**
Std. Dev.		**0.04**	**0.00**	**0.04**	**0.00**	**0.01**	**0.00**	**0.00**	**0.01**	**0.02**	**0.04**	**0.00**	**0.00**	**0.00**	**0.03**
SAMPLE	**Pt#**	**SiO_2**	**TiO_2**	**Al_2O_3**	**Cr_2O_3**	**FeO**	**NiO**	**MnO**	**MgO**	**CaO**	**Na_2O**	**K_2O**	**Cl**	**F**	**TOTAL**
ANALCIME in clay matrix															
EBS 24 clay A3 zeolite	22	61.38	0.03	25.00	0.00	0.08	0.00	0.00	0.01	2.84	4.28	0.03	0.01	0.00	93.64
EBS 24 clay A1 zeolites	2	59.57	0.03	25.14	0.00	0.22	0.00	0.00	0.11	3.90	3.80	0.08	0.01	0.18	92.85

EBS 24 clay A1 zeolites	3	60.34	0.03	25.76	0.00	0.12	0.00	0.00	0.00	3.46	4.21	0.04	0.01	0.02	93.98
EBS 24 clay A1 zeolites	4	58.60	0.02	23.84	0.00	0.21	0.00	0.01	0.09	5.19	3.69	0.03	0.01	0.02	91.67
AVERAGE	**59.97**	**0.03**	**24.93**	**0.00**	**0.15**	**0.00**	**0.00**	**0.05**	**3.85**	**3.99**	**0.05**	**0.01**	**0.06**	**93.04**	**59.97**
Std. Dev.	**1.02**	**0.00**	**0.69**	**0.00**	**0.06**	**0.00**	**0.00**	**0.05**	**0.86**	**0.25**	**0.02**	**0.00**	**0.07**	**0.89**	**1.02**
12 oxygen atoms per formula unit (sum excludes F & Cl)															
		Si	**Ti**	**Al**	**Cr**	**Fe**	**Ni**	**Mn**	**Mg**	**Ca**	**Na**	**K**	**Cl**	**F**	**SUM**
EBS 24 clay A3 zeolite	22	4.23	0.00	2.03	0.00	0.00	0.00	0.00	0.00	0.21	0.57	0.00	0.00	0.00	7.05
EBS 24 clay A1 zeolites	2	4.16	0.00	2.07	0.00	0.01	0.00	0.00	0.01	0.29	0.51	0.01	0.00	0.04	7.07
EBS 24 clay A1 zeolites	3	4.16	0.00	2.09	0.00	0.01	0.00	0.00	0.00	0.26	0.56	0.00	0.00	0.01	7.08
EBS 24 clay A1 zeolites	4	4.16	0.00	2.00	0.00	0.01	0.00	0.00	0.01	0.39	0.51	0.00	0.00	0.01	7.09
AVERAGE		**4.18**	**0.00**	**2.05**	**0.00**	**0.01**	**0.00**	**0.00**	**0.01**	**0.29**	**0.54**	**0.00**	**0.00**	**0.01**	**7.07**
Std. Dev.		**0.03**	**0.00**	**0.04**	**0.00**	**0.00**	**0.00**	**0.00**	**0.00**	**0.07**	**0.03**	**0.00**	**0.00**	**0.02**	**0.02**
SAMPLE	**Pt#**	**SiO_2**	**TiO_2**	**Al_2O_3**	**Cr_2O_3**	**FeO**	**NiO**	**MnO**	**MgO**	**CaO**	**Na_2O**	**K_2O**	**Cl**	**F**	**TOTAL**
GARRONITE															
EBS 24 clay A2 zeolite	19	48.56	0.00	22.79	0.00	0.08	0.00	0.01	0.00	8.01	0.55	0.02	0.01	0.00	80.05
EBS 24 clay A4 zeolites	29	51.69	0.00	23.02	0.01	0.05	0.00	0.00	0.00	8.04	2.74	0.02	0.00	0.00	85.55
EBS 24 clay A1 zeolites	11	51.58	0.02	24.08	0.00	0.21	0.00	0.00	0.06	8.83	0.98	0.06	0.03	0.00	85.85
EBS 24 clay A3 zeolite	24	53.06	0.01	23.93	0.00	0.11	0.00	0.00	0.01	7.75	1.35	0.08	0.07	0.02	86.37
EBS 24 clay A3 zeolite	26	56.00	0.00	23.37	0.01	0.03	0.02	0.00	0.00	7.64	1.38	0.04	0.03	0.00	88.51
EBS 24 clay A2 zeolite	18	55.67	0.01	23.61	0.01	0.17	0.00	0.00	0.01	7.85	1.13	0.08	0.01	0.00	88.54
EBS 24 clay A3 zeolite	23	56.25	0.00	24.26	0.00	0.07	0.00	0.01	0.01	7.26	1.39	0.06	0.03	0.02	89.34
EBS 24 clay A3 zeolite	25	57.78	0.01	22.64	0.00	0.06	0.01	0.02	0.00	7.73	1.10	0.05	0.03	0.00	89.42
EBS 24 clay A1 zeolites	12	56.03	0.01	24.04	0.01	0.06	0.01	0.00	0.00	8.50	1.16	0.02	0.00	0.00	89.83
EBS 24 clay A1 zeolites	10	56.64	0.01	24.78	0.00	0.07	0.00	0.00	0.02	8.41	1.23	0.03	0.02	0.00	91.22
EBS 24 clay A1 zeolites	14	60.85	0.01	23.74	0.00	0.08	0.01	0.01	0.00	8.30	1.32	0.03	0.02	0.09	94.37
AVERAGE		**54.92**	**0.01**	**23.66**	**0.00**	**0.09**	**0.00**	**0.00**	**0.01**	**8.03**	**1.30**	**0.04**	**0.02**	**0.01**	**88.10**
Std. Dev.		**3.25**	**0.00**	**0.63**	**0.00**	**0.05**	**0.01**	**0.01**	**0.02**	**0.43**	**0.51**	**0.02**	**0.02**	**0.03**	**3.50**
8 oxygen atoms per formula unit (sum excludes F & Cl)															
		Si	**Ti**	**Al**	**Cr**	**Fe**	**Ni**	**Mn**	**Mg**	**Ca**	**Na**	**K**	**Cl**	**F**	**SUM**
EBS 24 clay A2 zeolite	19	2.65	0.00	1.47	0.00	0.00	0.00	0.00	0.00	0.47	0.06	0.00	0.00	0.00	4.65

EBS 24 clay A4 zeolites	29	2.66	0.00	1.40	0.00	0.00	0.00	0.00	0.00	0.44	0.27	0.00	0.00	0.00	4.78
EBS 24 clay A1 zeolites	11	2.64	0.00	1.45	0.00	0.01	0.00	0.00	0.00	0.48	0.10	0.00	0.00	0.00	4.69
EBS 24 clay A3 zeolite	24	2.68	0.00	1.43	0.00	0.00	0.00	0.00	0.00	0.42	0.13	0.00	0.01	0.00	4.67
EBS 24 clay A3 zeolite	26	2.75	0.00	1.35	0.00	0.00	0.00	0.00	0.00	0.40	0.13	0.00	0.00	0.00	4.64
EBS 24 clay A2 zeolite	18	2.74	0.00	1.37	0.00	0.01	0.00	0.00	0.00	0.41	0.11	0.00	0.00	0.00	4.64
EBS 24 clay A3 zeolite	23	2.73	0.00	1.39	0.00	0.00	0.00	0.00	0.00	0.38	0.13	0.00	0.00	0.00	4.64
EBS 24 clay A3 zeolite	25	2.80	0.00	1.29	0.00	0.00	0.00	0.00	0.00	0.40	0.10	0.00	0.00	0.00	4.61
EBS 24 clay A1 zeolites	12	2.72	0.00	1.37	0.00	0.00	0.00	0.00	0.00	0.44	0.11	0.00	0.00	0.00	4.65
EBS 24 clay A1 zeolites	10	2.71	0.00	1.40	0.00	0.00	0.00	0.00	0.00	0.43	0.11	0.00	0.00	0.00	4.65
EBS 24 clay A1 zeolites	14	2.80	0.00	1.29	0.00	0.00	0.00	0.00	0.00	0.41	0.12	0.00	0.00	0.01	4.62
AVERAGE		**2.72**	**0.00**	**1.38**	**0.00**	**0.00**	**0.00**	**0.00**	**0.00**	**0.43**	**0.13**	**0.00**	**0.00**	**0.00**	**4.66**
Std. Dev.		**0.05**	**0.00**	**0.05**	**0.00**	**0.00**	**0.00**	**0.00**	**0.00**	**0.03**	**0.05**	**0.00**	**0.00**	**0.00**	**0.04**
SAMPLE	**Pt#**	**SiO_2**	**TiO_2**	**Al_2O_3**	**Cr_2O_3**	**FeO**	**NiO**	**MnO**	**MgO**	**CaO**	**Na_2O**	**K_2O**	**Cl**	**F**	**TOTAL**
K-FELDSPAR															
EBS 24 clay A1 feldspar	16	63.55	0.00	20.60	0.00	0.10	0.02	0.00	0.00	0.19	3.14	11.54	0.01	0.00	99.14
EBS 24 clay A3 feldspars	28	64.32	0.01	20.29	0.00	0.11	0.00	0.00	0.00	0.23	2.88	11.28	0.00	0.00	99.12
EBS 24 clay A4 feldspars	32	63.71	0.01	20.41	0.00	0.10	0.00	0.02	0.00	0.21	3.12	11.61	0.00	0.03	99.19
EBS 24 clay A4 feldspars	33	65.28	0.00	20.62	0.00	0.15	0.01	0.00	0.00	0.20	3.17	11.61	0.00	0.00	101.04
EBS 24 clay A4 feldspars	34	64.28	0.01	20.87	0.00	0.11	0.01	0.00	0.00	0.36	3.18	10.18	0.00	0.00	99.00
EBS 24 clay A5 feldspars	37	63.86	0.01	20.52	0.00	0.16	0.00	0.00	0.00	0.19	3.02	11.23	0.01	0.00	99.00
EBS 24 clay A5 feldspars	38	64.25	0.01	19.70	0.00	0.15	0.00	0.00	0.01	0.15	2.99	11.54	0.01	0.00	98.81
EBS 24 clay A5 feldspars	39	64.95	0.01	20.32	0.00	0.13	0.01	0.00	0.02	0.23	2.99	11.49	0.01	0.00	100.14
AVERAGE		**64.34**	**0.01**	**20.35**	**0.00**	**0.14**	**0.00**	**0.00**	**0.01**	**0.23**	**3.05**	**11.11**	**0.01**	**0.00**	**99.24**
Std. Dev.		**0.39**	**0.00**	**0.43**	**0.00**	**0.02**	**0.01**	**0.00**	**0.01**	**0.08**	**0.08**	**0.55**	**0.00**	**0.00**	**0.53**
8 oxygen atoms per formula unit (sum excludes F & Cl)															
		Si	**Ti**	**Al**	**Cr**	**Fe**	**Ni**	**Mn**	**Mg**	**Ca**	**Na**	**K**	**Cl**	**F**	**SUM**
EBS 24 clay A1 feldspar	16	2.92	0.00	1.11	0.00	0.00	0.00	0.00	0.00	0.01	0.28	0.68	0.00	0.00	5.00
EBS 24 clay A3 feldspars	28	2.91	0.00	1.13	0.00	0.00	0.00	0.00	0.00	0.01	0.26	0.68	0.00	0.00	5.00

EBS 24 clay A4 feldspars	32	2.92	0.00	1.10	0.00	0.00	0.00	0.00	0.00	0.01	0.28	0.68	0.00	0.00	5.00
EBS 24 clay A4 feldspars	33	2.94	0.00	1.09	0.00	0.01	0.00	0.00	0.00	0.01	0.28	0.67	0.00	0.00	4.99
EBS 24 clay A4 feldspars	34	2.88	0.00	1.17	0.00	0.00	0.00	0.00	0.00	0.02	0.29	0.62	0.00	0.00	4.99
EBS 24 clay A5 feldspars	37	2.93	0.00	1.11	0.00	0.01	0.00	0.00	0.00	0.01	0.27	0.66	0.00	0.00	4.98
EBS 24 clay A5 feldspars	38	2.96	0.00	1.07	0.00	0.01	0.00	0.00	0.00	0.01	0.27	0.68	0.00	0.00	4.98
EBS 24 clay A5 feldspars	39	2.94	0.00	1.09	0.00	0.00	0.00	0.00	0.00	0.01	0.26	0.66	0.00	0.00	4.98
AVERAGE		**2.92**	**0.00**	**1.11**	**0.00**	**0.00**	**0.00**	**0.00**	**0.00**	**0.01**	**0.27**	**0.67**	**0.00**	**0.00**	**4.99**
Std. Dev.		**0.02**	**0.00**	**0.03**	**0.00**	**0.00**	**0.00**	**0.00**	**0.00**	**0.00**	**0.01**	**0.02**	**0.00**	**0.00**	**0.01**
SAMPLE	**Pt#**	**SiO_2**	**TiO_2**	**Al_2O_3**	**Cr_2O_3**	**FeO**	**NiO**	**MnO**	**MgO**	**CaO**	**Na_2O**	**K_2O**	**Cl**	**F**	**TOTAL**
Plagioclase															
EBS 24 clay A1 zeolites	9	59.11	0.01	25.46	0.00	0.24	0.00	0.02	0.00	5.58	7.01	1.02	0.00	0.02	98.46
EBS 24 clay A1 feldspar	15	61.38	0.00	24.98	0.00	0.22	0.00	0.01	0.00	5.56	7.07	1.02	0.00	0.00	100.25
EBS 24 clay A3 feldspars	27	58.10	0.00	27.80	0.00	0.17	0.00	0.01	0.00	7.52	6.43	0.65	0.00	0.07	100.69
EBS 24 clay A5 feldspars	36	62.54	0.01	22.98	0.00	0.18	0.00	0.00	0.01	5.77	6.97	0.95	0.00	0.09	99.41
AVERAGE		**60.28**	**0.00**	**25.30**	**0.00**	**0.20**	**0.00**	**0.01**	**0.00**	**6.11**	**6.87**	**0.91**	**0.00**	**0.04**	**99.70**
Std. Dev.		**1.77**	**0.00**	**1.71**	**0.00**	**0.03**	**0.00**	**0.01**	**0.00**	**0.82**	**0.26**	**0.15**	**0.00**	**0.04**	**0.85**
8 oxygen atoms per formula unit (sum excludes F & Cl)															
		Si	**Ti**	**Al**	**Cr**	**Fe**	**Ni**	**Mn**	**Mg**	**Ca**	**Na**	**K**	**Cl**	**F**	**SUM**
EBS 24 clay A1 zeolites	9	2.67	0.00	1.36	0.00	0.01	0.00	0.00	0.00	0.27	0.61	0.06	0.00	0.00	4.98
EBS 24 clay A1 feldspar	15	2.69	0.00	1.34	0.00	0.01	0.00	0.00	0.00	0.26	0.60	0.06	0.00	0.00	4.96
EBS 24 clay A3 feldspars	27	2.58	0.00	1.45	0.00	0.01	0.00	0.00	0.00	0.36	0.55	0.04	0.00	0.01	4.99
EBS 24 clay A5 feldspars	36	2.71	0.00	1.33	0.00	0.01	0.00	0.00	0.00	0.27	0.59	0.05	0.00	0.01	4.95
AVERAGE		**2.66**	**0.00**	**1.37**	**0.00**	**0.01**	**0.00**	**0.00**	**0.00**	**0.29**	**0.59**	**0.05**	**0.00**	**0.01**	**4.97**
Std. Dev.		**0.05**	**0.00**	**0.05**	**0.00**	**0.00**	**0.00**	**0.00**	**0.00**	**0.04**	**0.02**	**0.01**	**0.00**	**0.00**	**0.02**
SAMPLE	**Pt#**	**SiO_2**	**TiO_2**	**Al_2O_3**	**Cr_2O_3**	**FeO**	**NiO**	**MnO**	**MgO**	**CaO**	**Na_2O**	**K_2O**	**Cl**	**F**	**TOTAL**
ANALCIME in porous cement matrix															
EBS 24 cement A1 zeolites	4	59.28	0.00	24.67	0.00	0.06	0.02	0.00	0.00	2.92	5.20	0.03	0.00	0.08	92.18
EBS 24 cement A1 zeolites	7	59.66	0.00	25.83	0.00	0.04	0.01	0.00	0.00	2.96	5.43	0.03	0.00	0.00	93.95

EBS 24 cement A2 zeolites	10	59.78	0.00	25.99	0.00	0.05	0.00	0.01	0.00	2.98	5.12	0.01	0.01	0.00	93.95
EBS 24 cement A1 zeolites	2	60.45	0.02	25.18	0.00	0.09	0.00	0.00	0.00	3.04	5.14	0.02	0.00	0.05	93.94
EBS 24 cement A1 zeolites	6	60.25	0.00	26.26	0.00	0.04	0.00	0.00	0.00	3.05	5.58	0.02	0.00	0.11	95.21
EBS 24 cement A2 zeolites	8	59.95	0.00	27.33	0.00	0.05	0.00	0.01	0.00	3.05	5.31	0.03	0.01	0.00	95.74
EBS 24 cement A2 zeolites	9	59.84	0.01	25.56	0.01	0.05	0.00	0.00	0.00	3.07	4.96	0.02	0.01	0.00	93.52
EBS 24 cement A3 zeolites	19	58.73	0.00	24.33	0.00	0.03	0.00	0.00	0.01	3.15	5.12	0.03	0.00	0.00	91.40
EBS 24 cement A4 zeolites	22	59.39	0.01	24.38	0.00	0.05	0.00	0.02	0.01	3.19	5.13	0.01	0.00	0.00	92.18
EBS 24 cement A3 zeolites	17	58.95	0.00	25.67	0.00	0.05	0.01	0.01	0.00	3.27	5.15	0.01	0.01	0.09	93.12
EBS 24 cement A4 zeolites	23	60.87	0.00	25.73	0.00	0.08	0.00	0.00	0.00	3.44	5.37	0.02	0.00	0.08	95.52
EBS 24 cement A4 zeolites	20	55.59	0.01	26.75	0.00	0.04	0.01	0.00	0.00	3.48	5.36	0.02	0.00	0.00	91.27
EBS 24 cement A4 zeolites	21	59.77	0.00	25.01	0.00	0.07	0.00	0.00	0.00	3.63	5.23	0.02	0.01	0.01	93.74
EBS 24 cement A1 zeolites	3	54.07	0.00	24.98	0.00	0.05	0.03	0.00	0.01	3.72	5.32	0.02	0.01	0.00	88.20
EBS 24 cement A1 zeolites	1	60.37	0.00	27.63	0.00	0.05	0.01	0.01	0.00	3.84	5.56	0.02	0.00	0.01	97.49
AVERAGE		**59.13**	**0.00**	**25.69**	**0.00**	**0.05**	**0.01**	**0.00**	**0.00**	**3.25**	**5.26**	**0.02**	**0.00**	**0.03**	**93.43**
Std. Dev.		**1.79**	**0.01**	**0.96**	**0.00**	**0.02**	**0.01**	**0.01**	**0.00**	**0.29**	**0.17**	**0.01**	**0.00**	**0.04**	**2.16**
12 oxygen atoms per formula unit (sum excludes F & Cl)															
		Si	**Ti**	**Al**	**Cr**	**Fe**	**Ni**	**Mn**	**Mg**	**Ca**	**Na**	**K**	**Cl**	**F**	**SUM**
EBS 24 cement A1 zeolites	4	4.17	0.00	2.05	0.00	0.00	0.00	0.00	0.00	0.22	0.71	0.00	0.00	0.02	7.16
EBS 24 cement A1 zeolites	7	4.13	0.00	2.11	0.00	0.00	0.00	0.00	0.00	0.22	0.73	0.00	0.00	0.00	7.19
EBS 24 cement A2 zeolites	10	4.13	0.00	2.12	0.00	0.00	0.00	0.00	0.00	0.22	0.69	0.00	0.00	0.00	7.16
EBS 24 cement A1 zeolites	2	4.17	0.00	2.05	0.00	0.01	0.00	0.00	0.00	0.22	0.69	0.00	0.00	0.01	7.15
EBS 24 cement A1 zeolites	6	4.12	0.00	2.11	0.00	0.00	0.00	0.00	0.00	0.22	0.74	0.00	0.00	0.02	7.20
EBS 24 cement A2 zeolites	8	4.07	0.00	2.19	0.00	0.00	0.00	0.00	0.00	0.22	0.70	0.00	0.00	0.00	7.19
EBS 24 cement A2 zeolites	9	4.15	0.00	2.09	0.00	0.00	0.00	0.00	0.00	0.23	0.67	0.00	0.00	0.00	7.14
EBS 24 cement A3 zeolites	19	4.17	0.00	2.04	0.00	0.00	0.00	0.00	0.00	0.24	0.70	0.00	0.00	0.00	7.16
EBS 24 cement A4 zeolites	22	4.18	0.00	2.02	0.00	0.00	0.00	0.00	0.00	0.24	0.70	0.00	0.00	0.00	7.16
EBS 24 cement A3 zeolites	17	4.12	0.00	2.11	0.00	0.00	0.00	0.00	0.00	0.24	0.70	0.00	0.00	0.02	7.18
EBS 24 cement A4 zeolites	23	4.15	0.00	2.07	0.00	0.00	0.00	0.00	0.00	0.25	0.71	0.00	0.00	0.02	7.18
EBS 24 cement A4 zeolites	20	3.98	0.00	2.26	0.00	0.00	0.00	0.00	0.00	0.27	0.74	0.00	0.00	0.00	7.26

EBS 24 cement A4 zeolites	21	4.15	0.00	2.05	0.00	0.00	0.00	0.00	0.00	0.27	0.70	0.00	0.00	0.00	7.18
EBS 24 cement A1 zeolites	3	4.02	0.00	2.19	0.00	0.00	0.00	0.00	0.00	0.30	0.77	0.00	0.00	0.00	7.27
EBS 24 cement A1 zeolites	1	4.04	0.00	2.18	0.00	0.00	0.00	0.00	0.00	0.28	0.72	0.00	0.00	0.00	7.23
AVERAGE		**4.12**	**0.00**	**2.11**	**0.00**	**0.00**	**0.00**	**0.00**	**0.00**	**0.24**	**0.71**	**0.00**	**0.00**	**0.01**	**7.18**
Std. Dev.		**0.06**	**0.00**	**0.07**	**0.00**	**0.00**	**0.00**	**0.00**	**0.00**	**0.02**	**0.02**	**0.00**	**0.00**	**0.01**	**0.04**
SAMPLE	**Pt#**	**SiO_2**	**TiO_2**	**Al_2O_3**	**Cr_2O_3**	**FeO**	**NiO**	**MnO**	**MgO**	**CaO**	**Na_2O**	**K_2O**	**Cl**	**F**	**TOTAL**
ANACLIME in porous cement matrix (High Ca)															
EBS 24 cement A3 zeolites	18	56.08	0.01	25.71	0.00	0.04	0.01	0.00	0.00	5.90	4.85	0.01	0.02	0.00	92.63
EBS 24 cement A1 zeolites	5	55.54	0.01	24.72	0.00	0.15	0.00	0.00	0.02	6.83	4.55	0.08	0.03	0.00	91.93
EBS 24 cement A2 zeolites	11	56.92	0.00	23.69	0.00	0.15	0.00	0.00	0.12	7.22	3.36	0.05	0.13	0.04	91.64
AVERAGE		**56.18**	**0.01**	**24.70**	**0.00**	**0.11**	**0.00**	**0.00**	**0.05**	**6.65**	**4.26**	**0.05**	**0.06**	**0.01**	**92.07**
Std. Dev.		56.08	0.01	25.71	0.00	0.04	0.01	0.00	0.00	5.90	4.85	0.01	0.02	0.00	92.63
12 oxygen atoms per formula unit (sum excludes F & Cl)															
		Si	**Ti**	**Al**	**Cr**	**Fe**	**Ni**	**Mn**	**Mg**	**Ca**	**Na**	**K**	**Cl**	**F**	**SUM**
EBS 24 cement A3 zeolites	18	3.99	0.00	2.16	0.00	0.00	0.00	0.00	0.00	0.45	0.67	0.00	0.00	0.00	7.27
EBS 24 cement A1 zeolites	5	4.00	0.00	2.10	0.00	0.01	0.00	0.00	0.00	0.53	0.64	0.01	0.00	0.00	7.28
EBS 24 cement A2 zeolites	11	4.09	0.00	2.01	0.00	0.01	0.00	0.00	0.01	0.56	0.47	0.00	0.02	0.01	7.14
AVERAGE		**4.03**	**0.00**	**2.09**	**0.00**	**0.01**	**0.00**	**0.00**	**0.00**	**0.51**	**0.59**	**0.00**	**0.01**	**0.00**	**7.23**
Std. Dev.		**0.05**	**0.00**	**0.06**	**0.00**	**0.00**	**0.00**	**0.00**	**0.01**	**0.04**	**0.09**	**0.00**	**0.01**	**0.00**	**0.06**
SAMPLE	**Pt#**	**SiO_2**	**TiO_2**	**Al_2O_3**	**Cr_2O_3**	**FeO**	**NiO**	**MnO**	**MgO**	**CaO**	**Na_2O**	**K_2O**	**Cl**	**F**	**TOTAL**
K-FELDSPAR															
EBS 24 cement A2 feldspar	12	65.27	0.01	19.67	0.00	0.12	0.00	0.00	0.00	0.20	2.37	13.03	0.00	0.00	100.68
EBS 24 cement A2 feldspar	13	65.17	0.01	19.82	0.00	0.11	0.00	0.00	0.01	0.22	3.40	11.92	0.01	0.02	100.68
EBS 24 cement A3 feldspar	14	65.37	0.00	19.61	0.00	0.13	0.02	0.01	0.01	0.26	3.38	11.86	0.01	0.04	100.65
AVERAGE		**65.27**	**0.01**	**19.70**	**0.00**	**0.12**	**0.01**	**0.00**	**0.01**	**0.23**	**3.05**	**12.27**	**0.01**	**0.02**	**100.67**
Std. Dev.		**0.08**	**0.00**	**0.09**	**0.00**	**0.01**	**0.01**	**0.00**	**0.00**	**0.03**	**0.48**	**0.54**	**0.00**	**0.02**	**0.01**
8 oxygen atoms per formula unit (sum excludes F & Cl)															
		Si	**Ti**	**Al**	**Cr**	**Fe**	**Ni**	**Mn**	**Mg**	**Ca**	**Na**	**K**	**Cl**	**F**	**SUM**

EBS 24 cement A2 feldspar	12	2.96	0.00	1.05	0.00	0.00	0.00	0.00	0.00	0.01	0.21	0.75	0.00	0.00	4.99
EBS 24 cement A2 feldspar	13	2.96	0.00	1.05	0.00	0.00	0.00	0.00	0.00	0.01	0.30	0.68	0.00	0.00	5.00
EBS 24 cement A3 feldspar	14	2.96	0.00	1.05	0.00	0.00	0.00	0.00	0.00	0.01	0.30	0.68	0.00	0.01	5.01
AVERAGE		**2.96**	**0.00**	**1.05**	**0.00**	**0.00**	**0.00**	**0.00**	**0.00**	**0.01**	**0.27**	**0.71**	**0.00**	**0.00**	**5.00**
Std. Dev.		**0.00**	**0.00**	**0.00**	**0.00**	**0.00**	**0.00**	**0.00**	**0.00**	**0.00**	**0.04**	**0.03**	**0.00**	**0.00**	**0.01**
SAMPLE	**Pt#**	**SiO_2**	**TiO_2**	**Al_2O_3**	**Cr_2O_3**	**FeO**	**NiO**	**MnO**	**MgO**	**CaO**	**Na_2O**	**K_2O**	**Cl**	**F**	**TOTAL**
PLAGIOCLASE															
EBS 24 cement A3 feldspar	15	60.76	0.00	24.77	0.00	0.20	0.00	0.00	0.01	5.30	7.48	0.93	0.01	0.00	99.46
EBS 24 cement A3 feldspar	16	61.18	0.01	24.92	0.00	0.24	0.02	0.01	0.00	5.15	7.24	1.09	0.00	0.00	99.87
AVERAGE		**60.97**	**0.00**	**24.84**	**0.00**	**0.22**	**0.01**	**0.00**	**0.01**	**5.22**	**7.36**	**1.01**	**0.00**	**0.00**	**99.67**
Std. Dev.		**0.21**	**0.00**	**0.08**	**0.00**	**0.02**	**0.01**	**0.00**	**0.01**	**0.08**	**0.12**	**0.08**	**0.00**	**0.00**	**0.20**
8 oxygen atoms per formula unit (sum excludes F & Cl)															
		Si	**Ti**	**Al**	**Cr**	**Fe**	**Ni**	**Mn**	**Mg**	**Ca**	**Na**	**K**	**Cl**	**F**	**SUM**
EBS 24 cement A3 feldspar	15	2.74	0.00	1.26	0.00	0.01	0.00	0.00	0.00	0.26	0.65	0.05	0.00	0.00	4.98
EBS 24 cement A3 feldspar	16	2.76	0.00	1.26	0.00	0.01	0.00	0.00	0.00	0.24	0.60	0.06	0.00	0.00	4.94
AVERAGE		**2.75**	**0.00**	**1.26**	**0.00**	**0.01**	**0.00**	**0.00**	**0.00**	**0.25**	**0.63**	**0.06**	**0.00**	**0.00**	**4.96**
Std. Dev.		**0.01**	**0.00**	**0.00**	**0.00**	**0.00**	**0.00**	**0.00**	**0.00**	**0.01**	**0.03**	**0.00**	**0.00**	**0.00**	**0.02**
SAMPLE	**Pt#**	**SiO_2**	**TiO_2**	**Al_2O_3**	**Cr_2O_3**	**FeO**	**NiO**	**MnO**	**MgO**	**CaO**	**Na_2O**	**K_2O**	**Cl**	**F**	**TOTAL**
ANALCIME near steel surface															
EBS 24 Steel zeolites A1	1	60.82	0.01	22.17	0.07	0.38	0.06	0.01	0.00	5.43	3.02	0.04	0.02	0.01	92.03
EBS 24 Steel zeolites A1	2	60.45	0.01	22.19	0.06	0.41	0.04	0.02	0.00	3.18	4.65	0.03	0.01	0.01	91.04
EBS 24 Steel zeolites A1	3	60.60	0.03	22.23	0.12	0.43	0.07	0.00	0.00	4.52	3.20	0.02	0.02	0.05	91.23
EBS 24 Steel Zeolites A1	4	62.93	0.01	23.54	0.15	0.56	0.06	0.02	0.01	3.33	4.32	0.04	0.01	0.06	94.98
EBS 24 Steel Zeolites A1	5	61.80	0.03	22.93	0.25	1.37	0.12	0.02	0.11	3.18	3.43	0.02	0.03	0.01	93.29
EBS 24 Steel zeolites A2	6	63.39	0.02	22.92	0.05	0.14	0.01	0.00	0.05	3.10	4.32	0.02	0.01	0.05	94.04
EBS 24 Steel zeolites A2	7	61.14	0.01	22.95	0.03	0.14	0.00	0.02	0.03	2.62	4.48	0.01	0.01	0.02	91.42
EBS 24 Steel zeolites A2	8	59.48	0.00	22.21	0.17	0.29	0.04	0.01	0.01	2.43	5.27	0.03	0.01	0.00	89.94

EBS 24 Steel zeolites A2	9	61.53	0.01	21.74	0.15	0.22	0.01	0.00	0.00	2.19	5.09	0.04	0.02	0.00	90.98
AVERAGE		**61.35**	**0.02**	**22.54**	**0.12**	**0.44**	**0.05**	**0.01**	**0.02**	**3.33**	**4.20**	**0.03**	**0.01**	**0.02**	**92.11**
Std. Dev.		**1.16**	**0.01**	**0.54**	**0.07**	**0.36**	**0.03**	**0.01**	**0.03**	**0.98**	**0.76**	**0.01**	**0.01**	**0.02**	**1.55**
12 oxygen atoms per formula unit (sum excludes F & Cl)															
		Si	**Ti**	**Al**	**Cr**	**Fe**	**Ni**	**Mn**	**Mg**	**Ca**	**Na**	**K**	**Cl**	**F**	**SUM**
EBS 24 Steel zeolites A1	1	4.29	0.00	1.84	0.00	0.02	0.00	0.00	0.00	0.41	0.41	0.00	0.00	0.00	6.99
EBS 24 Steel zeolites A1	2	4.30	0.00	1.86	0.00	0.02	0.00	0.00	0.00	0.24	0.64	0.00	0.00	0.00	7.08
EBS 24 Steel zeolites A1	3	4.30	0.00	1.86	0.01	0.03	0.00	0.00	0.00	0.34	0.44	0.00	0.00	0.01	6.98
EBS 24 Steel Zeolites A1	4	4.29	0.00	1.89	0.01	0.03	0.00	0.00	0.00	0.24	0.57	0.00	0.00	0.01	7.05
EBS 24 Steel Zeolites A1	5	4.30	0.00	1.88	0.01	0.08	0.01	0.00	0.01	0.24	0.46	0.00	0.00	0.00	6.99
EBS 24 Steel zeolites A2	6	4.34	0.00	1.85	0.00	0.01	0.00	0.00	0.01	0.23	0.57	0.00	0.00	0.01	7.02
EBS 24 Steel zeolites A2	7	4.31	0.00	1.91	0.00	0.01	0.00	0.00	0.00	0.20	0.61	0.00	0.00	0.01	7.04
EBS 24 Steel zeolites A2	8	4.29	0.00	1.89	0.01	0.02	0.00	0.00	0.00	0.19	0.74	0.00	0.00	0.00	7.13
EBS 24 Steel zeolites A2	9	4.36	0.00	1.82	0.01	0.01	0.00	0.00	0.00	0.17	0.70	0.00	0.00	0.00	7.07
AVERAGE		**4.31**	**0.00**	**1.87**	**0.01**	**0.03**	**0.00**	**0.00**	**0.00**	**0.25**	**0.57**	**0.00**	**0.00**	**0.01**	**7.04**
Std. Dev.		**0.03**	**0.00**	**0.03**	**0.00**	**0.02**	**0.00**	**0.00**	**0.00**	**0.07**	**0.11**	**0.00**	**0.00**	**0.01**	**0.05**
SAMPLE	**Pt#**	**SiO_2**	**TiO_2**	**Al_2O_3**	**Cr_2O_3**	**FeO**	**NiO**	**MnO**	**MgO**	**CaO**	**Na_2O**	**K_2O**	**Cl**	**F**	**TOTAL**
CLAY															
EBS 24 Steel zeolites A3	15	31.93	0.14	13.34	0.22	4.25	0.05	0.04	2.37	3.07	0.71	0.89	0.27	0.10	57.27
EBS 24 Steel zeolites A3	16	33.85	0.45	13.33	0.26	5.46	0.08	0.05	2.98	4.41	0.58	0.57	0.29	0.12	62.30
AVERAGE		**32.89**	**0.29**	**13.34**	**0.24**	**4.86**	**0.07**	**0.04**	**2.67**	**3.74**	**0.64**	**0.73**	**0.28**	**0.11**	**59.78**
Std. Dev.		**0.96**	**0.16**	**0.01**	**0.02**	**0.61**	**0.02**	**0.01**	**0.31**	**0.67**	**0.06**	**0.16**	**0.01**	**0.01**	**2.52**
8 oxygen atoms per formula unit (sum excludes F & Cl)															
		Si	**Ti**	**Al**	**Cr**	**Fe**	**Ni**	**Mn**	**Mg**	**Ca**	**Na**	**K**	**Cl**	**F**	**SUM**
EBS 24 Steel zeolites A3	15	3.85	0.01	1.89	0.02	0.43	0.00	0.00	0.42	0.40	0.17	0.14	0.06	0.04	7.33
EBS 24 Steel zeolites A3	16	3.80	0.04	1.76	0.02	0.51	0.01	0.00	0.50	0.53	0.13	0.08	0.05	0.04	7.38
AVERAGE		**3.82**	**0.03**	**1.83**	**0.02**	**0.47**	**0.01**	**0.00**	**0.46**	**0.46**	**0.15**	**0.11**	**0.05**	**0.04**	**7.36**
Std. Dev.		**0.03**	**0.01**	**0.07**	**0.00**	**0.04**	**0.00**	**0.00**	**0.04**	**0.07**	**0.02**	**0.03**	**0.00**	**0.00**	**0.02**
SAMPLE	**Pt#**	**SiO_2**	**TiO_2**	**Al_2O_3**	**Cr_2O_3**	**FeO**	**NiO**	**MnO**	**MgO**	**CaO**	**Na_2O**	**K_2O**	**Cl**	**F**	**TOTAL**

Miscellaneous zeolite on steel															
EBS 24 Steel zeolites A2	13	65.63	0.00	20.31	0.05	0.16	0.01	0.00	0.00	0.21	3.22	12.03	0.00	0.00	101.63
EBS 24 Steel zeolites A2	10	65.32	0.01	24.17	0.06	0.23	0.01	0.00	0.00	4.25	8.18	1.11	0.00	0.00	103.35
EBS 24 Steel zeolites A2	11	51.03	0.01	31.07	0.07	0.41	0.01	0.00	0.02	12.92	3.90	0.22	0.00	0.07	99.68
12 oxygen atoms per formula unit (sum excludes F & Cl)															
		Si	**Ti**	**Al**	**Cr**	**Fe**	**Ni**	**Mn**	**Mg**	**Ca**	**Na**	**K**	**Cl**	**F**	**SUM**
EBS 24 Steel zeolites A2	13	4.41	0.00	1.61	0.00	0.01	0.00	0.00	0.00	0.02	0.42	1.03	0.00	0.00	7.50
EBS 24 Steel zeolites A2	10	4.19	0.00	1.83	0.00	0.01	0.00	0.00	0.00	0.29	1.02	0.09	0.00	0.00	7.44
EBS 24 Steel zeolites A2	11	4.19	0.00	1.83	0.00	0.01	0.00	0.00	0.00	0.29	1.02	0.09	0.00	0.00	7.44

EBS-25		**WEIGHT PERCENT**													
SAMPLE	**Pt#**	**SiO_2**	**TiO_2**	**Al_2O_3**	**Cr_2O_3**	**FeO**	**NiO**	**MnO**	**MgO**	**CaO**	**Na_2O**	**K_2O**	**Cl**	**F**	**TOTAL**
ZEOLITE in clay matrix															
EBS 25-clay zeolite A1	1	61.28	0.02	23.60	0.00	0.24	0.00	0.00	0.07	3.55	4.19	0.05	0.04	0.00	93.04
EBS 25-clay zeolites	3	60.99	0.01	24.43	0.00	0.11	0.00	0.00	0.01	3.07	5.05	0.03	0.01	0.04	93.71
EBS 25-clay zeolites	4	61.23	0.02	24.80	0.00	0.18	0.00	0.00	0.07	3.92	4.91	0.03	0.01	0.01	95.18
EBS 25-clay zeolites	5	62.84	0.01	23.18	0.00	0.31	0.01	0.00	0.02	2.96	3.85	0.04	0.02	0.00	93.23
EBS 25-clay zeolites	6	60.73	0.02	24.09	0.00	0.10	0.00	0.00	0.00	3.32	5.88	0.03	0.00	0.00	94.16
EBS 25-clay zeolites	7	62.88	0.02	23.52	0.00	0.15	0.00	0.00	0.04	2.38	6.00	0.03	0.00	0.00	95.03
EBS 25-clay zeolites	8	61.54	0.03	23.68	0.00	0.12	0.00	0.00	0.02	2.66	4.90	0.04	0.01	0.04	92.99
AVERAGE		**61.64**	**0.02**	**23.90**	**0.00**	**0.17**	**0.00**	**0.00**	**0.03**	**3.12**	**4.97**	**0.04**	**0.01**	**0.01**	**93.91**
Std. Dev.		**0.80**	**0.01**	**0.52**	**0.00**	**0.07**	**0.00**	**0.00**	**0.02**	**0.49**	**0.73**	**0.01**	**0.01**	**0.02**	**0.85**
12 oxygen atoms per formula unit (sum excludes F & Cl)															
		Si	**Ti**	**Al**	**Cr**	**Fe**	**Ni**	**Mn**	**Mg**	**Ca**	**Na**	**K**	**Cl**	**F**	**SUM**

EBS 25-clay zeolite A1	1	4.26	0.00	1.94	0.00	0.01	0.00	0.00	0.01	0.26	0.56	0.00	0.00	0.00	7.05
EBS 25-clay zeolites	3	4.22	0.00	1.99	0.00	0.01	0.00	0.00	0.00	0.23	0.68	0.00	0.00	0.01	7.12
EBS 25-clay zeolites	4	4.18	0.00	2.00	0.00	0.01	0.00	0.00	0.01	0.29	0.65	0.00	0.00	0.00	7.14
EBS 25-clay zeolites	5	4.34	0.00	1.89	0.00	0.02	0.00	0.00	0.00	0.22	0.52	0.00	0.00	0.00	6.98
EBS 25-clay zeolites	6	4.20	0.00	1.96	0.00	0.01	0.00	0.00	0.00	0.25	0.79	0.00	0.00	0.00	7.21
EBS 25-clay zeolites	7	4.29	0.00	1.89	0.00	0.01	0.00	0.00	0.00	0.17	0.79	0.00	0.00	0.00	7.16
EBS 25-clay zeolites	8	4.27	0.00	1.94	0.00	0.01	0.00	0.00	0.00	0.20	0.66	0.00	0.00	0.01	7.09
AVERAGE		**4.25**	**0.00**	**1.94**	**0.00**	**0.01**	**0.00**	**0.00**	**0.00**	**0.23**	**0.66**	**0.00**	**0.00**	**0.00**	**7.11**
Std. Dev.		**0.05**	**0.00**	**0.04**	**0.00**	**0.00**	**0.00**	**0.00**	**0.00**	**0.04**	**0.10**	**0.00**	**0.00**	**0.00**	**0.07**
SAMPLE	**Pt#**	**SiO_2**	**TiO_2**	**Al_2O_3**	**Cr_2O_3**	**FeO**	**NiO**	**MnO**	**MgO**	**CaO**	**Na_2O**	**K_2O**	**Cl**	**F**	**TOTAL**
GARRONITE															
EBS 25-steel zeolites A1	13	58.23	0.00	23.65	0.00	0.05	0.02	0.02	0.01	8.69	0.55	0.03	0.03	0.00	91.29
EBS 25-steel zeolites A1	14	58.92	0.00	23.09	0.00	0.03	0.00	0.02	0.00	8.67	0.84	0.02	0.02	0.01	91.62
EBS 25-steel zeolites A1	15	55.96	0.00	23.80	0.00	0.05	0.01	0.01	0.00	8.26	0.61	0.02	0.03	0.04	88.76
AVERAGE		**57.71**	**0.00**	**23.52**	**0.00**	**0.04**	**0.01**	**0.02**	**0.00**	**8.54**	**0.67**	**0.02**	**0.03**	**0.02**	**90.55**
Std. Dev.		**1.27**	**0.00**	**0.31**	**0.00**	**0.01**	**0.01**	**0.00**	**0.00**	**0.20**	**0.13**	**0.01**	**0.01**	**0.02**	**1.28**
8 oxygen atoms per formula unit (sum excludes F & Cl)															
		Si	**Ti**	**Al**	**Cr**	**Fe**	**Ni**	**Mn**	**Mg**	**Ca**	**Na**	**K**	**Cl**	**F**	**SUM**
EBS 25-steel zeolites A1	13	2.77	0.00	1.33	0.00	0.00	0.00	0.00	0.00	0.44	0.05	0.00	0.00	0.00	4.59
EBS 25-steel zeolites A1	14	2.79	0.00	1.29	0.00	0.00	0.00	0.00	0.00	0.44	0.08	0.00	0.00	0.00	4.60
EBS 25-steel zeolites A1	15	2.74	0.00	1.37	0.00	0.00	0.00	0.00	0.00	0.43	0.06	0.00	0.00	0.01	4.61
AVERAGE		**2.77**	**0.00**	**1.33**	**0.00**	**0.00**	**0.00**	**0.00**	**0.00**	**0.44**	**0.06**	**0.00**	**0.00**	**0.00**	**4.60**
Std. Dev.		**0.02**	**0.00**	**0.03**	**0.00**	**0.00**	**0.00**	**0.00**	**0.00**	**0.00**	**0.01**	**0.00**	**0.00**	**0.00**	**0.00**
SAMPLE	**Pt#**	**SiO_2**	**TiO_2**	**Al_2O_3**	**Cr_2O_3**	**FeO**	**NiO**	**MnO**	**MgO**	**CaO**	**Na_2O**	**K_2O**	**Cl**	**F**	**TOTAL**
FELDSPAR?															
EBS 25-clay A2 feldspar	10	66.55	0.15	21.30	0.00	0.45	0.00	0.01	0.07	1.25	6.84	4.03	0.04	0.08	100.69
EBS 25-clay A2 feldspar	12	65.46	0.03	20.93	0.00	0.49	0.00	0.02	0.07	1.80	4.30	5.96	0.10	0.00	99.16
AVERAGE		**66.00**	**0.09**	**21.11**	**0.00**	**0.47**	**0.00**	**0.02**	**0.07**	**1.53**	**5.57**	**5.00**	**0.07**	**0.04**	**99.93**
Std. Dev.		**0.54**	**0.06**	**0.19**	**0.00**	**0.02**	**0.00**	**0.00**	**0.00**	**0.28**	**1.27**	**0.97**	**0.03**	**0.04**	**0.77**

8 oxygen atoms per formula unit (sum excludes F & Cl)															
		Si	**Ti**	**Al**	**Cr**	**Fe**	**Ni**	**Mn**	**Mg**	**Ca**	**Na**	**K**	**Cl**	**F**	**SUM**
EBS 25-clay A2 feldspar	10	2.92	0.00	1.10	0.00	0.02	0.00	0.00	0.00	0.06	0.58	0.23	0.00	0.01	4.92
EBS 25-clay A2 feldspar	12	2.99	0.00	1.01	0.00	0.02	0.00	0.00	0.00	0.09	0.40	0.36	0.01	0.00	4.88
AVERAGE		**2.96**	**0.00**	**1.06**	**0.00**	**0.02**	**0.00**	**0.00**	**0.00**	**0.08**	**0.49**	**0.30**	**0.01**	**0.01**	**4.90**
Std. Dev.		**0.03**	**0.00**	**0.05**	**0.00**	**0.00**	**0.00**	**0.00**	**0.00**	**0.02**	**0.09**	**0.07**	**0.00**	**0.01**	**0.02**
SAMPLE	**Pt#**	**SiO_2**	**TiO_2**	**Al_2O_3**	**Cr_2O_3**	**FeO**	**NiO**	**MnO**	**MgO**	**CaO**	**Na_2O**	**K_2O**	**Cl**	**F**	**TOTAL**
BIOTITE															
EBS 25 clay biotite	9	34.33	3.14	15.04	0.00	22.80	0.00	0.18	8.12	0.04	0.34	8.85	0.20	0.45	93.05
12 oxygen atoms per formula unit (sum excludes F & Cl)															
		Si	**Ti**	**Al**	**Cr**	**Fe**	**Ni**	**Mn**	**Mg**	**Ca**	**Na**	**K**	**Cl**	**F**	**SUM**
EBS 25 clay biotite	9	3.00	0.21	1.55	0.00	1.67	0.00	0.01	1.06	0.00	0.06	0.99	0.03	0.12	8.54
SAMPLE	**Pt#**	**SiO_2**	**TiO_2**	**Al_2O_3**	**Cr_2O_3**	**FeO**	**NiO**	**MnO**	**MgO**	**CaO**	**Na_2O**	**K_2O**	**Cl**	**F**	**TOTAL**
ANALCIME in porous cement matrix															
EBS 25-cement analcime A2	28	59.32	0.02	23.68	0.00	0.13	0.01	0.00	0.01	3.48	4.13	0.02	0.00	0.08	90.81
EBS 25-cement analcime A3	37	60.09	0.03	23.41	0.00	0.10	0.00	0.00	0.00	3.56	3.67	0.03	0.01	0.00	90.91
EBS 25-cement analcime A1	14	59.77	0.02	24.06	0.00	0.11	0.02	0.01	0.00	3.01	3.87	0.02	0.02	0.00	90.93
EBS 25-cement analcime A1	3	58.98	0.02	24.27	0.00	0.09	0.00	0.01	0.01	3.10	4.43	0.05	0.01	0.09	90.97
EBS 25-cement analcime A2	24	59.59	0.03	23.62	0.00	0.11	0.02	0.01	0.00	3.68	3.95	0.02	0.01	0.02	91.02
EBS 25-cement analcime A1	5	59.67	0.03	24.09	0.00	0.07	0.00	0.00	0.00	3.28	3.88	0.04	0.01	0.05	91.06
EBS 25-cement analcime A2	26	60.42	0.01	22.90	0.00	0.18	0.01	0.00	0.04	3.90	3.73	0.03	0.02	0.02	91.25
EBS 25-cement analcime A2	27	59.64	0.02	23.93	0.00	0.15	0.02	0.01	0.00	3.40	4.38	0.02	0.01	0.01	91.58
EBS 25-cement analcime A3	33	60.10	0.02	23.90	0.00	0.10	0.00	0.00	0.00	3.28	4.14	0.03	0.01	0.00	91.58
EBS 25-cement analcime A1	6	59.67	0.02	23.76	0.00	0.11	0.00	0.00	0.02	4.45	3.57	0.02	0.01	0.00	91.63
EBS 25-cement analcime A3	31	59.74	0.03	24.00	0.01	0.12	0.00	0.00	0.00	3.39	4.33	0.03	0.00	0.00	91.65
EBS 25-cement analcime A1	9	60.24	0.02	23.70	0.01	0.10	0.02	0.00	0.00	3.93	3.82	0.01	0.01	0.00	91.85

EBS 25-cement analcime A3	36	59.95	0.03	23.89	0.00	0.07	0.00	0.00	0.00	3.70	4.21	0.00	0.01	0.02	91.86
EBS 25-cement analcime A3	30	60.05	0.02	23.99	0.00	0.09	0.00	0.00	0.00	3.64	4.10	0.01	0.01	0.00	91.91
EBS 25-cement analcime A3	32	60.39	0.02	24.04	0.00	0.17	0.02	0.02	0.01	3.30	3.94	0.02	0.01	0.13	91.93
EBS 25-cement analcime A2	20	60.78	0.04	23.99	0.00	0.11	0.00	0.00	0.00	2.99	4.03	0.03	0.01	0.00	91.98
EBS 25-cement analcime A2	23	59.43	0.03	24.02	0.00	0.09	0.00	0.01	0.01	4.79	3.67	0.02	0.01	0.00	92.09
EBS 25-cement analcime A1	18	60.33	0.02	24.13	0.00	0.12	0.00	0.03	0.02	3.54	3.93	0.02	0.01	0.00	92.12
EBS 25-cement analcime A2	25	58.62	0.05	23.31	0.00	0.30	0.00	0.00	0.16	6.01	3.56	0.06	0.09	0.00	92.16
EBS 25-cement analcime A2	22	60.90	0.02	24.12	0.00	0.10	0.01	0.02	0.00	2.98	3.97	0.03	0.01	0.10	92.17
EBS 25-cement analcime A1	10	60.50	0.02	24.28	0.01	0.09	0.02	0.00	0.00	3.82	3.45	0.02	0.01	0.00	92.22
EBS 25-cement analcime A1	2	60.59	0.03	24.34	0.00	0.09	0.00	0.01	0.00	3.27	3.95	0.03	0.01	0.00	92.31
EBS 25-cement analcime A3	35	61.12	0.03	23.96	0.00	0.10	0.02	0.00	0.00	3.18	3.93	0.03	0.01	0.00	92.39
EBS 25-cement analcime A1	15	60.60	0.02	24.34	0.00	0.11	0.00	0.03	0.00	3.17	4.13	0.03	0.01	0.03	92.44
EBS 25-cement analcime A3	34	61.35	0.03	23.87	0.00	0.09	0.00	0.00	0.00	3.40	3.70	0.02	0.01	0.00	92.47
EBS 25-cement analcime A1	4	60.57	0.03	24.26	0.00	0.10	0.00	0.00	0.00	3.35	4.14	0.02	0.01	0.01	92.48
EBS 25-cement analcime A1	7	60.63	0.02	24.37	0.00	0.09	0.00	0.01	0.00	3.86	3.65	0.02	0.01	0.05	92.67
EBS 25-cement analcime A2	21	60.96	0.03	23.66	0.00	0.20	0.00	0.00	0.07	4.38	3.50	0.04	0.01	0.10	92.84
EBS 25-cement analcime A1	1	61.11	0.02	24.48	0.00	0.09	0.00	0.00	0.00	3.26	3.94	0.04	0.01	0.04	92.96
EBS 25-cement analcime A1	16	61.87	0.03	24.80	0.00	0.12	0.01	0.01	0.00	2.75	4.16	0.04	0.01	0.00	93.80
EBS 25-cement analcime A1	12	62.19	0.02	24.87	0.00	0.11	0.01	0.00	0.00	3.12	4.24	0.03	0.00	0.12	94.59
EBS 25-cement analcime A1	13	62.15	0.01	25.09	0.00	0.12	0.00	0.00	0.00	2.98	4.38	0.05	0.01	0.05	94.79
EBS 25-cement analcime A1	11	62.15	0.01	26.08	0.00	0.09	0.01	0.01	0.03	3.83	3.07	0.01	0.01	0.00	95.30
AVERAGE		**60.41**	**0.02**	**24.10**	**0.00**	**0.12**	**0.01**	**0.01**	**0.01**	**3.57**	**3.93**	**0.03**	**0.01**	**0.03**	**92.20**
Std. Dev.		**0.88**	**0.01**	**0.55**	**0.00**	**0.04**	**0.01**	**0.01**	**0.03**	**0.62**	**0.30**	**0.01**	**0.02**	**0.04**	**1.08**
12 oxygen atoms per formula unit (sum excludes F & Cl)															
		Si	**Ti**	**Al**	**Cr**	**Fe**	**Ni**	**Mn**	**Mg**	**Ca**	**Na**	**K**	**Cl**	**F**	**SUM**
EBS 25-cement analcime A2	28	4.23	0.00	1.99	0.00	0.01	0.00	0.00	0.00	0.27	0.57	0.00	0.00	0.02	7.06
EBS 25-cement analcime A3	37	4.26	0.00	1.96	0.00	0.01	0.00	0.00	0.00	0.27	0.51	0.00	0.00	0.00	7.01
EBS 25-cement analcime A1	14	4.24	0.00	2.01	0.00	0.01	0.00	0.00	0.00	0.23	0.53	0.00	0.00	0.00	7.02
EBS 25-cement analcime A1	3	4.20	0.00	2.04	0.00	0.01	0.00	0.00	0.00	0.24	0.61	0.00	0.00	0.02	7.09
EBS 25-cement analcime A2	24	4.23	0.00	1.98	0.00	0.01	0.00	0.00	0.00	0.28	0.54	0.00	0.00	0.01	7.05
EBS 25-cement analcime A1	5	4.23	0.00	2.01	0.00	0.00	0.00	0.00	0.00	0.25	0.53	0.00	0.00	0.01	7.03

EBS 25-cement analcime A2	26	4.28	0.00	1.91	0.00	0.01	0.00	0.00	0.00	0.30	0.51	0.00	0.00	0.00	7.02
EBS 25-cement analcime A2	27	4.22	0.00	1.99	0.00	0.01	0.00	0.00	0.00	0.26	0.60	0.00	0.00	0.00	7.08
EBS 25-cement analcime A3	33	4.24	0.00	1.99	0.00	0.01	0.00	0.00	0.00	0.25	0.57	0.00	0.00	0.00	7.05
EBS 25-cement analcime A1	6	4.22	0.00	1.98	0.00	0.01	0.00	0.00	0.00	0.34	0.49	0.00	0.00	0.00	7.04
EBS 25-cement analcime A3	31	4.22	0.00	2.00	0.00	0.01	0.00	0.00	0.00	0.26	0.59	0.00	0.00	0.00	7.08
EBS 25-cement analcime A1	9	4.24	0.00	1.97	0.00	0.01	0.00	0.00	0.00	0.30	0.52	0.00	0.00	0.00	7.04
EBS 25-cement analcime A3	36	4.22	0.00	1.98	0.00	0.00	0.00	0.00	0.00	0.28	0.57	0.00	0.00	0.01	7.07
EBS 25-cement analcime A3	30	4.23	0.00	1.99	0.00	0.01	0.00	0.00	0.00	0.27	0.56	0.00	0.00	0.00	7.06
EBS 25-cement analcime A3	32	4.24	0.00	1.99	0.00	0.01	0.00	0.00	0.00	0.25	0.54	0.00	0.00	0.03	7.03
EBS 25-cement analcime A2	20	4.26	0.00	1.98	0.00	0.01	0.00	0.00	0.00	0.22	0.55	0.00	0.00	0.00	7.02
EBS 25-cement analcime A2	23	4.19	0.00	2.00	0.00	0.01	0.00	0.00	0.00	0.36	0.50	0.00	0.00	0.00	7.06
EBS 25-cement analcime A1	18	4.23	0.00	1.99	0.00	0.01	0.00	0.00	0.00	0.27	0.53	0.00	0.00	0.00	7.04
EBS 25-cement analcime A2	25	4.16	0.00	1.95	0.00	0.02	0.00	0.00	0.02	0.46	0.49	0.01	0.01	0.00	7.11
EBS 25-cement analcime A2	22	4.26	0.00	1.99	0.00	0.01	0.00	0.00	0.00	0.22	0.54	0.00	0.00	0.02	7.02
EBS 25-cement analcime A1	10	4.23	0.00	2.00	0.00	0.01	0.00	0.00	0.00	0.29	0.47	0.00	0.00	0.00	7.00
EBS 25-cement analcime A1	2	4.23	0.00	2.00	0.00	0.01	0.00	0.00	0.00	0.25	0.53	0.00	0.00	0.00	7.03
EBS 25-cement analcime A3	35	4.26	0.00	1.97	0.00	0.01	0.00	0.00	0.00	0.24	0.53	0.00	0.00	0.00	7.02
EBS 25-cement analcime A1	15	4.23	0.00	2.00	0.00	0.01	0.00	0.00	0.00	0.24	0.56	0.00	0.00	0.01	7.05
EBS 25-cement analcime A3	34	4.27	0.00	1.96	0.00	0.01	0.00	0.00	0.00	0.25	0.50	0.00	0.00	0.00	7.00
EBS 25-cement analcime A1	4	4.23	0.00	2.00	0.00	0.01	0.00	0.00	0.00	0.25	0.56	0.00	0.00	0.00	7.05
EBS 25-cement analcime A1	7	4.23	0.00	2.00	0.00	0.01	0.00	0.00	0.00	0.29	0.49	0.00	0.00	0.01	7.02
EBS 25-cement analcime A2	21	4.25	0.00	1.94	0.00	0.01	0.00	0.00	0.01	0.33	0.47	0.00	0.00	0.02	7.02
EBS 25-cement analcime A1	1	4.24	0.00	2.00	0.00	0.01	0.00	0.00	0.00	0.24	0.53	0.00	0.00	0.01	7.02
EBS 25-cement analcime A1	16	4.25	0.00	2.01	0.00	0.01	0.00	0.00	0.00	0.20	0.55	0.00	0.00	0.00	7.03
EBS 25-cement analcime A1	12	4.24	0.00	2.00	0.00	0.01	0.00	0.00	0.00	0.23	0.56	0.00	0.00	0.03	7.04
EBS 25-cement analcime A1	13	4.23	0.00	2.01	0.00	0.01	0.00	0.00	0.00	0.22	0.58	0.00	0.00	0.01	7.05
EBS 25-cement analcime A1	11	4.20	0.00	2.08	0.00	0.01	0.00	0.00	0.00	0.28	0.40	0.00	0.00	0.00	6.96
AVERAGE		**4.23**	**0.00**	**1.99**	**0.00**	**0.01**	**0.00**	**0.00**	**0.00**	**0.27**	**0.53**	**0.00**	**0.00**	**0.01**	**7.04**
Std. Dev.		**0.02**	**0.00**	**0.03**	**0.00**	**0.00**	**0.00**	**0.00**	**0.00**	**0.05**	**0.04**	**0.00**	**0.00**	**0.01**	**0.03**

SAMPLE	Pt#	SiO_2	TiO_2	Al_2O_3	Cr_2O_3	FeO	NiO	MnO	MgO	CaO	Na_2O	K_2O	Cl	F	TOTAL
TOBEMORITE															
EBS 25-cement zeolite A4	45	44.39	0.08	10.26	0.00	1.71	0.00	0.03	0.66	17.80	0.16	0.30	0.55	0.09	75.94
EBS 25-cement zeolite A4	46	38.47	0.01	4.34	0.01	0.24	0.00	0.04	0.03	22.03	0.27	0.10	0.64	0.04	66.18
EBS 25-cement zeolite A4	47	40.49	0.07	9.02	0.00	1.84	0.02	0.03	0.59	20.03	0.19	0.25	0.61	0.15	73.14
EBS 25-cement zeolite A4	48	41.98	0.07	9.27	0.00	1.52	0.01	0.01	0.48	18.59	0.16	0.30	0.67	0.13	73.08
EBS 25-cement zeolite A4	49	31.57	0.15	10.41	0.00	1.62	0.00	0.02	0.82	12.92	0.18	0.52	0.67	0.04	58.88
EBS 25-cement zeolite A4	50	33.74	0.04	4.13	0.00	0.59	0.02	0.02	0.14	19.47	0.13	0.05	0.62	0.19	58.96
AVERAGE		**38.44**	**0.07**	**7.91**	**0.00**	**1.26**	**0.01**	**0.02**	**0.45**	**18.47**	**0.18**	**0.25**	**0.63**	**0.11**	**67.70**
Std. Dev.		**4.50**	**0.04**	**2.64**	**0.00**	**0.61**	**0.01**	**0.01**	**0.28**	**2.81**	**0.04**	**0.15**	**0.04**	**0.06**	**6.87**
16 oxygen atoms per formula unit (sum excludes F & Cl)															
		Si	**Ti**	**Al**	**Cr**	**Fe**	**Ni**	**Mn**	**Mg**	**Ca**	**Na**	**K**	**Cl**	**F**	**SUM**
EBS 25-cement zeolite A4	45	5.51	0.01	1.50	0.00	0.18	0.00	0.00	0.12	2.37	0.04	0.05	0.12	0.04	9.77
EBS 25-cement zeolite A4	46	5.65	0.00	0.75	0.00	0.03	0.00	0.00	0.01	3.47	0.08	0.02	0.16	0.02	10.01
EBS 25-cement zeolite A4	47	5.34	0.01	1.40	0.00	0.20	0.00	0.00	0.12	2.83	0.05	0.04	0.14	0.06	9.99
EBS 25-cement zeolite A4	48	5.47	0.01	1.42	0.00	0.17	0.00	0.00	0.09	2.60	0.04	0.05	0.15	0.05	9.85
EBS 25-cement zeolite A4	49	5.12	0.02	1.99	0.00	0.22	0.00	0.00	0.20	2.24	0.06	0.11	0.19	0.02	9.95
EBS 25-cement zeolite A4	50	5.59	0.01	0.81	0.00	0.08	0.00	0.00	0.04	3.45	0.04	0.01	0.17	0.10	10.03
AVERAGE		**5.45**	**0.01**	**1.31**	**0.00**	**0.15**	**0.00**	**0.00**	**0.09**	**2.83**	**0.05**	**0.05**	**0.15**	**0.05**	**9.94**
Std. Dev.		**0.18**	**0.01**	**0.42**	**0.00**	**0.07**	**0.00**	**0.00**	**0.06**	**0.48**	**0.01**	**0.03**	**0.02**	**0.03**	**0.09**
SAMPLE	**Pt#**	SiO_2	TiO_2	Al_2O_3	Cr_2O_3	FeO	NiO	MnO	MgO	CaO	Na_2O	K_2O	Cl	F	TOTAL
K-FELDSPAR															
EBS 25-cement feldspar A3	40	64.81	0.00	19.54	0.00	0.10	0.00	0.00	0.01	0.21	2.91	11.59	0.00	0.00	99.18
EBS 25-cement feldspar A3	41	64.76	0.01	19.92	0.00	0.14	0.01	0.02	0.00	0.23	3.26	11.37	0.00	0.00	99.72
EBS 25-cement feldspar A4	44	64.28	0.00	20.58	0.00	0.11	0.02	0.00	0.00	0.19	3.11	11.61	0.01	0.03	99.92
AVERAGE		**64.62**	**0.00**	**20.01**	**0.00**	**0.12**	**0.01**	**0.01**	**0.00**	**0.21**	**3.09**	**11.53**	**0.00**	**0.01**	**99.61**
Std. Dev.		**0.24**	**0.00**	**0.43**	**0.00**	**0.02**	**0.01**	**0.01**	**0.00**	**0.02**	**0.14**	**0.11**	**0.00**	**0.01**	**0.31**
8 oxygen atoms per formula unit (sum excludes F & Cl)															
		Si	**Ti**	**Al**	**Cr**	**Fe**	**Ni**	**Mn**	**Mg**	**Ca**	**Na**	**K**	**Cl**	**F**	**SUM**
EBS 25-cement feldspar A3	40	2.96	0.00	1.07	0.00	0.00	0.00	0.00	0.00	0.01	0.26	0.69	0.00	0.00	4.98

EBS 25-cement feldspar A3	41	2.94	0.00	1.08	0.00	0.01	0.00	0.00	0.00	0.01	0.29	0.67	0.00	0.00	5.00
EBS 25-cement feldspar A4	44	2.93	0.00	1.10	0.00	0.00	0.00	0.00	0.00	0.01	0.27	0.67	0.00	0.00	5.00
AVERAGE		**2.94**	**0.00**	**1.08**	**0.00**	**0.00**	**0.00**	**0.00**	**0.00**	**0.01**	**0.28**	**0.68**	**0.00**	**0.00**	**4.99**
Std. Dev.		**0.01**	**0.00**	**0.02**	**0.00**	**0.00**	**0.00**	**0.00**	**0.00**	**0.00**	**0.01**	**0.01**	**0.00**	**0.00**	**0.01**
SAMPLE	**Pt#**	**SiO_2**	**TiO_2**	**Al_2O_3**	**Cr_2O_3**	**FeO**	**NiO**	**MnO**	**MgO**	**CaO**	**Na_2O**	**K_2O**	**Cl**	**F**	**TOTAL**
PLAGIOCLASE															
EBS 25-cement feldspar A3	42	60.83	0.00	25.78	0.01	0.21	0.03	0.00	0.00	6.10	7.12	0.77	0.00	0.00	100.84
EBS 25-cement feldspar A3	43	58.33	0.02	26.51	0.00	0.26	0.00	0.00	0.00	7.50	6.14	0.54	0.00	0.00	99.30
AVERAGE		**59.58**	**0.01**	**26.14**	**0.00**	**0.23**	**0.02**	**0.00**	**0.00**	**6.80**	**6.63**	**0.65**	**0.00**	**0.00**	**100.07**
Std. Dev.		**1.25**	**0.01**	**0.37**	**0.00**	**0.02**	**0.01**	**0.00**	**0.00**	**0.70**	**0.49**	**0.12**	**0.00**	**0.00**	**0.77**
8 oxygen atoms per formula unit (sum excludes F & Cl)															
		Si	**Ti**	**Al**	**Cr**	**Fe**	**Ni**	**Mn**	**Mg**	**Ca**	**Na**	**K**	**Cl**	**F**	**SUM**
EBS 25-cement feldspar A3	42	2.68	0.00	1.34	0.00	0.01	0.00	0.00	0.00	0.29	0.61	0.04	0.00	0.00	4.97
EBS 25-cement feldspar A3	43	2.60	0.00	1.42	0.00	0.01	0.00	0.00	0.00	0.37	0.54	0.03	0.00	0.00	4.97
AVERAGE		**2.64**	**0.00**	**1.38**	**0.00**	**0.01**	**0.00**	**0.00**	**0.00**	**0.33**	**0.57**	**0.04**	**0.00**	**0.00**	**4.97**
Std. Dev.		**0.04**	**0.00**	**0.04**	**0.00**	**0.00**	**0.00**	**0.00**	**0.00**	**0.04**	**0.03**	**0.01**	**0.00**	**0.00**	**0.00**
SAMPLE	**Pt#**	**SiO_2**	**TiO_2**	**Al_2O_3**	**Cr_2O_3**	**FeO**	**NiO**	**MnO**	**MgO**	**CaO**	**Na_2O**	**K_2O**	**Cl**	**F**	**TOTAL**
ANALCIME near steel surface															
EBS 25-steel zeolites A1	1	63.95	0.02	24.66	0.04	0.15	0.01	0.00	0.00	2.09	4.37	0.05	0.00	0.00	95.34
EBS 25-steel zeolites A1	2	64.29	0.03	24.31	0.06	0.17	0.00	0.01	0.02	2.07	3.91	0.06	0.01	0.03	94.94
EBS 25-steel zeolites A1	3	62.84	0.03	24.83	0.04	0.15	0.00	0.02	0.01	2.41	4.31	0.04	0.01	0.02	94.67
EBS 25-steel zeolites A1	4	63.67	0.02	24.22	0.08	0.21	0.00	0.00	0.00	2.16	4.20	0.05	0.00	0.03	94.63
EBS 25-steel zeolites A1-maybe some clay	5	62.60	0.03	24.14	0.06	0.85	0.00	0.01	0.49	2.33	4.13	0.06	0.01	0.00	94.71
EBS 25-steel zeolites A1	9	63.31	0.03	24.25	0.05	0.24	0.00	0.02	0.02	2.15	4.06	0.05	0.01	0.00	94.19
AVERAGE		**63.44**	**0.03**	**24.40**	**0.05**	**0.30**	**0.00**	**0.01**	**0.09**	**2.20**	**4.16**	**0.05**	**0.01**	**0.01**	**94.75**
Std. Dev.		**0.60**	**0.01**	**0.25**	**0.01**	**0.25**	**0.00**	**0.01**	**0.18**	**0.13**	**0.15**	**0.01**	**0.00**	**0.01**	**0.35**
12 oxygen atoms per formula unit (sum excludes F & Cl)															

		Si	Ti	Al	Cr	Fe	Ni	Mn	Mg	Ca	Na	K	Cl	F	SUM
EBS 25-steel zeolites A1	1	4.31	0.00	1.96	0.00	0.01	0.00	0.00	0.00	0.15	0.57	0.00	0.00	0.00	7.00
EBS 25-steel zeolites A1	2	4.34	0.00	1.93	0.00	0.01	0.00	0.00	0.00	0.15	0.51	0.01	0.00	0.01	6.95
EBS 25-steel zeolites A1	3	4.27	0.00	1.99	0.00	0.01	0.00	0.00	0.00	0.18	0.57	0.00	0.00	0.00	7.02
EBS 25-steel zeolites A1	4	4.32	0.00	1.94	0.00	0.01	0.00	0.00	0.00	0.16	0.55	0.00	0.00	0.01	6.99
EBS 25-steel zeolites A1-maybe some clay	5	4.27	0.00	1.94	0.00	0.05	0.00	0.00	0.05	0.17	0.55	0.01	0.00	0.00	7.03
EBS 25-steel zeolites A1	9	4.31	0.00	1.95	0.00	0.01	0.00	0.00	0.00	0.16	0.54	0.00	0.00	0.00	6.98
AVERAGE		**4.30**	**0.00**	**1.95**	**0.00**	**0.02**	**0.00**	**0.00**	**0.01**	**0.16**	**0.55**	**0.00**	**0.00**	**0.00**	**7.00**
Std. Dev.		**0.03**	**0.00**	**0.02**	**0.00**	**0.01**	**0.00**	**0.00**	**0.02**	**0.01**	**0.02**	**0.00**	**0.00**	**0.00**	**0.03**
SAMPLE	**Pt#**	**SiO_2**	**TiO_2**	**Al_2O_3**	**Cr_2O_3**	**FeO**	**NiO**	**MnO**	**MgO**	**CaO**	**Na_2O**	**K_2O**	**Cl**	**F**	**TOTAL**
ZEOLITE with variable cation composition															
EBS 25-steel zeolites A2	10	60.84	0.16	22.94	0.05	1.88	0.01	0.02	0.38	3.45	3.33	0.06	0.01	0.02	93.14
EBS 25-steel zeolites A2	12	56.79	0.05	22.25	0.09	0.33	0.04	0.02	0.19	6.95	3.30	0.04	0.06	0.08	90.11
EBS 25-steel zeolites A2 rim	13	59.74	0.00	25.08	0.03	0.10	0.01	0.00	0.00	3.23	5.09	0.03	0.00	0.00	93.31
EBS 25-steel zeolites A2 core	14	59.98	0.00	25.08	0.02	0.11	0.00	0.01	0.01	4.44	4.03	0.00	0.00	0.00	93.68
EBS 25-zeolites A4	19	61.97	0.01	22.70	0.02	0.21	0.02	0.03	0.00	2.41	4.60	0.03	0.00	0.03	92.01
EBS 25-zeolites A4	20	62.56	0.00	22.76	0.03	0.24	0.01	0.00	0.00	2.34	4.61	0.04	0.00	0.00	92.58
EBS 25-zeolites A4	21	61.32	0.00	24.55	0.02	0.35	0.02	0.02	0.00	5.71	6.85	0.98	0.00	0.03	99.81
12 oxygen atoms per formula unit (sum excludes F & Cl)															
		Si	**Ti**	**Al**	**Cr**	**Fe**	**Ni**	**Mn**	**Mg**	**Ca**	**Na**	**K**	**Cl**	**F**	**SUM**
EBS 25-steel zeolites A2	10	4.25	0.01	1.89	0.00	0.11	0.00	0.00	0.04	0.26	0.45	0.01	0.00	0.00	7.02
EBS 25-steel zeolites A2	12	4.15	0.00	1.91	0.01	0.02	0.00	0.00	0.02	0.54	0.47	0.00	0.01	0.02	7.13
EBS 25-steel zeolites A2 rim	13	4.16	0.00	2.06	0.00	0.01	0.00	0.00	0.00	0.24	0.69	0.00	0.00	0.00	7.16
EBS 25-steel zeolites A2 core	14	4.16	0.00	2.05	0.00	0.01	0.00	0.00	0.00	0.33	0.54	0.00	0.00	0.00	7.09
EBS 25-zeolites A4	19	4.34	0.00	1.87	0.00	0.01	0.00	0.00	0.00	0.18	0.62	0.00	0.00	0.01	7.04
EBS 25-zeolites A4	20	4.35	0.00	1.86	0.00	0.01	0.00	0.00	0.00	0.17	0.62	0.00	0.00	0.00	7.03
EBS 25-zeolites A4	21	4.09	0.00	1.93	0.00	0.02	0.00	0.00	0.00	0.41	0.89	0.08	0.00	0.01	7.42
EBS 25-steel zeolites A2	10	4.25	0.01	1.89	0.00	0.11	0.00	0.00	0.04	0.26	0.45	0.01	0.00	0.00	7.02

SAMPLE	**Pt#**	**SiO_2**	**TiO_2**	**Al_2O_3**	**Cr_2O_3**	**FeO**	**NiO**	**MnO**	**MgO**	**CaO**	**Na_2O**	**K_2O**	**Cl**	**F**	**TOTAL**
GARRONITE															
EBS 25-steel zeolites A1	6	58.02	0.00	15.79	0.02	0.16	0.00	0.00	0.03	7.15	0.24	0.49	0.04	0.05	81.95
EBS 25-steel zeolites A1	7	59.02	0.00	23.29	0.00	0.07	0.00	0.01	0.00	8.46	1.10	0.02	0.01	0.00	91.98
EBS 25-steel zeolites A1	8	52.48	0.01	23.25	0.01	0.07	0.01	0.00	0.00	8.61	0.94	0.02	0.03	0.03	85.41
AVERAGE		**56.51**	**0.00**	**20.78**	**0.01**	**0.10**	**0.00**	**0.00**	**0.01**	**8.07**	**0.76**	**0.18**	**0.03**	**0.03**	**86.45**
Std. Dev.		**2.88**	**0.01**	**3.52**	**0.01**	**0.04**	**0.00**	**0.00**	**0.02**	**0.65**	**0.37**	**0.22**	**0.01**	**0.02**	**4.16**
8 oxygen atoms per formula unit (sum excludes F & Cl)															
		Si	**Ti**	**Al**	**Cr**	**Fe**	**Ni**	**Mn**	**Mg**	**Ca**	**Na**	**K**	**Cl**	**F**	**SUM**
EBS 25-steel zeolites A1	6	3.05	0.00	0.98	0.00	0.01	0.00	0.00	0.00	0.40	0.02	0.03	0.00	0.01	4.49
EBS 25-steel zeolites A1	7	2.79	0.00	1.30	0.00	0.00	0.00	0.00	0.00	0.43	0.10	0.00	0.00	0.00	4.62
EBS 25-steel zeolites A1	8	2.69	0.00	1.40	0.00	0.00	0.00	0.00	0.00	0.47	0.09	0.00	0.00	0.00	4.66
AVERAGE		**2.84**	**0.00**	**1.23**	**0.00**	**0.00**	**0.00**	**0.00**	**0.00**	**0.43**	**0.07**	**0.01**	**0.00**	**0.00**	**4.59**
Std. Dev.		**0.15**	**0.00**	**0.18**	**0.00**	**0.00**	**0.00**	**0.00**	**0.00**	**0.03**	**0.03**	**0.01**	**0.00**	**0.00**	**0.07**
SAMPLE	**Pt#**	**SiO_2**	**TiO_2**	**Al_2O_3**	**Cr_2O_3**	**FeO**	**NiO**	**MnO**	**MgO**	**CaO**	**Na_2O**	**K_2O**	**Cl**	**F**	**TOTAL**
TOBERMORITE															
EBS 25-steel zeolites A4	23	32.10	0.05	5.14	0.01	1.08	0.06	0.09	0.26	18.80	0.13	0.05	0.60	0.08	58.37
EBS 25-steel zeolites A4	24	35.17	0.04	4.96	0.01	1.28	0.13	0.09	0.25	18.73	0.16	0.04	0.75	0.17	61.61
EBS 25-steel zeolites A4	25	27.56	0.05	4.54	0.01	1.31	0.11	0.07	0.41	14.20	0.12	0.07	0.92	0.11	49.39
EBS 25-steel zeolites A4	26	24.55	0.04	4.21	0.01	1.19	0.08	0.07	0.26	13.44	0.14	0.03	0.85	0.04	44.88
AVERAGE		**29.85**	**0.05**	**4.71**	**0.01**	**1.21**	**0.10**	**0.08**	**0.29**	**16.29**	**0.14**	**0.05**	**0.78**	**0.10**	**53.56**
Std. Dev.		**4.09**	**0.00**	**0.36**	**0.00**	**0.09**	**0.03**	**0.01**	**0.07**	**2.49**	**0.01**	**0.01**	**0.12**	**0.05**	**6.72**
16 oxygen atoms per formula unit (sum excludes F & Cl)															
		Si	**Ti**	**Al**	**Cr**	**Fe**	**Ni**	**Mn**	**Mg**	**Ca**	**Na**	**K**	**Cl**	**F**	**SUM**
EBS 25-steel zeolites A4	23	5.40	0.01	1.02	0.00	0.15	0.01	0.01	0.07	3.39	0.04	0.01	0.17	0.04	10.11
EBS 25-steel zeolites A4	24	5.57	0.01	0.92	0.00	0.17	0.02	0.01	0.06	3.18	0.05	0.01	0.20	0.09	9.99
EBS 25-steel zeolites A4	25	5.48	0.01	1.06	0.00	0.22	0.02	0.01	0.12	3.02	0.05	0.02	0.31	0.07	10.01
EBS 25-steel zeolites A4	26	5.40	0.01	1.09	0.00	0.22	0.01	0.01	0.08	3.17	0.06	0.01	0.32	0.03	10.08

AVERAGE		5.46	0.01	1.03	0.00	0.19	0.01	0.01	0.08	3.19	0.05	0.01	0.25	0.06	10.05
Std. Dev.		0.07	0.00	0.06	0.00	0.03	0.00	0.00	0.03	0.13	0.01	0.00	0.06	0.02	0.05
SAMPLE	Pt#	SiO_2	TiO_2	Al_2O_3	Cr_2O_3	FeO	NiO	MnO	MgO	CaO	Na_2O	K_2O	Cl	F	TOTAL
MISCELLANEOUS															
EBS 25-steel feldspar A2	15	64.36	0.01	19.63	0.01	0.14	0.00	0.01	0.01	0.21	2.29	12.44	0.00	0.07	99.12
EBS 25-steel feldspar A3	17	57.25	0.00	26.93	0.00	0.29	0.00	0.00	0.02	8.09	5.72	0.76	0.00	0.02	99.06
EBS 25-steel feldspar A3 (possible zeolite/glass?)	18	64.64	0.09	10.59	0.02	0.18	0.00	0.02	0.04	4.25	0.46	0.25	0.03	0.00	80.57
8 oxygen atoms per formula unit (sum excludes F & Cl)															
		Si	Ti	Al	Cr	Fe	Ni	Mn	Mg	Ca	Na	K	Cl	F	SUM
EBS 25-steel feldspar A2	15	2.96	0.00	1.06	0.00	0.01	0.00	0.00	0.00	0.01	0.20	0.73	0.00	0.01	4.97
EBS 25-steel feldspar A3	17	2.59	0.00	1.43	0.00	0.01	0.00	0.00	0.00	0.39	0.50	0.04	0.00	0.00	4.97
EBS 25-steel feldspar A3 (possible zeolite/glass?)	18	3.37	0.00	0.65	0.00	0.01	0.00	0.00	0.00	0.24	0.05	0.02	0.00	0.00	4.33

EBS-26		WEIGHT PERCENT													
SAMPLE	Pt#	SiO_2	TiO_2	Al_2O_3	Cr_2O_3	FeO	NiO	MnO	MgO	CaO	Na_2O	K_2O	Cl	F	TOTAL
ANALCIME in clay matrix															
EBS 26 Clay zeolites A1	26	56.94	0.03	20.64	0.01	0.16	0.00	0.00	0.04	6.59	2.85	0.02	0.01	0.08	87.28
EBS 26 Clay zeolites A2	4	58.53	0.02	21.88	0.00	0.12	0.00	0.01	0.01	4.77	3.14	0.04	0.02	0.13	88.55
EBS 26 Clay zeolites A4	38	56.80	0.04	19.69	0.00	0.20	0.00	0.01	0.02	9.53	2.48	0.04	0.01	0.00	88.82
EBS 26 Clay zeolites A2	7	60.97	0.01	21.35	0.00	0.17	0.00	0.01	0.00	4.19	3.18	0.03	0.02	0.14	89.92
EBS 26 Clay zeolites A2	2	61.36	0.03	22.15	0.00	0.12	0.00	0.01	0.01	2.81	3.90	0.02	0.01	0.02	90.42
EBS 26 Clay zeolites A2	3	59.90	0.03	22.26	0.01	0.12	0.01	0.00	0.00	5.07	3.12	0.04	0.01	0.05	90.57
EBS 26 Clay zeolites A2	8	60.68	0.03	22.84	0.00	0.12	0.01	0.00	0.00	3.17	3.98	0.03	0.00	0.08	90.87
EBS 26 Clay zeolites A4	40	60.02	0.02	22.70	0.00	0.23	0.02	0.00	0.09	3.96	3.94	0.03	0.03	0.03	91.04

EBS 26 Clay zeolites A4	37	60.08	0.04	22.10	0.00	0.17	0.00	0.00	0.00	5.20	3.57	0.03	0.01	0.00	91.22
EBS 26 Clay zeolites A2	6	61.33	0.02	23.06	0.00	0.09	0.00	0.02	0.01	2.76	4.02	0.04	0.01	0.00	91.35
EBS 26 Clay zeolites A2	1	61.92	0.02	22.70	0.00	0.07	0.00	0.00	0.00	2.85	3.93	0.03	0.00	0.13	91.52
EBS 26 Clay zeolites A2	5	61.52	0.01	22.76	0.00	0.10	0.00	0.00	0.00	2.27	4.92	0.02	0.00	0.00	91.60
EBS 26 Clay zeolites A4	39	60.96	0.02	23.22	0.00	0.35	0.01	0.00	0.21	3.50	3.60	0.03	0.03	0.00	91.93
EBS 26 Clay zeolites A2	9	61.57	0.01	22.80	0.00	0.06	0.00	0.00	0.00	2.56	5.02	0.03	0.00	0.05	92.06
EBS 26 Clay zeolites A4	36	61.85	0.02	23.37	0.00	0.11	0.01	0.01	0.01	2.83	4.33	0.03	0.00	0.00	92.58
AVERAGE		**60.30**	**0.02**	**22.24**	**0.00**	**0.15**	**0.00**	**0.00**	**0.03**	**4.14**	**3.73**	**0.03**	**0.01**	**0.05**	**90.65**
Std. Dev.		**1.60**	**0.01**	**0.98**	**0.00**	**0.07**	**0.01**	**0.01**	**0.05**	**1.86**	**0.69**	**0.01**	**0.01**	**0.05**	**1.41**
12 oxygen atoms per formula unit (sum excludes F & Cl)															
		Si	**Ti**	**Al**	**Cr**	**Fe**	**Ni**	**Mn**	**Mg**	**Ca**	**Na**	**K**	**Cl**	**F**	**SUM**
EBS 26 Clay zeolites A1	26	4.26	0.00	1.82	0.00	0.01	0.00	0.00	0.00	0.53	0.41	0.00	0.00	0.02	7.04
EBS 26 Clay zeolites A2	4	4.28	0.00	1.89	0.00	0.01	0.00	0.00	0.00	0.37	0.45	0.00	0.00	0.03	7.00
EBS 26 Clay zeolites A4	38	4.23	0.00	1.73	0.00	0.01	0.00	0.00	0.00	0.76	0.36	0.00	0.00	0.00	7.09
EBS 26 Clay zeolites A2	7	4.37	0.00	1.80	0.00	0.01	0.00	0.00	0.00	0.32	0.44	0.00	0.00	0.03	6.95
EBS 26 Clay zeolites A2	2	4.36	0.00	1.86	0.00	0.01	0.00	0.00	0.00	0.21	0.54	0.00	0.00	0.00	6.98
EBS 26 Clay zeolites A2	3	4.28	0.00	1.88	0.00	0.01	0.00	0.00	0.00	0.39	0.43	0.00	0.00	0.01	7.00
EBS 26 Clay zeolites A2	8	4.30	0.00	1.91	0.00	0.01	0.00	0.00	0.00	0.24	0.55	0.00	0.00	0.02	7.01
EBS 26 Clay zeolites A4	40	4.27	0.00	1.90	0.00	0.01	0.00	0.00	0.01	0.30	0.54	0.00	0.00	0.01	7.05
EBS 26 Clay zeolites A4	37	4.28	0.00	1.85	0.00	0.01	0.00	0.00	0.00	0.40	0.49	0.00	0.00	0.00	7.04
EBS 26 Clay zeolites A2	6	4.32	0.00	1.91	0.00	0.01	0.00	0.00	0.00	0.21	0.55	0.00	0.00	0.00	7.00
EBS 26 Clay zeolites A2	1	4.35	0.00	1.88	0.00	0.00	0.00	0.00	0.00	0.21	0.53	0.00	0.00	0.03	6.98
EBS 26 Clay zeolites A2	5	4.33	0.00	1.89	0.00	0.01	0.00	0.00	0.00	0.17	0.67	0.00	0.00	0.00	7.06
EBS 26 Clay zeolites A4	39	4.28	0.00	1.92	0.00	0.02	0.00	0.00	0.02	0.26	0.49	0.00	0.00	0.00	7.00
EBS 26 Clay zeolites A2	9	4.32	0.00	1.88	0.00	0.00	0.00	0.00	0.00	0.19	0.68	0.00	0.00	0.01	7.08
EBS 26 Clay zeolites A4	36	4.30	0.00	1.92	0.00	0.01	0.00	0.00	0.00	0.21	0.58	0.00	0.00	0.00	7.03
AVERAGE		**4.30**	**0.00**	**1.87**	**0.00**	**0.01**	**0.00**	**0.00**	**0.00**	**0.32**	**0.51**	**0.00**	**0.00**	**0.01**	**7.02**
Std. Dev.		**0.04**	**0.00**	**0.05**	**0.00**	**0.00**	**0.00**	**0.00**	**0.01**	**0.15**	**0.09**	**0.00**	**0.00**	**0.01**	**0.04**

SAMPLE	Pt#	SiO_2	TiO_2	Al_2O_3	Cr_2O_3	FeO	NiO	MnO	MgO	CaO	Na_2O	K_2O	Cl	F	TOTAL
ANALCIME coating O.C. fragments															
EBS 26 Clay zeolites A1	27	62.55	0.01	23.14	0.00	0.14	0.00	0.00	0.01	2.08	4.52	0.04	0.00	0.00	92.49
EBS 26 Clay zeolites A4	41	62.46	0.01	23.13	0.00	0.16	0.00	0.00	0.00	2.57	4.30	0.04	0.00	0.05	92.67
EBS 26 Clay zeolites A4	42	63.20	0.01	23.45	0.00	0.13	0.00	0.00	0.00	2.61	4.69	0.03	0.00	0.00	94.12
AVERAGE		**62.74**	**0.01**	**23.24**	**0.00**	**0.14**	**0.00**	**0.00**	**0.00**	**2.42**	**4.50**	**0.03**	**0.00**	**0.02**	**93.09**
Std. Dev.		**0.33**	**0.00**	**0.15**	**0.00**	**0.01**	**0.00**	**0.00**	**0.00**	**0.24**	**0.16**	**0.01**	**0.00**	**0.02**	**0.73**
12 oxygen atoms per formula unit (sum excludes F & Cl)															
		Si	**Ti**	**Al**	**Cr**	**Fe**	**Ni**	**Mn**	**Mg**	**Ca**	**Na**	**K**	**Cl**	**F**	**SUM**
EBS 26 Clay zeolites A1	27	4.34	0.00	1.89	0.00	0.01	0.00	0.00	0.00	0.15	0.61	0.00	0.00	0.00	7.01
EBS 26 Clay zeolites A4	41	4.33	0.00	1.89	0.00	0.01	0.00	0.00	0.00	0.19	0.58	0.00	0.00	0.01	7.01
EBS 26 Clay zeolites A4	42	4.32	0.00	1.89	0.00	0.01	0.00	0.00	0.00	0.19	0.62	0.00	0.00	0.00	7.04
AVERAGE		**4.33**	**0.00**	**1.89**	**0.00**	**0.01**	**0.00**	**0.00**	**0.00**	**0.18**	**0.60**	**0.00**	**0.00**	**0.00**	**7.02**
Std. Dev.		**0.01**	**0.00**	**0.00**	**0.00**	**0.00**	**0.00**	**0.00**	**0.00**	**0.02**	**0.02**	**0.00**	**0.00**	**0.00**	**0.01**
SAMPLE	**Pt#**	**SiO_2**	**TiO_2**	**Al_2O_3**	**Cr_2O_3**	**FeO**	**NiO**	**MnO**	**MgO**	**CaO**	**Na_2O**	**K_2O**	**Cl**	**F**	**TOTAL**
GARRONITE															
EBS 26 Clay zeolites A2	16	42.20	0.01	15.68	0.00	0.11	0.00	0.02	0.00	6.27	1.57	0.06	0.01	0.04	65.92
EBS 26 Clay zeolites A2	20	44.79	0.02	16.36	0.00	0.20	0.00	0.00	0.00	6.61	1.42	0.07	0.01	0.00	69.47
EBS 26 Clay zeolites A4	43	45.63	0.00	17.74	0.00	0.14	0.00	0.00	0.00	8.00	0.70	0.05	0.01	0.00	72.27
EBS 26 Clay zeolites A2	18	53.12	0.02	22.28	0.01	0.35	0.00	0.00	0.20	6.58	1.89	0.14	0.02	0.00	84.62
EBS 26 Clay zeolites A4	44	56.54	0.00	21.38	0.00	0.09	0.01	0.00	0.01	7.97	0.52	0.04	0.01	0.03	86.59
EBS 26 Clay zeolites A1	31	56.98	0.01	23.78	0.00	0.13	0.01	0.00	0.03	6.24	1.47	0.11	0.04	0.00	88.80
AVERAGE		**49.88**	**0.01**	**19.54**	**0.00**	**0.17**	**0.00**	**0.00**	**0.04**	**6.94**	**1.26**	**0.08**	**0.02**	**0.01**	**77.95**
Std. Dev.		**5.89**	**0.01**	**3.09**	**0.00**	**0.09**	**0.00**	**0.01**	**0.07**	**0.75**	**0.49**	**0.04**	**0.01**	**0.02**	**9.00**
12 oxygen atoms per formula unit (sum excludes F & Cl)															
		Si	**Ti**	**Al**	**Cr**	**Fe**	**Ni**	**Mn**	**Mg**	**Ca**	**Na**	**K**	**Cl**	**F**	**SUM**
EBS 26 Clay zeolites A2	16	4.20	0.00	1.84	0.00	0.01	0.00	0.00	0.00	0.67	0.30	0.01	0.00	0.01	7.03
EBS 26 Clay zeolites A2	20	4.23	0.00	1.82	0.00	0.02	0.00	0.00	0.00	0.67	0.26	0.01	0.00	0.00	7.00
EBS 26 Clay zeolites A4	43	4.15	0.00	1.90	0.00	0.01	0.00	0.00	0.00	0.78	0.12	0.01	0.00	0.00	6.97

EBS 26 Clay zeolites A2	18	4.11	0.00	2.03	0.00	0.02	0.00	0.00	0.02	0.54	0.28	0.01	0.00	0.00	7.03
EBS 26 Clay zeolites A4	44	4.24	0.00	1.89	0.00	0.01	0.00	0.00	0.00	0.64	0.08	0.00	0.00	0.01	6.86
EBS 26 Clay zeolites A1	31	4.16	0.00	2.05	0.00	0.01	0.00	0.00	0.00	0.49	0.21	0.01	0.00	0.00	6.93
AVERAGE		**4.18**	**0.00**	**1.92**	**0.00**	**0.01**	**0.00**	**0.00**	**0.00**	**0.63**	**0.21**	**0.01**	**0.00**	**0.00**	**6.97**
Std. Dev.		**0.05**	**0.00**	**0.09**	**0.00**	**0.01**	**0.00**	**0.00**	**0.01**	**0.09**	**0.08**	**0.00**	**0.00**	**0.00**	**0.06**
SAMPLE	**Pt#**	**SiO_2**	**TiO_2**	**Al_2O_3**	**Cr_2O_3**	**FeO**	**NiO**	**MnO**	**MgO**	**CaO**	**Na_2O**	**K_2O**	**Cl**	**F**	**TOTAL**
K-FELDSPAR															
EBS 26 Clay feldspars A2	23	65.23	0.01	19.02	0.00	0.13	0.00	0.00	0.00	0.20	2.94	11.83	0.00	0.06	99.36
EBS 26 Clay feldspars A2	24	65.39	0.01	20.01	0.00	0.11	0.00	0.00	0.00	0.27	3.19	11.54	0.00	0.01	100.52
EBS 26 Clay feldspars A2	25	65.33	0.02	19.59	0.00	0.13	0.00	0.00	0.00	0.21	3.25	11.48	0.00	0.05	100.02
EBS 26 Clay feldspars A1	33	64.76	0.00	19.51	0.00	0.13	0.00	0.00	0.00	0.21	3.33	11.75	0.01	0.15	99.71
EBS 26 Clay feldspars A1	35	64.69	0.02	19.62	0.00	0.13	0.00	0.00	0.00	0.21	3.31	11.76	0.00	0.00	99.74
EBS 26 Clay feldspars A4	46	65.10	0.01	19.31	0.00	0.11	0.00	0.01	0.00	0.18	3.14	11.48	0.00	0.14	99.33
EBS 26 Clay feldspars A4	47	65.91	0.02	19.43	0.00	0.17	0.01	0.01	0.00	0.31	2.48	12.49	0.00	0.02	100.82
AVERAGE		**65.20**	**0.01**	**19.50**	**0.00**	**0.13**	**0.00**	**0.00**	**0.00**	**0.23**	**3.09**	**11.76**	**0.00**	**0.06**	**99.93**
Std. Dev.		**0.38**	**0.01**	**0.28**	**0.00**	**0.02**	**0.00**	**0.00**	**0.00**	**0.04**	**0.28**	**0.33**	**0.00**	**0.06**	**0.52**
8 oxygen atoms per formula unit (sum excludes F & Cl)															
		Si	**Ti**	**Al**	**Cr**	**Fe**	**Ni**	**Mn**	**Mg**	**Ca**	**Na**	**K**	**Cl**	**F**	**SUM**
EBS 26 Clay feldspars A2	23	2.98	0.00	1.03	0.00	0.00	0.00	0.00	0.00	0.01	0.26	0.69	0.00	0.01	4.98
EBS 26 Clay feldspars A2	24	2.97	0.00	1.06	0.00	0.00	0.00	0.00	0.00	0.01	0.27	0.63	0.00	0.00	4.95
EBS 26 Clay feldspars A2	25	2.97	0.00	1.05	0.00	0.00	0.00	0.00	0.00	0.01	0.29	0.67	0.00	0.01	4.98
EBS 26 Clay feldspars A1	33	2.96	0.00	1.05	0.00	0.01	0.00	0.00	0.00	0.01	0.29	0.68	0.00	0.02	5.01
EBS 26 Clay feldspars A1	35	2.95	0.00	1.06	0.00	0.01	0.00	0.00	0.00	0.01	0.29	0.69	0.00	0.00	5.01
EBS 26 Clay feldspars A4	46	2.98	0.00	1.04	0.00	0.00	0.00	0.00	0.00	0.01	0.28	0.67	0.00	0.02	4.98
EBS 26 Clay feldspars A4	47	2.98	0.00	1.03	0.00	0.01	0.00	0.00	0.00	0.02	0.22	0.72	0.00	0.00	4.97
AVERAGE		**2.97**	**0.00**	**1.05**	**0.00**	**0.00**	**0.00**	**0.00**	**0.00**	**0.01**	**0.27**	**0.68**	**0.00**	**0.01**	**4.98**
Std. Dev.		**0.01**	**0.00**	**0.01**	**0.00**	**0.00**	**0.00**	**0.00**	**0.00**	**0.00**	**0.03**	**0.03**	**0.00**	**0.01**	**0.02**

SAMPLE	Pt#	SiO_2	TiO_2	Al_2O_3	Cr_2O_3	FeO	NiO	MnO	MgO	CaO	Na_2O	K_2O	Cl	F	TOTAL
Plagioclase															
EBS 26 Clay feldspars A2	21	54.98	0.00	28.73	0.00	0.20	0.00	0.01	0.00	10.39	5.07	0.34	0.00	0.00	99.70
EBS 26 Clay feldspars A2	22	62.89	0.00	24.24	0.01	0.21	0.00	0.01	0.01	5.66	6.80	1.05	0.00	0.00	100.88
EBS 26 Clay feldspars A1	32	61.36	0.00	24.99	0.00	0.16	0.01	0.00	0.01	5.73	6.74	0.96	0.00	0.05	99.98
AVERAGE		**59.75**	**0.00**	**25.99**	**0.00**	**0.19**	**0.00**	**0.01**	**0.01**	**7.26**	**6.20**	**0.78**	**0.00**	**0.02**	**100.19**
Std. Dev.		**3.43**	**0.00**	**1.96**	**0.00**	**0.02**	**0.01**	**0.01**	**0.01**	**2.21**	**0.80**	**0.32**	**0.00**	**0.02**	**0.50**
8 oxygen atoms per formula unit (sum excludes F & Cl)															
		Si	**Ti**	**Al**	**Cr**	**Fe**	**Ni**	**Mn**	**Mg**	**Ca**	**Na**	**K**	**Cl**	**F**	**SUM**
EBS 26 Clay feldspars A2	21	2.48	0.00	1.53	0.00	0.01	0.00	0.00	0.00	0.50	0.44	0.02	0.00	0.00	4.98
EBS 26 Clay feldspars A2	22	2.76	0.00	1.25	0.00	0.01	0.00	0.00	0.00	0.27	0.58	0.06	0.00	0.00	4.93
EBS 26 Clay feldspars A1	32	2.72	0.00	1.31	0.00	0.01	0.00	0.00	0.00	0.27	0.58	0.05	0.00	0.01	4.94
AVERAGE		**2.66**	**0.00**	**1.36**	**0.00**	**0.01**	**0.00**	**0.00**	**0.00**	**0.35**	**0.53**	**0.04**	**0.00**	**0.00**	**4.95**
Std. Dev.		**0.12**	**0.00**	**0.12**	**0.00**	**0.00**	**0.00**	**0.00**	**0.00**	**0.11**	**0.06**	**0.02**	**0.00**	**0.00**	**0.02**
SAMPLE	**Pt#**	**SiO_2**	**TiO_2**	**Al_2O_3**	**Cr_2O_3**	**FeO**	**NiO**	**MnO**	**MgO**	**CaO**	**Na_2O**	**K_2O**	**Cl**	**F**	**TOTAL**
TOBERMORITE															
EBS 26 Clay zeolites A2	10	34.33	0.03	4.62	0.00	0.62	0.00	0.02	0.18	20.52	0.06	0.06	0.34	0.00	60.78
EBS 26 Clay zeolites A2	11	29.67	0.04	4.83	0.00	0.71	0.01	0.02	0.18	19.00	0.06	0.08	0.35	0.04	54.95
EBS 26 Clay zeolites A2	12	35.62	0.05	5.18	0.01	0.63	0.01	0.00	0.18	21.51	0.10	0.05	0.43	0.01	63.77
EBS 26 Clay zeolites A2	13	32.13	0.05	5.23	0.00	0.66	0.00	0.01	0.25	19.87	0.10	0.05	0.37	0.00	58.71
EBS 26 Clay zeolites A2	14	33.93	0.11	5.16	0.00	1.09	0.00	0.00	0.22	21.10	0.09	0.11	0.46	0.03	62.27
AVERAGE		**33.14**	**0.05**	**5.00**	**0.00**	**0.74**	**0.01**	**0.01**	**0.20**	**20.40**	**0.08**	**0.07**	**0.39**	**0.02**	**60.10**
Std. Dev.		**1.79**	**0.01**	**0.96**	**0.00**	**0.02**	**0.01**	**0.01**	**0.00**	**0.29**	**0.17**	**0.01**	**0.00**	**0.04**	**2.16**
16 oxygen atoms per formula unit (sum excludes F & Cl)															
		Si	**Ti**	**Al**	**Cr**	**Fe**	**Ni**	**Mn**	**Mg**	**Ca**	**Na**	**K**	**Cl**	**F**	**SUM**
EBS 26 Clay zeolites A2	10	5.51	0.00	0.87	0.00	0.08	0.00	0.00	0.04	3.53	0.02	0.01	0.09	0.00	10.07
EBS 26 Clay zeolites A2	11	5.32	0.01	1.02	0.00	0.11	0.00	0.00	0.05	3.65	0.02	0.02	0.11	0.02	10.19
EBS 26 Clay zeolites A2	12	5.46	0.01	0.93	0.00	0.08	0.00	0.00	0.04	3.53	0.03	0.01	0.11	0.01	10.09
EBS 26 Clay zeolites A2	13	5.36	0.01	1.03	0.00	0.09	0.00	0.00	0.06	3.55	0.03	0.01	0.11	0.00	10.14

EBS 26 Clay zeolites A2	14	5.37	0.01	0.96	0.00	0.14	0.00	0.00	0.05	3.58	0.03	0.02	0.12	0.01	10.16
AVERAGE		**5.40**	**0.01**	**0.96**	**0.00**	**0.10**	**0.00**	**0.00**	**0.05**	**3.57**	**0.03**	**0.01**	**0.11**	**0.01**	**10.13**
Std. Dev.		**0.07**	**0.00**	**0.06**	**0.00**	**0.02**	**0.00**	**0.00**	**0.01**	**0.04**	**0.01**	**0.00**	**0.01**	**0.01**	**0.04**
SAMPLE	**Pt#**	**SiO_2**	**TiO_2**	**Al_2O_3**	**Cr_2O_3**	**FeO**	**NiO**	**MnO**	**MgO**	**CaO**	**Na_2O**	**K_2O**	**Cl**	**F**	**TOTAL**
ZEOLITE															
EBS 26 Clay zeolites A2	17	46.78	0.45	31.95	0.02	2.27	0.00	0.01	1.62	3.55	0.44	7.91	0.04	0.19	95.04
12 oxygen atoms per formula unit (sum excludes F & Cl)															
		Si	**Ti**	**Al**	**Cr**	**Fe**	**Ni**	**Mn**	**Mg**	**Ca**	**Na**	**K**	**Cl**	**F**	**SUM**
EBS 26 Clay zeolites A2	17	3.42	0.02	2.75	0.00	0.14	0.00	0.00	0.18	0.28	0.06	0.74	0.01	0.04	7.58
SAMPLE	**Pt#**	**SiO_2**	**TiO_2**	**Al_2O_3**	**Cr_2O_3**	**FeO**	**NiO**	**MnO**	**MgO**	**CaO**	**Na_2O**	**K_2O**	**Cl**	**F**	**TOTAL**
ANALCIME in porous cement matrix															
EBS 26 cement A3 zeolites	19	55.84	0.02	25.71	0.00	0.18	0.03	0.00	0.05	2.97	5.66	0.05	0.01	0.10	90.51
EBS 26 cement A1 zeolites	4	59.34	0.00	23.63	0.00	0.04	0.01	0.01	0.01	2.84	4.75	0.02	0.00	0.05	90.66
EBS 26 cement A4 zeolites	23	63.62	0.00	24.92	0.01	0.07	0.00	0.01	0.00	2.34	4.77	0.05	0.01	0.00	95.78
EBS 26 cement A3 zeolites	18	60.63	0.02	23.01	0.00	0.68	0.01	0.01	0.41	2.77	4.84	0.09	0.03	0.03	92.51
EBS 26 cement A4 zeolites	22	60.47	0.01	24.40	0.00	0.14	0.01	0.00	0.01	2.78	4.87	0.04	0.00	0.01	92.72
EBS 26 cement A1 zeolites	1	60.30	0.00	24.85	0.00	0.05	0.00	0.00	0.00	2.58	5.28	0.03	0.01	0.02	93.09
EBS 26 cement A2 zeolites	9	60.36	0.00	25.19	0.01	0.07	0.00	0.01	0.00	2.53	4.90	0.03	0.00	0.00	93.11
EBS 26 cement A2 zeolites	7	60.68	0.01	24.66	0.00	0.05	0.00	0.00	0.00	3.02	4.71	0.01	0.00	0.00	93.13
EBS 26 cement A2 zeolites	8	61.03	0.00	24.76	0.00	0.06	0.00	0.00	0.00	2.84	4.86	0.02	0.01	0.00	93.58
EBS 26 cement A1 zeolites	3	60.74	0.00	24.68	0.00	0.05	0.00	0.00	0.01	3.23	4.96	0.01	0.00	0.02	93.67
AVERAGE		**60.30**	**0.01**	**24.58**	**0.00**	**0.14**	**0.01**	**0.00**	**0.05**	**2.79**	**4.96**	**0.03**	**0.01**	**0.02**	**92.88**
Std. Dev.		**1.81**	**0.01**	**0.73**	**0.00**	**0.19**	**0.01**	**0.00**	**0.12**	**0.25**	**0.28**	**0.02**	**0.01**	**0.03**	**1.43**
12 oxygen atoms per formula unit (sum excludes F & Cl)															
		Si	**Ti**	**Al**	**Cr**	**Fe**	**Ni**	**Mn**	**Mg**	**Ca**	**Na**	**K**	**Cl**	**F**	**SUM**
EBS 26 cement A3 zeolites	19	4.03	0.00	2.19	0.00	0.01	0.00	0.00	0.01	0.23	0.79	0.00	0.00	0.02	7.27

EBS 26 cement A1 zeolites	4	4.23	0.00	1.99	0.00	0.00	0.00	0.00	0.00	0.22	0.66	0.00	0.00	0.01	7.10
EBS 26 cement A4 zeolites	23	4.28	0.00	1.97	0.00	0.00	0.00	0.00	0.00	0.17	0.62	0.00	0.00	0.00	7.05
EBS 26 cement A3 zeolites	18	4.26	0.00	1.90	0.00	0.04	0.00	0.00	0.04	0.21	0.66	0.01	0.00	0.01	7.12
EBS 26 cement A4 zeolites	22	4.22	0.00	2.01	0.00	0.01	0.00	0.00	0.00	0.21	0.66	0.00	0.00	0.00	7.11
EBS 26 cement A1 zeolites	1	4.20	0.00	2.04	0.00	0.00	0.00	0.00	0.00	0.19	0.71	0.00	0.00	0.00	7.14
EBS 26 cement A2 zeolites	9	4.19	0.00	2.06	0.00	0.00	0.00	0.00	0.00	0.19	0.66	0.00	0.00	0.00	7.11
EBS 26 cement A2 zeolites	7	4.21	0.00	2.02	0.00	0.00	0.00	0.00	0.00	0.22	0.63	0.00	0.00	0.00	7.09
EBS 26 cement A2 zeolites	8	4.22	0.00	2.02	0.00	0.00	0.00	0.00	0.00	0.21	0.65	0.00	0.00	0.00	7.10
EBS 26 cement A1 zeolites	3	4.20	0.00	2.01	0.00	0.00	0.00	0.00	0.00	0.24	0.67	0.00	0.00	0.00	7.12
AVERAGE		**4.20**	**0.00**	**2.02**	**0.00**	**0.01**	**0.00**	**0.00**	**0.01**	**0.21**	**0.67**	**0.00**	**0.00**	**0.00**	**7.12**
Std. Dev.		**0.06**	**0.00**	**0.07**	**0.00**	**0.01**	**0.00**	**0.00**	**0.01**	**0.02**	**0.05**	**0.00**	**0.00**	**0.01**	**0.05**
SAMPLE	**Pt#**	**SiO_2**	**TiO_2**	**Al_2O_3**	**Cr_2O_3**	**FeO**	**NiO**	**MnO**	**MgO**	**CaO**	**Na_2O**	**K_2O**	**Cl**	**F**	**TOTAL**
ANALCIME coating O.C. fragments															
EBS 26 cement A4 zeolites	24	63.09	0.03	24.37	0.00	0.13	0.00	0.00	0.00	2.51	4.35	0.04	0.01	0.01	94.52
EBS 26 cement A4 zeolites	25	60.36	0.12	21.87	0.00	0.46	0.00	0.02	1.16	3.73	3.06	0.04	0.18	0.00	90.98
AVERAGE		**61.72**	**0.07**	**23.12**	**0.00**	**0.29**	**0.00**	**0.01**	**0.58**	**3.12**	**3.71**	**0.04**	**0.09**	**0.01**	**92.75**
Std. Dev.		**1.37**	**0.04**	**1.25**	**0.00**	**0.17**	**0.00**	**0.01**	**0.58**	**0.61**	**0.64**	**0.00**	**0.08**	**0.01**	**1.77**
12 oxygen atoms per formula unit (sum excludes F & Cl)															
		Si	**Ti**	**Al**	**Cr**	**Fe**	**Ni**	**Mn**	**Mg**	**Ca**	**Na**	**K**	**Cl**	**F**	**SUM**
EBS 26 cement A4 zeolites	24	63.09	0.03	24.37	0.00	0.13	0.00	0.00	0.00	2.51	4.35	0.04	0.01	0.01	94.52
EBS 26 cement A4 zeolites	25	60.36	0.12	21.87	0.00	0.46	0.00	0.02	1.16	3.73	3.06	0.04	0.18	0.00	90.98
AVERAGE		**61.72**	**0.07**	**23.12**	**0.00**	**0.29**	**0.00**	**0.01**	**0.58**	**3.12**	**3.71**	**0.04**	**0.09**	**0.01**	**92.75**
Std. Dev.		**1.37**	**0.04**	**1.25**	**0.00**	**0.17**	**0.00**	**0.01**	**0.58**	**0.61**	**0.64**	**0.00**	**0.08**	**0.01**	**1.77**
SAMPLE	**Pt#**	**SiO_2**	**TiO_2**	**Al_2O_3**	**Cr_2O_3**	**FeO**	**NiO**	**MnO**	**MgO**	**CaO**	**Na_2O**	**K_2O**	**Cl**	**F**	**TOTAL**
CASH (very low totals)															
EBS 26 cement A1 clay	5	17.11	0.06	3.64	0.00	0.84	0.00	0.00	0.61	14.13	0.29	0.07	0.74	0.00	37.48
EBS 26 cement A1 clay	6	17.59	0.01	3.49	0.00	0.40	0.01	0.00	1.03	10.46	0.22	0.09	0.79	0.01	34.08
AVERAGE		**17.35**	**0.04**	**3.56**	**0.00**	**0.62**	**0.00**	**0.00**	**0.82**	**12.29**	**0.26**	**0.08**	**0.76**	**0.01**	**35.78**

Std. Dev.		**0.24**	**0.02**	**0.08**	**0.00**	**0.22**	**0.00**	**0.00**	**0.21**	**1.83**	**0.03**	**0.01**	**0.03**	**0.01**	**1.70**
16 oxygen atoms per formula unit (sum excludes F & Cl)															
		Si	**Ti**	**Al**	**Cr**	**Fe**	**Ni**	**Mn**	**Mg**	**Ca**	**Na**	**K**	**Cl**	**F**	**SUM**
EBS 26 cement A1 clay	5	4.74	0.01	1.19	0.00	0.19	0.00	0.00	0.25	4.19	0.16	0.02	0.35	0.00	10.75
EBS 26 cement A1 clay	6	5.14	0.00	1.20	0.00	0.10	0.00	0.00	0.45	3.28	0.13	0.03	0.39	0.01	10.33
AVERAGE		**4.94**	**0.01**	**1.19**	**0.00**	**0.15**	**0.00**	**0.00**	**0.35**	**3.73**	**0.14**	**0.03**	**0.37**	**0.01**	**10.54**
Std. Dev.		**0.20**	**0.00**	**0.01**	**0.00**	**0.05**	**0.00**	**0.00**	**0.10**	**0.46**	**0.01**	**0.00**	**0.02**	**0.01**	**0.21**
SAMPLE	**Pt#**	**SiO_2**	**TiO_2**	**Al_2O_3**	**Cr_2O_3**	**FeO**	**NiO**	**MnO**	**MgO**	**CaO**	**Na_2O**	**K_2O**	**Cl**	**F**	**TOTAL**
K-FELDSPAR															
EBS 26 cement A3 feldspars	13	64.74	0.00	19.19	0.00	0.12	0.02	0.01	0.00	0.21	3.08	11.63	0.00	0.06	99.01
EBS 26 cement A3 feldspars	14	64.67	0.01	19.63	0.00	0.15	0.00	0.00	0.11	0.46	3.34	11.76	0.02	0.02	100.15
EBS 26 cement A3 feldspars	16	64.74	0.00	19.10	0.00	0.10	0.00	0.00	0.02	0.29	2.46	12.58	0.04	0.00	99.33
EBS 26 cement A4 feldspars	31	64.46	0.01	20.05	0.00	0.12	0.02	0.01	0.01	0.20	3.21	11.74	0.00	0.00	99.82
EBS 26 cement A4 feldspars	33	63.86	0.01	20.10	0.01	0.12	0.01	0.01	0.00	0.22	2.86	12.42	0.01	0.10	99.62
AVERAGE		**64.49**	**0.01**	**19.61**	**0.00**	**0.12**	**0.01**	**0.01**	**0.03**	**0.27**	**2.99**	**12.02**	**0.01**	**0.03**	**99.58**
Std. Dev.		**0.33**	**0.01**	**0.42**	**0.00**	**0.02**	**0.01**	**0.00**	**0.04**	**0.10**	**0.31**	**0.39**	**0.01**	**0.04**	**0.39**
8 oxygen atoms per formula unit (sum excludes F & Cl)															
		Si	**Ti**	**Al**	**Cr**	**Fe**	**Ni**	**Mn**	**Mg**	**Ca**	**Na**	**K**	**Cl**	**F**	**SUM**
EBS 26 cement A3 feldspars	13	2.97	0.00	1.04	0.00	0.00	0.00	0.00	0.00	0.01	0.27	0.68	0.00	0.01	4.98
EBS 26 cement A3 feldspars	14	2.93	0.00	1.08	0.00	0.01	0.00	0.00	0.01	0.02	0.29	0.67	0.00	0.00	5.01
EBS 26 cement A3 feldspars	16	2.96	0.00	1.05	0.00	0.00	0.00	0.00	0.00	0.01	0.22	0.75	0.00	0.00	5.00
EBS 26 cement A4 feldspars	31	2.94	0.00	1.08	0.00	0.00	0.00	0.00	0.00	0.01	0.28	0.68	0.00	0.00	5.00
EBS 26 cement A4 feldspars	33	2.93	0.00	1.09	0.00	0.00	0.00	0.00	0.00	0.01	0.25	0.73	0.00	0.01	5.02
AVERAGE		**2.95**	**0.00**	**1.07**	**0.00**	**0.00**	**0.00**	**0.00**	**0.00**	**0.01**	**0.26**	**0.70**	**0.00**	**0.01**	**5.00**
Std. Dev.		**0.02**	**0.00**	**0.02**	**0.00**	**0.00**	**0.00**	**0.00**	**0.00**	**0.00**	**0.02**	**0.03**	**0.00**	**0.01**	**0.01**
SAMPLE	**Pt#**	**SiO_2**	**TiO_2**	**Al_2O_3**	**Cr_2O_3**	**FeO**	**NiO**	**MnO**	**MgO**	**CaO**	**Na_2O**	**K_2O**	**Cl**	**F**	**TOTAL**
PLAGIOCLASE															

EBS 26 cement A1 zeolites	2	62.19	0.01	25.97	0.00	0.17	0.01	0.03	0.01	5.67	6.93	1.11	0.00	0.00	102.10
EBS 26 cement A2 feldspars	10	59.98	0.01	25.06	0.00	0.18	0.01	0.01	0.00	6.28	6.64	0.89	0.00	0.00	99.06
EBS 26 cement A2 feldspars	11	59.54	0.00	25.64	0.00	0.21	0.01	0.00	0.00	6.78	6.42	0.89	0.00	0.05	99.51
EBS 26 cement A2 feldspars	12	60.35	0.00	24.96	0.01	0.22	0.01	0.00	0.00	5.14	7.39	1.04	0.00	0.00	99.11
EBS 26 cement A3 feldspars	15	63.15	0.01	22.78	0.00	0.15	0.00	0.01	0.00	3.74	7.59	1.15	0.00	0.11	98.60
EBS 26 cement A4 feldspars	32	59.08	0.01	25.38	0.00	0.18	0.00	0.01	0.00	5.77	6.86	1.02	0.00	0.00	98.30
AVERAGE		**60.72**	**0.01**	**24.97**	**0.00**	**0.18**	**0.01**	**0.01**	**0.00**	**5.56**	**6.97**	**1.02**	**0.00**	**0.03**	**99.45**
Std. Dev.		**1.46**	**0.00**	**1.03**	**0.00**	**0.02**	**0.00**	**0.01**	**0.00**	**0.96**	**0.41**	**0.10**	**0.00**	**0.04**	**1.25**
8 oxygen atoms per formula unit (sum excludes F & Cl)															
		Si	**Ti**	**Al**	**Cr**	**Fe**	**Ni**	**Mn**	**Mg**	**Ca**	**Na**	**K**	**Cl**	**F**	**SUM**
EBS 26 cement A1 zeolites	2	2.70	0.00	1.33	0.00	0.01	0.00	0.00	0.00	0.26	0.58	0.06	0.00	0.00	4.95
EBS 26 cement A2 feldspars	10	2.69	0.00	1.33	0.00	0.01	0.00	0.00	0.00	0.30	0.58	0.05	0.00	0.00	4.96
EBS 26 cement A2 feldspars	11	2.67	0.00	1.35	0.00	0.01	0.00	0.00	0.00	0.33	0.56	0.05	0.00	0.01	4.96
EBS 26 cement A2 feldspars	12	2.78	0.00	1.25	0.00	0.01	0.00	0.00	0.00	0.23	0.61	0.06	0.00	0.00	4.93
EBS 26 cement A3 feldspars	15	2.82	0.00	1.20	0.00	0.01	0.00	0.00	0.00	0.18	0.66	0.07	0.00	0.02	4.94
EBS 26 cement A4 feldspars	32	2.68	0.00	1.35	0.00	0.01	0.00	0.00	0.00	0.28	0.60	0.06	0.00	0.00	4.98
AVERAGE		**2.72**	**0.00**	**1.30**	**0.00**	**0.01**	**0.00**	**0.00**	**0.00**	**0.26**	**0.60**	**0.06**	**0.00**	**0.00**	**4.95**
Std. Dev.		**0.06**	**0.00**	**0.06**	**0.00**	**0.00**	**0.00**	**0.00**	**0.00**	**0.05**	**0.03**	**0.01**	**0.00**	**0.01**	**0.02**
SAMPLE	**Pt#**	**SiO_2**	**TiO_2**	**Al_2O_3**	**Cr_2O_3**	**FeO**	**NiO**	**MnO**	**MgO**	**CaO**	**Na_2O**	**K_2O**	**Cl**	**F**	**TOTAL**
TOBERMORITE															
EBS 26 cement A4 zeolites	26	26.28	0.06	6.28	0.01	1.03	0.00	0.00	0.28	16.95	0.17	0.09	0.62	0.23	51.77
EBS 26 cement A4 zeolites	27	31.56	0.06	7.25	0.00	1.09	0.00	0.00	0.26	19.16	0.19	0.12	0.65	0.08	60.32
EBS 26 cement A4 zeolites	28	25.10	0.06	5.27	0.01	1.07	0.01	0.02	0.17	18.60	0.26	0.10	0.60	0.00	51.26
EBS 26 cement A4 zeolites	29	39.82	0.05	7.27	0.00	1.14	0.00	0.02	0.37	18.77	0.67	0.18	0.59	0.28	68.87
EBS 26 cement A4 zeolites	30	31.02	0.06	6.39	0.00	1.24	0.00	0.01	0.36	15.38	0.22	0.13	0.59	0.08	55.40
AVERAGE		**30.76**	**0.06**	**6.49**	**0.00**	**1.11**	**0.00**	**0.01**	**0.29**	**17.77**	**0.30**	**0.12**	**0.61**	**0.13**	**57.53**
Std. Dev.		**5.19**	**0.00**	**0.74**	**0.00**	**0.07**	**0.00**	**0.01**	**0.08**	**1.41**	**0.19**	**0.03**	**0.02**	**0.11**	**6.53**
16 oxygen atoms per formula unit (sum excludes F & Cl)															
		Si	**Ti**	**Al**	**Cr**	**Fe**	**Ni**	**Mn**	**Mg**	**Ca**	**Na**	**K**	**Cl**	**F**	**SUM**
EBS 26 cement A4 zeolites	26	5.04	0.01	1.42	0.00	0.17	0.00	0.00	0.08	3.48	0.06	0.02	0.20	0.14	10.28

EBS 26 cement A4 zeolites	27	5.15	0.01	1.39	0.00	0.15	0.00	0.00	0.06	3.35	0.06	0.02	0.18	0.04	10.19
EBS 26 cement A4 zeolites	28	4.96	0.01	1.23	0.00	0.18	0.00	0.00	0.05	3.94	0.10	0.03	0.20	0.00	10.48
EBS 26 cement A4 zeolites	29	5.54	0.01	1.19	0.00	0.13	0.00	0.00	0.08	2.80	0.18	0.03	0.14	0.12	9.96
EBS 26 cement A4 zeolites	30	5.41	0.01	1.31	0.00	0.18	0.00	0.00	0.09	2.87	0.07	0.03	0.17	0.04	9.98
AVERAGE		**5.22**	**0.01**	**1.31**	**0.00**	**0.16**	**0.00**	**0.00**	**0.07**	**3.29**	**0.10**	**0.03**	**0.18**	**0.07**	**10.18**
Std. Dev.		**0.22**	**0.00**	**0.09**	**0.00**	**0.02**	**0.00**	**0.00**	**0.02**	**0.42**	**0.04**	**0.00**	**0.02**	**0.05**	**0.20**
SAMPLE	**Pt#**	**SiO_2**	**TiO_2**	**Al_2O_3**	**Cr_2O_3**	**FeO**	**NiO**	**MnO**	**MgO**	**CaO**	**Na_2O**	**K_2O**	**Cl**	**F**	**TOTAL**
ANALCIME near steel surface															
EBS 26 Steel zeolites A2	5	63.88	0.04	24.45	0.02	0.33	0.01	0.00	0.11	2.96	3.65	0.05	0.05	0.07	95.53
EBS 26 Steel zeolites A2	6	62.78	0.01	23.51	0.00	0.23	0.01	0.01	0.00	2.55	3.42	0.03	0.01	0.00	92.56
EBS 26 Steel zeolites A1	9	61.26	0.04	24.17	0.00	0.95	0.00	0.00	0.41	2.94	2.66	0.26	0.26	0.02	92.95
EBS 26 Steel zeolites A1	12	61.36	0.01	24.16	0.00	0.20	0.01	0.00	0.01	3.19	3.90	0.03	0.00	0.01	92.87
AVERAGE		**62.32**	**0.02**	**24.07**	**0.01**	**0.43**	**0.01**	**0.00**	**0.13**	**2.91**	**3.41**	**0.09**	**0.08**	**0.02**	**93.48**
Std. Dev.		**1.08**	**0.01**	**0.35**	**0.01**	**0.30**	**0.00**	**0.00**	**0.17**	**0.23**	**0.46**	**0.10**	**0.11**	**0.03**	**1.19**
12 oxygen atoms per formula unit (sum excludes F & Cl)															
		Si	**Ti**	**Al**	**Cr**	**Fe**	**Ni**	**Mn**	**Mg**	**Ca**	**Na**	**K**	**Cl**	**F**	**SUM**
EBS 26 Steel zeolites A2	5	4.30	0.00	1.94	0.00	0.02	0.00	0.00	0.01	0.21	0.48	0.00	0.01	0.01	6.97
EBS 26 Steel zeolites A2	6	4.34	0.00	1.92	0.00	0.01	0.00	0.00	0.00	0.19	0.46	0.00	0.00	0.00	6.93
EBS 26 Steel zeolites A1	9	4.26	0.00	1.98	0.00	0.05	0.00	0.00	0.04	0.22	0.36	0.02	0.03	0.01	6.94
EBS 26 Steel zeolites A1	12	4.26	0.00	1.98	0.00	0.01	0.00	0.00	0.00	0.24	0.53	0.00	0.00	0.00	7.02
AVERAGE		**4.29**	**0.00**	**1.95**	**0.00**	**0.02**	**0.00**	**0.00**	**0.01**	**0.21**	**0.45**	**0.01**	**0.01**	**0.01**	**6.96**
Std. Dev.		**0.04**	**0.00**	**0.03**	**0.00**	**0.02**	**0.00**	**0.00**	**0.02**	**0.02**	**0.06**	**0.01**	**0.01**	**0.01**	**0.03**
SAMPLE	**Pt#**	**SiO_2**	**TiO_2**	**Al_2O_3**	**Cr_2O_3**	**FeO**	**NiO**	**MnO**	**MgO**	**CaO**	**Na_2O**	**K_2O**	**Cl**	**F**	**TOTAL**
GARRONITE															
EBS 26 Steel zeolites A3	15	58.23	0.04	20.26	0.00	0.43	0.00	0.01	0.11	10.55	2.63	0.04	0.07	0.06	92.37
EBS 26 Steel zeolites A3	16	57.28	0.10	19.75	0.00	1.63	0.03	0.06	0.16	9.73	2.78	0.04	0.03	0.32	91.58
AVERAGE		**57.75**	**0.07**	**20.00**	**0.00**	**1.03**	**0.01**	**0.04**	**0.14**	**10.14**	**2.70**	**0.04**	**0.05**	**0.19**	**91.97**

Std. Dev.		**0.48**	**0.03**	**0.26**	**0.00**	**0.60**	**0.01**	**0.02**	**0.02**	**0.41**	**0.08**	**0.00**	**0.02**	**0.13**	**0.39**
8 oxygen atoms per formula unit (sum excludes F & Cl)															
		Si	**Ti**	**Al**	**Cr**	**Fe**	**Ni**	**Mn**	**Mg**	**Ca**	**Na**	**K**	**Cl**	**F**	**SUM**
EBS 26 Steel zeolites A3	15	2.79	0.00	1.15	0.00	0.02	0.00	0.00	0.01	0.54	0.24	0.00	0.01	0.01	4.76
EBS 26 Steel zeolites A3	16	2.79	0.00	1.13	0.00	0.07	0.00	0.00	0.01	0.51	0.26	0.00	0.00	0.05	4.78
AVERAGE		**2.79**	**0.00**	**1.14**	**0.00**	**0.04**	**0.00**	**0.00**	**0.01**	**0.52**	**0.25**	**0.00**	**0.00**	**0.03**	**4.77**
Std. Dev.		**0.00**	**0.00**	**0.01**	**0.00**	**0.02**	**0.00**	**0.00**	**0.00**	**0.02**	**0.01**	**0.00**	**0.00**	**0.02**	**0.01**
SAMPLE	**Pt#**	**SiO_2**	**TiO_2**	**Al_2O_3**	**Cr_2O_3**	**FeO**	**NiO**	**MnO**	**MgO**	**CaO**	**Na_2O**	**K_2O**	**Cl**	**F**	**TOTAL**
HIGH-Fe ANALCIME MATRIX															
EBS 26 Steel zeolites A2	3	59.06	0.11	22.85	0.01	1.28	0.00	0.01	0.27	4.48	2.80	0.03	0.08	0.00	90.99
EBS 26 Steel zeolites A2	4	59.69	0.04	22.80	0.00	0.68	0.00	0.00	0.11	4.06	3.61	0.04	0.03	0.13	91.07
EBS 26 Steel zeolites A2	2	59.93	0.06	23.78	0.00	1.95	0.01	0.00	0.82	3.44	2.59	0.06	0.13	0.05	92.77
EBS 26 Steel zeolites A1	14	61.96	0.02	23.40	0.01	0.84	0.00	0.01	0.12	3.30	3.69	0.03	0.05	0.00	93.42
EBS 26 Steel zeolites A1	10	61.96	0.06	23.33	0.01	0.81	0.01	0.01	0.39	3.92	2.94	0.03	0.05	0.00	93.51
EBS 26 Steel zeolites A2	7	63.34	0.05	24.19	0.01	1.97	0.01	0.00	0.35	3.22	3.66	0.05	0.11	0.08	96.95
AVERAGE		**60.99**	**0.06**	**23.39**	**0.01**	**1.25**	**0.00**	**0.01**	**0.34**	**3.74**	**3.21**	**0.04**	**0.07**	**0.04**	**93.12**
Std. Dev.		**1.52**	**0.03**	**0.49**	**0.00**	**0.53**	**0.00**	**0.00**	**0.24**	**0.46**	**0.45**	**0.01**	**0.04**	**0.05**	**1.99**
12 oxygen atoms per formula unit (sum excludes F & Cl)															
		Si	**Ti**	**Al**	**Cr**	**Fe**	**Ni**	**Mn**	**Mg**	**Ca**	**Na**	**K**	**Cl**	**F**	**SUM**
EBS 26 Steel zeolites A2	3	4.23	0.01	1.93	0.00	0.08	0.00	0.00	0.03	0.34	0.39	0.00	0.01	0.00	7.00
EBS 26 Steel zeolites A2	4	4.25	0.00	1.92	0.00	0.04	0.00	0.00	0.01	0.31	0.50	0.00	0.00	0.03	7.04
EBS 26 Steel zeolites A2	2	4.20	0.00	1.97	0.00	0.11	0.00	0.00	0.09	0.26	0.35	0.01	0.02	0.01	6.99
EBS 26 Steel zeolites A1	14	4.29	0.00	1.91	0.00	0.05	0.00	0.00	0.01	0.24	0.50	0.00	0.01	0.00	7.00
EBS 26 Steel zeolites A1	10	4.28	0.00	1.90	0.00	0.05	0.00	0.00	0.04	0.29	0.39	0.00	0.01	0.00	6.96
EBS 26 Steel zeolites A2	7	4.25	0.00	1.91	0.00	0.11	0.00	0.00	0.03	0.23	0.48	0.00	0.01	0.02	7.03
AVERAGE		**4.25**	**0.00**	**1.92**	**0.00**	**0.07**	**0.00**	**0.00**	**0.04**	**0.28**	**0.43**	**0.00**	**0.01**	**0.01**	**7.00**
Std. Dev.		**0.03**	**0.00**	**0.02**	**0.00**	**0.03**	**0.00**	**0.00**	**0.02**	**0.04**	**0.06**	**0.00**	**0.00**	**0.01**	**0.02**
SAMPLE	**Pt#**	**SiO_2**	**TiO_2**	**Al_2O_3**	**Cr_2O_3**	**FeO**	**NiO**	**MnO**	**MgO**	**CaO**	**Na_2O**	**K_2O**	**Cl**	**F**	**TOTAL**

ZEOLITES with variable cation composition															
EBS 26 Steel zeolites A3	20	62.17	0.03	24.04	0.01	0.19	0.01	0.01	0.00	4.21	3.65	0.02	0.01	0.12	94.36
EBS 26 Steel zeolites A1	11	63.32	0.01	24.31	0.00	0.44	0.00	0.00	0.04	3.07	4.05	0.02	0.01	0.00	95.27
EBS 26 Steel zeolites A1	13	61.60	0.02	24.52	0.00	0.30	0.00	0.00	0.01	3.12	4.25	0.02	0.00	0.03	93.85
EBS 26 Steel zeolites A3	18	60.45	0.05	22.47	0.00	0.41	0.00	0.00	0.18	6.36	3.05	0.07	0.06	0.07	93.10
12 oxygen atoms per formula unit (sum excludes F & Cl)															
		Si	**Ti**	**Al**	**Cr**	**Fe**	**Ni**	**Mn**	**Mg**	**Ca**	**Na**	**K**	**Cl**	**F**	**SUM**
EBS 26 Steel zeolites A3	20	4.26	0.00	1.94	0.00	0.01	0.00	0.00	0.00	0.31	0.49	0.00	0.00	0.03	7.01
EBS 26 Steel zeolites A1	11	4.29	0.00	1.94	0.00	0.02	0.00	0.00	0.00	0.22	0.53	0.00	0.00	0.00	7.01
EBS 26 Steel zeolites A1	13	4.24	0.00	1.99	0.00	0.02	0.00	0.00	0.00	0.23	0.57	0.00	0.00	0.01	7.05
EBS 26 Steel zeolites A3	18	4.24	0.00	1.86	0.00	0.02	0.00	0.00	0.02	0.48	0.42	0.01	0.01	0.02	7.04

F. SEM and EMP Images: EBS-23 to EBS-31

EBS-23

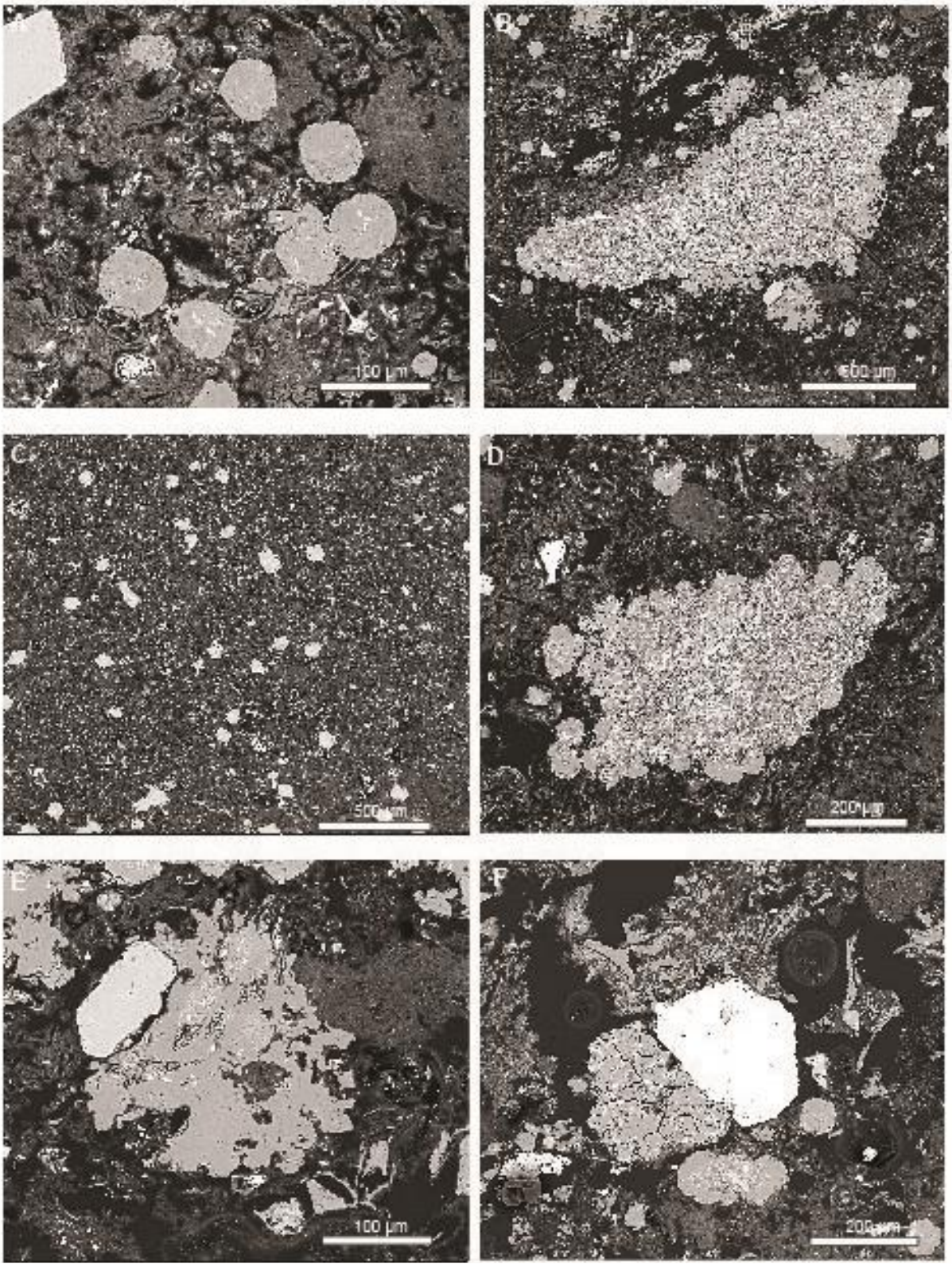

Figure F-1. EBS-23. BSE images of EBS-23 thin sections. [**A**] Analcime crystals in porous clay matrix. [**B**] Opalinus Clay fragment rimmed by analcime. [**C**] Analcime dispersed in porous cement matrix. [**D**] Analcime mantling an Opalinus Clay fragment. [**E**] Feldspar crystal adjacent to garronite. [**F**] Bright Fe-oxide crystal next to analcime and garronite.

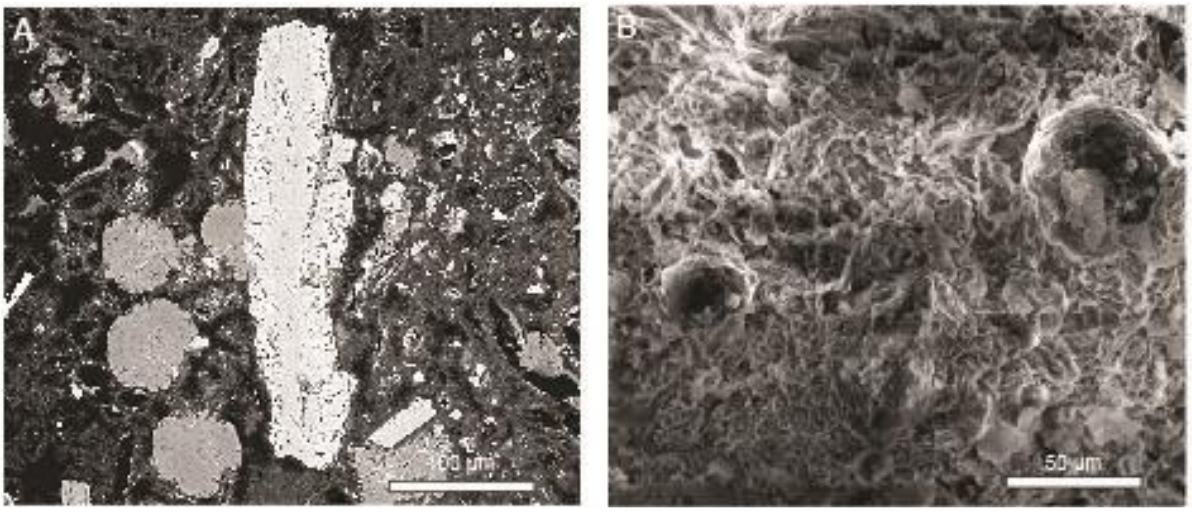

Figure F-2. EBS-23. BSE image of calcite crystal (center) surrounded by analcime. [**A**] Analcime removed from the calcite crystal is Na-rich, whereas analcime attached to the calcite is Ca-rich (determined by EMPA). [**B**] Analcime embedded in smectite.

EBS-24

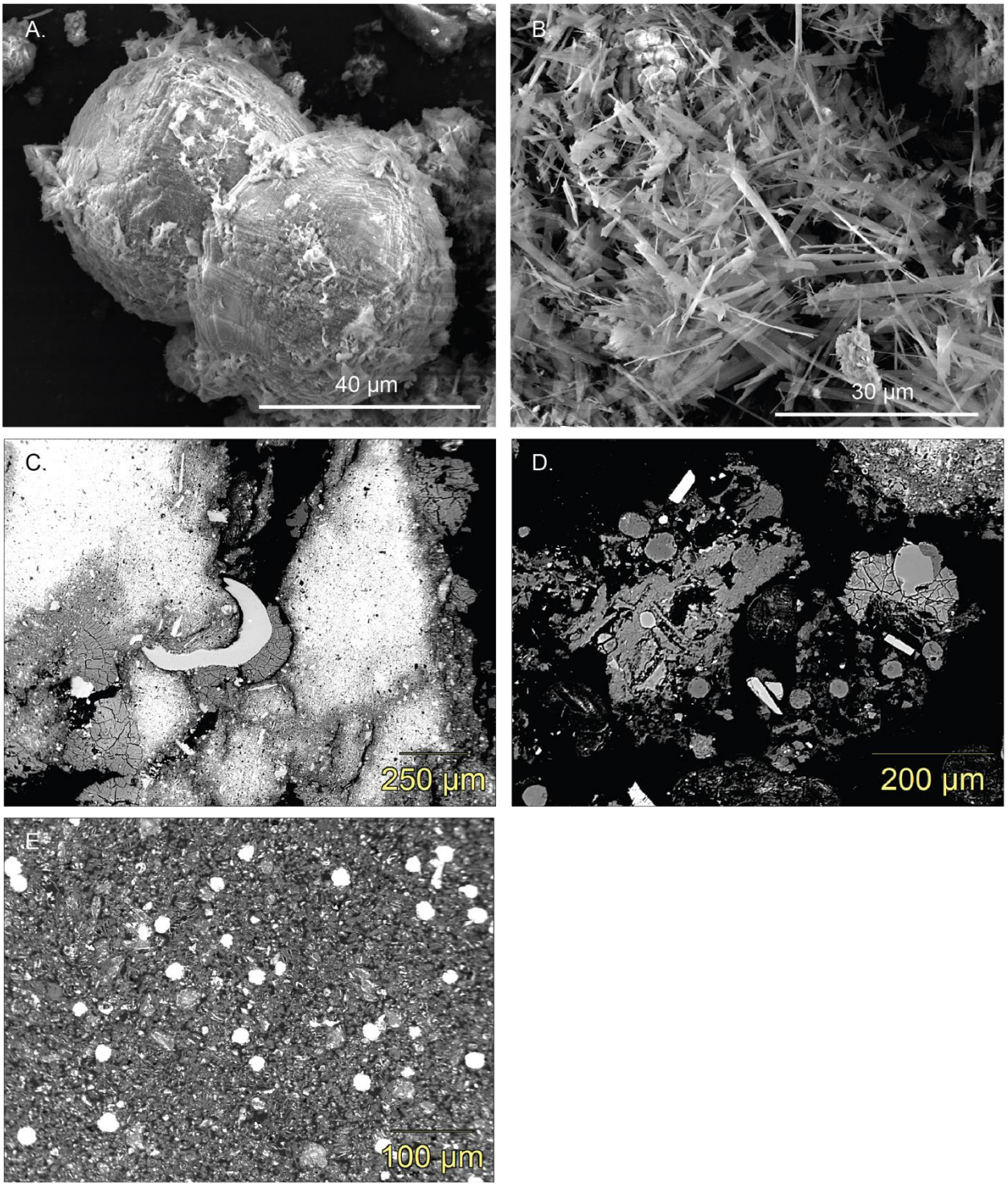

Figure F-3. EBS-24. SEM images of cement and clay [**A**] SE image of rough analcime (possible intergrowth of other phases?) spheres. [**B**] SE image of fibrous xonotlite. [**C**] BSE image of calcite (crescent shape) and adjacent garronite (gray, cracked mineral) in a fracture of an Opalinus Clay fragment (bright white zones). [**D**] BSE image of analcime, feldspar, and garronite in the clay fraction. [**E**] BSE image of analcime crystals dispersed in a porous cement matrix.

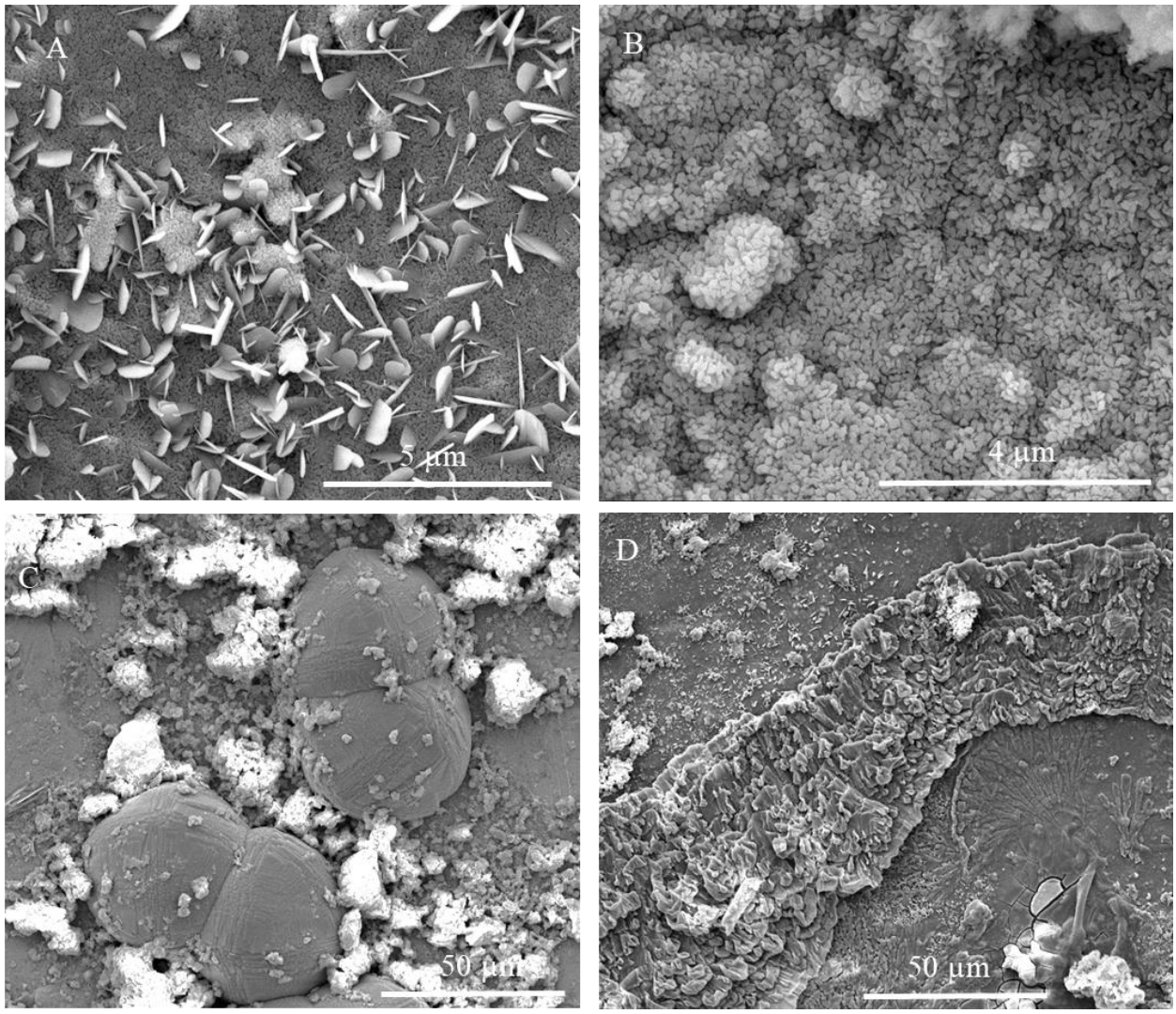

Figure F-4. EBS-24. SEM images of post-reaction 316SS. [**A**] Fe-Ni-Cr oxide on the SS surface. [**B**] Fe-oxide on SS surface. [**C**] Analcime with clay on the stainless-steel surface. [**D**] Calcite (central band) with Fe-Ni-Cr oxides on the steel.

EBS-25

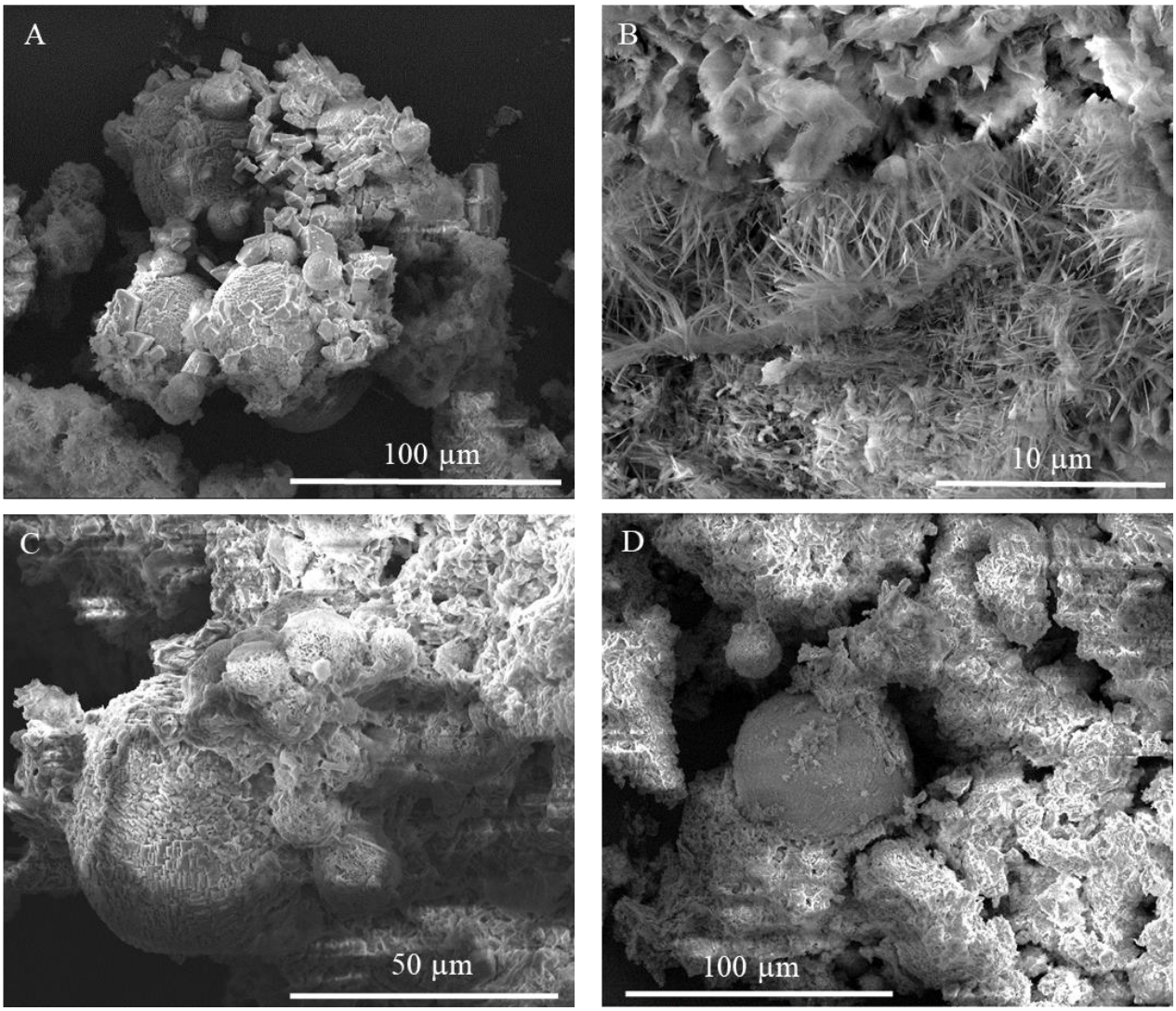

Figure F-5. EBS-25. SEM images of clay and cement. [**A**] Analcime with anorthite and tobermorite rosettes in the porous cement matrix. [**B**] Fibrous minerals in the cement fraction (potential xonotolite). [**C**] Intergrowth of garronite to analcime in the clay fraction. [**D**] Analcime sphere in smectite in the clay fraction.

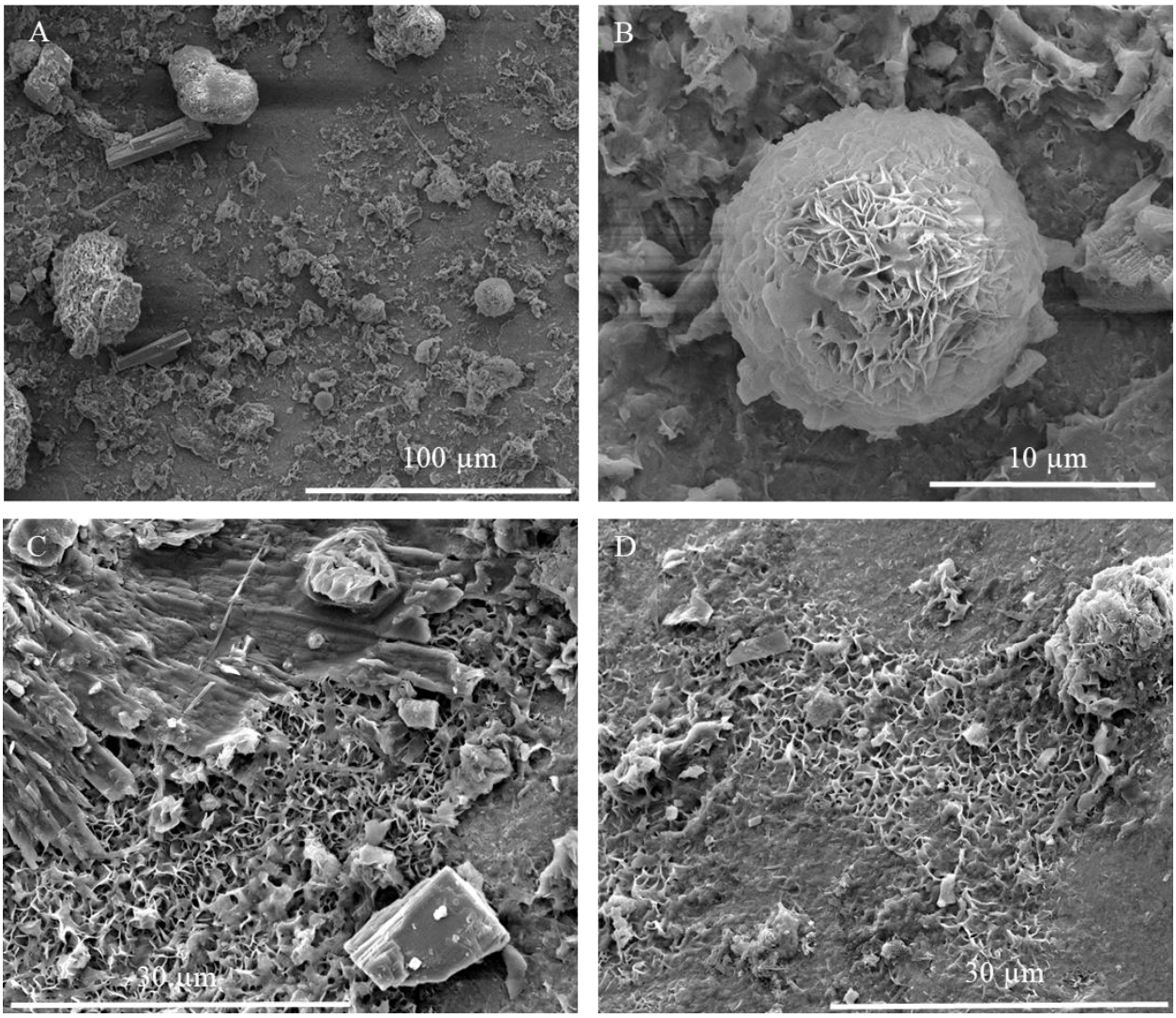

Figure F-6. EBS-25. SEM images of post-reaction 304 SS. [**A**] Overview of the stainless-steel surface with zeolite, gypsum, and CSH phases. [**B**] Tobermorite rosette. [**C**] Calcite spray overlaying mat of CSH minerals. [**D**] CSH mineral proto-rosette layer on steel.

EBS-26

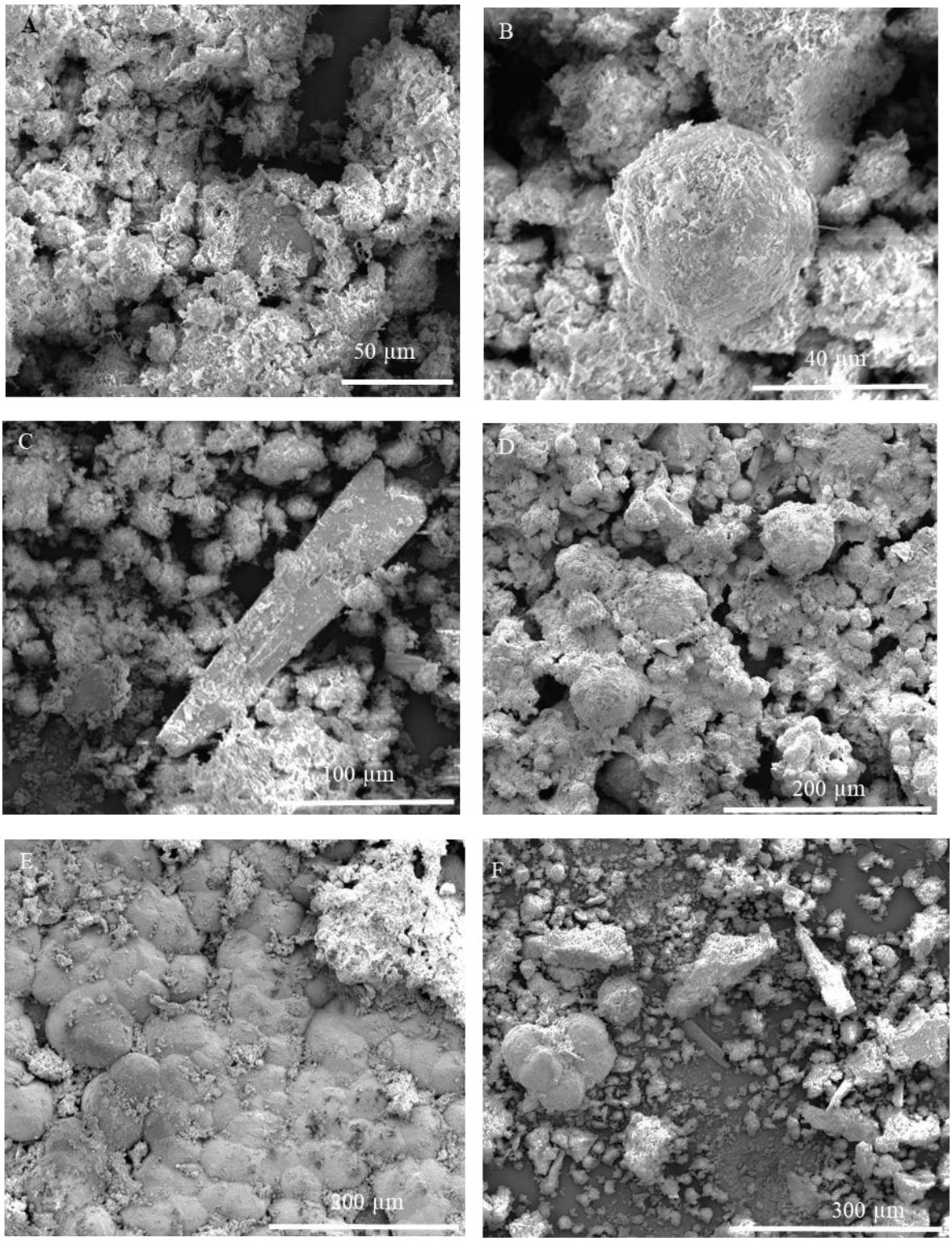

Figure F-7. EBS-26 SEM images. [**A**] Zeolite with CSH minerals and clays in the porous cement fraction. [**B**] Zeolite with tobermorite in the clay fraction. [**C**] Gypsum on clay minerals on the stainless-steel surface. [**D**] Zeolite with CSH and clay minerals on stainless steel. [**E**] Zeolite mat on the stainless steel. [**F**] Overview of LCS with zeolites, gypsum, and Fe-oxides.

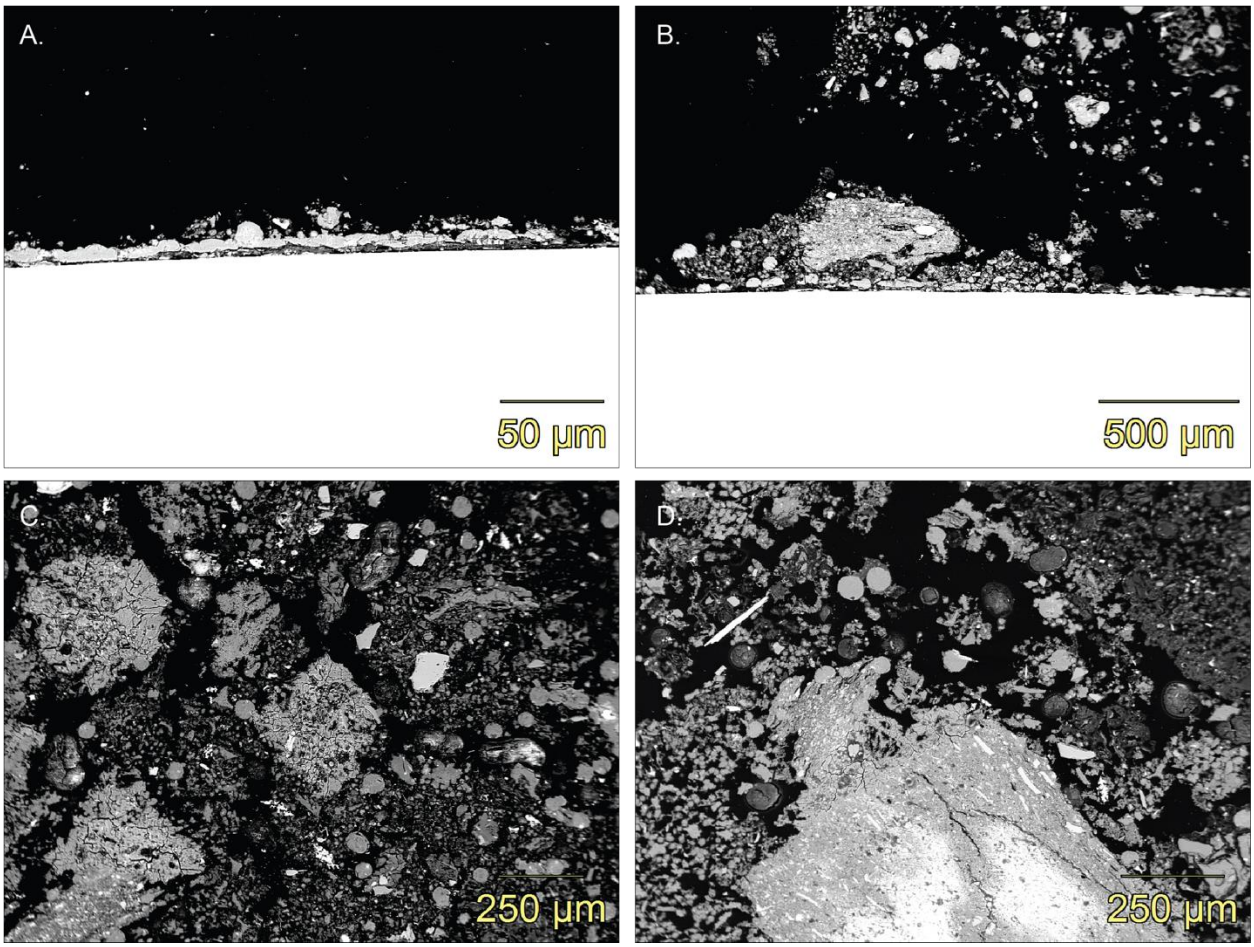

Figure F-8. EBS-26 BSE images. [**A, B**] Surface of LCS coupon (white) depicting zeolite layer. In [**B**], an Opalinus Clay fragment is observed adjacent to the surface. [**C, D**] Analcime (small spheres) and garronite clusters (porous, larger spheres) near Opalinus Clay fragments (light, fine grained) in the clay fraction of EBS-26. An example of a cluster of tobermorite is in the bottom left corner of [**D**].

EBS-27

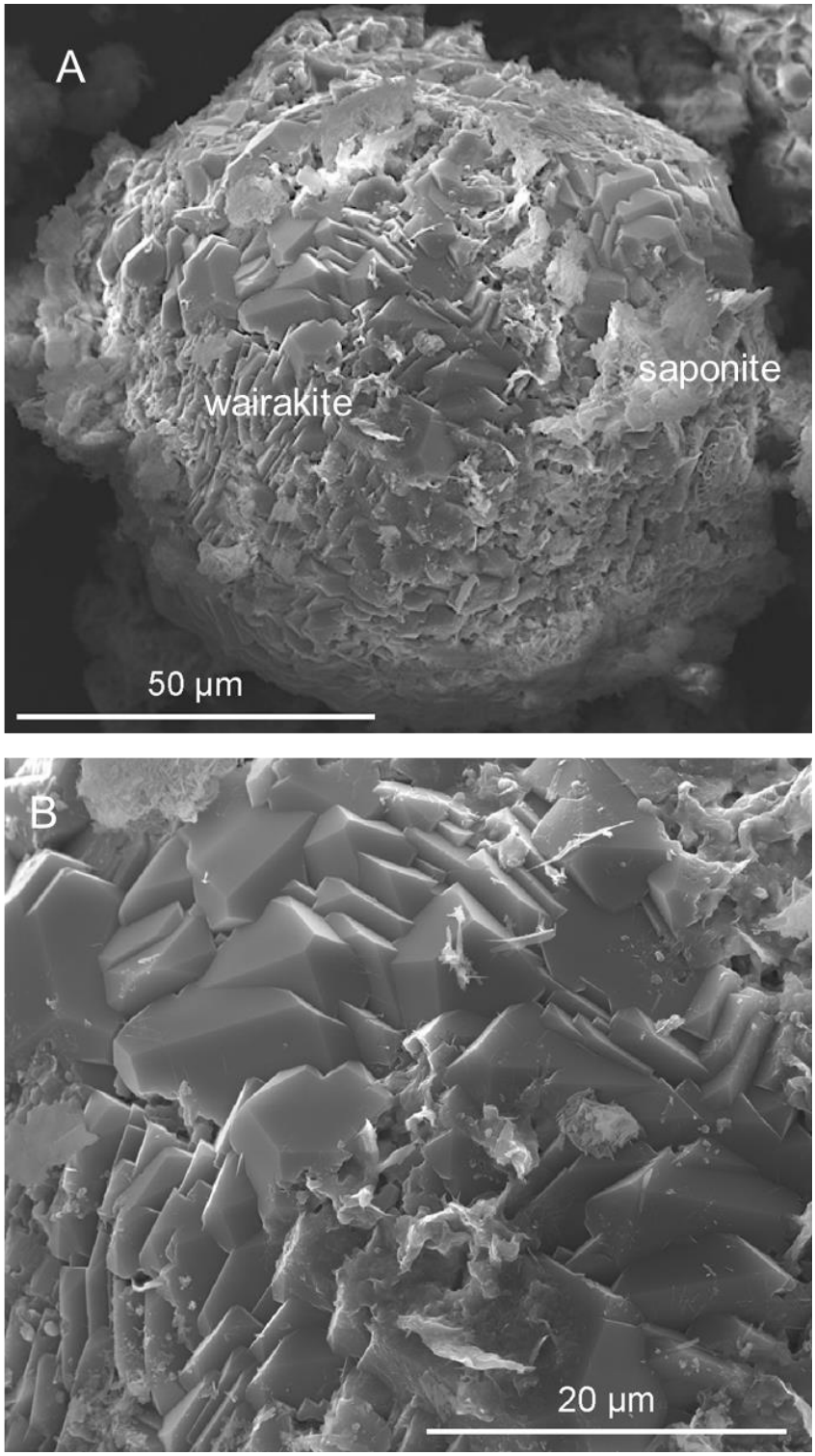

Figure F-9. EBS-27 SEM images of post-reaction products from top of the reaction cell. [**A**] Wairakite with saponite [**B**] Inset of wairakite texture [A]

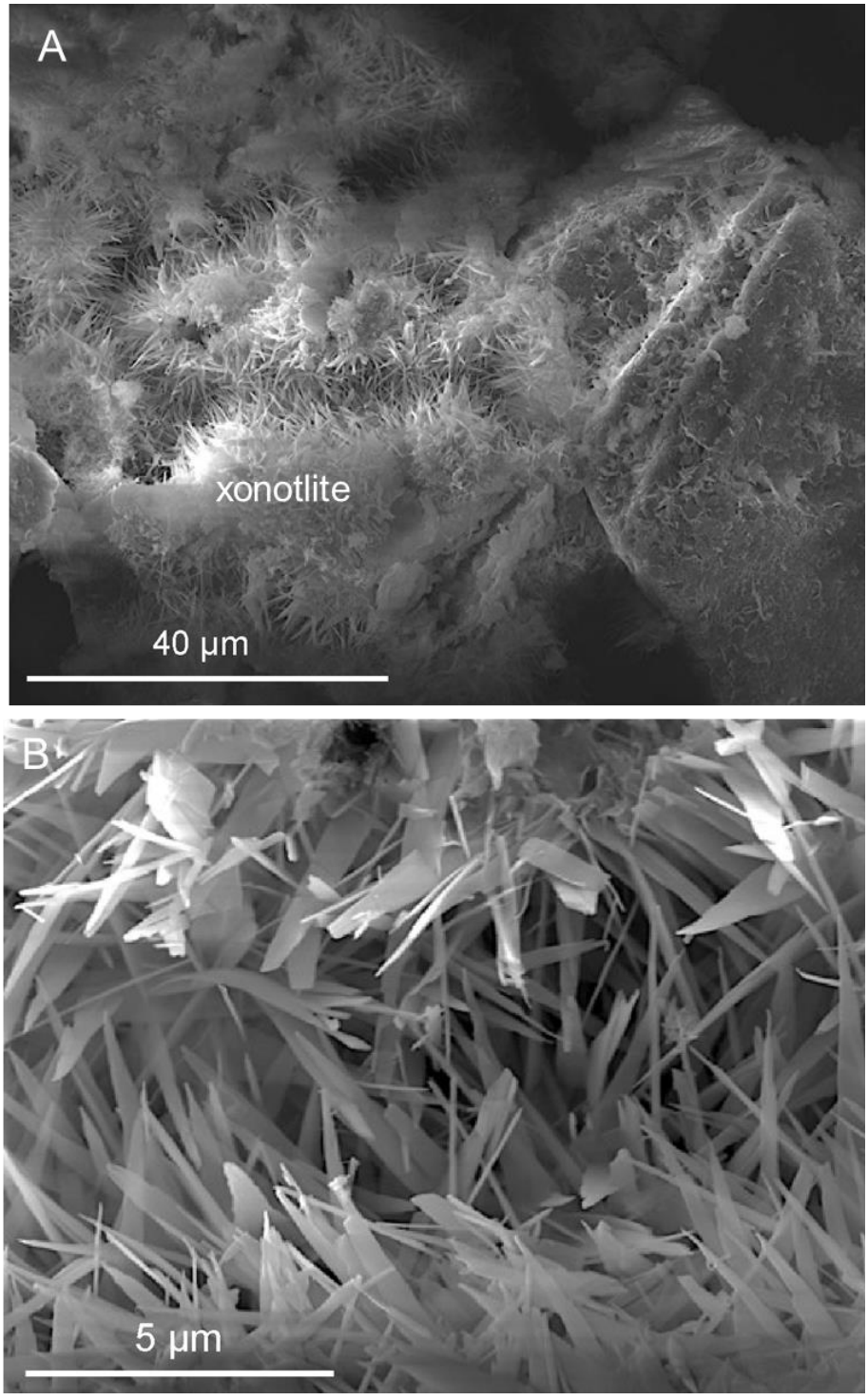

Figure F-10. EBS-27 SEM images of post-reaction post-reaction products from top of reaction cell. [**A**] Xonotlite in clay matrix [**B**] Inset image of fibrous xonotlite from [A]

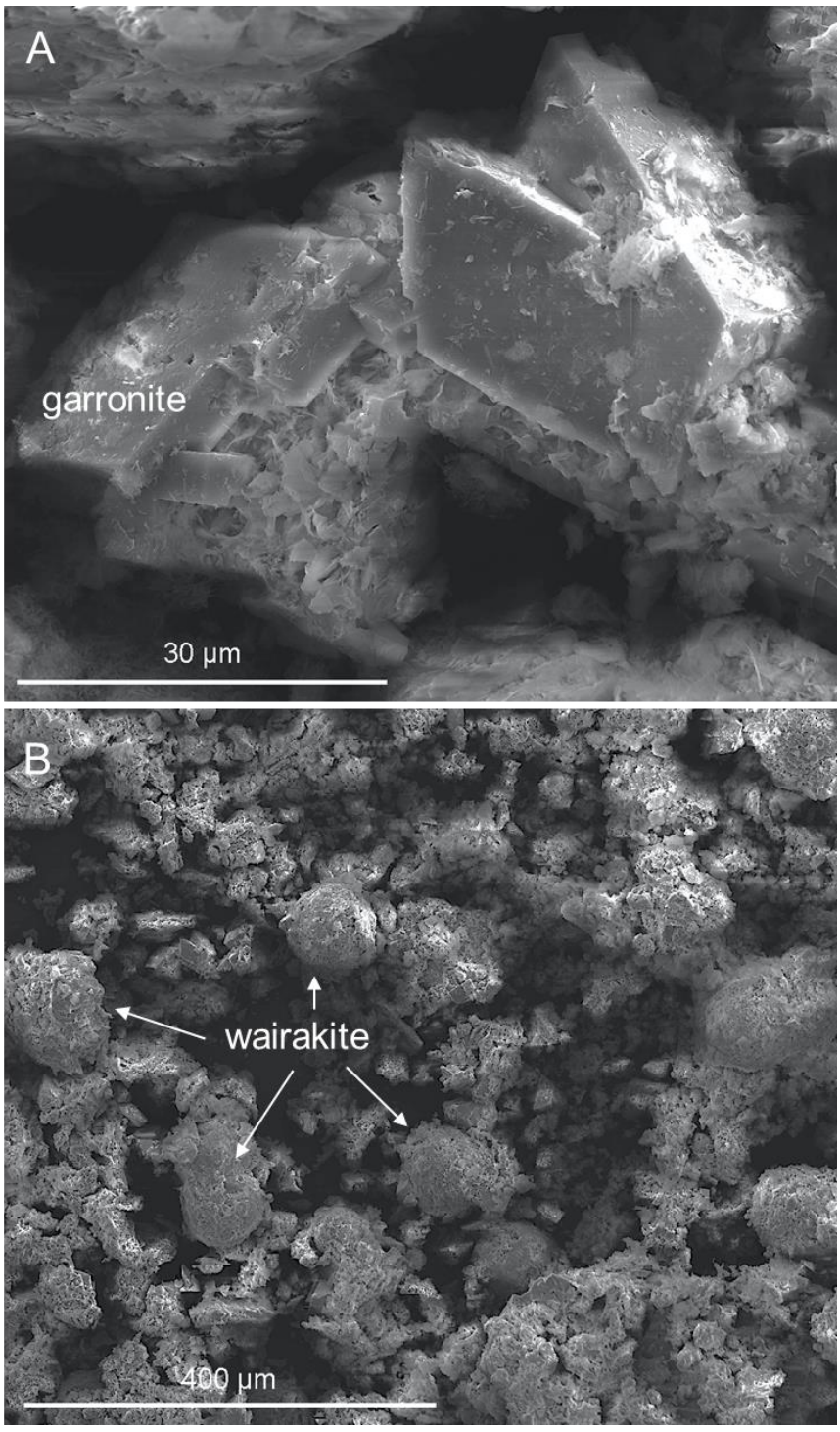

Figure F-11. EBS-27 SEM images of post-reaction products from bottom of bottom of reaction cell. [**A**] Garronite with Fe-saponite [**B**] Wairakite in a CSH-clay matrix.

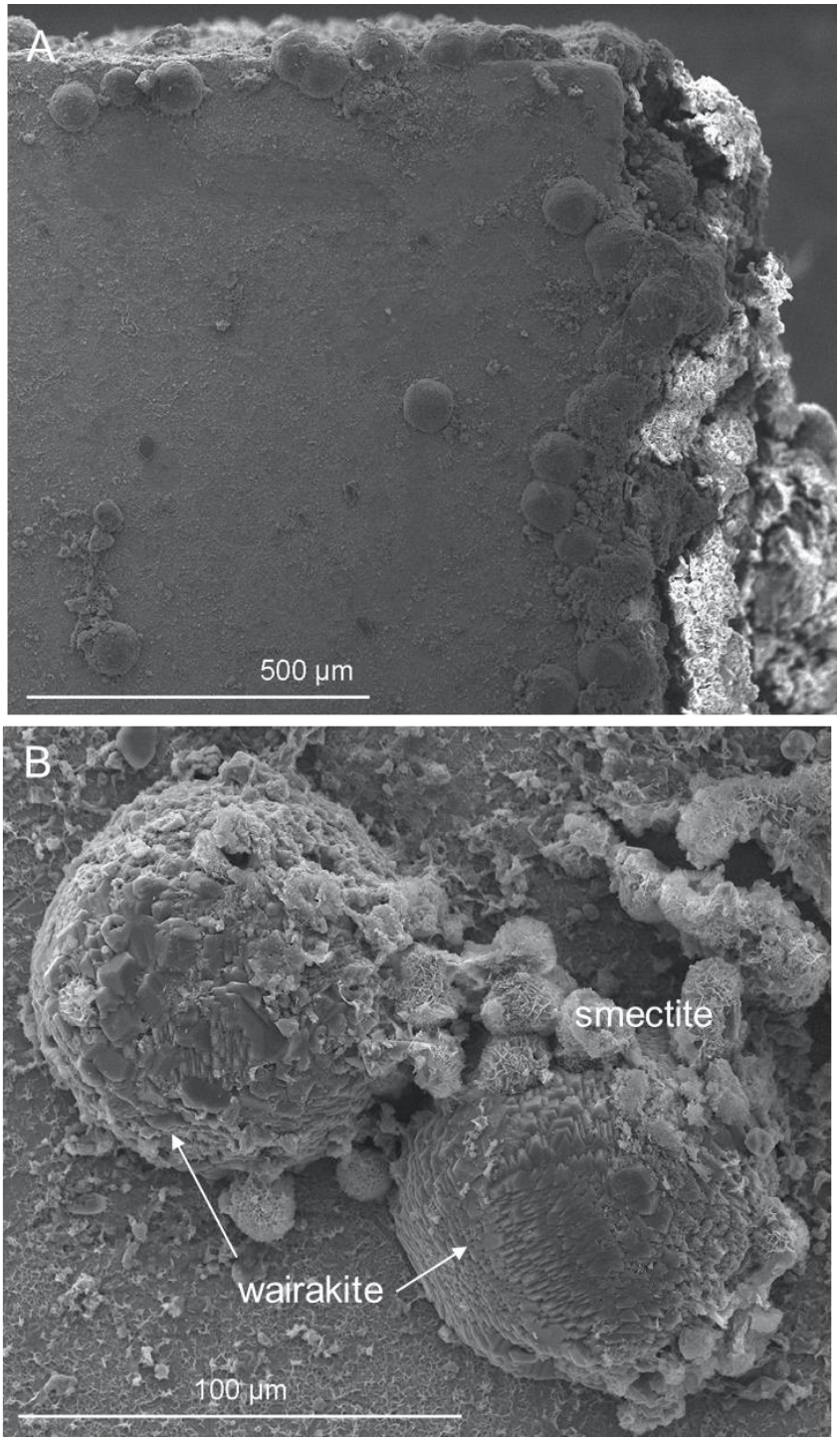

Figure F-12. EBS-27 SEM images of post-reaction products from 316SS. [**A**] Overview of SS with large wairakite crystals [**B**] Wairakite with smectite rosettes.

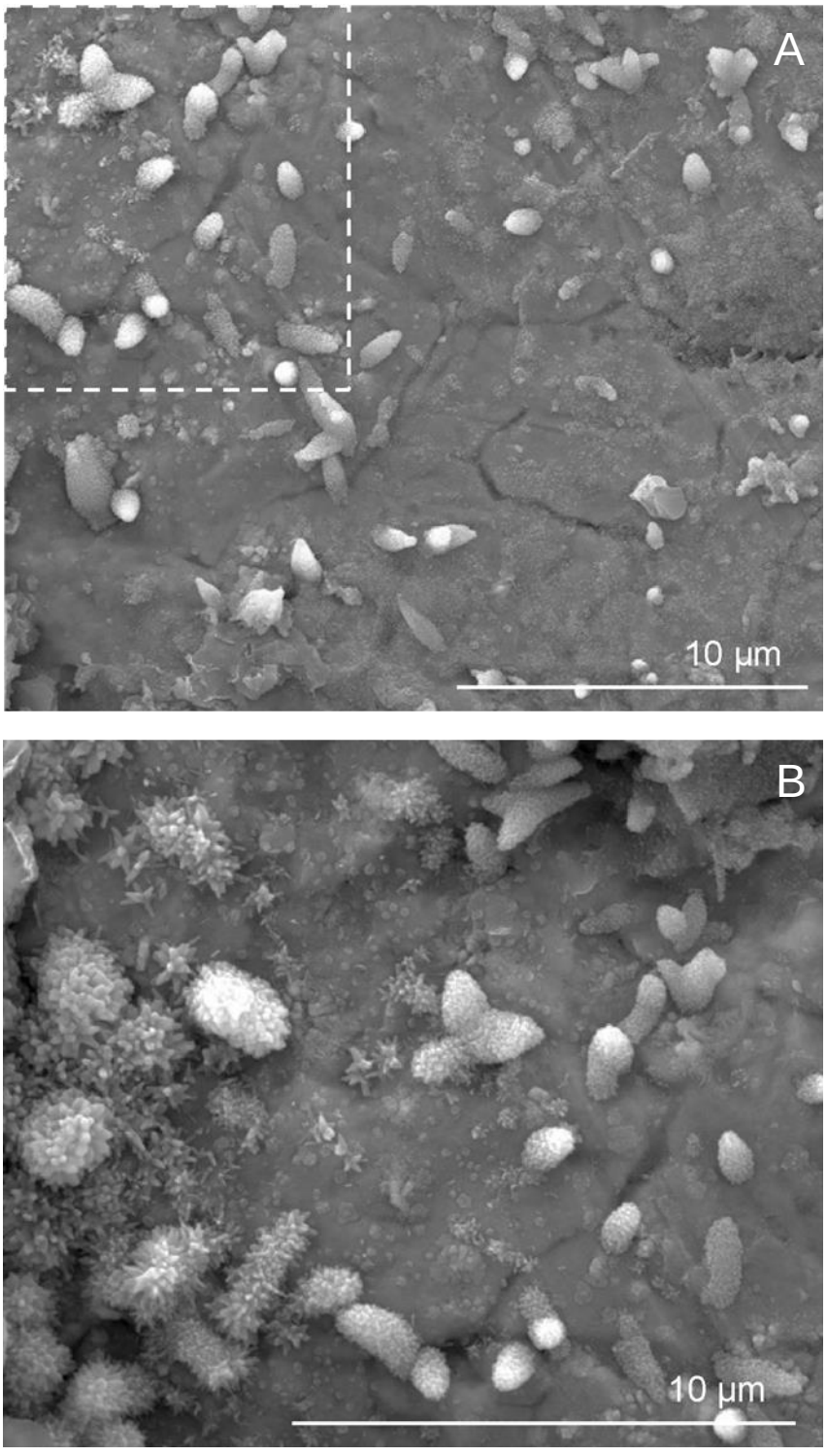

Figure F-13. EBS-27 SEM images of post-reaction products from the 316SS surface. [**A**] Iron oxide on steel surface [**B**] Inset image of iron oxides from [A]

EBS-28

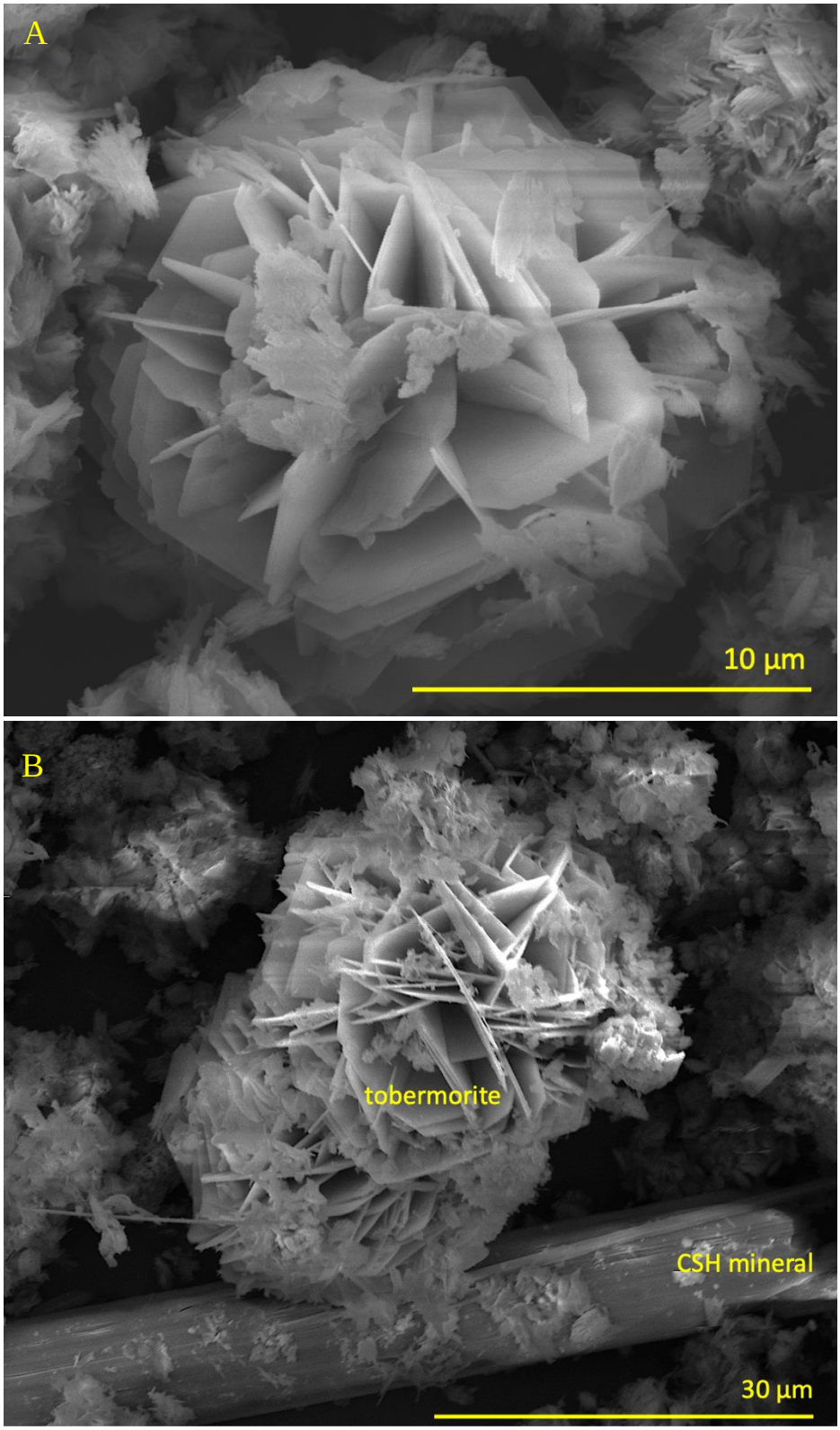

Figure F-14. EBS-28 SEM images of clay-cement mixture. [**A**] Tobermorite rosette [**B**] Tobermorite rosette with CSH minerals

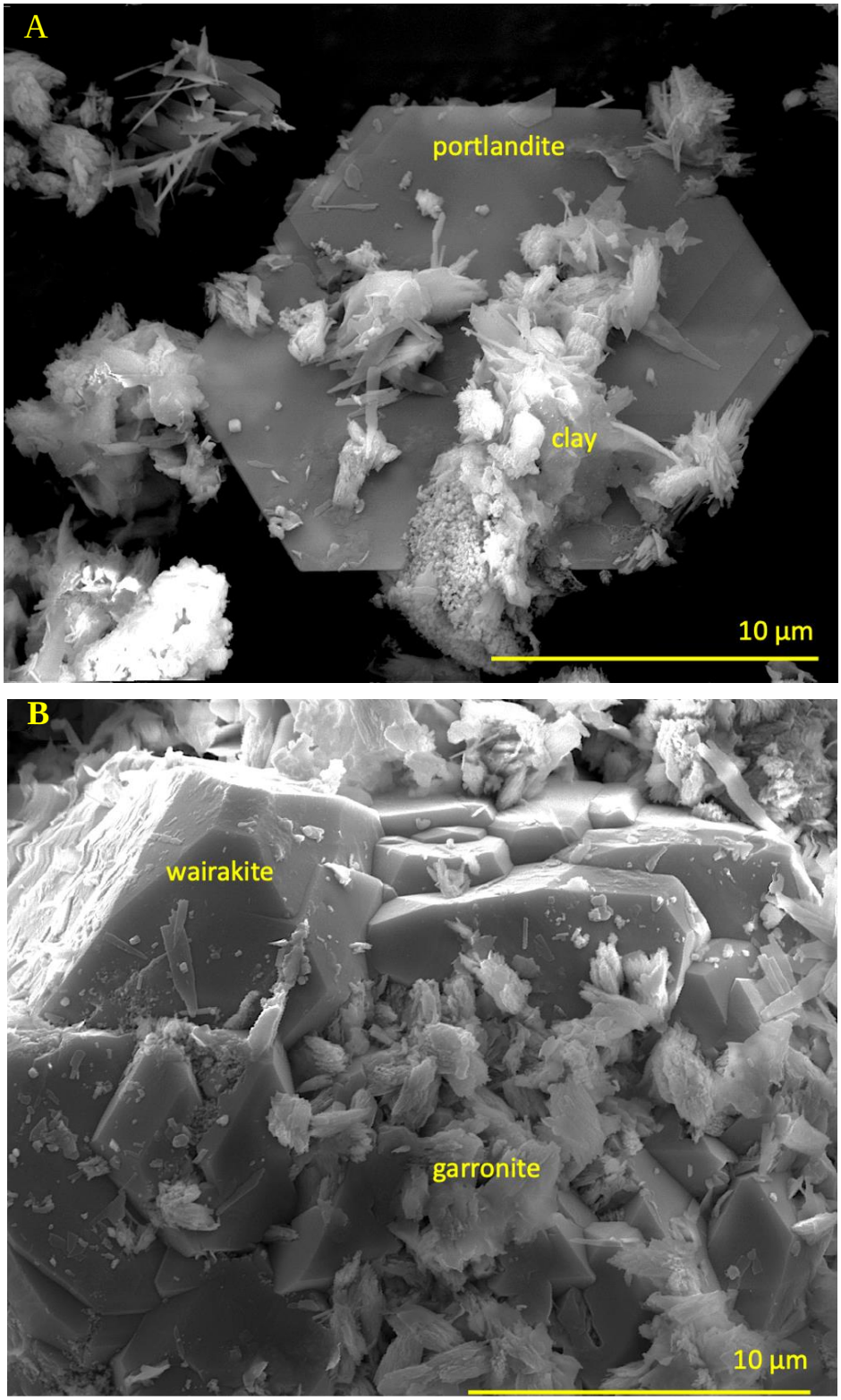

Figure F-15. EBS-28 SEM images of clay-cement mixture. [**A**] Portlandite plate with clay [**B**] Wairakite with garronite

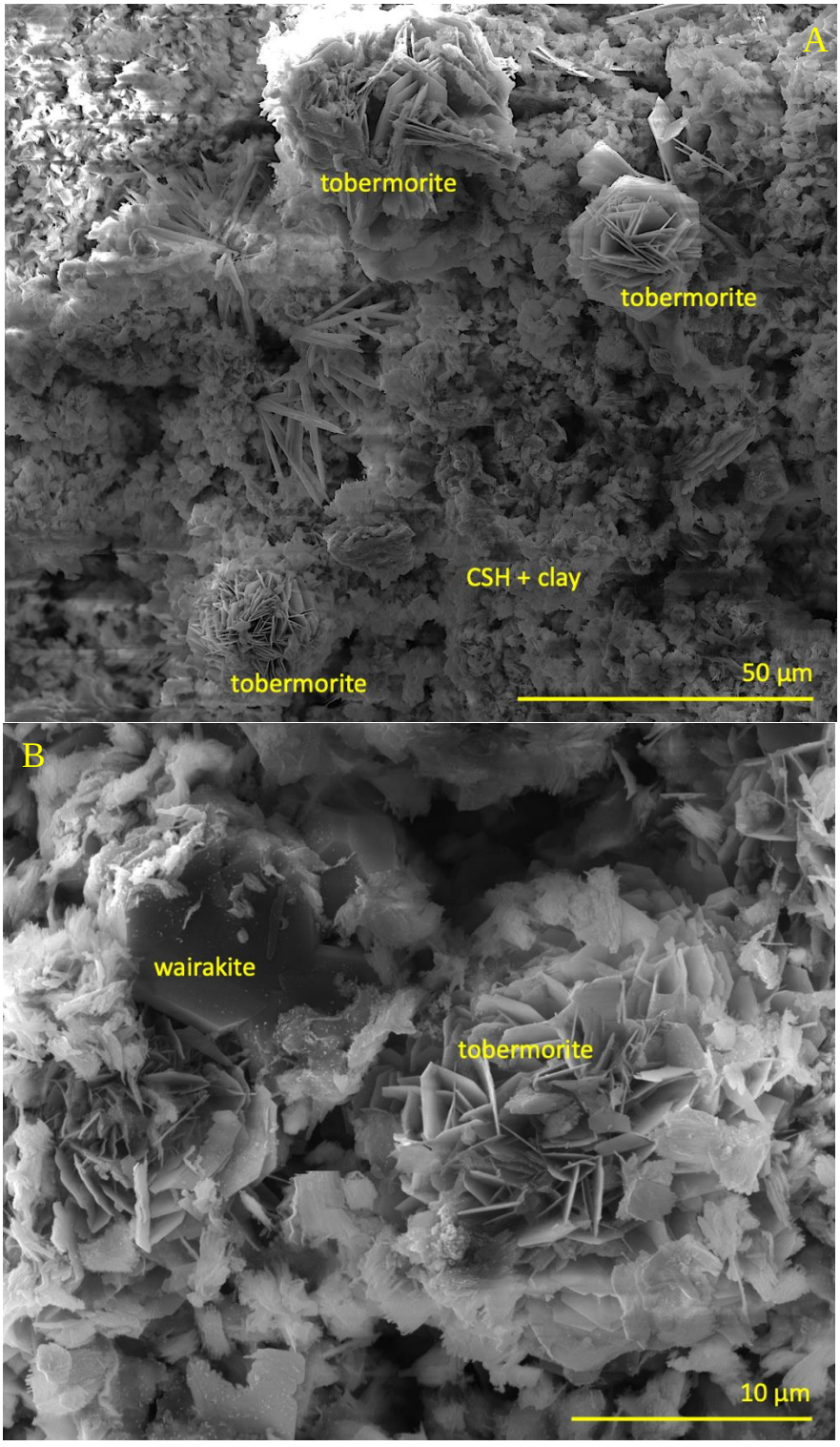

Figure F-16. EBS-28 SEM images of post-reaction products on the 316SS. [**A**] Multiple tobermorite rosettes in a CSH-clay matrix. [**B**] Wairakite and tobermorite in CSH-clay matrix.

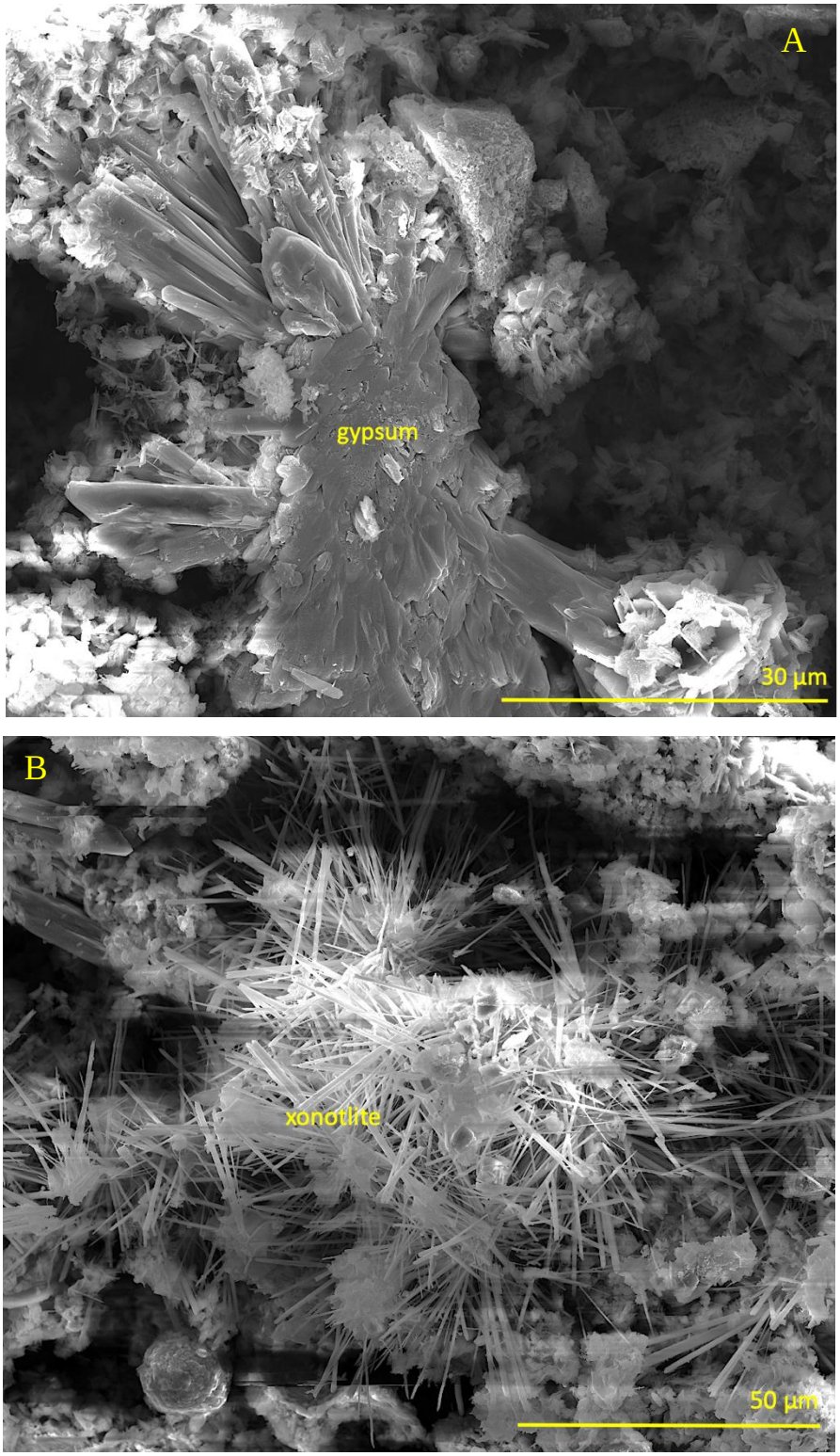

Figure F-17. EBS-28 SEM images of post-reaction products on the 316SS. [**A**] Gypsum in CSH-clay matrix [**B**] Xonotlite in CSH-clay matrix.

EBS-29

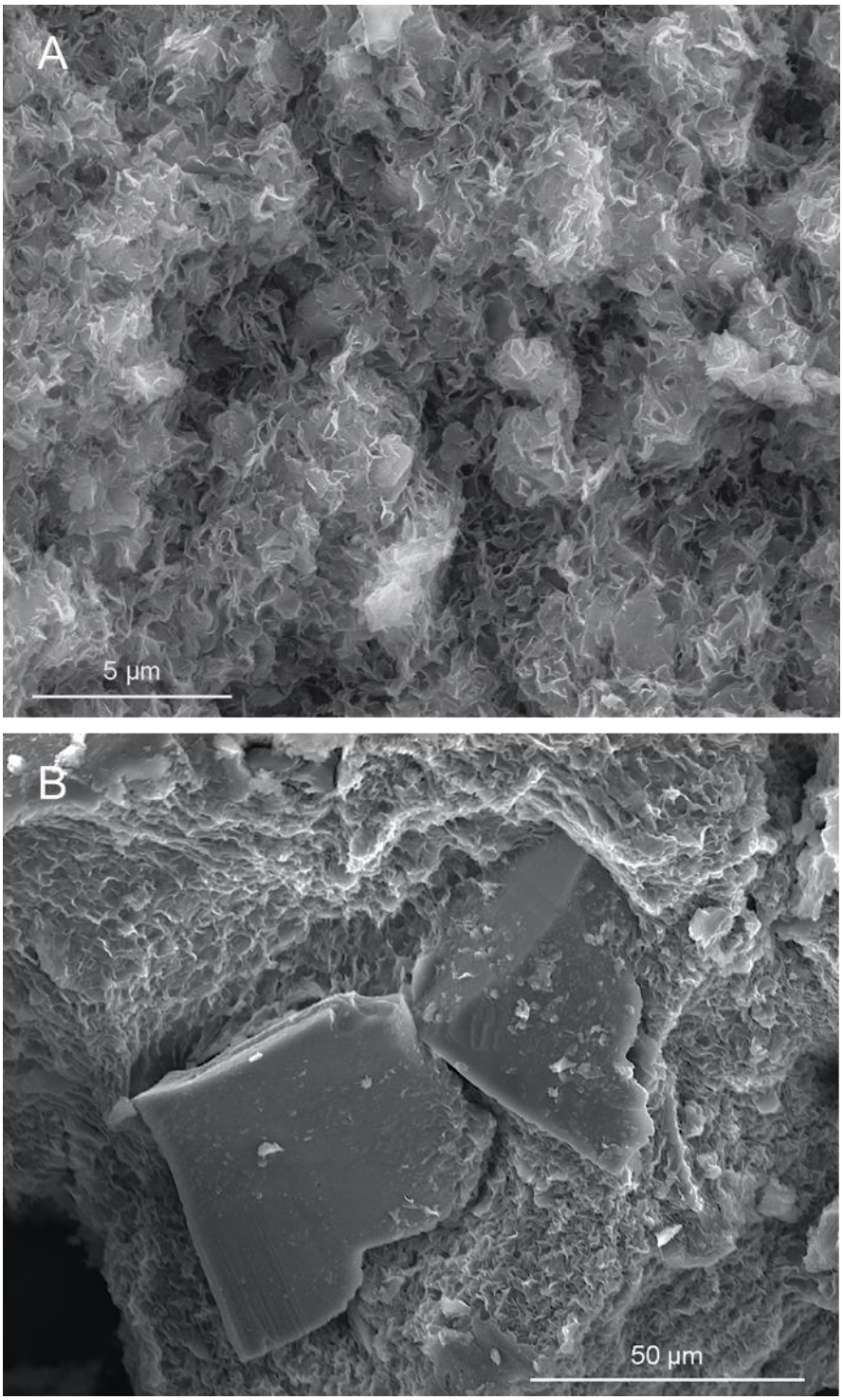

Figure F-18. EBS-29 SEM images of post-reaction products WY bentonite. [**A**] Fe-saponite [**B**] Plagioclase phenocryst in Fe-saponite

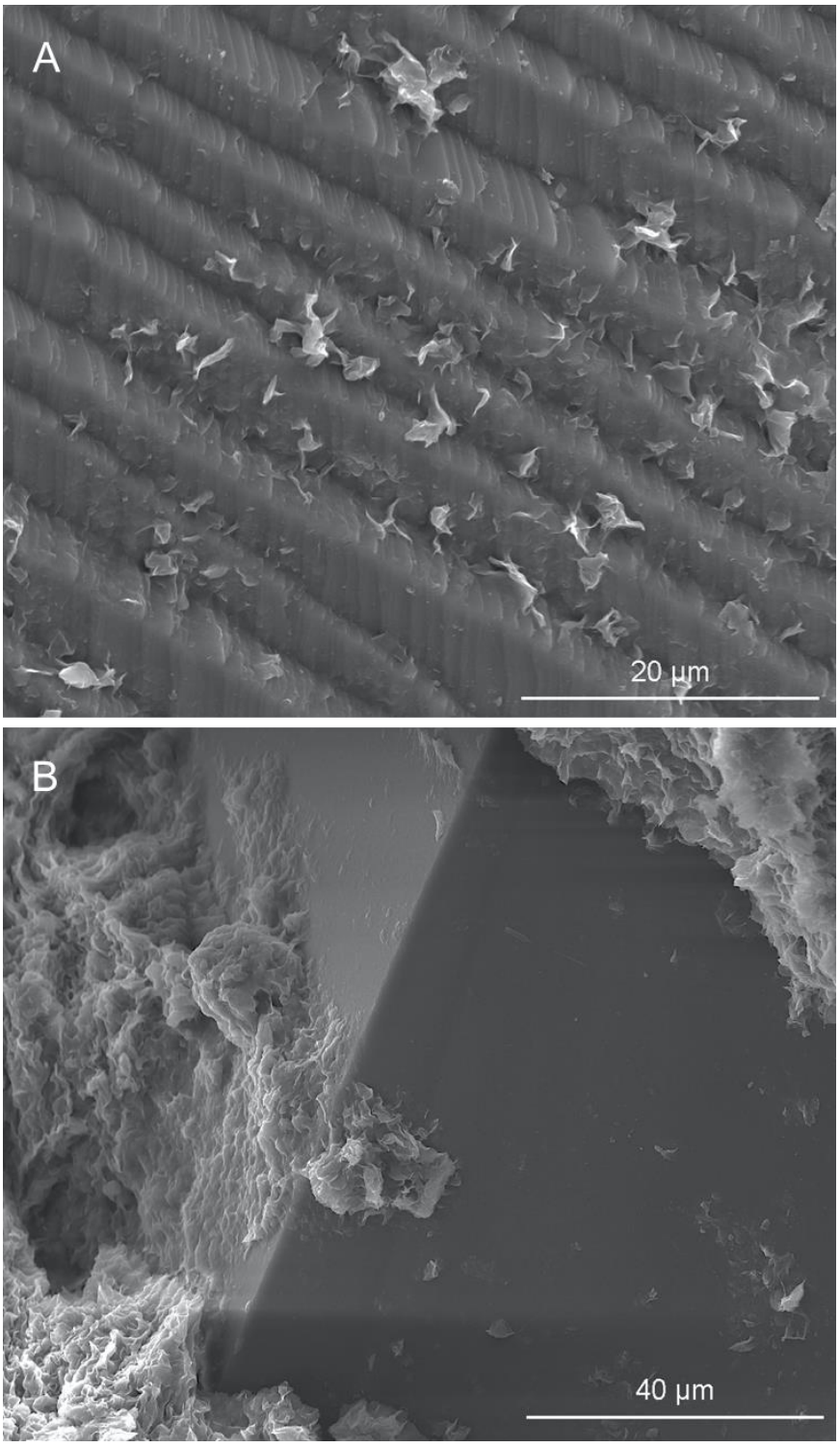

Figure F-19. EBS-29 SEM images of post-reaction products of apatite from WY bentonite. [**A**] Apatite surface with dissolution features [**B**] Apatite coated in smectite

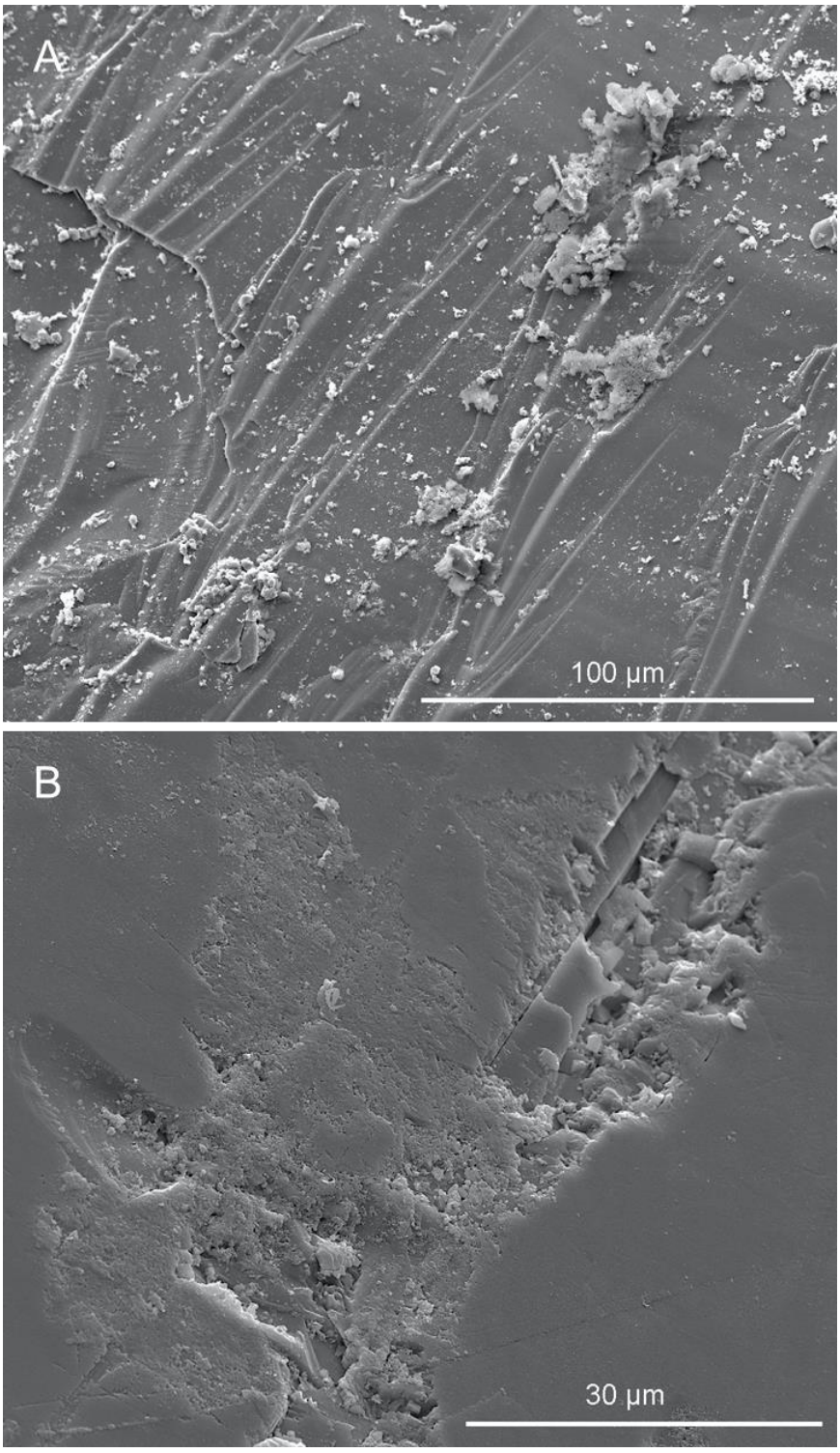

Figure F-20. EBS-29 SEM images of post-reaction products from apatite-only capsules. [**A**] Apatite with surface impurities [**B**] Pitting on apatite surface.

EBS-30

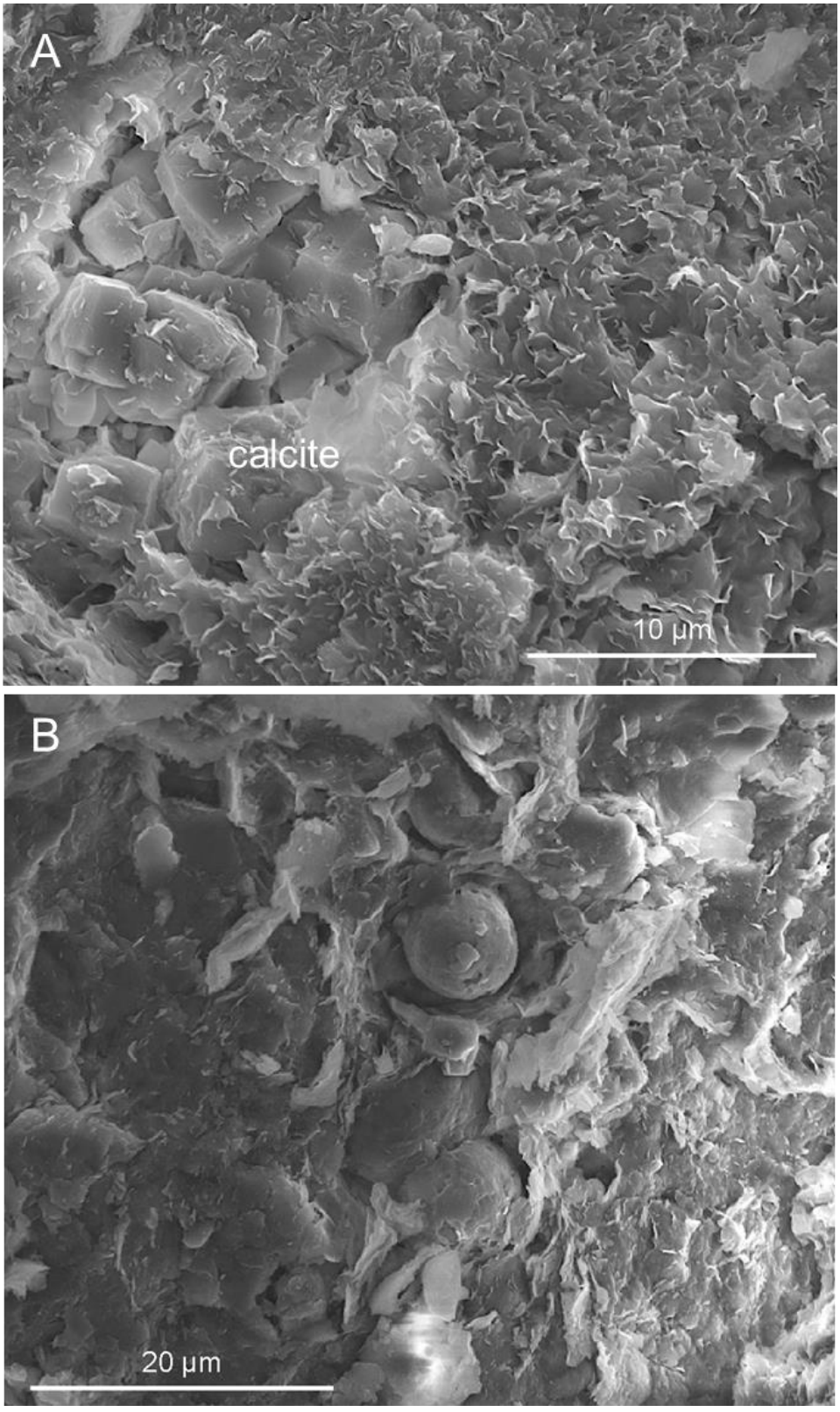

Figure F-21. EBS-30 SEM images of post-reaction products from OPC and WY bentonite. [**A**] Calcite embedded in smectite. [**B**] Calcite spheres, likely fossils from Opalinus Clay, imbedded in a clay matrix.

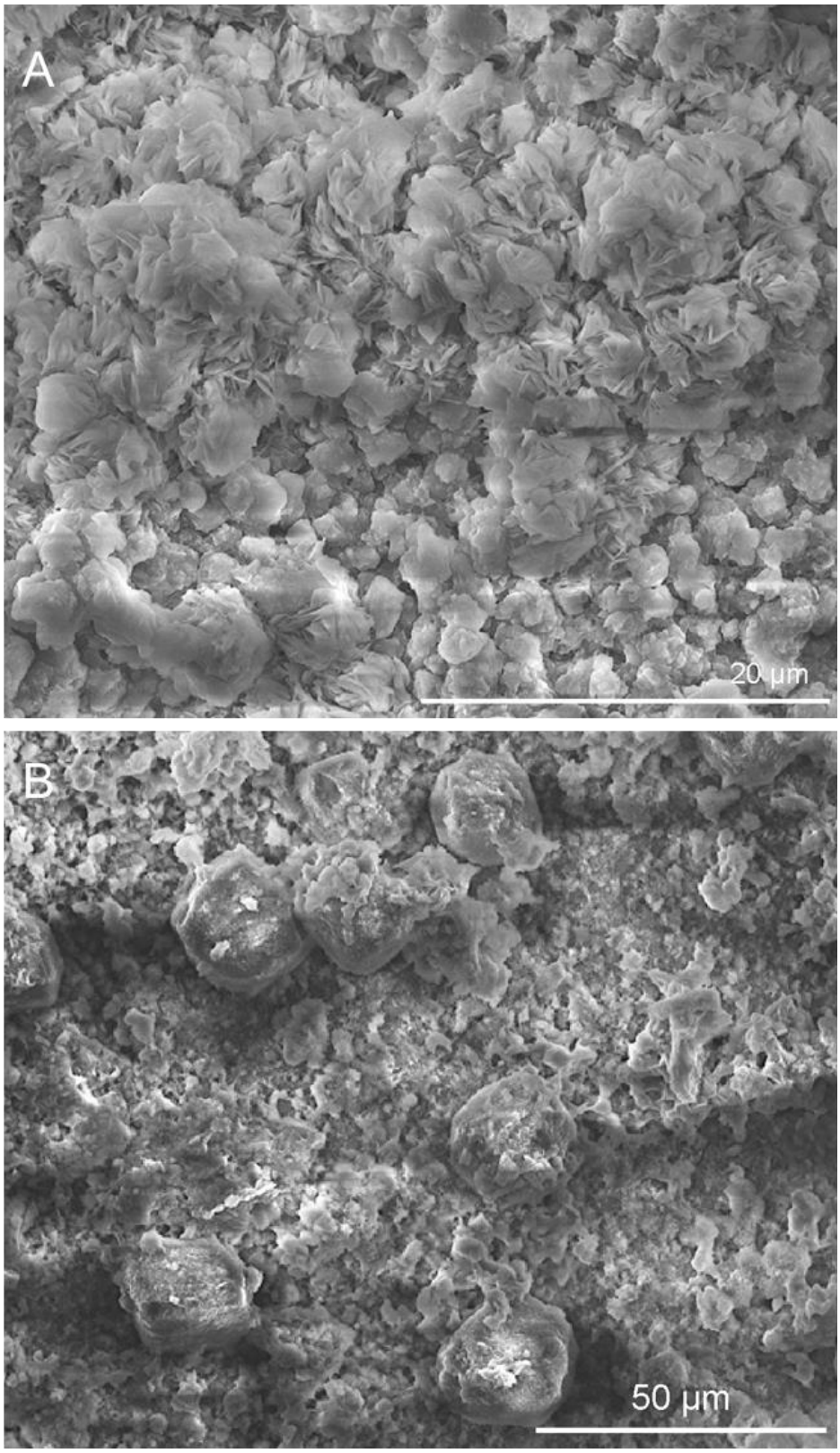

Figure F-22. EBS-30 SEM images of post-reaction cement chip surface. [**A**] CSH gel-smectite matrix [**B**] Calcite aggregates in the CSH/smectite matrix.

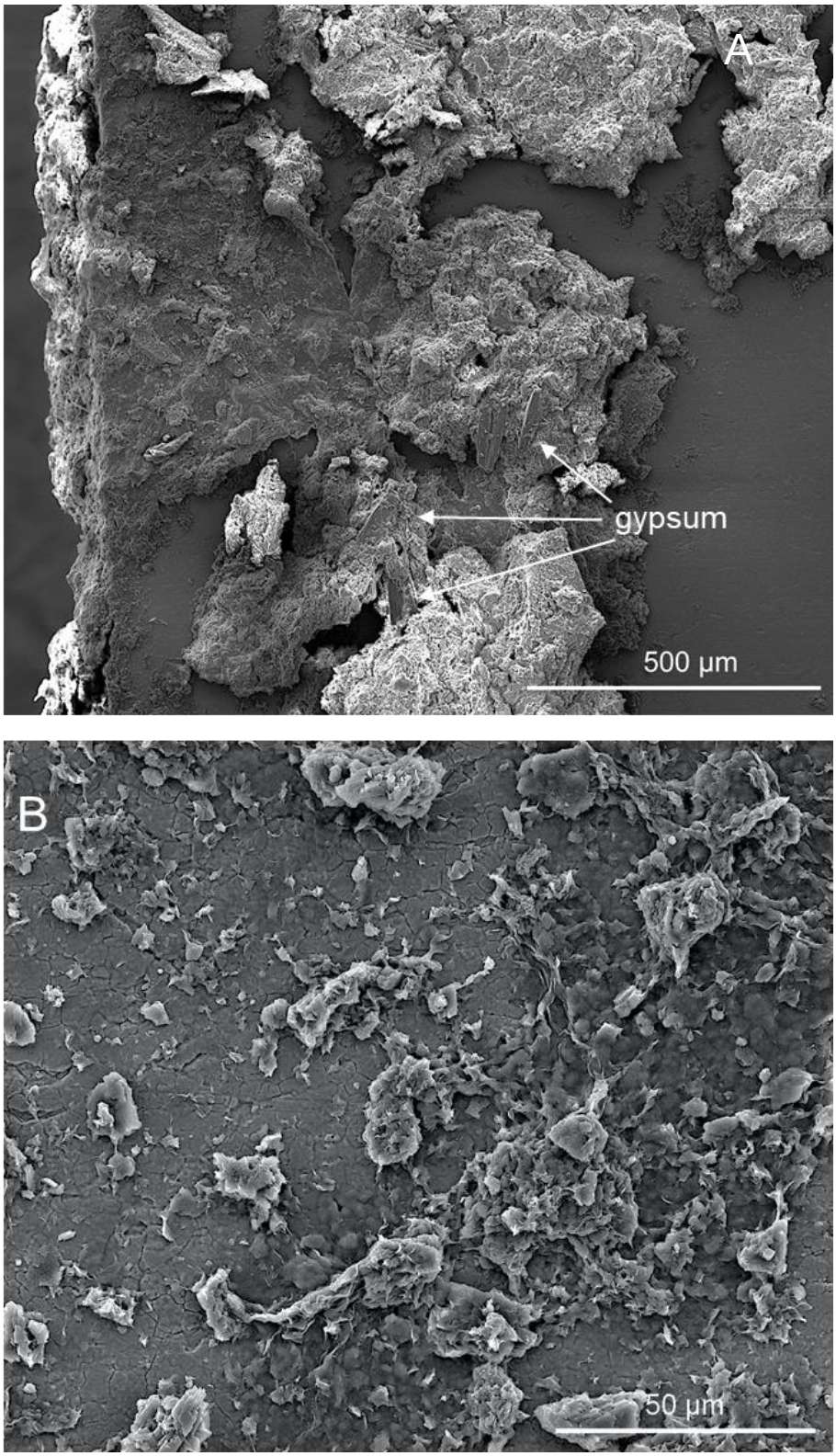

Figure F-23. EBS-30 SEM images of post-reaction products from the 316SS surface. [**A**] Large gypsum crystals in CSH-clay matrix [**B**] Smectite coating of the surface of the steel.

EBS-31

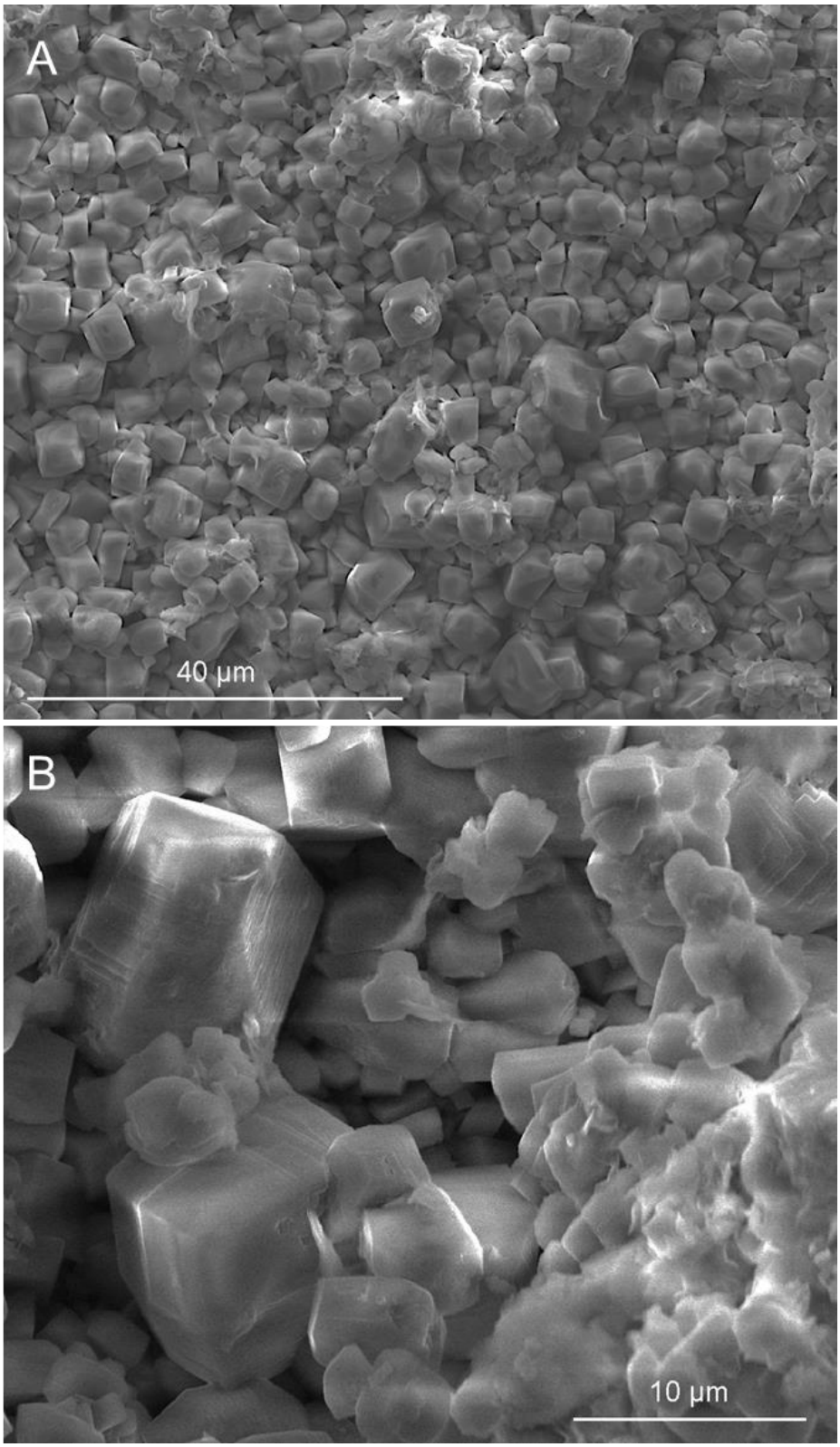

Figure F-24. EBS-31 SEM images of post-reaction cement surface. [**A**] Calcite covering the cement chip surface [**B**] Calcite with smectite.

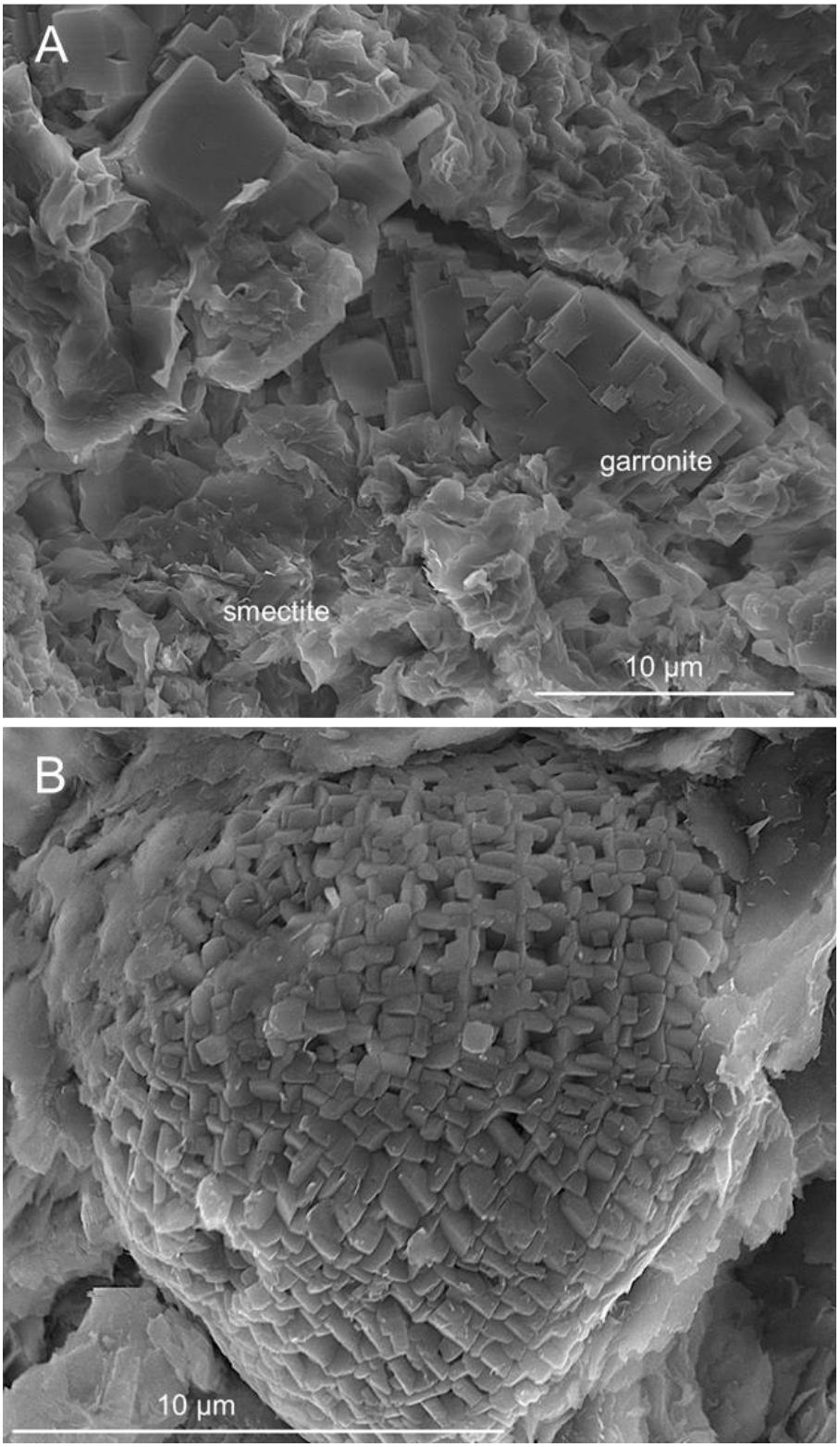

Figure F-25. EBS-31 SEM images of the WY bentonite and Opalinus Clay. [**A**] Garronite in a smectite matrix. [**B**] Lime or CSH sphere in smectite.

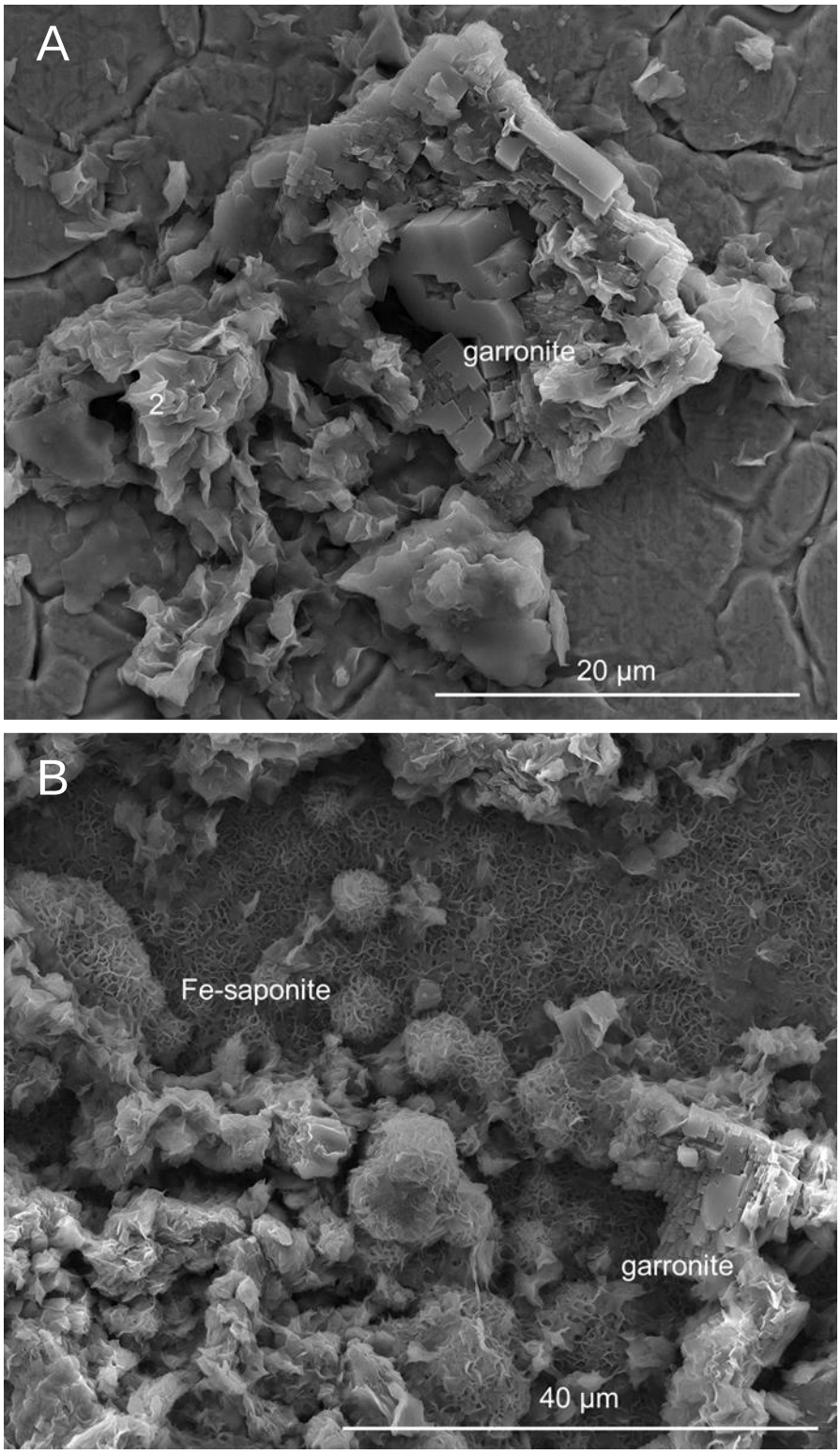

Figure F-26. EBS-31 SEM images of the post-reaction 304SS surface. [**A**] Garronite in a smectite matrix on the steel surface. [**B**] Fe-saponite honeycombs with minor garronite.